

### Geophysical-Petrological Modeling of the Crust and Upper Mantle within the Central Mediterranean and Topographic Implications

Wentao Zhang



Aquesta tesi doctoral està subjecta a la llicència <u>Reconeixement 4.0. Espanya de</u> <u>Creative Commons.</u>

Esta tesis doctoral está sujeta a la licencia <u>Reconocimiento 4.0. España de Creative</u> <u>Commons.</u>

This doctoral thesis is licensed under the <u>Creative Commons Attribution 4.0. Spain</u> <u>License.</u>

# Geophysical-Petrological Modeling of the Crust and Upper Mantle within the Central Mediterranean and Topographic Implications

Tesis presentada por

### Wentao Zhang

Para obtener el título de doctor en Ciencias de la Tierra por la Universidad de Barcelona

Tesis realizada en el marco del programa de doctorado de Ciencias de la Tierra de la

Universidad de Barcelona

Directoras:

Dr. Ivone Jiménez-Munt

**GEO3BCN-CSIC** 

**Dr. Montserrat Torné Escasany** 

**GEO3BCN-CSIC** 

Dr. Ana María Negredo Moreno

Universidad Complutense de Madrid

Tutor:

Dr. Alex Marcuello Pascual

Universitat de Barcelona

Barcelona, Septiembre 2024









# Geophysical-Petrological Modeling of the Crust and Upper Mantle within the Central Mediterranean and Topographic Implications

Thesis presented by

Wentao Zhang

To obtain the degree of doctor in Earth Sciences from the University of Barcelona

Thesis conducted within the framework of the doctoral program in Earth Sciences at
the University of Barcelona

Supervisors:

Dr. Ivone Jiménez-Munt

**GEO3BCN-CSIC** 

**Dr. Montserrat Torné Escasany** 

**GEO3BCN-CSIC** 

Dr. Ana María Negredo Moreno

Universidad Complutense de Madrid

Tutor:

Dr. Alex Marcuello Pascual

Universitat de Barcelona

Barcelona, September 2024









### **ACKNOWLEDGMENTS**

First and foremost, I wish to express my heartfelt gratitude for my supervisors at Geosciences Barcelona (GEO3BCN), Dr. Ivone Jiménez-Munt and Montserrat Torné Escasany. Your support and guidance throughout my studies have been invaluable. I am extremely grateful for your recommendation letter, which played a crucial role in securing my scholarship from the Chinese government. I feel very fortunate and deeply grateful that you accepted me as your student. You have been like a true friend and the key to helping me complete my studies in Barcelona. This journey as a PhD student has been an incredible experience, offering numerous opportunities for learning and personal growth. Your enthusiasm and inclusiveness have been truly inspiring and helping me build confidence and independence as a young researcher. I wanted to thank you immensely for all your help again.

To my co-supervisor at Madrid, Dr. Ana María Negredo Moreno (UCM), your guidance, patience, and support are invaluable throughout my studies in Spain. Regardless of how tough things got, our discussions always left me feeling more confident and optimistic about our work. You have gone beyond the role of a supervisor, becoming a true friend and mentor. Your constant encouragement has motivated me to overcome challenges and achieve my goals. I also extend my heartfelt thanks to my tutor, Dr. Alex Marcuello Pascual at UB. Your collaboration and assistance are crucial in navigating the procedures necessary to complete my Ph.D. at the Universitat de Barcelona.

Once again, I want to extend my heartfelt thanks to all my supervisors and tutor for their invaluable assistance throughout my studies. Your extensive knowledge and rich experience have been tremendously helpful during my doctoral studies. In addition, your encouragement and ongoing support allowed me to spend my years in Barcelona engaged in positive and meaningful experiences.

I extend my gratitude to all members of the Group of Dynamics of the Lithosphere (GDL) for the enriching discussions and learning experiences during workshops, field trips, and training events integral to this thesis. Special thanks to the researchers here, Jaume Vergés, Daniel García-Castellanos, Gema Llorens, David Cruset, and Marc Viaplana for the enjoyable times and the invaluable geological knowledge shared over the years. Your friendship has made the past years truly memorable, and I feel fortunate to have gained

a new family through our experiences together. Thank you sincerely for your invaluable contributions.

I also want to express my gratitude to my friends and colleagues in Barcelona for the wonderful times we shared both in the work and life, including Abraham, Ajay, Alejandra, Ángela, Daniela, Estefania, Erandi, Hanneke, Handoyo, Hongqiang, Josep, Lara, Mahdi, Mario, Núria, Olaya, Ozgench, Paula, Samuel, Yuenchao, and Xavi. Their companionship made my time in Barcelona fulfilling and enjoyable. Thank you for your friendship and the unforgettable moments we experienced together.

Finally, to my parents and sister for everything.

Muchas gracias a todos.

### **Publications**

### Fist author publications included in this thesis:

Zhang, W., Jiménez-Munt, I., Torne, M., Vergés, J., Bravo-Gutiérrez, E., Negredo, A. M., & García-Castellanos, D. (2024). The Lithosphere and Upper Mantle of the Western-Central Mediterranean Region From Integrated Geophysical-Geochemical Modeling. Journal of Geophysical Research: Solid Earth, 129(4), e2023JB028435. https://doi.org/10.1029/2023JB028435

Zhang, W., Jiménez-Munt, I., Torne, M., Vergés, J., Bravo-Gutiérrez, E., Negredo, A. M., Carminati, E., García-Castellanos, D., & Fernàndez, M. (2022). Geophysical-Petrological Model for Bidirectional Mantle Delamination of the Adria Microplate Beneath the Northern Apennines and Dinarides Orogenic Systems. Journal of Geophysical Research: Solid Earth, 127(12), e2022JB024800. https://doi.org/10.1029/2022JB024800

### Co-author publications not included in this thesis:

Bravo-Gutiérrez, E., Vergés, J., Torne, M., García-Castellanos, D., Negredo, A. M., Zhang, W., Cruset, D., Viaplana-Muzas, M., & Jiménez-Munt, I. (2024). Preshortening reconstruction of the adria microplate: Balanced and restored cross-sections through the Southern Apennines—Dinarides (Central Mediterranean Sea). *Marine and Petroleum Geology*, 169, 107055. https://doi.org/10.1016/j.marpetgeo.2024.107055

Sheng, C., Xu, H., Zhang, Y., Zhang, W., & Ren, Z. Hydrological Properties of Calcareous Sands and Its Influence on Formation of Underground Freshwater Lenson Islands. *Journal of Jilin University (Earth Science Edition)*, 2020, 50(4): 1127-1138. http://dx.doi.org/10.13278/j.cnki.jjuese.20180331

### **Funding**

This thesis is funded by GeoCAM (PGC2018-095154-B-I00) and GEOADRIA (PID2022-139943NB-I00) from the Spanish Government, the Generalitat de Catalunya Grant (AGAUR, 2021 SGR 00410), and the China Scholarship Council (CSC-201904910470) from Chinese Government. This thesis has been done using the facilities of the Laboratory of Geodynamic Modeling from Geo3BCN-CSIC.

### **Table of contents**

ABSTRACT	I
RESUM	iii
RESUMEN	v
CHAPTER 1 General Introduction	1
1.1. Motivation and overview	3
1.2. Tectonic setting	8
1.2.1. Tyrrhenian Basin	12
1.2.2. Apennines fold-thrust belt	13
1.2.3. Dinarides fold-thrust belt	14
1.2.4. Pannonian Basin	15
1.3. Objectives	16
1.4. Outline	17
CHAPTER 2 Fundamentals and Methodology	19
2.1. Fundamental concepts	21
2.1.1. Internal structure of the Earth	21
2.1.2. Composition of the upper mantle	26
2.1.3. Topography	28
2.2. Methodology	30
2.2.1. General workflow	31
2.2.2. Thermal modeling and boundary conditions	32
2.2.3. Potential field: Gravity and Geoid Height Anomalies	33
2.2.4. Mantle composition	34
2.2.5. Densities distribution	36
2.2.6. Mantle seismic velocities	37
2.2.7. Elevation	38
2.3. Geophysical data	43
2.3.1. Elevation	43

2.3.2. Gravity anomaly	44
2.3.3. Geoid	45
2.3.4. Surface heat flow	46
2.3.5. Mantle seismic velocities	47
CHAPTER 3 Geophysical-Petrological Model of the Crust and	
Mantle Beneath the Northern Apennines and Dinarides Oroger Systems	
3.1. Crustal structure from previous studies	54
3.2. Mantle characterisation from previous studies	58
3.3. Results	60
3.3.1. Crustal structure	60
3.3.2. The LAB and upper mantle physical properties and composition	66
3.3.3. Isostatic and dynamic topography	68
3.4. Discussion	71
3.4.1. Crustal and lithospheric structure	71
3.4.2. Mantle composition and sublithospheric anomalies	72
3.4.3. Geodynamic implications	73
3.5. Chapter conclusions	76
CHAPTER 4 Geophysical-Petrological Model of the Crust and Mantle Beneath the Southern Apennines and Dinarides Orogei Systems	nic
4.1. Model parameters and constraints	82
4.2. Results	86
4.2.1. Crustal structure	86
4.2.2. The LAB and upper mantle physical properties and composition	92
4.2.3. Isostatic and dynamic topography	96
4.3. Discussion	100
4.3.1. Crustal and lithospheric structure	100
4.3.2. Mantle composition and sublithospheric anomalies	101
4.3.3. Geodynamic implications	104
4.4. Chapter conclusions	107

CHAPTER 5 General Discussion	109
5.1. Present-day crustal and lithospheric structure	111
5.2. Mantle composition and anomalies	114
5.3. Dynamic topography	118
5.4. Geodynamic implications	123
CHAPTER 6 Conclusions, limitations and future work	129
List of Figures and Tables	137
List of Figures	139
List of Tables	147
References	149
Annex	189

### **ABSTRACT**

The Central Mediterranean region is a highly active seismic zone with unique tectonic characteristics, forming part of the Alpine-Mediterranean belt that extends from southern Iberia to the western Aegean Sea. This belt originated from the convergence of the African and Eurasian plates since the Late Cretaceous. The post-collision counterclockwise rotation of the Adria microplate triggered the opening of the asymmetric Tyrrhenian Basin and synchronous tectonic tightening along all its margins: the Apennines, the Calabria belt, the Dinarides-Hellenic belt, the Alps, and the Carpathian belt.

Applying an integrated geophysical-petrological modeling (LitMod2D\_2.0), this thesis investigates the thermochemical structure of the lithosphere and sublithospheric mantle beneath the Adria microplate and its margins and explores the geometry and depth continuity of the Adria slabs. Two transects have been modeled down to 400 km, spanning from the Tyrrhenian Basin to the Carpathians-Balkanides region, in a roughly SW-NE direction. The northern transect, approximately 1000 km long, crosses the Tyrrhenian Sea, the northern Apennines, the Adriatic Sea, the Dinarides and the Pannonian Basin. The southern transect spans approximately 1250 km, crossing the southern Tyrrhenian Basin, the southern Apennines, the Adriatic Sea, the southern Dinarides, and the Carpathians-Balkanides. In addition, I developed new numerical modeling codes of mantle flow to evaluate the topographic response of opposed subductions along these transects and discuss their implications in the evolution of the region.

In the northern transect, results show a more complex structure and slightly higher average crustal density of Adria compared to Tisza microplate. Below the Tyrrhenian Sea and Western Apennines, Moho lays at <25 km depth while along the Eastern Apennines it is as deep as 55 km. The modeled lithosphere-asthenosphere boundary (LAB) below the Tyrrhenian Sea and Pannonian Basin is flat lying at ~75 and 90 km, respectively. Below the External Apennines and Dinarides the LAB deepens to 150 km, slightly shallowing toward the Adriatic foreland basin at 125 km depth. My results are consistent with the presence of two mantle wedges, resulting from the rollback of the Ligurian-Tethys and Vardar-NeoTethys oceanic slabs followed by continental mantle delamination of the eastern and western distal margins of Adria. These two opposed slabs beneath the Apennines and Dinarides are modeled as two thermal sublithospheric anomalies of ~200 °C.

In the southern transect, the modeling shows the presence of two asthenospheric mantle wedges aligning with the Apenninic and Dinaric continental mantle slab rollback,

along with cold (-200 °C) sublithospheric anomalies beneath Adria's NE and SW margins. In the northern Adria region, the lithosphere undergoes synchronous thinning in the Tyrrhenian domain and thickening toward the forefront of the northern Apennines. This is associated with the northeastward rollback of the SW Adriatic slab, leading to subsequent delamination of the continental mantle. In the southern Adria region, the complex deep structure results from the variably oriented lithospheric slabs, and nearly 90-degree shift of the tectonic grain between the southern Apennines and the Calabrian Arc. At the SW Adria margin, beneath the northern Apennines, the thermal sublithospheric anomaly is attached to the shallower lithosphere, while a slab gap is modeled in the southern Apennines. One possibility is that the gap is due to a recent horizontal slab tear. Along the NE margin of Adria, the thermal anomaly penetrates to depths of about 200 km in the northern Dinarides and 280 km in the southern Dinarides, shallower than the SW Adria anomaly, which extends to at least 400 km depth.

Most elevation along the profiles is attributed to thermal isostasy. Elevation in the External Apennines, Dinarides, and Sava Suture Zone can be explained by regional isostasy with an elastic thickness of 20-30 km. The numerical modeling of dynamic topography permitted the identification of the dynamic deflection caused by deep mantle flow and buoyancy forces related to density contrasts. This modeling indicates that the denser attached slabs trigger downwelling mantle flow and negative dynamic topography. A longer slab beneath the northern Apennines leads to higher mantle flow and larger amplitudes of dynamic topography, -400 m. Residual topography in the northern Apennines can be explained by the cold thermal anomaly associated with the northern Apenninic slab. The rest of mantle anomalies produce a negligible dynamic topography, either because of being detached in the case of the southern Apennines, or because of their reduced size below the Dinarides.

### **RESUM**

La regió del Mediterrània central és una zona sísmica molt activa amb característiques tectòniques úniques, formant part del sistema orogènic Alpí-Mediterrani s'estén des del sud d'Iberia fins l'extrem occidental del mar Egeu. Aquest cinturó orogènic s'originà per la convergència de les plaques africana i eurasiàtica des del Cretaci superior. La rotació en sentit antihorari de la microplaca d'Adria, després de la col·lisió, va desencadenar l'obertura asimètrica de la Conca del Tirrè i l'aprimament tectònic al llarg de tots els seus marges: els Apenins, el cinturó de Calàbria, el cinturó Dinàric-Hel·lènic, els Alps i el cinturó dels Carpats.

Aplicant un model geofísic-petrològic (LitMod2D\_2.0), aquesta tesi investiga l'estructura termoquímica de la litosfera i del mantell sublitosfèric sota la microplaca d'Adria i els seus marges, i explora la geometria i la continuïtat en profunditat de les llosses litosfèriques (*slabs*) del marges d'Adria. Així, s'han modelat dos perfils, fins a 400 km de profunditat, que s'estenen des de la Conca del Tirrè fins a la regió dels Carpats-Balcans, en una direcció aproximadament NE-SO. El perfil del nord, d'uns 1000 km de llargada, travessa la Conca del Tirrè, els Apenins septentrionals, el mar Adriàtic, els Dinaris i la Conca del Panònic. El perfil del sud abasta uns 1250 km, travessant la Conca del Tirrè, els Apenins meridionals, el mar Adriàtic, els Dinaris meridionals i els Carpats-Balcans. A més, en aquesta tesi he desenvolupat un nou codi de modelització numèrica del flux del mantell, per avaluar la resposta topogràfica de les dues llosses que subdueixen amb vergència oposada al llarg d'aquests perfils i discuteixo les seves implicacions geodinàmiques en l'evolució de la regió.

Al perfil nord, els resultats mostren que la microplaca d'Adria té una estructura més complexa i una densitat mitjana lleugerament superior en comparació amb la microplaca de Tisza. Sota la Conca del Tirrè i els Apenins occidentals, la Moho es troba a una profunditat inferior a 25 km, mentre que als Apenins orientals arriba fins als 55 km de profunditat. El límit litosfera-astenosfera (LAB) sota les conques del Tirrè i del Panònic és pla i es troba a ~75 i 90 km, respectivament. Sota els Apenins externs i els Dinaris, el LAB s'aprofundeix fins als 150 km, mentre que es menys profund cap a la conca adriàtica arribant als 125 km de profunditat. Els meus resultats són consistents amb la presència de dues cunyes de mantell, resultat del retrocés de les llosses oceàniques del Ligúria-Tetis al SO i Vardar-NeoTetis al NE, seguit de la delaminació del mantell continental corresponent als marges distals oriental i occidental d'Adria. Aquestes dues llosses de vergència oposada, localitzades sota els Apenins i els Dinaris s'han modelat com dues anomalies tèrmiques sublitosfèriques de ~200°C.

Al perfil sud, els resultats mostren la presència de dues cunyes de mantell astenosfèric alineades amb el retrocés de les llosses del mantell continental apeninic i dinàric, juntament amb anomalies tèrmiques (-200 °C) sublitosfèriques sota els marges NE i SO d'Adria. Al nord d'Adria, s'observa aprimament de la litosfera en el domini del Tirrè i engruiximent cap al front dels Apenins septentrionals. Aquest fet està associat amb el retrocés cap al NE de la llosa del SO d'Adria, que provoca la subsequent delaminació del mantell continental. Al sud d'Adria, l'estructura que s'observa es conseqüència de que la orientació de les llosses litosfèriques es variable i d'un canvi, gairebé de 90 graus, de les direccions tectòniques entre les dels Apenins meridionals i les de l'arc calabrès. Al marge SO d'Adria, sota els Apenins septentrionals, l'anomalia tèrmica sublitosfèrica està connectada a la litosfera més superficial, mentre que en els Apenins meridionals l'anomalia tèrmica n'està desenganxada. Una possibilitat és que aquest desenganxament sigui degut a una ruptura horitzontal recent de la llosa (tearing). Al llarg del marge NE d'Adria, l'anomalia tèrmica penetra fins a profunditats d'uns 200 km als Dinaris septentrionals i fins a 280 km als Dinaris meridionals. En ambdós casos, la seva extensió en profunditat es menor que la de les anomalies que s'observen en el marge occidental d'Adria, que s'estenen fins a almenys 400 km de profunditat.

La major part de l'elevació al llarg dels perfils s'explica per isostàsia tèrmica. La elevació actual dels Apenins externs, Dinaris i la zona de sutura de Sava es pot explicar per isostàsia regional amb un gruix elàstic de la litosfera de 20-30 km. La modelització numèrica de la topografia dinàmica m'ha permès identificar la deflexió dinàmica causada pel flux del mantell profund i les forces de flotabilitat relacionades amb els contrastos de densitat. Aquesta modelització indica que les llosses litosfèriques (slabs) quan estan enganxades a la litosfera, al ser més denses, desencadenen fluxos de mantell descendents i una topografia dinàmica negativa. La llosa sota els Apenins septentrionals, al aprofundir-se més, produeix un flux del mantell més gran, i, per tant, resulta en una major amplitud de la topografia dinàmica, -400 m. La topografia residual en els Apenins septentrionals es pot explicar per l'anomalia tèrmica freda associada amb la llosa sota aquesta part del Apenins. La resta d'anomalies del mantell produeixen una topografia dinàmica negligible. Això és perquè o bé estan desenganxades en el cas dels Apenins meridionals, o bé perquè la seva mida reduïda sota els Dinaris.

### RESUMEN

La región del Mediterráneo central es una zona sísmica muy activa con características tectónicas únicas, formando parte del sistema orogénico Alpino-Mediterráneo, se extiende desde el sur de Iberia hasta el extremo occidental del mar Egeo. Este cinturón orogénico se originó por la convergencia de las placas africana y euroasiática desde el Cretácico superior. La rotación en sentido antihorario de la microplaca de Adria, después de la colisión, desencadenó la apertura asimétrica de la Cuenca del Tirreno y el adelgazamiento tectónico a lo largo de todos sus márgenes: los Apeninos, el cinturón de Calabria, el cinturón Dinárico-Helénico, los Alpes y el cinturón de los Cárpatos.

Utilizando un modelo geofísico-petrológico (LitMod2D\_2.0), esta tesis investiga la estructura termoquímica de la litosfera y del manto sublitosférico bajo la microplaca de Adria y sus márgenes, explorando la geometría y la continuidad en profundidad de las losas litosféricas (*slabs*) de los márgenes de Adria. Así, se han modelado dos perfiles, hasta 400 km de profundidad, que se extienden desde la Cuenca del Tirreno hasta la región de los Cárpatos-Balcanes, en una dirección aproximadamente NE-SO. El perfil del norte, de unos 1000 km de longitud, atraviesa la Cuenca del Tirreno, los Apeninos septentrionales, el mar Adriático, los Dinárides y la Cuenca Panónica. El perfil del sur abarca unos 1250 km, atravesando la Cuenca del Tirreno, los Apeninos meridionales, el mar Adriático, los Dinárides meridionales y los Cárpatos-Balcanes. Además, en esta tesis he desarrollado un nuevo código de modelización numérica del flujo del manto para evaluar la respuesta topográfica de las dos subducciones de vergencia opuesta a lo largo de estos perfiles y discuto sus implicaciones geodinámicas en la evolución de la región.

En el perfil norte, los resultados muestran que la microplaca de Adria tiene una estructura más compleja y una densidad media ligeramente superior en comparación con la microplaca de Tisza. Bajo la Cuenca del Tirreno y los Apeninos occidentales, la Moho se encuentra a una profundidad inferior a 25 km, mientras que en los Apeninos orientales llega hasta los 55 km. El límite litosfera-astenosfera (LAB) bajo las cuencas del Tirreno y Panónica es plano y se encuentra a ~75 y 90 km, respectivamente. Bajo los Apeninos externos y los Dinárides, el LAB (Límite Litosfera-Astenosfera) alcanza los 150 km, mientras que es menos profundo hacia la cuenca adriática llegando a los 125 km de profundidad. Mis resultados son consistentes con la presencia de dos cuñas de manto astenosférico, resultado del retroceso de las losas oceánicas del Ligúrico-Tetis al SO y Vardar-NeoTetis al NE, seguido de la delaminación del manto continental en los márgenes distales oriental y occidental de Adria. Estas dos losas de vergencia opuesta, localizadas

bajo los Apeninos y los Dinárides, se han modelado como dos anomalías térmicas sublitosféricas de −200°C.

En el perfil sur, los resultados muestran la presencia de dos cuñas de manto astenosférico alineadas con el retroceso de las losas del manto continental apenínico y dinárico, junto con anomalías térmicas (-200 °C) sublitosféricas bajo los márgenes NE y SO de Adria. Al norte de Adria, se observa adelgazamiento de la litosfera en el dominio del Tirreno y engrosamiento hacia el frente de los Apeninos septentrionales. Este hecho está asociado con el retroceso hacia el NE de la losa del SO de Adria, que provoca la subsecuente delaminación del manto continental. Al sur de Adria, la estructura que se observa es consecuencia de que la orientación de las losas litosféricas es variable y de un cambio, casi de 90 grados, de las direcciones tectónicas entre las de los Apeninos meridionales y las del arco calabrés. En el margen SO de Adria, bajo los Apeninos septentrionales, la anomalía térmica sublitosférica está conectada a la litosfera más superficial, mientras que en los Apeninos meridionales la anomalía térmica está desconectada. Este hecho puede estar asociada a una ruptura horizontal reciente de la losa (tearing). A lo largo del margen NE de Adria, la anomalía térmica penetra hasta profundidades de unos 200 km en los Dinárides septentrionales y hasta 280 km en los Dinárides meridionales. En ambos casos alcanzan una profundidad inferior a la de las anomalías que se observan en el margen occidental de Adria, que se extienden hasta al menos 400 km de profundidad.

La mayor parte de la elevación a lo largo de los perfiles se explica por isostasia térmica. La elevación actual de los Apeninos externos, Dinárides y la zona de sutura de Sava se puede explicar por isostasia regional con un grosor elástico de la litosfera de 20-30 km. Los modelización numérica de la topografía dinámica muestra que cuando las losas están conectadas a la litosfera, al ser más densas, desencadenan flujos de manto descendentes y una topografía dinámica negativa. La losa bajo los Apeninos septentrionales, al alcanzar una mayor profundidad, produce un flujo del manto mayor, y, por lo tanto, resulta en una mayor amplitud de la topografía dinámica, -400 m. La topografía residual en los Apeninos del Norte se puede explicar por la anomalía térmica fría asociada a la losa que subduce en esta zona. El resto de las anomalías del manto producen una topografía dinámica insignificante, ya sea por estar desenganchadas en el caso de los Apeninos del Sur, o por su tamaño reducido bajo los Alpes Dináricos.

### CHAPTER 1 General Introduction

### **Chapter 1. General Introduction**

### 1.1. Motivation and overview

The Central Mediterranean region is a highly active seismic zone, known for its unique tectonic characteristics. It forms part of the Alpine-Mediterranean belt that extends from southern Iberia to the western Aegean Sea (Figure 1.1). The belt originated from the convergence of the African and Eurasian plates since the Late Cretaceous (e.g., Dewey et al., 1989; Handy et al., 2010). It encompasses pre-orogenic rifting and oceanization, activation of several subduction zones and the complete consumption of the Alpine-Ligurian Tethys and Neotethyan oceanic lithospheres, within the continental collision between the Corsica-Sardinia block and Adria microplate during the Late Oligocene-Early Miocene times. Post-collision counterclockwise rotation of the Adria microplate triggered the opening of the asymmetric Tyrrhenian Basin and the synchronous tectonic tightening along all its margins: the Apennines, the Calabria belt, the Dinarides-Hellenic belt, the Alps and the Carpathian belt (e.g., Jolivet and Faccenna, 2000; Wortel and Spakman, 2000; Carminati et al., 2012, 2020; Handy et al., 2015; van Hinsbergen et al., 2019, 2020; Schmid et al., 2020).

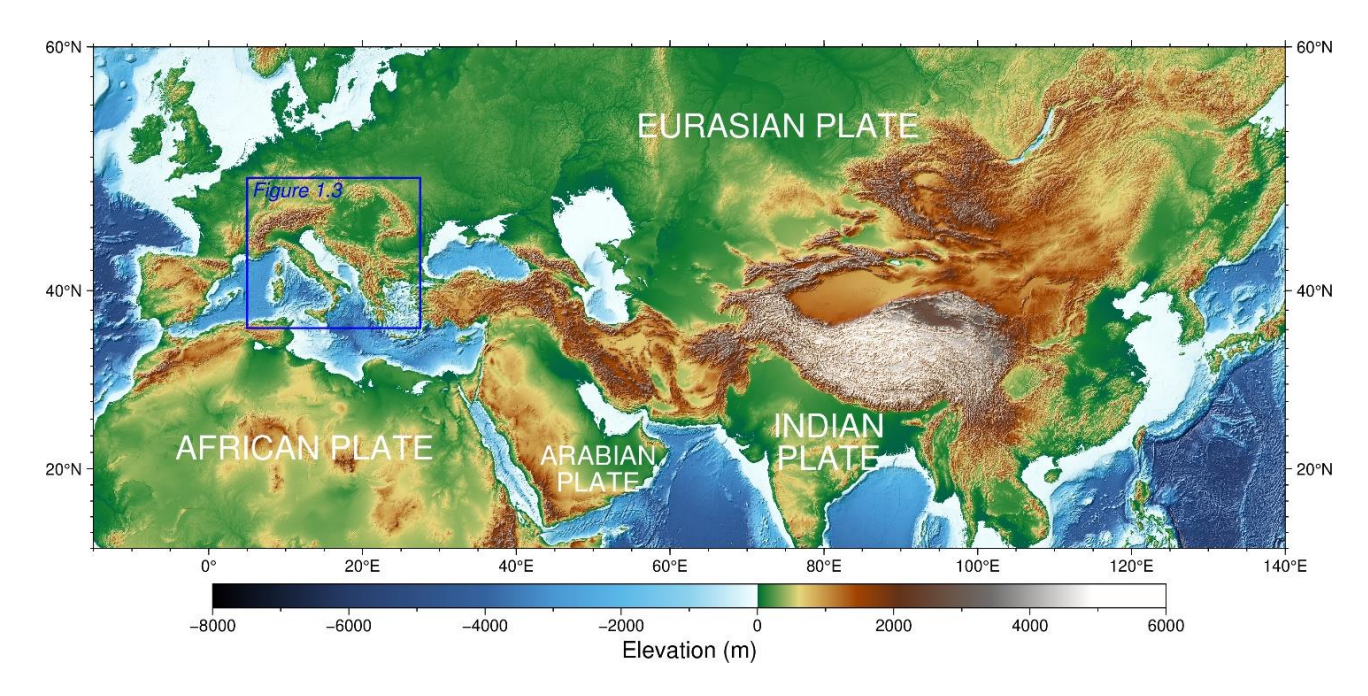


**Figure 1.1** Topography map of the Alpine-Himalayan collision zone. The area inside the blue box locates the study region (Figure 1.3).

During the opening and subsequent closure of the Alpine-Ligurian Tethys and Vardar oceans, small continental blocks, such as the Alcapa, Tisza, and Dacia microplates, broke away from the Eurasian Plate. These microplates subsequently collided with Adria with the extrusion of blocks and slab-retreat processes resulting in the formation of the present-day belts and foredeep basins. The Adria microplate is believed to have separated from the African Plate during the early Mesozoic, having drifted toward the NNE with a slight counter clockwise rotation (e.g., Le Breton et al., 2017; Handy et al., 2021; Jolivet, 2023). Consequently, Adria is surrounded by extensively deformed convergent margins, characterized by three plate subductions with different plate polarities. An interesting aspect of these subducted and delaminated slabs is their segmentation and variable lengths at depth, as evidenced by the tomography studies listed below.

The N-S convergence between the African and Eurasian plates since the Late Cretaceous is recognized as the primary causal mechanism for the squeezing of intervening microplates, bounded by narrow branches of the Neo-Tethys Ocean (e.g., Dewey et al., 1989). In particular, it drove to the development of subduction and collision orogens in the Central-Western Mediterranean region, which is a part of the active Alpine-Mediterranean mobile belt. The Adria microplate plays a key role in this geodynamic puzzle since Jurassic times, when the Vardar ophiolitic obduction started, followed by continental collisions with the Tisza microplate and Eurasian plate (Schmid et al., 2020). Subsequently, the NW-SE trending Dinarides orogenic belt developed along the NE margin of Adria whereas the NW-SE trending Apennines fold-thrust belt evolved in its SW margin. The Adria-Eurasia convergence also produced the almost 1000 km long ENE-WSW trending Alps orogenic belt (Figure 1.1) (e.g., Dewey et al., 1989; Stampfli and Borel, 2002; Handy et al., 2010).

Therefore, the Central Mediterranean region is a challenging area characterized by structural heterogeneity and tectonic complexity. For a comprehensive review of the current geology and geodynamics of the area the reader is referred to the works of Faccenna et al. (2001), Carminati et al. (2012), Chiarabba et al. (2014), Handy et al. (2015), van Hinsbergen et al. (2019, 2020), Schmid et al. (2020), Balling et al. (2021), Carminati and Chiarabba (2023), and Jolivet (2023). All these deep geodynamic processes have a direct effect on the topography of the orogenic belts, producing the so-called dynamic topography (e.g., Faccenna et al., 2014; Kumar et al., 2021).

Understanding the geodynamic processes within this complex tectonic region requires reliable knowledge of the present-day lithospheric and sublithospheric mantle structure, particularly the evolution of the subducting lithosphere (Giacomuzzi et al., 2022; Magrini et al., 2022), which is described after decades of careful studies of its geology and

geophysics. These studies reconstructed its crustal orogenic fold-belt and upper mantle structure in three dimensions, interpreted as the result of subducted lithospheric slabs displaying abrupt changes in subduction polarity across transfer fault zones (e.g., Rosenbaum et al., 2008; Vignaroli et al., 2008, 2009). However, despite the wealth of data and research published about the study region (e.g., Carminati and Doglioni, 2012; Artemieva and Thybo, 2013; Kapuralić et al., 2019; Kästle et al., 2020), some issues regarding its current lithospheric structure and the topographic implications of lithospheric and sublithospheric anomalies are still under debate. In particular, there is significant uncertainty about the shapes and sizes of the subducting slabs, and whether they are attached or detached from the lithosphere (Figure 1.2).

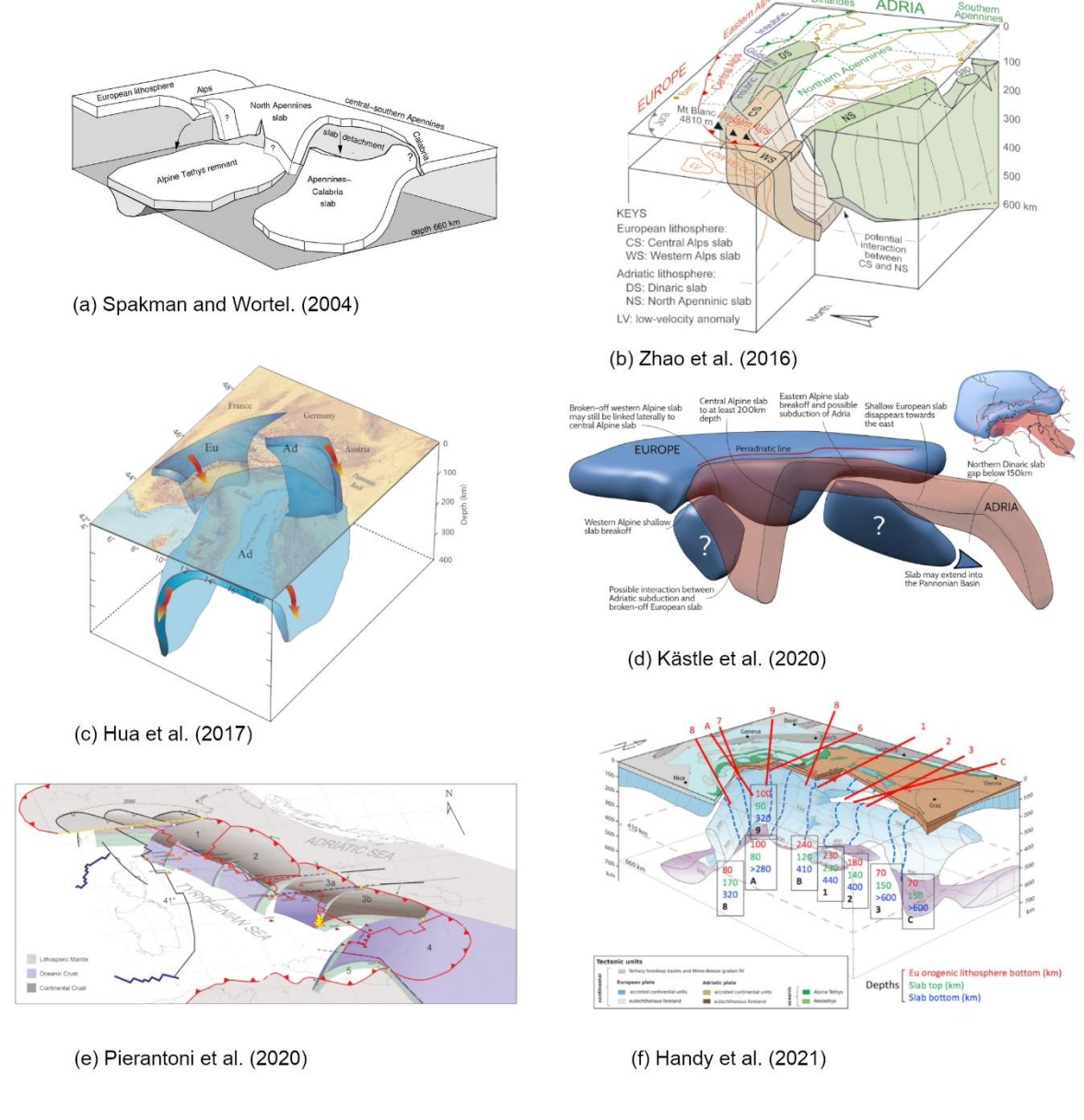


**Figure 1.2** Collection of images of the Adriatic slab beneath the Apennines according to different interpretations: a) Spakman and Wortel (2004), b) Zhao et al. (2016), c) Hua et al. (2017), d) Kästle et al. (2020), e) Pierantoni et al. (2020), f) Handy et al. (2021).

Global or regional tomography studies, for example, Lucente et al. (1999); Piromallo and Morelli (2003); Spakman and Wortel (2004); Giacomuzzi et al. (2011, 2022); Blom et al. (2020); El-Sharkawy et al. (2020); Belinić et al. (2021) and Rappisi et al. (2022), have not provided conclusive evidence on the details of the mantle structure in the study area. Piromallo and Morelli (2003) show a pronounced, wide and well-resolved fast velocity anomaly below the southern Apennines while Spakman and Wortel (2004) propose that a short (300-400 km) slab is hanging below them. In the Central Apennines, a slab window is imaged ranging from 140 km (Giacomuzzi et al., 2011) to 250 km (Spakman and Wortel, 2004) depth. In the southern Apennines, the deep fast Vp velocity anomalies appear continuously connected to the Calabrian slab (e.g., Rappisi et al., 2022).

Three-dimensional anisotropic teleseismic P-wave tomography and S-wave models suggest a positive velocity anomaly under the whole Dinarides (Koulakov et al., 2015; Šumanovac and Dudjak, 2016; Belinić et al., 2021). Positive Vp and Vs regional anomalies beneath the Apennines and Dinarides, located at different depths, are interpreted to be the westward and eastward descending margins of the Adria microplate. Király et al. (2018) describe the two dipping regional anomalies as the bidirectional subduction of Adria. The large amount of deep geophysical data supports the interpretation that the sub-crustal structure beneath Adria is shaped by an intricate array of segmented slabs (e.g., 3-D mapping by Rappisi et al., 2022). These slabs are remnants of the thinned continental margins of Adria that formed during the Pangea break-up, and were subsequently subducted by both the eastwards drift of Adria during the Triassic-Early Cretaceous and by the convergence between Africa and Eurasia since the Late Cretaceous (e.g., Pierantoni et al., 2020).

Considering the longitudinal variations in plate-scale geometries previously identified in various studies of the Apennines and Dinarides slabs, my primary goal is to investigate the geometry and depth continuity of the opposing Apennines and Dinarides slabs. To achieve that, I have derived the present-day crust and upper mantle structure along two transects (Figure 1.3). The northern transect, approximately 1000 km long, crosses the Tyrrhenian Sea, the northern Apennines, the Adriatic Sea, the Dinarides and the Pannonian Basin in a SW-NE direction. Similarly, the southern transect spans approximately 1250 km, crossing the southern Tyrrhenian Basin, the southern Apennines, the Adriatic Sea, the southern Dinarides, and the Carpathians-Balkanides in a roughly SW-NE direction. Additionally, based on the results of lithospheric modeling, I will briefly explore the implications of thermal anomalies identified in both the lithospheric and sublithospheric mantle on present-day elevation, particularly in the context of dynamic topography.

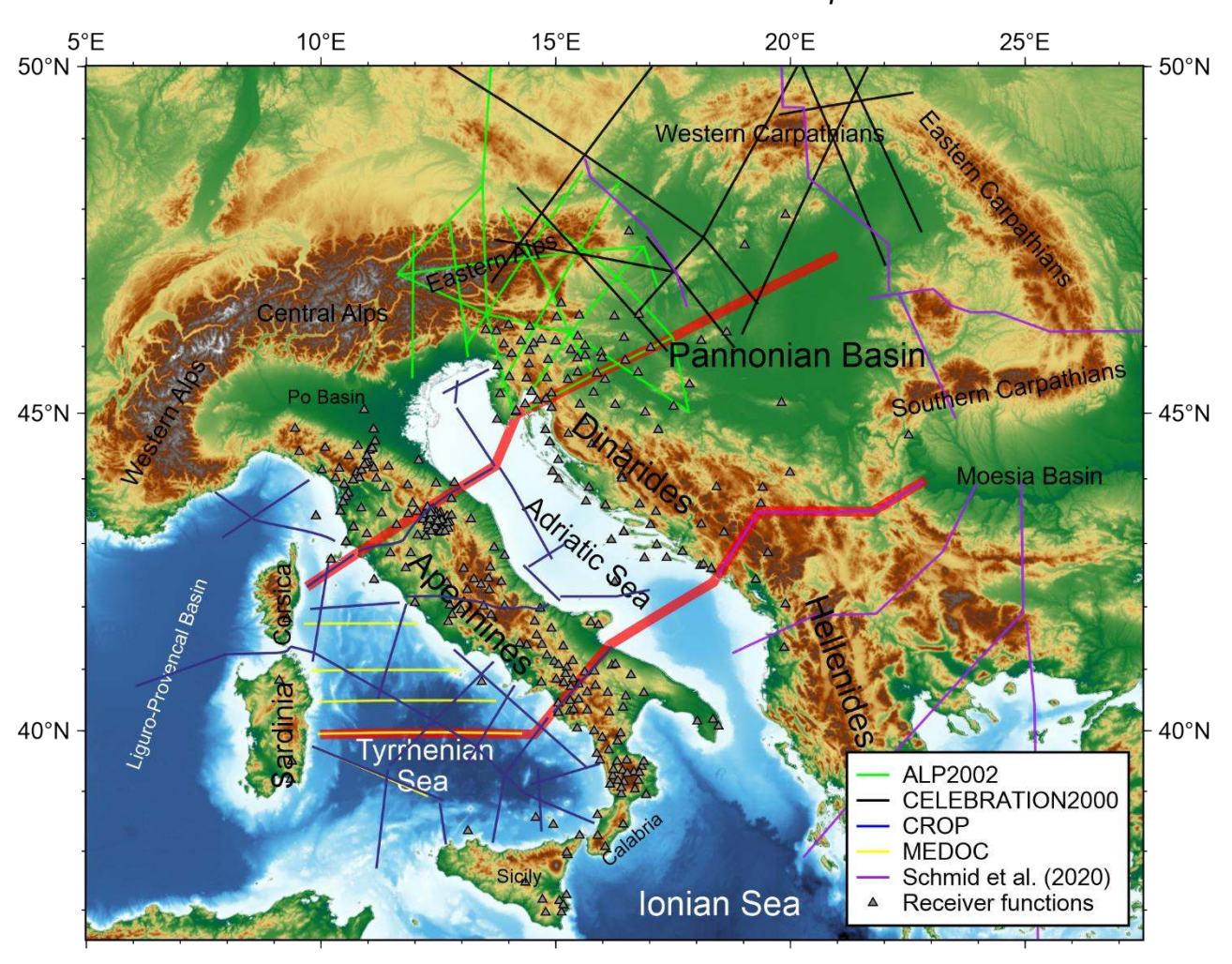


**Figure 1.3** Elevation map of the Central Mediterranean featuring the main orogenic belts and foreland basins. The red lines show the locations of the northern and southern transects (Chapter 3, Zhang et al., 2022; and Chapter 4, Zhang et al., 2024, respectively). The seismic profiles and receiver functions (RF) data used to constrain the crustal structure are also shown, according to the color legend displayed in the lower right inset.

To determine the lithospheric structure along these two transects I applied an integrated geophysical-petrological modeling tool (LitMod2D\_2.0), which combines surface heat flow (SHF), Bouguer anomaly, geoid height, elevation and petrological data to produce the thermal, density, and seismic velocity structure of the crust and upper mantle as described in Kumar et al. (2020). LitMod2D\_2.0 allows for obtaining the present-day crust and upper mantle structure, down to 400 km depth, by integrating available geophysical and petrological data within a self-consistent thermodynamic framework. A similar approach was used to study the deep structure of the Gibraltar Arc region (Jiménez-Munt et al., 2019) and along the Algerian and Alboran basins of the Western Mediterranean (Kumar et al., 2021). Both studies demonstrated that the pull force of hanging lithospheric slabs is markedly different if the slab is still attached to the continental lithosphere or is detached after break-off processes. They also permitted to determine the

up-down direction, amount and extent of the dynamic topography linked to the sublithospheric forces as well as its impact at the surface.

The results along the transects are the 2D temperature, bulk density, seismic velocity (Vp and Vs), and compositional structure for the entire lithosphere, along with the distribution of temperature anomalies for the sublithospheric mantle. The crustal and lithospheric structures obtained in this study are compared with previous interpretations and discussed in terms of the geodynamic evolution of studied tectonic domains within the complex and long-term evolving Alpine-Mediterranean mobile belt. Lastly, the contribution of deep geodynamic processes in the build-up of present orogenic topographic relief is discussed.

Hence, the geophysical-geochemical integrated model presented here offers valuable insights into the lithospheric and thermochemical structure of the upper mantle beneath the Apennines and Dinarides fold-thrust belts. In this thesis I integrate the results from both the northern and southern Adria transects with independent geological and geophysical data to investigate the role of the Adria microplate in the geodynamic evolution of the Central Mediterranean region.

It is important to note that a comprehensive study of the Adria microplate requires interdisciplinary research at multiple scales. Therefore, this PhD thesis has been carried out in close collaboration with the research conducted by Estefanía Bravo-Gutiérrez, whose thesis examines the same transects across the Adria microplate, addressing its crustal structure and temporal reconstruction. It is important to highlight that our research is interdependent, with the results of both studies complementing each other.

### 1.2. Tectonic setting

The Central Alpine Mediterranean orogenic system is the result of the interplay between the Eurasian plate and the Adria, Tisza and Dacia microplates (originally separated by the Vardar oceanic domain, a northern branch of the Neo-Tethys) in the framework of the Africa-Eurasia convergence (Figure 1.4). At upper crustal levels, the main tectonic domains that evolved on the Adria microplate are, from west to east, the Apennines and the Dinarides orogens with their common foreland basin along the entire Adriatic Sea. The Apennines mainly developed during the W- to SW-dipping subduction of the Alpine Tethys oceanic domain (that separated Adria microplate from Eurasian plate) and the following subduction of the Adria thinned margin (Doglioni, 1991; Faccenna et al., 2001; Molli, 2008), that drove to the deformation of cover rocks of the SW margin of Adria. The eastward retreat of the subducting-plate hinge generated the ENE-directed

Apennines orogenic system and the development of a complex back-arc basin system (e.g., Malinverno and Ryan, 1986; Patacca et al., 1990; Royden, 1993; Doglioni et al., 1997; Lacombe and Jolivet, 2005; Le Breton et al., 2017; Romagny et al., 2020).

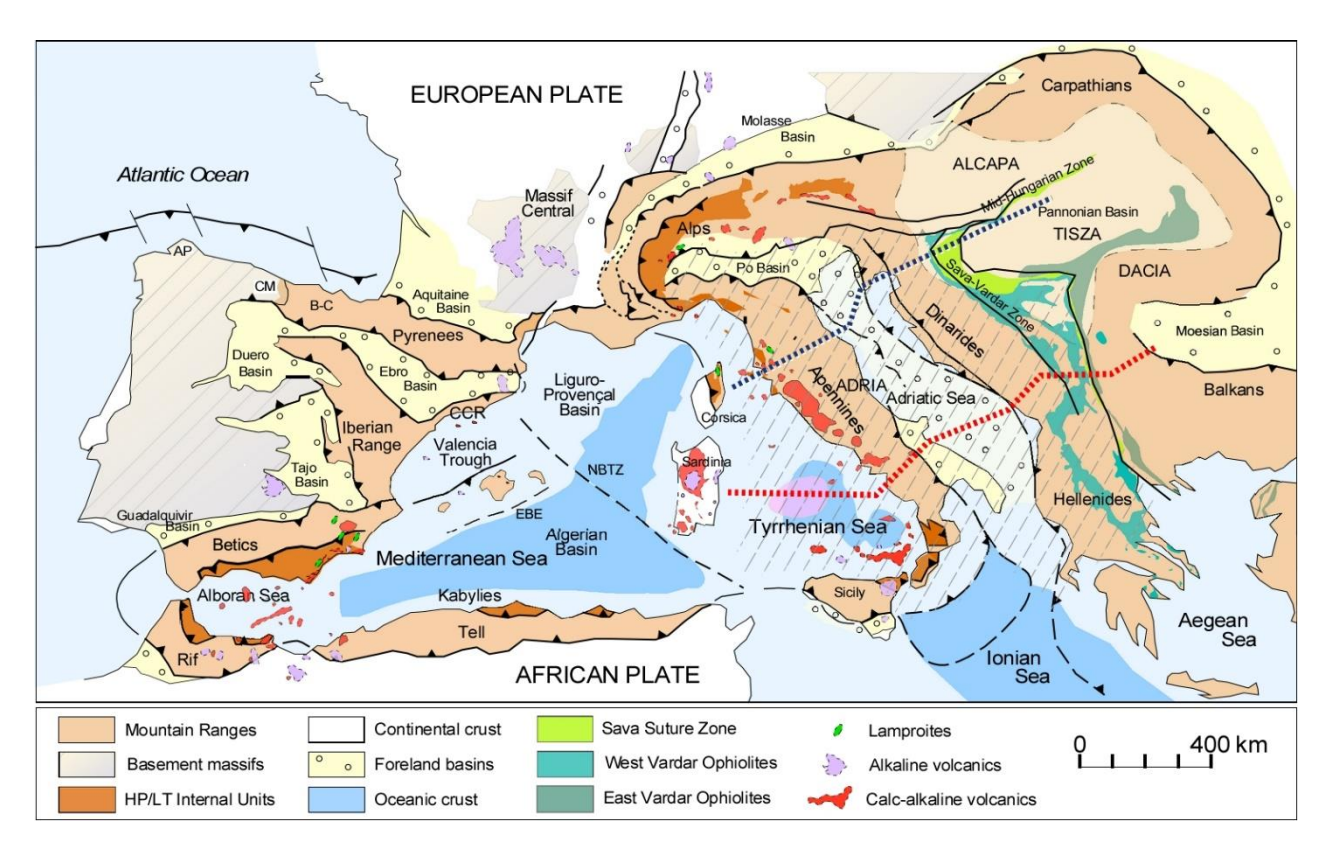


**Figure 1.4** Simplified tectonic map of the Central Mediterranean region with the main orogenic belts and foreland basins (based on Vergés and Sàbat, 1999; Melchiorre et al., 2017; Schmid et al., 2020). The blue dashed line shows the location of the northern transect. The red dashed line shows the location of the southern transect. The gray dashed area shows the location of Adria microplate.

The Corsica-Sardinia lithosphere was drifted from the southern Europe continental margin (Doglioni et al., 1997; Romagny et al., 2020), and it is located between the Liguro-Provencal and Tyrrhenian back-arc basins. The Dinarides lie along the deformed NE margin of Adria and have a longer and more complex history that includes subduction of the Vardar Ocean basin. This long-term subduction produced a first late Jurassic obduction of oceanic lithosphere and a later continental collision between Adria and Tisza microplates (Channell et al., 1996; Schmid et al., 2020), presently forming the thinned crust flooring the northern region of the Pannonian Basin along the easternmost segment of the transect. The Tisza crustal domain is welded to the Eurasian plate (Figure 1.4).

It is widely acknowledged that the Adria microplate has continuously influenced the evolution of the Alpine-Mediterranean region since its formation (Handy et al., 2010, 2015; Faccenna et al., 2014; Le Breton et al., 2017; Király et al., 2018; Lo Bue et al., 2021).

Post-collision counterclockwise rotation of the Adria microplate triggered the opening of the asymmetric Tyrrhenian Basin and the synchronous tightening along all its margins, in addition to the formation of the Apennines, the Calabria belt, the Dinarides-Hellenic belt, the Alps and the Carpathian belt (e.g., Carminati et al., 2012, 2020; Handy et al., 2015; van Hinsbergen et al., 2019, 2020; Schmid et al., 2020). During the opening and subsequent closure of the Alpine-Ligurian Tethys and Vardar oceans, small continental blocks, such as the Alcapa, Tisza, and Dacia microplates (see Figure 1.4), broke away from the Eurasian Plate. These microplates subsequently collided with Adria with the extrusion of blocks and slab-retreat processes resulting in the formation of the present-day belts and foredeep basins. The Adria microplate is believed to have separated from the African Plate during the early Mesozoic, having drifted toward the NNE with a slight counter clockwise rotation (e.g., Le Breton et al., 2017; Handy et al., 2021; Jolivet, 2023). Consequently, Adria is surrounded by extensively deformed convergent margins, characterized by three plate subductions with different plate polarities.

As illustrated in Figure 1.5, most active faults and seismic activity are widespread across extensive areas and elongated zones, primarily along the orogenic belts, such as the Alps-Carpathians belt, Apennines-Calabria belt, and Dinarides-Hellenic belt. The zones are typically located along the boundaries of plates and microplates, including Adria, Eurasia, Tisza, and Dacia. The active tectonics in the area is heterogeneous (Billi et al., 2007; Serpelloni et al., 2010; Wrigley et al., 2015). The boundary of the Adria microplate is surrounded by active compression, except for the southern region. The south-Tyrrhenian is mainly under compression, which terminates in Sicily, as the African plate squeezes northeastward compared to the Eurasian plate (Billi et al., 2007; Serpelloni et al., 2010). The seismicity is characterized by frequent occurrences of low-to-moderate magnitude events, alongside occasional occurrences of large earthquakes (>7) (e.g., Vannucci et al., 2004; Guidoboni et al., 2007; Serpelloni et al., 2007; Godey et al., 2013). The deepest seismic zone is situated beneath the Calabrian Arc, where a Wadati-Benioff zone with a dip angle of approximately 70° extends from depths of 50 km to 450 km (Giardini and Velonà, 1991; Selvaggi and Chiarabba, 1995).

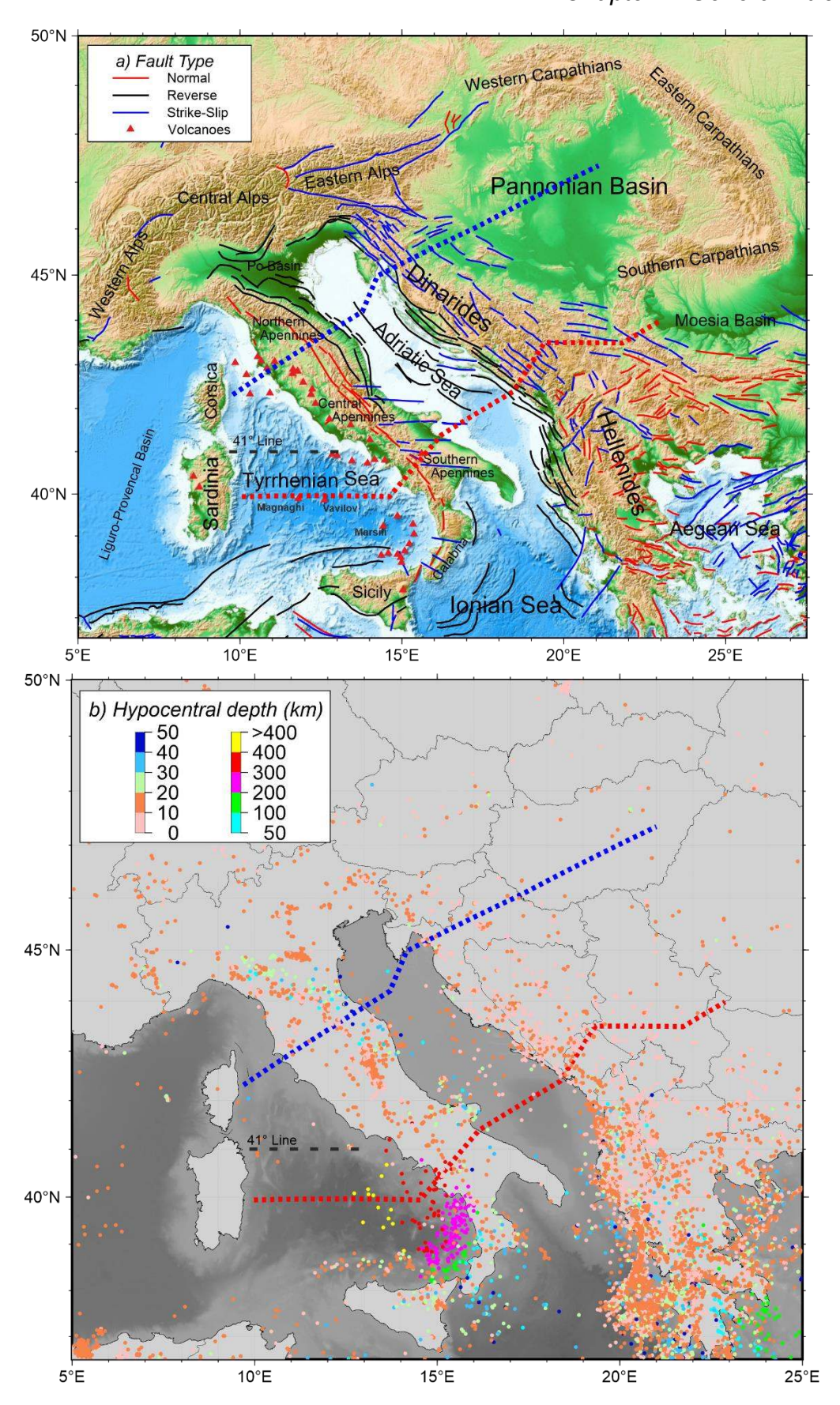


**Figure 1.5** (a) Distribution of the active faults in the study region. The faults are colored by their kinematics; red faults are normal, black faults are reverse and blue faults are strike-slip. The data are taken from Global Active Faults Database (Styron and Pagani, 2020). Red trigangles show the location of main volcanoes

(Pierantoni et al., 2020). The dashed line represents the 41° Parallel Line. (b) Distribution of the earthquake epicenters, M>3.0, in the same region between 2008 and 2021. The data are taken from the International Seismological Centre (ISC). Colored circles mark the hypocentral depths (color scale is shown at the bottom left inset). Blue and red dashed lines indicate the locations of the study transects.

### 1.2.1. Tyrrhenian Basin

The Tyrrhenian basin, a triangular shaped basin situated in the central Mediterranean Sea, is surrounded by the Apennines orogen to the east, the Calabrian arc and Sicily to the south, and the Corsica-Sardinia block to the west (Figure 1.4). The basin is regarded as the youngest back-arc basin of the Mediterranean, having developed from Middle Miocene to the present (e.g., Malinverno and Ryan, 1986; Zitellini et al., 2019; Pierantoni et al., 2020; Loreto et al., 2021). The opening of the Tyrrhenian Basin occurred after the cessation of seafloor spreading in the Liguro-Provençal basin (~30-16 Ma, Burrus, 1984; Gattacceca et al., 2007; Gailler et al., 2009; Bache et al., 2010). The formation of the basin was mainly driven by slab rollback of the east-southeastward migration of the Apennines-Calabrian subduction system (e.g., Malinverno and Ryan, 1986; Faccenna et al., 2001; Turco et al., 2012). The initiation of the Tyrrhenian extension may have occurred during the Tortonian (~11-9 Ma, Trincardi and Zitellini, 1987; Mascle and Rehault, 1990; Sartori, 1990; Sartori et al., 2001) or Langhian/ Serravallian time (~16-12 Ma, Loreto et al., 2021).

As already pointed out by several authors (e.g., Prada et al., 2014, 2016; Faccenna and Becker, 2020), the Tyrrhenian Basin exhibits a very distinct organization north and south of 41°N latitude. In the northern Tyrrhenian Basin, the bathymetry and the crustal structure corresponds to that of a thin continental crust, with widespread volcanism, extending to the Tuscany Magmatic Province (e.g., Pandeli et al., 2013; Sani et al., 2016). In the southern region, the deep bathymetry, the amount of the extension and the crustal structure indicate the presence of an oceanic type crust, particularly in the deep Vavilov and Marsili basins (Prada et al., 2014, 2015). The opening and oceanization of the Vavilov Basin commenced during Upper Messinian/Lower Pliocene period and ceased in the upper Pliocene, subsequently, extension shifted southeastward, leading to the opening of the Marsili Basin during the lower Pleistocene (2 Ma) (e.g., Kastens et al., 1988; Sartori et al., 2004; Loreto et al., 2021). As in the northern region, volcanism is widespread extending to the onshore Campanian Plain. Magmatism in the central Tyrrhenian Basin is likely triggered by both extension-induced melting (back-arc basin magmatism) and continental delamination-related processes. Moreover, the offshore and onshore continental platform is characterized by volcanic arc-type magmatism. Peccerillo (2017) concludes that magmatism from the Tuscany Province of the northern Apennines to the Aeolian Arc northwest of Calabria exhibits geochemical markers of source regions that have undergone metasomatism related to subduction processes (involving fluids and subducted sediments).

### 1.2.2. Apennines fold-thrust belt

The NE directed Apennines fold-thrust belt mainly developed during the W- to SW-dipping subduction of the Alpine Tethys oceanic domain (that separated the Adria microplate from the Eurasian plate) and the following subduction of the Adria thinned margin (Doglioni, 1991; Faccenna et al., 2001; Molli, 2008). Convergence between the African and European plates commenced in the Late Cretaceous, resulting in the closure of the Tethys Ocean and the subsequent formation of the Apennines during the Late Oligocene-Pleistocene period, as evidenced by the ages of siliciclastic deposits (Boccaletti et al., 1990). Throughout the Middle/Late Miocene to Late Pliocene, the Apennines experienced simultaneous occurrences of normal and thrust faults along the western and eastern margins of the belt, respectively (Molli, 2008). Extension persisted into the Pleistocene-Holocene epochs and continues to be active today, exerting control over seismic activity along the mountain belt.

The Apennines are characterized by two tectonic domains; the Internal (western) Apennines including the Ligurian-Tuscan-Tyrrhenian regions toward the WSW and the External (eastern) Apennines comprising the Apennines fold-thrust belt and the Adriatic foreland basin toward the ENE (e.g., Barchi et al., 1998, 2003; Scrocca, 2006; Molli, 2008; Cosentino et al., 2010). The belt and its undeformed foreland show a complex ENEdirected system of thrust imbricate structures, involving mainly thin-skinned and possibly thick-skinned structural styles (e.g., Mostardini and Merlini, 1986; Bally, 1987; Patacca et al., 1990; Keller and Coward, 1996; Barchi et al., 1998; Mazzoli et al., 2005; Massoli et al., 2006; Molli et al., 2010). Compression migrated from the Tyrrhenian area toward the Adriatic foreland from Oligocene to Pliocene-Pleistocene (Doglioni et al., 1996; Keller and Coward, 1996; Noguera and Rea, 2000; Patacca and Scandone, 2001, 2007), whereas coeval extension collapsed the Internal Apennines (Patacca et al., 1990; Cavinato and De Celles, 1999). From North to South, the belt can be subdivided into two arcuate segments: The northern and southern segments, connected by the intermediate pivotal segment of the Central Apennines (e.g., Cavazza et al., 2004). The northern Apennines consist of a regular, in-sequence system of N- and NE-verging thrust imbricates. In contrast, the ENEand E-verging southern Apennines are characterized by duplex geometries and out-ofsequence thrusting, with N-verging thrusts along the pivotal Central Apennines (Cavazza

et al., 2004). The analysis of syn-orogenic and thrust top deposits allowed the recognition of  $\sim$ 100 and  $\sim$ 200 km progressive eastward migration of the thrust fronts in the last 25 My in the northern and central Apennines, respectively (Boccaletti et al., 1990; Vezzani et al., 2010), with a shortening of the frontal thrust system of 45 km in the last 17 My at shortening rates of 2.9 mm/yr (Basili and Barba, 2007).

### 1.2.3. Dinarides fold-thrust belt

The WSW-directed Dinarides orogenic system is built by multiple orogenic processes related to the progressive closure of the Vardar Ocean since Late Jurassic time (e.g., Channell et al., 1996; Chiari et al., 2011; Gallhofer et al., 2017; Maffione and van Hinsbergen, 2018). The first of these large-scale plate tectonic processes was the obduction of the Western Vardar Ophiolite Unit on top of the NE Dinarides with a total displacement of ~180 km. The end of the Vardar oceanic subduction led to the continental collision between Adria (lower plate) and Eurasian (upper plate) along the Sava Suture Zone (Pamić et al., 1998; Schmid et al., 2008, 2020; Ustaszewski et al., 2010; Handy et al., 2015).

The Dinarides fold-thrust belt is divided into the Internal Dinarides in the east, directly in contact with the Sava Suture Zone, and the External Dinarides in the west (Tari, 2002; Schmid et al., 2004; Tomljenović et al., 2008; Placer et al., 2010). The Internal Dinarides consist of composite thrust sheets (Schmid et al., 2008, 2020; Balling et al., 2021), including the obducted Western Vardar Ophiolites (Robertson et al., 2009) and Mesozoic cover rocks (platform carbonates and foredeep deposits) belonging to the NE distal margin of Adria (Tari, 2002; Tomljenović et al., 2008). The External Dinarides are characterized by thrust imbricates of sedimentary cover units, locally involving Paleozoic basement, belonging to the NE margin of the Adria microplate shortened from the Eocene to the Present, although shortening was interrupted by a period of extension in Miocene time (e.g., Tari, 2002; Schmid et al., 2008; Van Unen et al., 2019). Shortening propagated in-sequence from the Sava Suture Zone in the east to the Adriatic foreland in the west (Ustaszewski et al., 2010). Total shortening increases from 50 to 130 km toward the south of Dinarides (Schmid et al., 2008, 2020; Balling et al., 2021), although these estimates can vary significantly owing to different paleogeographic reconstructions (Pamić et al., 2002; Korbar, 2009). The internal parts of the Dinarides are characterized by abundant Paleogene-middle Miocene calc-alkaline to ultrapotassic magmatism, (e.g., Kovács et al., 2007, and references therein).

### 1.2.4. Pannonian Basin

The Pannonian Basin, to the NE of the Sava Suture Zone, is surrounded by the Alpine, Carpathians and Dinarides orogenic belts and is a Miocene to Present extensional backarc basin underlain by thinned continental lithosphere (e.g., Horváth, 1995; Horváth et al., 2006; Koroknai et al., 2020). The basement of the Pannonian Basin is made up by two distinct megatectonic units (Figure 1.4): The Alpine-Carpathian-Pannonian (Alcapa) and the Tisza, separated by the WNW-ENE Mid-Hungarian Shear Zone (Csontos and Nagymarosy, 1998; Schmid et al., 2008; Hetényi et al., 2015). The indentation of the Adria microplate during the Pliocene-Quaternary triggered mild compression through the Pannonian Basin (Horváth et al., 2006; Bada et al., 2007; Matenco and Radivojević, 2012).

The Pannonian Basin hosts Miocene to recent magmatic rocks with diverse compositions (calc-alkaline, K-alkalic, ultrapotassic and Na-alkalic; Seghedi and Downes, 2011). The basin is of extensional origin and its formation was accompanied by intensive calc-alkaline magmatism with a paroxysm of silicic volcanism during the Early and Middle Miocene climax of rifting. Thin crust and lithosphere, alongside with high heat flow and temperature gradient values, characterize the Pannonian region (Horváth et al., 2006, 2015). Thick sedimentary sequences, dominate the basin, in response to tectonic subsidence and sedimentation. These sedimentary deposits consist of various lithologies, including clastic sediments, evaporites, and carbonates (Seghedi and Downes, 2011; Kalmár et al., 2021).

### 1.3. Objectives

The general objective of this thesis is to better comprehend how the Adria microplate has been accommodated between the two major plates, Africa and Eurasia. In particular, I am interested in understanding how the Adria microplate has been tectonically consumed along the active belts of the Apennines and Dinarides, and in characterizing the presentday signal of this process in terms of slabs geometries. Therefore, the primary goal of this thesis is to improve the understanding of the lithosphere and upper mantle structure and composition of the Adria microplate and its margins. To achieve that, I have derived the present-day crust and upper mantle structure along two lithospheric transects, crossing the northern and southern regions of the Apennines and Dinarides orogenic belts, from the back-arc Tyrrhenian basin to the Panonnian and Carpathians-Balkanides in a roughly SW-NE direction. The two transects are almost perpendicular to the main trend of the belts, and coincide with wide-angle reflection/refraction seismic experiments and receiver functions analysis, that have allowed to further constrain the main crustal and upper mantle structure of the region. Additionally, based on the results of the lithospheric modeling presented in this thesis, I explore the implications of the identified mantle thermal anomalies on the present-day elevation, particularly in the context of dynamic topography.

The specific objectives include:

- 1) Determine the crustal structure along the modeled lithospheric profiles and compare the northern and southern regions.
- 2) Constrain the crustal and upper mantle structure in terms of density and temperature distribution, geometry and depth of the base of the crust and the lithosphere-asthenosphere boundary, and the upper mantle composition, along the two profiles.
- 3) Characterize the different tectonic domains of the region in terms of variations in the chemical composition of the mantle and tectonic evolution, and its influence on the resulting density and surface topography.
- 4) Determine the geometry and continuation at depth of the existing slabs beneath the Apennines and Dinarides.
- 5) Compare the obtained results along the two modeled profiles and discuss their tectonic significance in terms of the geodynamic evolution of the study area.
- 6) Evaluate the implications of deep tectonics on the surface dynamic topography responsible for the topographic evolution in the Central Alpine Mediterranean Orogenic System.
  - 7) Discuss the geodynamic implications of the results.

In summary, my results of the lithosphere and upper mantle structure integrating all available geological and geophysical data in a 2D forward modeling have allowed me to investigate the role of the Adria microplate in the geodynamic evolution of the Central Mediterranean region.

#### 1.4. Outline

The thesis dissertation is divided into six chapters.

Chapter 2 introduces the fundamental concepts and methodology used for the 2D lithospheric modeling (LitMod2D\_2.0 by Kumar et al., 2020). I also summarize the main geophysical data used, which are elevation, gravity, geoid height, surface heat flow, crustal seismic data and mantle seismic velocities. The methodology I have used integrates geological, geophysical and geochemical data. This methodology allows to obtain an integrated model of the thermochemical structure of the lithosphere and uppermost mantle down to a depth of 400 km.

Chapter 3 presents the results of the integrated lithospheric and uppermost mantle modeling along a northern transect which extends approximately 1000 km, crossing in a SW-NE direction the Tyrrhenian Sea, the northern Apennines, the Adriatic Sea, the Dinarides and the Pannonian Basin. The main aim of this chapter is to derive the present-day crust and upper mantle structure of the study area up to a depth of 400 km, using the methodology described in Chapter 2. The crustal and lithospheric structure is compared with previous interpretations and discussed in terms of the geodynamic evolution of the studied tectonic domains within the complex and long-term evolving Alpine-Mediterranean mobile belt. I demonstrate that bidirectional subducting continental mantle delamination of the Adria microplate can explain the main lithospheric and sublithospheric mantle features observed in the modeled transect. Lastly, I discuss the contribution of deep geodynamic processes in the build-up of present orogenic topographic relief.

Chapter 4 presents a nearly parallel southern transect employing the same approach as in the northern transect. The southern transect is about 1250 km long, crossing through the southern Tyrrhenian Sea, southern Apennines, the Adriatic Sea, the southern Dinarides, and the Balkans in a SW-NE direction. My primary goal is to investigate the lateral continuity between the opposing Apennines and Dinarides slabs, which has already been discussed for the northern region in Chapter 3. In this chapter, I am expanding my analysis to encompass the southern Apennines and Dinarides regions. Hence, the geophysical-geochemical integrated model presented here, in conjunction with findings from the northern Transect (Chapter 3), offers valuable insights into the lithospheric and

thermochemical structure of the upper mantle beneath the Apennines and Dinarides foldthrust belts.

Chapter 5 presents the general discussion on the two transects and their implication for the geodynamic evolution of the area. In this chapter, I delve into the primary findings of this thesis, addressing: i) the crustal and lithospheric structure of Adria and its margins along both the northern and southern transects. I analyze and compare the different crustal and mantle lithospheric domains; ii) I examine the distribution of density and temperature in the lithosphere and uppermost mantle along both transects, revealing significant thermal anomalies in the lithospheric and sublithospheric mantle; iii) I discuss findings regarding the different mantle compositions, noting a slightly depleted mantle for the Adria and Dacia microplates, contrasted with a more fertile mantle below the southern Tyrrhenian and Apennines; iv) I explore the sublithospheric anomalies modeled beneath the northern and southern Apennines and the Dinarides, highlighting variations in slab geometries. I discuss and provide an integrated view on the deep structure of Adria (Apennines-Dinarides) and Dacia (Carpathian-Balkanides) microplates, together with information on the slabs located along the western and eastern Adria margins. Finally, I integrate the results from the northern and southern Adria transects to investigate the role of the Adria microplate in the geodynamic evolution of the Central Mediterranean region

Chapter 6 presents the final conclusions of this thesis.

# CHAPTER 2 Fundamentals and Methodology

# Chapter 2. Fundamentals and Methodology

This thesis integrates a wide range of geological and geophysical data to investigate the density, thermochemical, and seismic velocity structure of the lithosphere and sublithospheric mantle. However, before delving into the methodology employed, I will initially introduce some fundamental concepts. First, I will summarize the basic principles of the crust, lithosphere, and sublithosphere, alongside the geophysical observables utilized in my research. Subsequently, I delve into the methodology that I have used and the fundamental concepts underpinning my integrated geophysical-petrological modeling and discuss the implications of mantle anomalies. Additionally, I provide a brief overview of the methodology of dynamic topography applied in this thesis.

#### 2.1. Fundamental concepts

#### 2.1.1. Internal structure of the Earth

Earth's interior is typically divided into several layers based on distinct physical and compositional characteristics (Figure 2.1). It consists of three major compositional layers: the crust, mantle, and core. Considering the mode of deformation or rheology, it can be divided into five main mechanical layers: lithosphere, asthenosphere, lower mantle, outer core, and inner core. The mechanical divisions of the interior of the Earth do not necessarily match the compositional layers. This thesis focuses on the Earth structure until the top of the transition zone between the upper and lower mantle (~ 400 km). Hence, the sublithospheric mantle is introduced to describe a mechanically weaker layer (i.e., asthenosphere) that spans from the Lithosphere-Asthenosphere Boundary (thereinafter LAB) to the base of upper mantle.

#### The crust

The crust is the outermost layer of the Earth's lithosphere. The Mohorovičić (Moho) discontinuity, the base of the crust, is a significant global seismic velocity discontinuity from the felsic crust to the mafic upper mantle, which indicates the major changes in properties such as petrology, chemistry, seismic wave velocity, density, and rheology (Jarchow and Thompson, 1989). It is usually corresponding to be the level where compressional seismic (P-wave) velocity first increases rapidly or gradually overtakes 7.6

km/s (Thybo et al., 2013). The crust can be divided into two different types, oceanic and continental crust. Oceanic crust and continental crust have different characteristics.

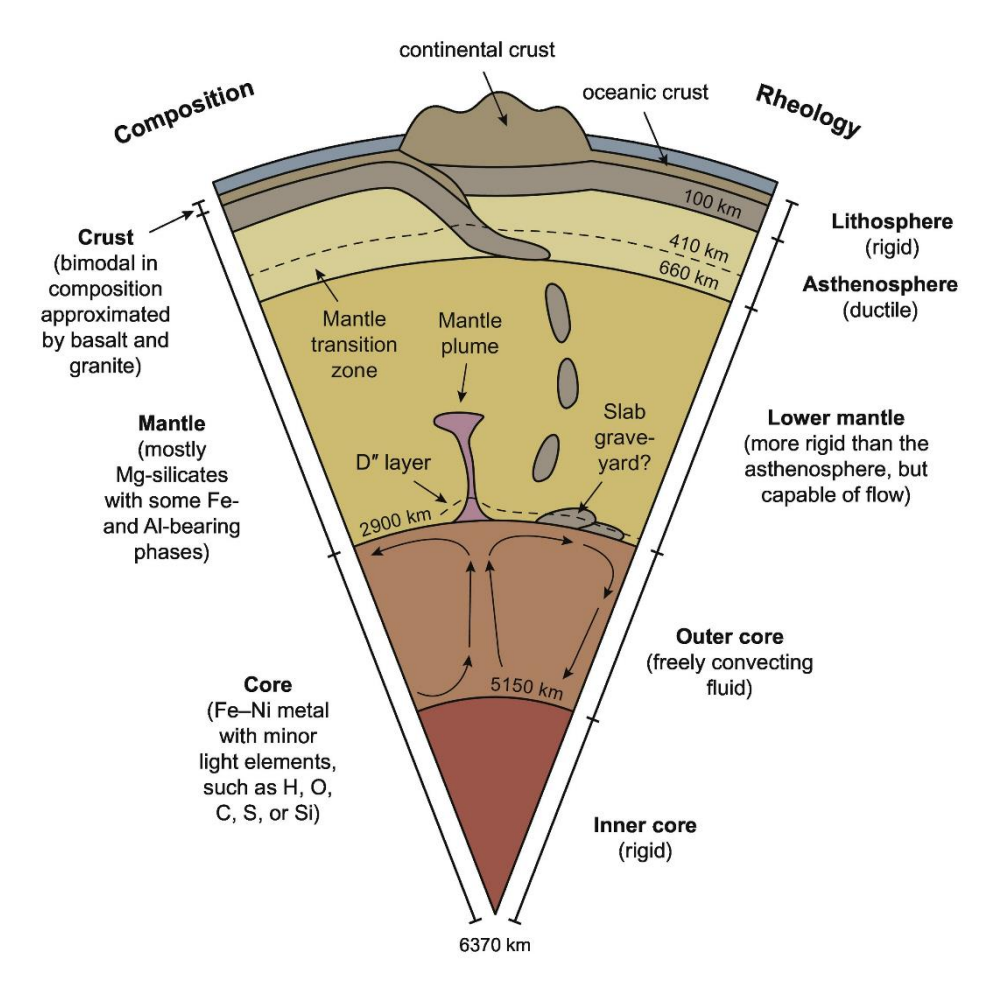


**Figure 2.1** Two views of the internal structure of the Earth (modified from Palin et al., 2020). Not to scale. The Moho discontinuity separates the crust and mantle. The LAB separates the lithosphere and sublithospheric mantle (i.e., asthenosphere).

The oceanic crust is on average about 7 km thick and has a roughly basaltic composition. This type of crust is generated at mid-ocean ridges as a result of decompression melting in the upwelling mantle, and it is consumed in subduction zones. The rocks of the oceanic crust thus are younger (usually, < 180 million years old) and denser (density about 3000 kg/m³) than continental rocks (2700-2800 kg/m³). A large number of geological and geophysical studies have identified that the oceanic crust typically consists of three layers (Kennett, 1982): an uppermost sedimentary layer, a middle basaltic volcanic layer, and a lowermost layer of gabbroic plutonic rocks.

The continental crust is thicker (the average Archean crust is ~35 km and the Proterozoic crust is ~45 km thick) and it is primarily composed of igneous, metamorphic and sedimentary rocks. It is formed through a complex amalgamation of diverse geological events and has a significantly longer lifespan. The continental crust has a relatively low

average density of about 2700-2800 kg/m³, which leads to continental crust having more buoyancy and cannot be readily subducted into the deep mantle. So, the continents on each side collide, generating new orogenic belts when the intervening ocean basin is completely consumed by subduction. Christensen and Mooney (1995) based on global seismic models proposed a three-layer crust: The upper crust, extending from the surface to about 10-20 km deep and characterized by relatively low velocities, consists predominantly of a variable thick sedimentary cover, overlain the crystalline basement composed of felsic rocks like granite and granodiorite, and is less dense and more brittle. Below this, the middle crust, reaching depths of 20-30 km, contains a mix of felsic and mafic rocks, including amphibolite and metamorphic rocks, and exhibits intermediate density and mechanical properties. The lower crust, extending to the Moho at depths of 35 km or more, consists mainly of dense, ductile mafic rocks such as gabbro and granulite, allowing it to flow under stress at difference with the upper and middle crust, the lower crust is depleted in heat generating elements.

#### The Lithosphere

The lithosphere is regarded as a mechanically rigid layer floating on the warmer and weaker asthenosphere. Plate tectonics theory suggests the rigid lithosphere is divided into several tectonic plates and provides a robust framework that describes and predicts its behavior in space and time. The lithosphere includes the crust and the uppermost part of the mantle (the so-called lithospheric mantle).

The lithosphere-asthenosphere boundary (LAB) separates the lithosphere from the underlying convecting mantle and represents a mechanical transition between them. However, where exactly this transition occurs and what is the best definition of the lithosphere is still debated (Eaton et al., 2009; Artemieva, 2011). The lithosphere has various definitions (Figure 2.2) depending on the property adopted for its definition:

- The thermal lithosphere is defined as the thermal boundary layer where the heat is primarily transferred by conduction. The base of the lithosphere or LAB is commonly defined by the depth of a constant isotherm (e.g., Gerya, 2019) or the intersection between a conductive geotherm and the mantle adiabat (e.g., Turcotte and Schubert, 2014).
- The seismological lithosphere is defined as the high-seismic velocity layer which typically overlays the Low Velocity Zone (LVZ) in the upper mantle (Carlson et al.,

2005; Anderson, 2007). Some studies associate the LAB with a distinct change in seismic anisotropy (e.g., Plomerová and Babuška, 2010).

- The geochemical lithosphere is defined as a layer that retains distinct geochemical and isotopic signatures from the underlying convecting mantle for longer periods (Griffin et al., 1999; O'Reilly and Griffin, 2010). Chemically, the base of the lithosphere should divide a lithospheric mantle that is variably depleted in basaltic components from a more fertile asthenosphere.
- The electrical lithosphere is defined as the resistive layer of the Earth overlying more conductive material (Jones and Craven, 2004)
- The mechanical lithosphere is defined as a layer that has the ability to retain no significant deformation with high differential tectonic stresses over geological periods. It is constrained by rheological parameters (Eaton et al., 2009) and is always thinner than the seismological, thermal, or geochemical lithosphere (Burov, 2011).

Of course, the different definitions result in different LAB depths. In this thesis, the lithosphere is defined by a thermochemical condition, which encompasses both the thermal and geochemical definitions. This definition assumes that the lithosphere has dominating conductive heat transfer, above the convective mantle with an adiabatic geothermal gradient. Furthermore, the definition considers the heterogeneity of the upper mantle, with the LAB being a chemical boundary that marks the transition from depleted to undepleted/fertile composition. This preferred definition is chosen for the following reasons:

- a) The thermal definition is practical and intuitive, and usually used in geodynamics.
- b) The thermal structure has a reliable relationship with the mechanical properties of the lithosphere.
- c) The correlation between the depth where the mantle composition changes from depleted to undepleted and the associated isotherm has been widely confirmed.
- d) Both temperature and composition are fundamental conditions for other widely used definitions, e.g., seismic, electrical, elastic, etc.
  - e) This definition effectively eliminates ambiguities existing with other methods.

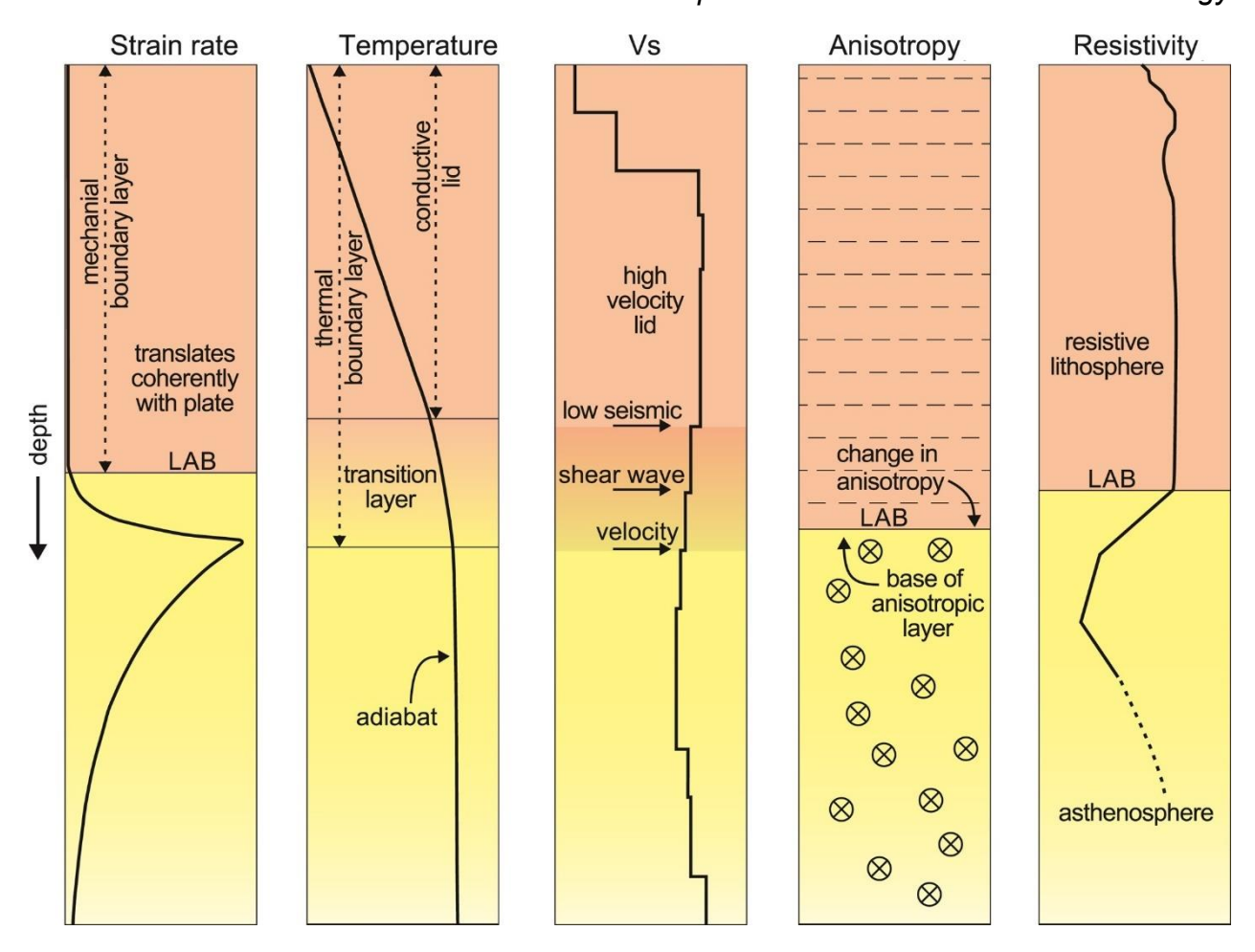


**Figure 2.2** Schematic definition of the lithosphere and common geophysical proxies used to estimate its thickness. Taken from Eaton et al. (2009)

#### Sublithospheric mantle

The sublithospheric upper mantle (i.e., asthenosphere) in this thesis describes the mechanically weaker layer which spans from the LAB to a depth of ~ 400 km (the lower limit of my model), which is dominated by an adiabatic geothermal gradient because of its convective activity (e.g., Hofmann, 1988). The sublithospheric upper mantle is characterized by general low seismic velocities, high attenuation and high electrical conductivity (Shankland et al., 1981). Due to high temperature and pressure conditions, this layer exhibits weaker and more ductile behavior compared to the lithosphere over geological time scales. This behavior results in the "floating" and slowly "drift" of lithospheric plates, leading to the occurrence of plate tectonics. The progressive melting of the mantle during the Earth's earliest evolution led to the formation of a depleted mantle and a continental crust enriched in highly incompatible elements. The sublithospheric mantle has long served as a chemical reservoir for overlying oceanic and continental lithosphere (e.g., Hofmann, 1997; Workman and Hart, 2005; Hofmann et al., 2022).

#### 2.1.2. Composition of the upper mantle

The Earth's upper mantle extends from the base of the crust (Moho) to about 670 km, which is the discontinuity between the upper and lower mantle (Figure 2.1). Although the overall composition of the upper mantle can be approximated as peridotite, major geodynamic processes (subduction, rifting, continental collision, and mantle upwelling) can easily change this average composition. The composition of the upper mantle is primarily derived from deep peridotite massifs, mantle-derived xenoliths and volcanic rocks and has been studied for several decades (e.g., Klein and Langmuir, 1987; Langmuir et al., 1992; Niu, 1997, 2021; Griffin et al., 1999, 2009; Johnson et al., 2016; Melchiorre et al., 2017; Hofmann et al., 2022; Mantovani et al., 2022). However, the precise composition of the lithospheric mantle remains a topic of ongoing investigation and has not yet been resolved (Griffin et al., 2009; Sani et al., 2023), due to its compositional heterogeneity (O'Reilly and Griffin, 2006; Tommasi and Vauchez, 2015; Melchiorre et al., 2017). Partial melting experiments on peridotite reveal that incompatible elements (such as Na, K, Ca, and Al) preferentially partition into the melt, and compatible elements (such as Mg and Fe) preferentially stay behind in the residual mantle. The Magnesium number Mg# = 100 × Mg / (Mg + Fe), as a potential tracer, usually indicates the depleted degree of mantle (Bernstein et al., 2007).

The lithospheric mantle can be oceanic (associated with the oceanic crust) or continental (associated with the continental crust).

The oceanic lithospheric mantle is formed at mid-ocean ridges (MORs) from partial melting of the convective mantle. The process produces a depleted oceanic residual lithosphere mantle and a basaltic crust. Despite of the presence of lateral thermal variation (Turcotte and Schubert, 2014), geophysical-petrological modeling indicates that the vertical stratification of its composition predominates (Afonso et al., 2008; Liao et al., 2013). One of the most influential models (Klein and Langmuir, 1987, Langmuir et al., 1992; Gale et al., 2014; Dalton et al., 2014) suggests that variations in mantle potential temperature at the mid-ocean ridges play a crucial role in controlling the depth and pressure of mantle melting. The model considers that hotter mantle regions have taller melting columns, more extensive melting, thicker crust, and shallower ridge depths because of the earlier beginning of melting at deeper depths.

The continental lithospheric mantle is highly heterogeneous and its mean composition is highly depleted. Several studies (Griffin et al., 1999, 2009; Gaul et al., 2000; O'Reilly et al., 2001; O'Reilly and Griffin, 2006) have confirmed that the degree of depletion in subcontinental lithospheric mantle varies with the tectonothermal age of the overlying crust (Figure 2.3 and Table 2.1), at least from higher depleting Archean (>2.5 Ga), to

middle depleting Proterozoic (2.5-1.0 Ga), and to lighter depleting Phanerozoic (<1.0 Ga) continental lithospheres. The Archean lithospheric mantle with highly depleted chemical composition is characterized by its great thickness (up to 300 km), low density, depleted basaltic components, high refractory (i.e., less likely to melt), and low temperature gradient (Lee et al., 2011; Wang et al., 2023).

On other hand, the composition of the sublithospheric mantle is nearly homogeneous, although this remains a topic of debate. McDonough and Sun (1995) estimated a homogeneous sublithospheric mantle with a primitive upper mantle (PUM) chemical composition assuming no influence from deep mantle. However, its composition could be changed by various mantle upwelling, subduction, and/or delamination (O'Reilly and Griffin, 2006; Tommasi and Vauchez, 2015; Melchiorre et al., 2017). Overall, it is slightly depleted relative to estimates of the primitive mantle whereas less fertile (i.e., less likely to melt) than the depleted lithospheric mantle (Workman and Hart, 2005; Stracke, 2021; Hofmann et al., 2022). Kumar et al. (2020) has tested the different available compositions of the sublithospheric mantle and indicated that the depleted mid-ocean ridge basalt mantle (DMM, Workman and Hart, 2005) provides the best overall fits among them. The DMM is depleted and characterized by a significant depletion in the incompatible trace elements compared to the primitive upper mantle and I use it as a reference composition for the sublithospheric mantle.

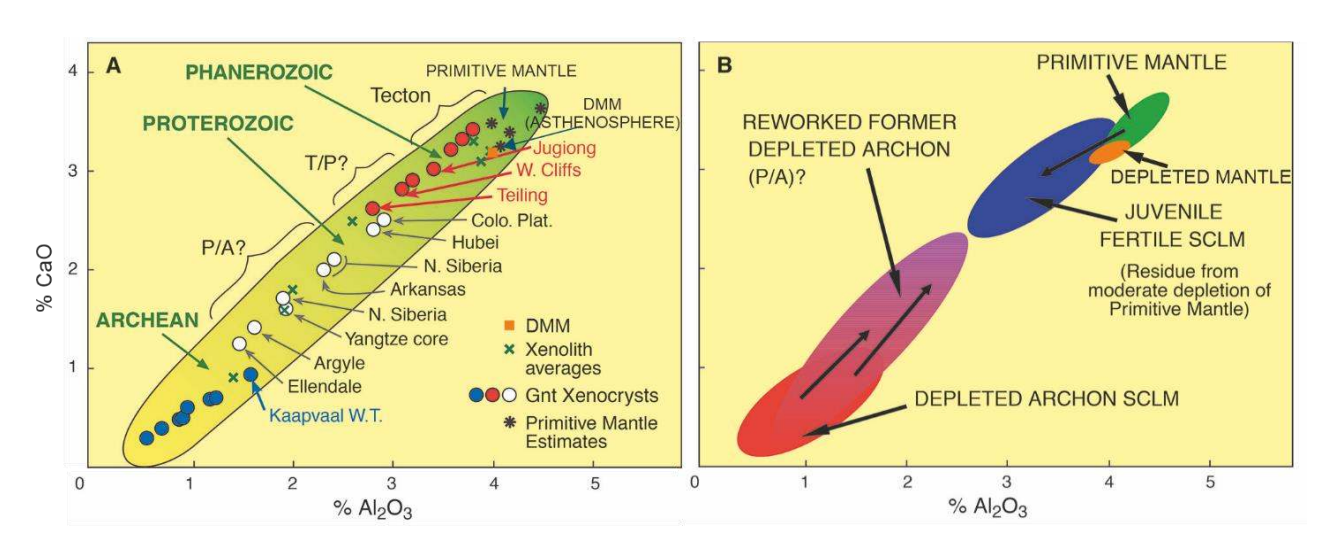


**Figure 2.3** A. Estimates of the mean CaO and Al<sub>2</sub>O<sub>3</sub> contents in continental lithospheric mantle of different tectonothermal age based on the compositions of garnet xenocryst populations (circles) and xenolith populations (crosses) in volcanic rocks (modified from Griffin et al., 2009). B. Interpretation of the data in (A) in terms of depletion-refertilization processes.

**Table 2.1** Bulk compositions and characteristics of different lithospheric mantle compositions which come from Griffin et al., 2009. DMM: Depleted mid-ocean ridge basalt mantle (Workman and Hart, 2005; Kumar et al., 2020) is the composition attributed to the sublithospheric mantle.

	Archons	Protons	Tectons	DMM
Age / Ga	>2.5	1.0-1.5 <1.0		/
Thickness / km	180-250	150-180	150-180 60-140	
SiO <sub>2</sub> / %wt	41.7-46.6	43.9-45.4 44.0-45.0		44.71
Al <sub>2</sub> O <sub>3</sub> / %wt	0.3-2.2	0.64-3.7 2.3-3.9		3.98
FeO / %wt	6.4-8.1	7.9-8.3	9-8.3 8.1-8.4	
MgO / %wt	43.8-50.4	39.9-46.0	38.7-41.4	38.73
CaO / %wt	0.12-1.66	0.43-3.2	2.2-3.2	3.17
Na <sub>2</sub> O / %wt	0.26-0.34	0.08-0.26	3-0.26 0.24-0.27	
Mg#	90.5-93.1	90.4-91.9	89.5-89.9	89.4

#### 2.1.3. Topography

The surface topography of Earth is always assumed to be influenced by lateral density heterogeneity in the lithosphere and/or uppermost mantle, and is typically assumed to be in isostatic equilibrium. However, sublithospheric mantle processes play a significant role in sculpting Earth's surface landscapes (Braun, 2010; Flament et al., 2013). Deep mantle flow, resulting in surface vertical deformation known as dynamic topography (Figure 2.4), was first proposed by Pekeris (1935).

The records of dynamic topography and surface processes can be preserved in the geological setting (Burgess et al., 1997; Burgess and Moresi, 1999; Braun et al., 2013). Examples of are the Colorado Plateau (Moucha et al., 2009; Liu and Gurnis, 2010; Karlstrom et al., 2012; Braun et al., 2013), the Iceland Plateau (Bijwaard and Spakman, 1999; Maclennan et al., 2001), the South African Plateau (Gurnis et al., 2000; Moucha and Forte, 2011; Braun et al., 2014; Flament et al., 2014), the Australian continent (Sandiford, 2007; Matthews et al., 2011; Czarnota et al., 2013, 2014), and Mediterranean Sea (Boschi et al., 2010; Faccenna and Becker, 2010).

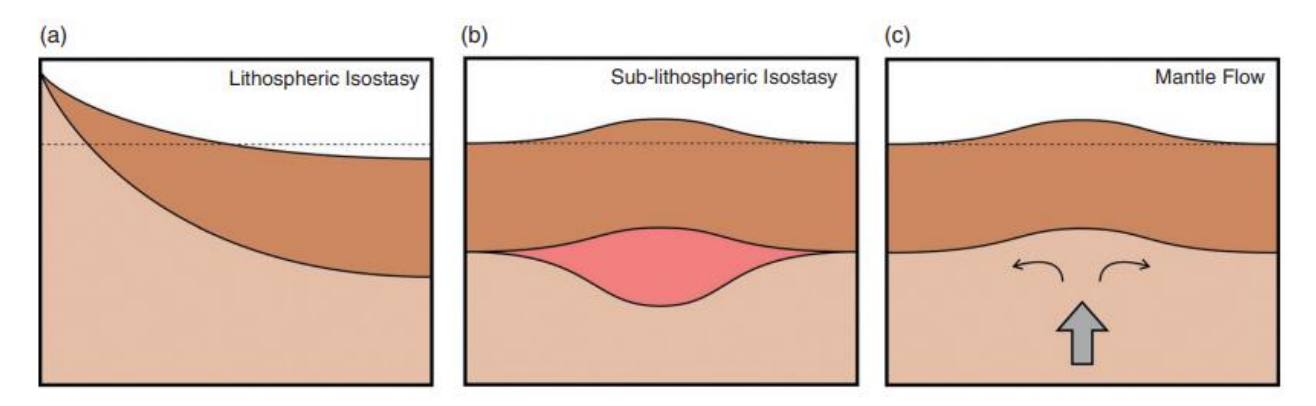


**Figure 2.4** Examples of processes producing dynamic topography and mechanisms causing evolving vertical motion. Taken from Hoggard et al. (2021). (a) lithospheric isostasy (both oceans and continents); (b) isostasy within the mantle (asthenosphere and deeper); (c) mantle flow.

Figure 2.4 shows three examples related to isostasy and mantle flow (Hoggard et al., 2021). First, buoyancy due to differences in the lithospheric thickness and temperature is isostatically compensated at the Earth's surface (Figure 2.4a), particularly in oceanic regions where older plates become colder and denser, leading to subsidence. Second, lateral variations in temperature and chemical composition within the asthenosphere and deeper mantle create density anomalies that can be isostatically compensated at the surface (Figure 2.4b), occurring even in the absence of vertical flow, for example in cratons. Third, mantle flow generates pressure gradients and vertical deviatoric stresses that exert forces on the overlying tectonic plates (Figure 2.4c).

There are two main methods of estimating the present-day dynamic topography: a) calculating the residual topography (Gvirtzman and Nur, 2001; Faccenna and Becker, 2020), which is typically defined as the remaining portion of topography once the isostatic component of the lithosphere has been subtracted from the observed topography. This calculation depends on the detail knowledge of the thermal and mechanical structure of the lithosphere. However, the uncertainty about the structure can lead to significant variations in the estimation of residual topography. b) numerical modeling of mantle flow (Lithgow-Bertelloni and Silver, 1998; Heller and Liu, 2016; Hu et al., 2018; Bodur and Rey, 2019; Wang et al., 2023), which usually employs seismically imaged anomalies to derive velocity and stress flow fields. However, this method tends to oversimplify mantle rheology, and the translation of seismic velocities to physical properties (e.g., density, temperature) introduces additional uncertainties (Cammarano et al., 2003).

#### 2.2. Methodology

The methodology employed in this thesis is based on LitMod2D\_2.0 (Kumar et al., 2020), an updated version of the original 2D software designed by Afonso et al. (2008). Both versions have a similar workflow and design concept, and are based on the finite element forward modeling approach. They are specifically developed to investigate the 2D structure of the crust and upper mantle, including thermal, density, and seismological structure, as well as composition, down to 400 km depth. This method integrates available geophysical and petrological data within a self-consistent thermodynamic framework (Figure 2.5), ensuring a comprehensive understanding of the subsurface structure. The approach has been successfully applied in different tectonic settings including continental margins (e.g., Fernàndez et al., 2010; Pedreira et al., 2015) and continental collisional regions (e.g., Carballo et al., 2015; Tunini et al., 2015; Jiménez-Munt et al., 2019; Ravikumar et al., 2020; Kumar et al., 2021).

This thesis adds a new post-processing calculation based on dynamic topography to assess the implications of deep mantle anomalies on surface topography. For a better understanding, this subsection describes the basic workflow, and details the procedures of this integrated geophysical-petrological approach.

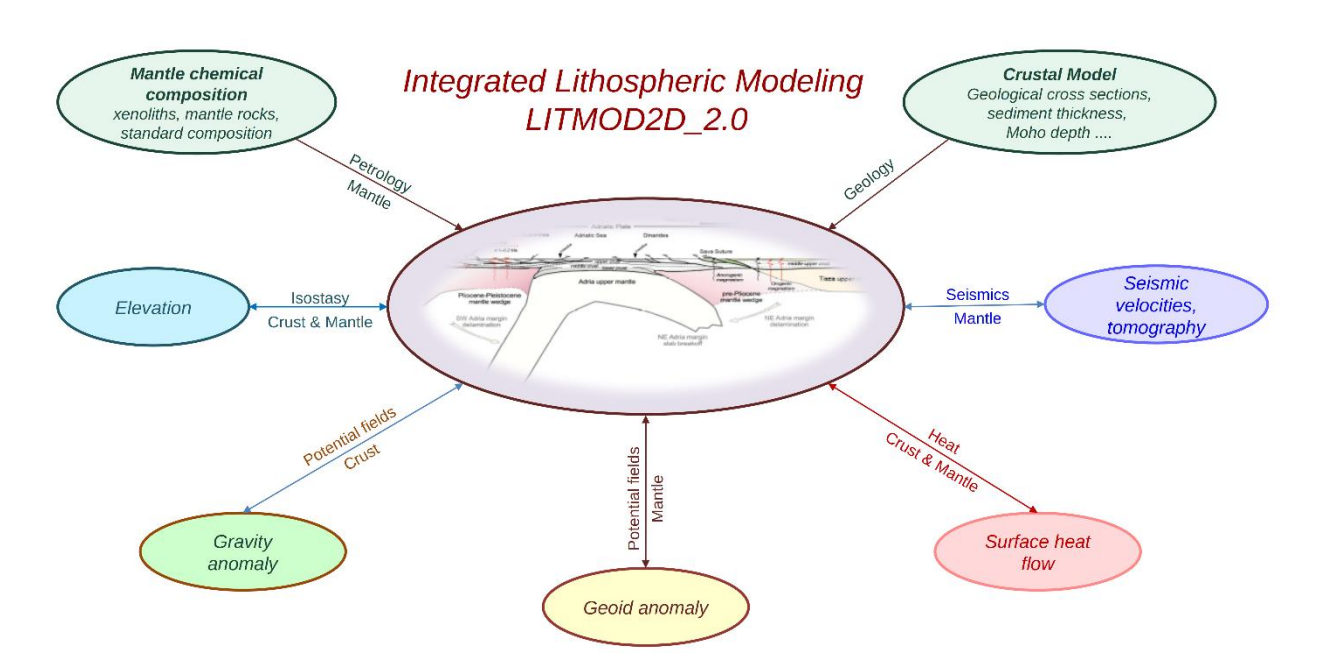


Figure 2.5 Simplified scheme of the LitMod2D\_2.0.

#### 2.2.1. General workflow

The methodology follows a forward modeling workflow (Figure 2.6); wherein each step involves comparing the model outputs (such as elevation, gravity and geoid anomalies, surface heat flow, and mantle seismic velocities distribution) with observed data (including geophysical observables, seismic velocities, and tomography images). The user has the flexibility to modify the input parameters and model geometry within the experimental uncertainties, employing a trial-and-error approach to achieve the best-fitting model. In essence, the software calculates the two-dimensional distribution of temperature, density, and mantle seismic velocities, along with the resulting surface heat flow, elevation, gravity, and geoid anomalies, to simultaneously fit all geophysical observables.

The model extends from the surface to 400 km depth and is composed of two domains: the crustal and the mantle domain. The strategy to define and assign properties to each domain is as follows:

The crustal bodies are described by the user defining thermo-physical parameters (density, thermal conductivity, volumetric heat production rate, coefficient of thermal expansion, etc.). The density can be constant or pressure-and/or temperature-dependent by setting the value of thermal expansion and compressibility. The thermal conductivity is set as constant depending on the lithology of the crustal rock. The volumetric heat production rate may be constant or exponentially decreasing with depth. Crustal geometry is mainly constrained by previous studies, including active and passive seismic experiments and geological cross-sections, which are discussed in the following subsection. Note that the geometry and properties of the crustal bodies should be assigned according to the pre-investigated geological structure and constrained by existing data.

The mantle bodies are described by their composition. The corresponding physical properties are calculated by thermodynamic modeling of the mantle phase equilibrium, considering its temperature and pressure. As explained in Section 2.1, the mantle is divided into two parts (lithospheric and sublithospheric mantle) by the LAB. The depleted mid-ocean ridge basalt mantle (DMM, Workman and Hart, 2005) is considered to be the reference composition for the sublithospheric mantle (see Section 2.1.2). The chemical composition of the lithospheric mantle is heterogeneous, and it is derived from xenoliths data when available, or according to its tectonothermal age (see Section 2.1.2 and 2.2.4). The LAB depth is subsequently refined based on the fitting of the geophysical observables: elevation, gravity anomaly, geoid high, surface heat flow and mantle seismic velocities.

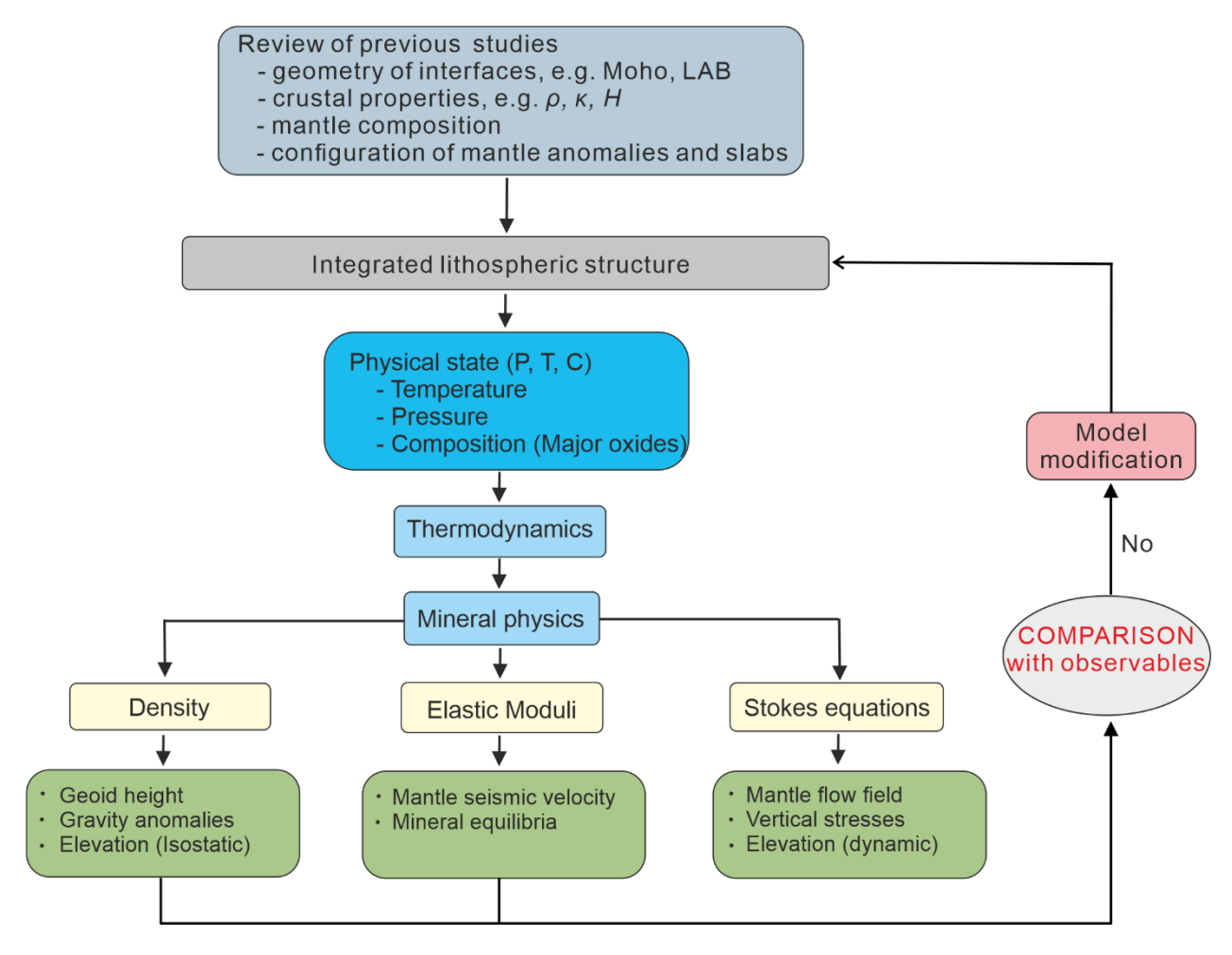


Figure 2.6 Simplified flowchart indicating the general modeling procedure used in LitMod 2D.

#### 2.2.2. Thermal modeling and boundary conditions

The methodology distinguishes two regions for thermal modeling: the lithospheric domain dominated by conduction and the sublithospheric domain dominated by convection. The temperature distribution within the lithosphere is calculated by solving the two-dimensional steady-state heat conduction equation:

$$\nabla \cdot (k \, \nabla T) + A(x, z) = 0 \tag{2.1}$$

where T is the temperature, [K]; k is the thermal conductivity, [W/(m·K)]; A is volumetric heat production rate, [W/m³]; V is the nabla operator; x and z represent the horizontal and vertical directions in the Cartesian coordinate system, respectively. As mentioned above, the thermo-physical parameters of the crust are user-defined. The volumetric heat production rate of the mantle is set to 0.02  $\mu$ W/m³, a value typical of the upper mantle (Turcotte and Schubert, 2002). The thermal conductivity of the mantle is calculated as a

function of composition, temperature, and pressure, following the model proposed by Grose and Afonso (2013). This model considers the combined contributions of lattice thermal conductivity ( $k_{lat}$ ) and radiative thermal conductivity ( $k_{rad}$ ):

$$k_{lat}(T) = \rho C_p[a + b \exp(-cT) + d \exp(-eT)]$$
(2.2)

$$k_{rad}(T,d) = A \exp\left(-\frac{(T-T_A)^2}{2x_A^2}\right) + B \exp\left(-\frac{(T-T_B)}{2x_B^2}\right)$$
 (2.3)

where T is the temperature;  $\rho$  is the density;  $C_p$  is the heat capacity; a, b, c, d and e are the coefficients corresponding to each mineral measured from laboratory; d is the grain size; A, B,  $T_A$ ,  $T_B$ ,  $x_A$  and  $x_B$  are a function of gain size (further details in Grose and Afonso, 2013).

The thermal equation (2.1) is solved by the Galerkin finite element method, dividing the numerical domain into triangular elements. The temperature boundary conditions are: a) 0 °C at the surface; b) 1320 °C at the LAB, values that are widely used in geodynamic modeling (e.g., Gerya et al., 2021); c) no heat flow across the lateral boundaries of the model. The temperature at the base of the model (at 400 km) is taken to be 1520 °C (Afonso et al., 2008; Kumar et al., 2019) which is consistent with high-pressure and high-temperature experiments on the phase equilibria of olivine-wadsleyite (Ito and Katsura, 1989; Katsura et al., 2004).

In the sublithospheric domain, the vertical temperature distribution is assumed to follow an adiabatic gradient, with values between 0.35 and 0.50 °C/km. In order to avoid abrupt thermal discontinuities between the conductive thermal gradient of the lithosphere and the adiabatic sublithospheric thermal gradient, the method incorporates a thermal buffer layer with a thickness of 40 km and a bottom constant temperature of 1400 °C.

#### 2.2.3. Potential field: Gravity and Geoid Height Anomalies

The gravitational field provides information about the lateral variations of the density within the Earth. Therefore, it is a very valuable measurement for determining mass distribution at depth.

Gravity anomalies provide valuable insights into the density distribution at shallower depths within the lithosphere regions, representing the shorter-wavelength component of the signal. On the other hand, geoidal height is particularly sensitive to deeper density anomalies and the depth of the Lithosphere-Asthenosphere boundary (LAB). This distinction arises from the fact that the geoid anomaly corresponds to the height disparity

between two equipotential surfaces, and is therefore influenced by a 1/r relationship rather than  $1/r^2$  for gravity, where r is the distance to the density anomaly (Turcotte and Schubert, 2002).

Gravity anomalies are calculated using the Talwani's algorithm for polygonal bodies (Talwani et al., 1959). This algorithm takes into consideration both horizontal and vertical variations of density by computing gravitational effects on the elements of the mesh. To mitigate the influence of boundary effects, the models are extended horizontally by 1 x  $10^5$  km beyond the limits of the profile.

Geoid height is computed by converting the neighboring elements of the numerical mesh into rectangular prisms. The integral of the gravity potential is then solved, the obtained result is substituted into Brun's formula, and finally the geoid height  $\Delta N$  is expressed as:

$$\Delta N = \frac{G\rho}{g_o} \iiint_{x_1, y_1, z_1}^{x_2, y_2, z_2} \frac{1}{\sqrt{x^2 + y^2 + z^2}} dx dy dz$$
 (2.4)

where G is the universal gravitational constant,  $g_0$ the normal gravity acceleration,  $\rho$  the rectangular prism density, and  $x_1$ ,  $x_2$ ,  $y_1$ ,  $y_2$ ,  $z_1$ ,  $z_2$  the prism boundary coordinates. By employing the analytical solution developed by Zeyen et al. (2005) for this equation, I can obtain 2.5-D geoid heights along the model.

#### 2.2.4. Mantle composition

The composition of the mantle is defined within the NCFMAS (Na<sub>2</sub>O-CaO-FeO-MgO-Al<sub>2</sub>O<sub>3</sub>-SiO<sub>2</sub>) system, from which stable mineral assemblages are determined by minimizing the Gibbs free energy (Connolly, 2005). The system considers the relative amounts of these six major elements which compose the ~98% of the Earth's mantle. The physical properties of each mineral and of the bulk mantle (density, thermal conductivity, thermal expansion coefficient, elastic parameters) are calculated as function of composition, temperature, pressure, and phase changes.

The composition of the lithospheric mantle is distinctive, and its heterogeneity has been widely confirmed (see Section 2.1.4 and Table 2.1). In the continent lithospheric mantle, I adopt the composition defined by Griffin et al., (2009), who categorize it into three groups based on the tectonothermal age of the overlying crust (Table 2.1): higher depleted Archean (>2.5 Ga), middle depleting Proterozoic (2.5-1.0 Ga), and lighter depleting Phanerozoic (<1.0 Ga).

The composition of oceanic lithospheric mantle is predicted by a theoretical model (Klein and Langmuir, 1987, Langmuir et al., 1992), that is based on the relationship between the degree of partial melting of the underlying mantle and the thickness of oceanic crust at the ridge. The model can also be applied to other tectonic setting such as continental rifts, back arc basins and intraplate hotspots. Here I update the formalism for extensional basins or continental rifts zone. Defining that the total amount of melt  $F_T$  present within a unit column is

$$F_T = \int_{P_0}^{P_f} F(P) dP$$
 (2.5)

where  $P_0$  is the pressure where partial melting starts,  $P_f$  is the pressure at which partial melting stops. Then, the mean fraction of melting  $\bar{F}$  is

$$\bar{F} = \frac{\int_{P_0}^{P_f} F(P) dP}{\left(P_0 - P_f\right)} \tag{2.6}$$

Assuming that the total amount of melt produced segregates to form the crust, then

$$\rho_c g h_c = \bar{F} \big( P_0 - P_f \big) \tag{2.7}$$

where  $\rho_c$  and  $h_c$  are the density and thickness of the crust, respectively. For example, for typical crust (Asimow et al., 2001) of  $\bar{F}=\sim 7.2\%$ ,  $P_0=2.75$  GPa,  $P_f=0.2$  GPa, and  $\rho_c=2880$  kg/m³, then gives  $h_c=6.5$  km. After the production and separation of melt from the underlying asthenosphere, there is a subsequent change in the chemical composition of the residue. The composition of this residue can be determined through mass-balance calculations using various parameters, including the initial concentration of elements or components in the system (e.g., major oxides), the bulk distribution coefficient (D), and the fraction of liquid ( $\bar{F}$ ). As a first-order approximation, the composition of the solid residue can be approximated using the approach proposed by Langmuir et al. (1992):

$$x_i^s = \frac{x_i^o}{\bar{F}/D_i + (1 - \bar{F})} \tag{2.8}$$

where  $x_i^o$  and  $x_i^s$  are the concentration of the *i*th oxide in the original source and residues (in wt %), respectively.  $D_i$  is its bulk partition coefficient (Niu, 1997).

In addition, the composition of sublithospheric mantle is assumed homogenous (see Section 2.1.2). And the depleted mid-ocean ridge basalt mantle (DMM, Workman and Hart, 2005) is assumed for the whole sublithospheric mantle (Kumar et al., 2020).

#### 2.2.5. Densities distribution

The density of each crustal body can be either constant or dependent on pressure and/or temperature. By setting the values of the thermal expansion coefficient and compressibility, the density can then be calculated as a function of pressure and temperature:

$$\rho(T, P) = \rho_0 - \rho_0 \alpha (T - T_0) + \rho_0 \beta (P - P_0)$$
(2.9)

where  $\rho_0$  is the reference density at reference temperature  $T_0$  (typically at 25 °C) and pressure  $P_0$  (typically 10<sup>5</sup> Pa=1 bar),  $\alpha$  is the thermal expansion coefficient and  $\beta$  is the compressibility. The reference density and thermodynamical parameters are related to tectonic setting and could be estimated from local or global studies.

Density within the mantle depends on temperature, pressure, and composition, and is computed using a Gibbs free energy minimization algorithm (Connolly, 2009). In this process, the chemical composition of the mantle domain is expressed using the NCFMAS system (Na<sub>2</sub>O-CaO-FeO-MgO-Al<sub>2</sub>O<sub>3</sub>-SiO<sub>2</sub>). To facilitate the calculations, I employed a modified version of the thermodynamic database developed by Holland and Powell (1998), as further refined by Afonso and Zlotnik (2011). By using the Perple-X software (Connolly, 2005; Connolly, 2009), all stable assemblages and relevant physical properties are generated and subsequently stored in "look-up" tables for use in next modeling.

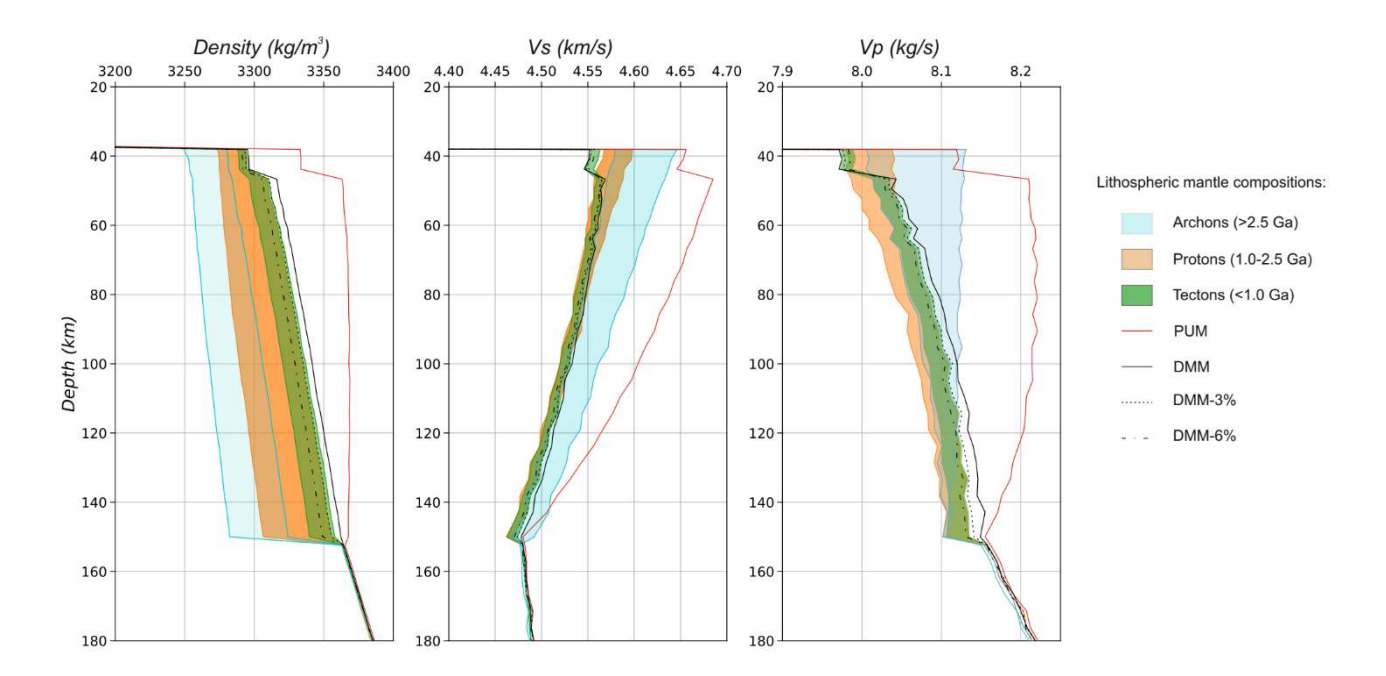


**Figure 2.7** Density, seismic velocities (Vs and Vp) changes with depth due to temperature and pressure variations for different lithospheric mantle compositions. The results are calculated with a model considering the Moho and the LAB discontinuities at depth of 35 km and 150 km, respectively. Here this model adopts

a constant grain size (10 mm) and constant oscillation period (75 s) for the mantle with a modified version of the thermodynamic database from Holland and Powell (1998), revised by Afonso and Zlotnik (2011). Compositions of lithospheric mantle are taken from Griffin et al. (2009), and the depleted mid-ocean ridge basalt mantle (DMM, Workman and Hart, 2005) is assumed for the sublithospheric mantle.

Figure 2.7 shows the correlation between calculated physical properties (density, seismic velocities) and different lithospheric mantle compositions. The results show that density and seismic wave velocity decrease and increase, respectively, as the tectonothermal age of the overlying crust increases. However, it remains the challenge of identifying mantle composition due to the lack of uniqueness in physical properties like density and seismic velocities. For example, some Archean and Phanerozoic mantles, despite having different density values (ranging from 3320 kg/m³ to 3340 kg/m³ and from 3280 kg/m³ to 3320 kg/m³, respectively, at a depth of 100 km), share a similar range of values in seismic velocities, particularly P-wave velocities. This lack of distinctiveness in physical properties could complicate efforts to differentiate between mantle compositions in various regions.

#### 2.2.6. Mantle seismic velocities

Mantle seismic velocities are calculated based on the composition, pressure, and temperature variables. To calculate them, it is necessary to have information about the elastic parameters, including the bulk and shear modulus, for each mineral, as well as the bulk rock density under the specific pressures and temperatures of interest. By considering these parameters, the isotropic anharmonic seismic compressional ( $V_p$ ) and shear ( $V_s$ ) wave velocities can be determined using the following equations:

$$V_p^2 \rho = K + \frac{4}{3}G \tag{2.10}$$

$$V_s^2 \rho = G \tag{2.11}$$

where  $\rho$  is the bulk rock density, which is obtained as described in the Section 2.2.5. K and G are the bulk and shear modulus of the aggregate (i.e., bulk rock), respectively. They are calculated by the following steps: The first step involves using a least squares procedure to determine the mole fractions of end-members mineral in each stable phase. Then, the moduli of each solution phase are obtained by calculating the arithmetic mean of the end-member moduli, based on their molar proportions. Next, the elastic moduli of the bulk rock are calculated using the Voigt-Reuss-Hill (VRH) average scheme (Hill, 1952):

$$M_B = \frac{1}{2} \left[ \left( \sum_{i=1}^n w_i / M_i \right)^{-1} + \sum_{i=1}^n w_i M_i \right]$$
 (2.12)

where  $M_i$  and  $w_i$  are the moduli of the phases present and their volumetric fractions.

In addition, the methodology considers the anelastic effects when calculating seismic velocities. The correction of the effects is important because its sensitivity to the temperature and compositional heterogeneities (Cammarano et al., 2003; Afonso et al., 2008). The anelastic effects are corrected as a function of grain size, oscillation period, temperature, and pressure (Kumar et al., 2020):

$$V_P = V_{P_0}(T, P) \left[ 1 - \frac{2}{9} \cot(\frac{\pi \alpha}{2}) Q_S^{-1} \right]$$
 (2.13)

$$V_S = V_{S_o}(T, P) \left[ 1 - \frac{1}{2} \cot(\frac{\pi \alpha}{2}) Q_S^{-1} \right]$$
 (2.14)

$$Q_S^{-1} = A \left[ T_o d^{-1} \exp\left(\frac{-E + VP}{RT}\right) \right]^{\alpha}$$
 (2.15)

where  $Q_P=\frac{9}{4}Q_S$  is assumed.  $V_{P_o}(T,P)$  and  $V_{S_o}(T,P)$  are the anharmonic seismic velocities at a given temperature and pressure for a given chemical composition, A, E, and  $\alpha$  are empirical parameters proposed by Jackson and Faul (2010), and A =  $816~s^{-\alpha}\mu m^{-\alpha}$ ,  $\alpha=0.36$  is the frequency dependence factor,  $E=293~{\rm kJ/mol}$  is the activation energy,  $V=1.2~{\rm x}~10^{-5}~{\rm m}^3/{\rm mol}$  is the activation volume, and R is the universal gas constant. Based on the optimal results from Kumar et al. (2020), I adopt a grain size of  $d=10~{\rm mm}$  and an oscillation period of  $T_o=75~{\rm s}$ .

#### 2.2.7. Elevation

According to the principle of isostasy, regions of the Earth with the same elevation are expected to exhibit the same buoyancy when referred to a common compensation level. In the case of the lithosphere and sublithospheric mantle, the approach commonly assumes that the compensation level is situated at a depth of 400 km (Afonso et al., 2008; Kumar et al., 2020). Selecting a global compensation level at this depth has two advantages: (1) it encompasses the entire spectrum of estimated lithospheric thicknesses, and (2) there is no requirement to adjust the calibration constants for different geographic regions.

In order to estimate the absolute elevation, the approach incorporates a reference column that represents a thermally stable oceanic lithosphere and the underlying sublithospheric mantle. The rationale behind selecting a thermally stable oceanic lithosphere is its relatively simpler relationship between temperature, pressure, and composition, compared to actively spreading mid-ocean ridges where complexities arise from factors like melt content and transient buoyancy sources (Kumar et al., 2020). Then the calculation of absolute elevation involves the following equations:

$$E_a = \int_{L_{top}}^{L_{bottom}} \frac{\rho_b - \rho_l(z)}{\rho_b} dz - \Pi$$
 for elevation > 0, above sea level (2.16)

$$E_b = E_a \frac{\rho_b}{\rho_b - \rho_w}$$
 for elevation < 0, below sea level (2.17)

where  $L_{top}$  and  $L_{bottom}$  are the top and bottom of the column,  $\rho_b$  is the density of the mantle at 400 km depth and  $\rho_l$  is the depth-dependent density of the column, and  $\rho_w$  is the seawater density.  $\Pi$  is a calibration constant which depends on the average density and the elevation of the reference column (Kumar et al., 2020).

#### Flexural isostasy

The lithosphere can also behave as an elastic plate floating over a viscous material, the asthenosphere. Then, the lithospheric plate is flexing under vertical loading and can be considered as an elastic plate with an effective elastic thickness. I account for the rigidity of the lithosphere to calculate the lithostatic equilibrium or flexural isostasy, and the resulting elevation.

To determine the flexural elevation, the first step is to calculate the lateral variations in lithostatic pressure at a compensation level based on the lithospheric structure derived from potential fields, following the procedure described in Jiménez-Munt et al. (2010). The vertical displacement (deflection) w for each column required to compensate these pressure variations, are calculated changing the elastic thickness values  $T_e$  between 0 (representing local isostasy) to 35 km, which is the expected value for the region (Faccenna et al., 2014). According to the elastic thin plate approach, the deflection of the lithosphere in response to vertical lithostatic pressure variations can be described as follows (Garcia-Castellanos et al., 1997; Watts, 2001):

$$D\frac{d^4w(x)}{dx^4} + (\rho_a - \rho_w)gw(x) = q(x) - \overline{q}$$
 (2.18)

$$D = \frac{ET_e^3}{12(1-v^2)} \tag{2.19}$$

where x is the position along the profile, D is the rigidity of the lithosphere, g is the gravitational acceleration,  $\rho_a$  and  $\rho_w$  are the densities of the asthenosphere and seawater,

respectively, q-  $\bar{q}$  is the lithostatic pressure anomaly (relative to the mean pressure along the transect), E is Young's modulus, v is the Poisson ratio and  $T_e$  is the lithospheric elastic thickness (assumed constant along the profile).

The pressure anomalies are calculated from a lithospheric geometry which incorporates the measured bathymetry; therefore, the calculated deflection should be small in amplitude and induce small changes in bathymetry along the section.

#### **Dynamic topography**

The flexural elevation is mainly based on the principle of flexural isostasy. However, this principle ignores the dynamic topography related to the convection of the mantle. The dynamic topography is the vertical deflection caused by viscous stresses generated by flow within the sublithospheric mantle (Braun, 2010; Section 2.1.3). Dynamic topography has been used to interpret the anomalous topography, including uplift and subsidence (e.g., Husson, 2006; Heller and Liu, 2016; Faccenna and Becker, 2020). In order to estimate the implications of deep mantle anomalies on the surface topographic evolution, I add a new post-processing calculation and develop a new code to obtain the present-day dynamic topography. The code uses 2-D finite difference and marker-in-cell methods to solve steady-state stokes equations in 2D Cartesian coordinate system, including the governing equations of conservation of mass, momentum, and the constitutive equations.

The conservation of mass equation (continuity equation) within incompressibility constraint is:

$$\frac{\partial v_x}{\partial x} + \frac{\partial v_z}{\partial z} = 0 {(2.20)}$$

where  $v_x$  and  $v_z$  are velocities in the horizontal x and vertical z directions, respectively. The conservation of momentum equations (Stokes equations) are:

$$\frac{\partial \sigma'_{xx}}{\partial x} + \frac{\partial \sigma'_{xz}}{\partial z} = \frac{\partial P}{\partial x}$$
 (2.21)

$$\frac{\partial \sigma'_{zx}}{\partial x} + \frac{\partial \sigma'_{zz}}{\partial z} = \frac{\partial P}{\partial z} - g\rho(C, P, T)$$
(2.22)

$$\sigma_{xx}' = \sigma_{xx} + P \tag{2.23}$$

$$\sigma_{zz}' = \sigma_{zz} + P \tag{2.24}$$

$$\sigma_{xz}' = \sigma_{xz} + P \tag{2.25}$$

where P is the dynamic pressure;  $\sigma_{xx}$ ,  $\sigma_{xz}$ , and  $\sigma_{zz}$  are the stress tensor components; g is the gravitational acceleration;  $\rho$  is the density of rocks that depends explicitly on pressure, temperature and chemical composition as explained in Section 2.2.5.  $\sigma'_{xx}$ ,  $\sigma'_{xz}$ , and  $\sigma'_{zz}$  are the deviatoric stress tensor components, with constitutive relations as follows:

$$\sigma'_{xx} = 2\eta_{eff} \dot{\epsilon}_{xx} \tag{2.26}$$

$$\sigma_{zz}' = 2\eta_{eff} \dot{\epsilon}_{zz} \tag{2.27}$$

$$\sigma'_{xz} = 2\eta_{eff} \dot{\epsilon}_{xz} \tag{2.28}$$

$$\dot{\epsilon}_{xx} = \frac{\partial v_x}{\partial x} \tag{2.29}$$

$$\dot{\epsilon}_{zz} = \frac{\partial v_z}{\partial z} \tag{2.30}$$

$$\dot{\epsilon}_{xz} = \frac{1}{2} \left( \frac{\partial v_x}{\partial z} + \frac{\partial v_z}{\partial x} \right) \tag{2.31}$$

where  $\dot{\epsilon}_{xx}$ ,  $\dot{\epsilon}_{xz}$ , and  $\dot{\epsilon}_{zz}$  are the strain rate components,  $\eta_{eff}$  is the effective viscosity that depends on the composition, pressure, temperature, and strain rate and it is controlled by a combination of creep diffusion and creep dislocation viscous flow laws (Hirth and Kohlstedt, 2003).

$$\eta_{eff} = \left(\frac{1}{\eta_{diff}} + \frac{1}{\eta_{disl}}\right)^{-1} \tag{2.32}$$

where  $\eta_{diff}$  and  $\eta_{disl}$  represent the viscosity for diffusion and dislocation creep respectively. They are calculated as

$$\eta_{diff \mid disl} = \frac{1}{2} A^{-\frac{1}{n}} d^{\frac{m}{n}} \dot{\epsilon}_{II}^{\frac{1-n}{n}} exp\left(\frac{PV_a + E_a}{nRT}\right)$$
(2.33)

where the index diff or disl denotes the creep mechanism (dislocation or diffusion). P and T are pressure and temperature, d is grain size, R is the gas constant, 8.314  $J \cdot K^{-1} \cdot mol^{-1}$ ,  $\dot{\epsilon}_{II} = \sqrt{\frac{1}{2}(\dot{\epsilon}_{xx}^2 + 2\dot{\epsilon}_{xz}^2 + \dot{\epsilon}_{zz}^2)}$  is the second invariant of strain rate tensor. And flow law parameters A is the pre-exponential factor, n is the stress exponent, m is the grain size exponent,  $V_a$  is the activation volume,  $E_a$  is the activation energy. They are determined from the laboratory experiments (Table 2.2, Hirth and Kohlstedt, 2003). In addition, the minimum and maximum viscosity limits at between  $10^{19}$  and  $10^{24}$  Pa·s (Negredo et al., 2020).

Table 2.2 Rheological parameters and viscosities used in this thesis

Symbol	Meaning	Sublithospheric mantle*		Crust	Lithospheric
		Dislocation	Diffusion	viscosity	<b>mantle</b> viscosity
A (Pa <sup>-n</sup> s <sup>-1</sup> )	Pre-exponential factor	2.28E-18	4.7E-16		
n	Stress exponent	3.5	1		
m	Grain size exponent	0	3	1E+21 Pa s	1E+22 Pa s
E (kJ/mol)	Activation energy	480	335		
V(10 <sup>-6</sup> m <sup>3</sup> /mol)	Activation volume	11	4		

<sup>\*</sup> Flow parameters from Hirth and Kohlstedt. (2003)

Therefore, the velocity field is determined based on the distribution of densities and viscosities within the model. Finally, the dynamic topography h is calculated from normal stresses at the surface as following:

$$h = \frac{\sigma_{zz \mid z=0}}{\delta \rho g} \tag{2.34}$$

where  $\sigma_{zz\,|\,z=0}$  is the normal stresses at the surface,  $\delta\rho$  is the density contrast between the crust and either air or water and g is the gravitational acceleration. The topography h calculated with the equation 2.34 is usually termed 'dynamic topography' in the literature (e.g., Braun, 2010; Davies et al., 2019). However, it is worth clarifying that it does not only reflect the convective mantle flow, but also all the buoyancy variations that arise from density contrasts (Figure 2.4 combination of panels a, b and c).

#### 2.3. Geophysical data

#### 2.3.1. Elevation

Elevation data (Figure 2.8) are compiled from topo\_19.1.img (Smith and Sandwell, 1997, updated 2019), which is a global elevation model with 1 × 1 min arc resolution. The northern Tyrrhenian Sea is characterized by a gentle bathymetry, with values ranging from 200 to 1000 m, that contrast with the southern region characterized by deep bathymetry (up to 3000 m) and several submarine mountains ranges, such as the Marsili Seamount (~-500 m), Vavilov Seamount (~-800 m), and Magnaghi Seamount (-1500 m). The northern Apennines reach up to 900 meters, with some peaks exceeding 2 km. The Central Apennines have the highest mean elevation (>1200 m) and the southern Apennines show a gradual decrease from 800 to 500 meters from west to east. The Adriatic Sea is bordered by coastal plains on both sides, with gentle slopes and low-lying terrain (~200 m). These plains are typically composed of sedimentary deposits and provide a transition between the sea and the adjacent land. The Pannonian Basin, a major flat area with an average elevation of around 100-200 meters, is surrounded by three different mountain ranges: Carpathian Mountains, with an average elevation of 1000-2000 m; the Dinarides (~2000 m) and the Alps (~3000 m).

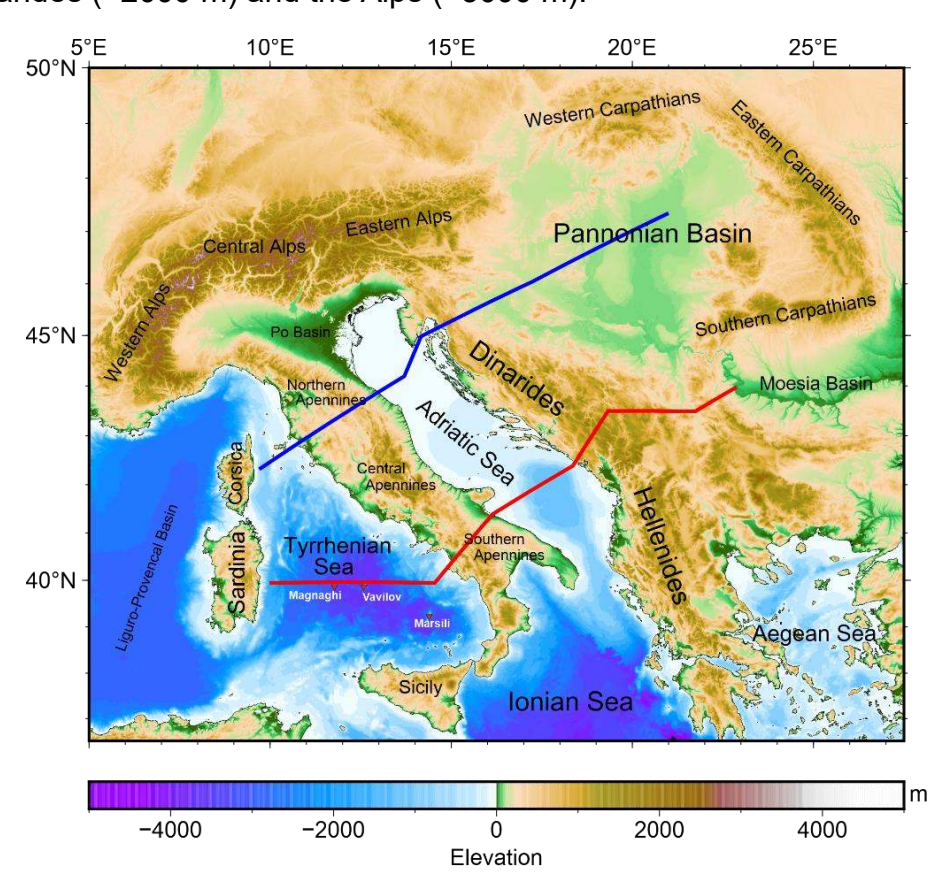


**Figure 2.8** Topography and bathymetry map of the study area. Elevation data comes from topo\_19.1.img (Smith and Sandwell, 1997, updated 2019). The blue and red lines show the locations of the northern and southern transects. Red trigangles show the location of three seamounts in the Tyrrennian Sea.

#### 2.3.2. Gravity anomaly

I use FA2BOUG software (Fullea et al., 2008) to calculate the Bouguer gravity anomaly map shown in Figure 2.9, applying a density reduction of 2670 kg/m³ and the complete Bouguer correction to the free-air gravity anomaly data of Sandwell et al. (2014, updated 2019). Stronger negative Bouguer anomalies are observed in higher altitude areas, such as the Alps, which have an anomaly of about -100 mGal, and in the Dinarides and the Apennines, with anomalies around -50 mGal. Positive anomalies are observed in the Tyrrhenian Basin (ranging from ~50 to ~300 mGal from north to south) and the southern Adriatic Sea (ranging from 0 to ~50 mGal from west to east). Additionally, the Pannonian Basin and the Po Basin are regions that exhibit relatively low gravity anomalies, with gravity values in these regions measured to be around 0 mGal.

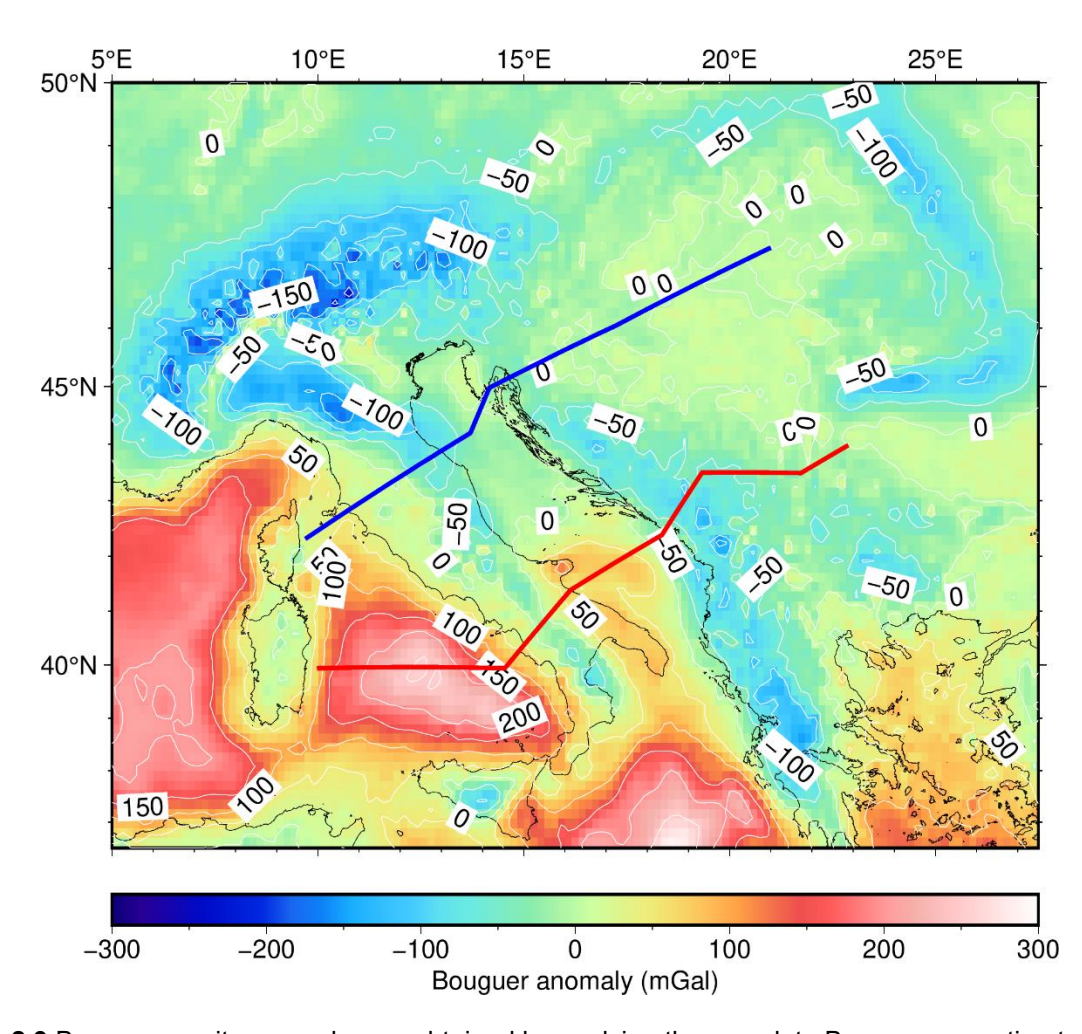


**Figure 2.9** Bouguer gravity anomaly was obtained by applying the complete Bouguer correction to the free air gravity anomaly data (Sandwell et al., 2014, updated 2019) using the software FA2BOUG (Fullea et al., 2008) with a density reduction of 2670 kg/m<sup>3</sup>. The blue and red lines show the locations of the northern and southern transects.

#### 2.3.3. Geoid

Geoid height data (Figure 2.10) are obtained from the global gravitational model GECO (Gilardoni et al., 2016), filtered up to degree and order 10, in order to capture geoid anomalies resulting from lateral density variations within the crust and upper mantle up to ~400 km depth. Across most of the study area, positive geoid values are observed, except in the Po Basin (about -1 m), the southern Adriatic Sea (~0 m), and the Ionian Sea (<-4 m). The orogenic belts, such as the Alps, the southern Apennines, and the southern Dinarides, are characterized by relative highs (above 8 m), while the northern Apennines and the northern Dinarides display values around 4 m. Moreover, the Pannonian Basin shows minimal values around 6 m. This distinctive feature reflects the complexity of the deep structure in the region.

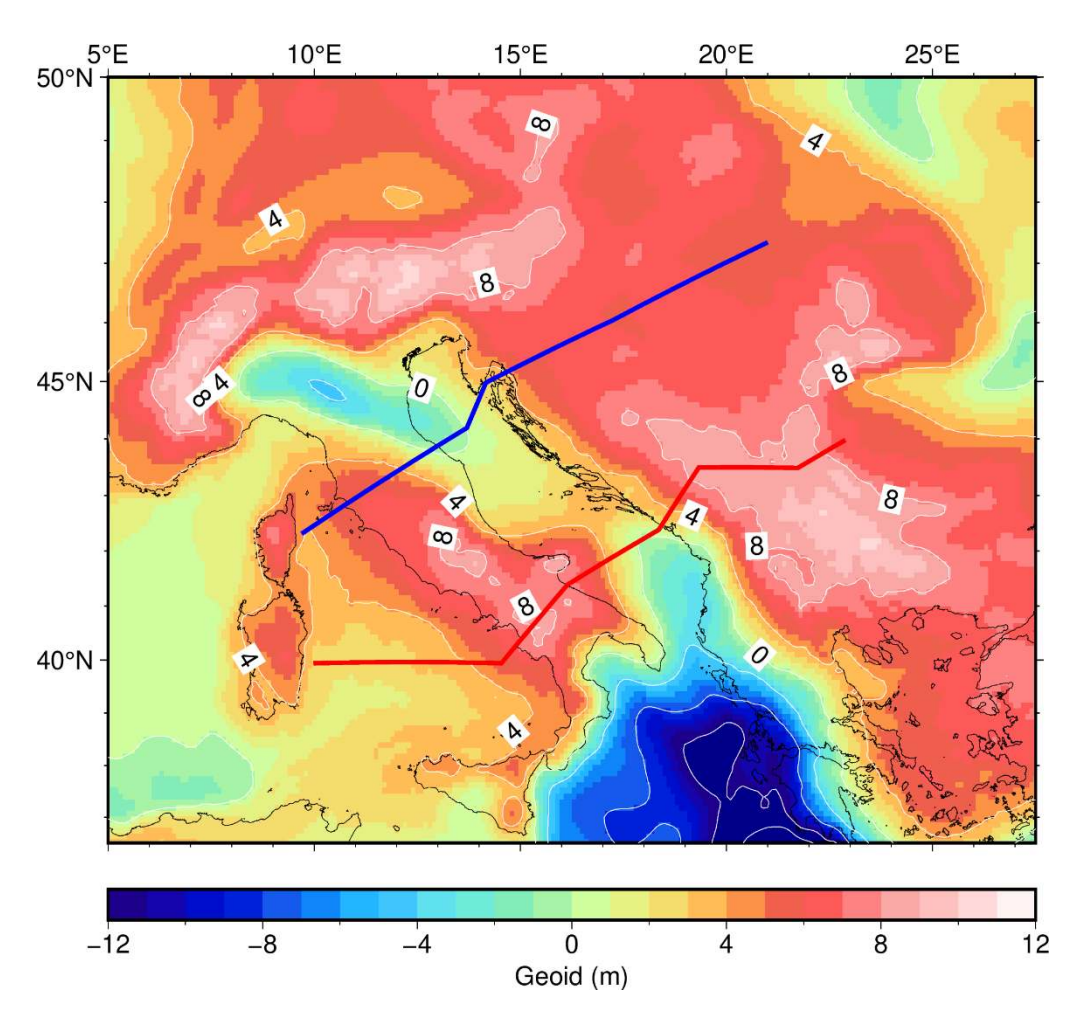


**Figure 2.10** Geoid height data were derived from the global gravitational model GECO (Gilardoni et al., 2016), filtered up to degree and order 10 for removing deep signals (>400 km). The blue and red lines show the locations of the northern and southern transects.

#### 2.3.4. Surface heat flow

Surface heat flow data (Figure 2.11) are compiled from the Global Heat Flow Database (Fuchs et al., 2021) and supplemented with data from the Italian National Geothermal Database (Trumpy and Manzella, 2017; Pauselli et al., 2019). The Tyrrhenian Sea and Tuscan domain are characterized by relatively high heat flow values, over 120 mW/m², which are likely related to the extension of the lithosphere associated with hotter mantle upwelling beneath the back-arc area (e.g., Tumanian et al., 2012). However, the External Apennine, the Adriatic Sea and Dinarides exhibit lower heat flow values ranging from 40 to 50 mW/m². The Pannonian Basin displays moderate heat flow values ranging from 60 to 80 mW/m². The heat flow characteristics in the Pannonian Basin are influenced by the tectonic processes that have shaped the basin.

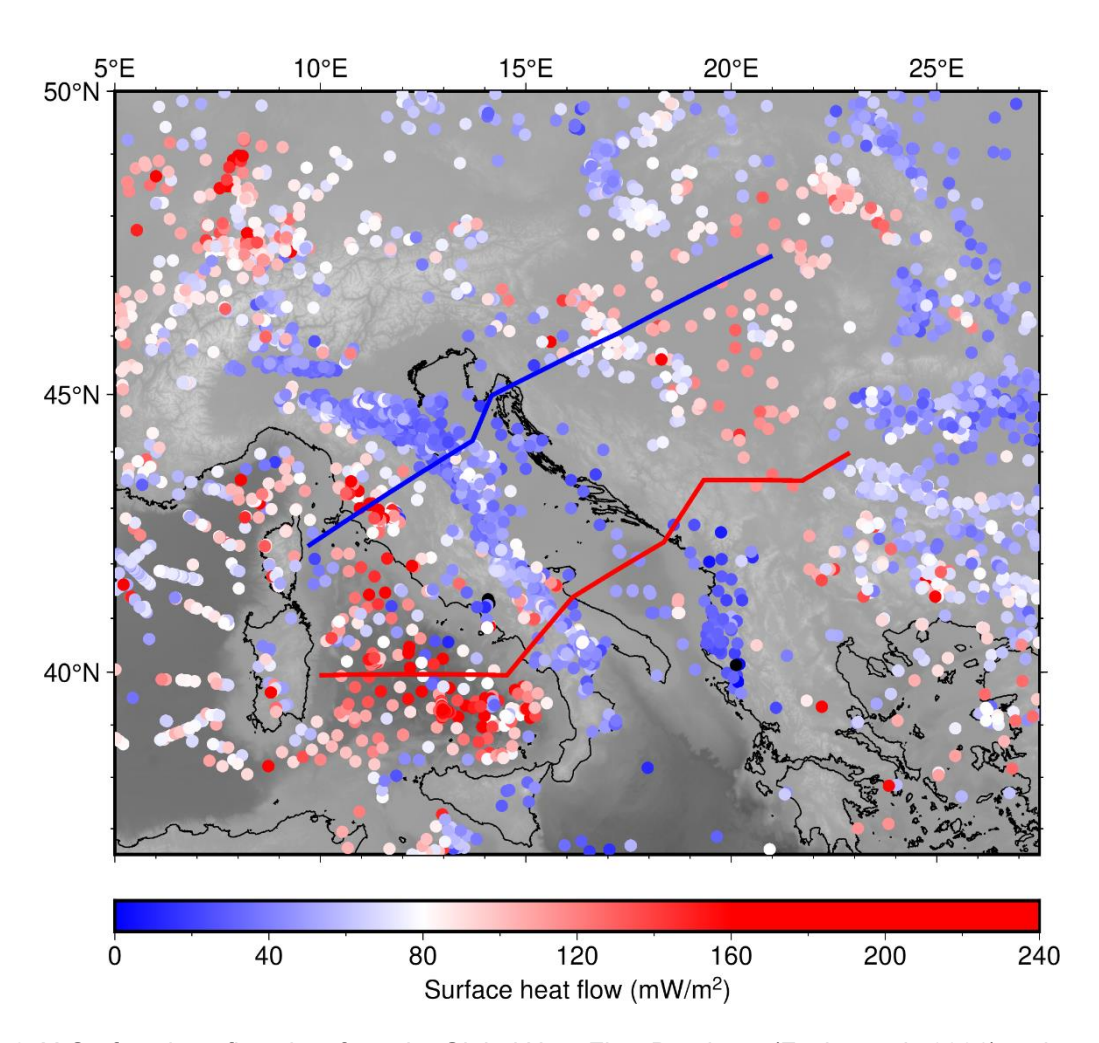


**Figure 2.11** Surface heat flow data from the Global Heat Flow Database (Fuchs et al., 2021) and completed with the Italian National Geothermal Database (Trumpy and Manzella, 2017; Pauselli et al., 2019). The blue and red lines show the locations of the northern and southern transects.

#### 2.3.5. Mantle seismic velocities

Mantle seismic velocities, based on seismic tomography, are usually considered the most powerful indicator to explore the structure of the upper mantle. Several seismic tomographic models have been developed in the study area over the last 25 years. Here I select seven representative global/regional tomography models (Figure 2.12) based on body waves (Amaru, 2007; Piromallo and Morelli 2003; Paffrath et al., 2021; Rappisi et al., 2022), surface waves (El-Sharkawy et al., 2020; Belinić et al., 2021) and both of them (Zhu et al., 2015). Horizontal cross-sections at lithospheric depth (about 100 and 300 km) of these tomographic models are shown in Figure 2.12, using the same color palette for facilitating their comparison.

Piromallo and Morelli (2003) showed the P-wave tomographic model of the Alpine-Mediterranean region, also called PM0.5. They imaged distinct velocity anomalies between the northern and southern Apennines in the top 200 km: A noticeable high-velocity anomaly in the northern, while a slow anomaly at these depths in the southern. These anomalies eventually combine into a single-continuous fast anomaly belt under 250 km. Along the Dinarides, a fast velocity anomaly can be identified, extending to a depth of 300 km in the southern Dinarides. Below the Calabrian Arc in the south, a fast velocity anomaly reappears in shallow layers (100–200 km depth). Additionally, a shallow slow anomaly is observed on the Tyrrhenian Sea, corresponding to the back-arc region, interpreted as evidence of asthenospheric upwelling.

Amaru (2007) presented a global P-wave velocity anomaly model, also known as UU-P07. Her results indicated the presence of a positive velocity anomalies in the upper mantle below the Alps, north Adriatic Sea, Apennines and Dinarides with various configurations. In contrast, lower velocity anomalies were observed in the upper mantle beneath the Pannonian Basin and the Tyrrhenian Sea. The high velocity anomaly beneath the Apennines exhibits a continuous body in the northern and discontinuous body in the southern region, and both reach the transition zone.

Zhu et al. (2015) presented P and S wave velocity and anisotropy of the European upper mantle based on joint tomography. They imaged a continuous belt of fast P and S velocities beneath the Alps, Adriatic region, and Hellenides extending to depths of 200 km. However, this continuous belt diminishes at greater depths, except in the Hellenic arc, where the subducting slab remains visible deep into the lower mantle. Deeper than 250 km, a distinct localized fast wave speed anomaly is observed in association with the Calabrian arc. Conversely, most parts of the Tyrrhenian Sea and Pannonian Basin are characterized by negative seismic velocity anomalies. Their anisotropic features indicated

horizontal upper mantle flow under the European continent and vertical mantle flow under subduction zones like the Apennines and the Hellenic arc.

El-Sharkawy et al. (2020) employed a high-resolution model of shear wave velocity in the Mediterranean upper mantle. A prominent fast-velocity anomaly is imaged beneath the northern Apennines and the southern Po Basin extending from 50 km to 250 km. In the central Apennines, there is a low-velocity anomaly from 70 km down to about 250 km, named by the Central Apenninic Slab Gap. At a depth of 250 km, a fast-velocity anomaly is detected below the central Apennines. In addition, a narrow, shallow, and northeast-dipping high-velocity anomaly is observed along the entire Dinarides. However, the depth extent of this anomaly varies: it reaches approximately 150 km in the northern and central Dinarides but extends to depths of 300 km in the southern Dinarides.

Belinić et al. (2021) showed a new shear-wave velocity structure focusing on the Dinarides. They imaged a high-velocity anomaly reaching depths of 160 km beneath the northern Dinarides and more than 200 km beneath the southern regions. The observed NE dipping fast anomalies in the northern region extend underneath the entire Dinarides fold-thrust belt, indicating the sinking of cold and rigid material of the Adria microplate. They interpreted low velocity zones under the southwestern Pannonian Basin and beneath the central part of Adria as results of lithospheric thinning and/or upwelling of hot asthenospheric material.

Paffrath et al. (2021) presented a P-wave travel-time tomography focusing on the greater Alpine area. The model came from AlpArray seismological network (Hetényi et al., 2018) and has been used to interpret the deep structure in the Alps region (Handy et al., 2021). This model is not covering the southern Apennines, Adriatic Sea and Dinarides. They also showed evidence that slabs in the Alps and northern Apennines have been partly to entirely detached from the orogenic edifices.

Rappisi et al. (2022) presented the 3D anisotropic P-wave tomography model of the upper mantle in the Central Mediterranean. A prominent high-velocity feature is observed extending along the Apennines. At shallow depths (<200 km), it is divided into northern and southern segments by a low velocity anomaly in the central Apennines. The segments are merged at greater depths (>150 km). These segments together with the Calabrian fast anomaly form a single, hook-shaped high-velocity belt that extends throughout the Italian peninsula, dipping towards the Tyrrhenian Basin. This high-speed belt can be traced to depths of up to 600 km. In addition, there is an elongated Dinaric fast anomaly running from the eastern Alps to Greece, following the trend of the Dinarides, extending from 50 to about 300 km.

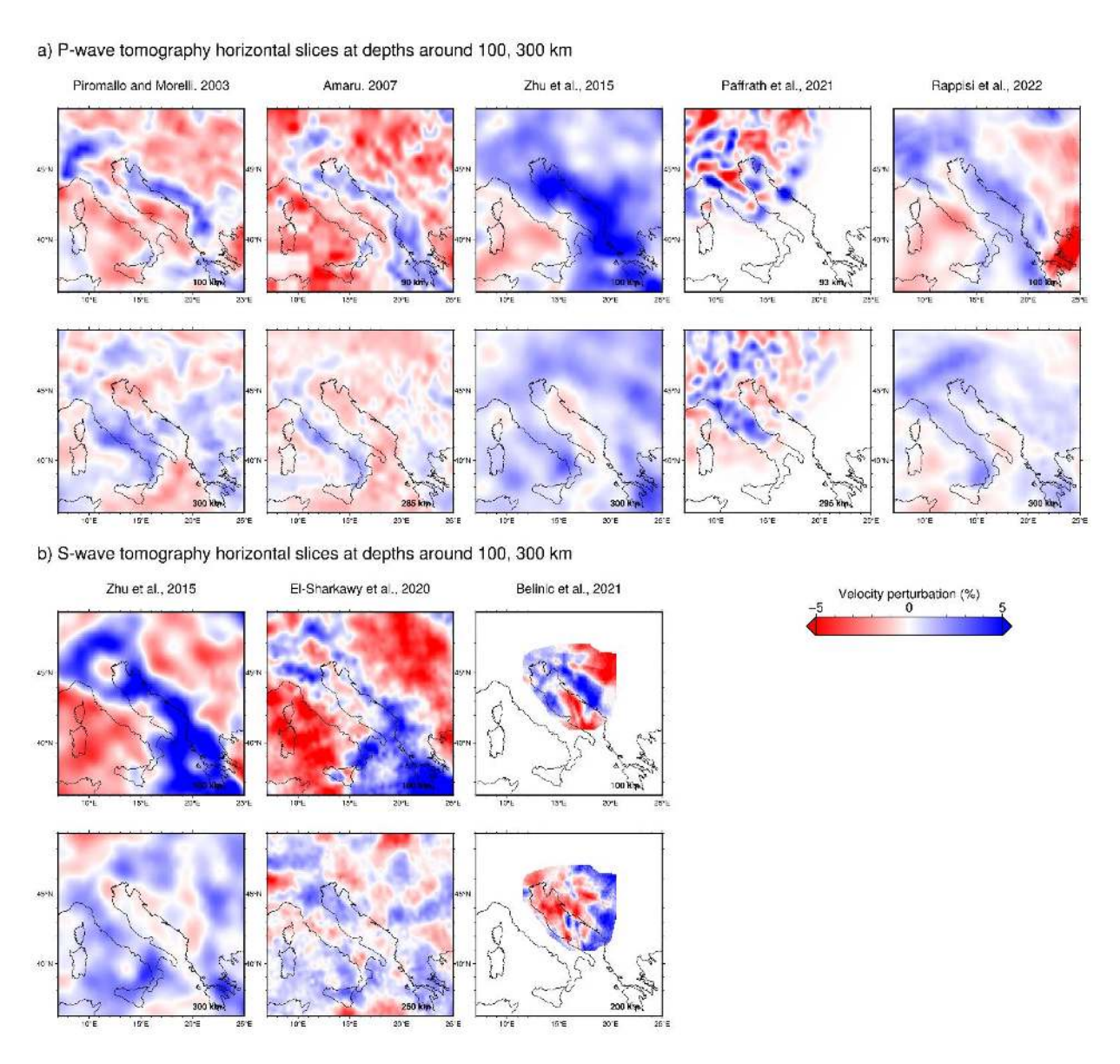


**Figure 2.12** Horizontal cross-sections of representative P and S wave tomographic models at depths of 100 km and 300 km within the upper mantle. All the images use the same color palette, which represents the velocity perturbation with respect to the reference model.

## Chapter 2. Fundamentals and Methodology

## **CHAPTER 3**

# Geophysical-Petrological Model of the Crust and Upper Mantle Beneath the Northern Apennines and Dinarides Orogenic Systems



## Chapter 3. Geophysical-Petrological Model of the Crust and Upper Mantle Beneath the Northern Apennines and Dinarides Orogenic Systems

In this Chapter, I present the crust and upper mantle structure (down to 400 km depth) along a ~1000 km transect, crossing in a SW-NE direction the northern Tyrrhenian Sea, the northern Apennines, the Adriatic Sea, the Dinarides and the Pannonian Basin (Figure 3.1). I model the temperature, density and seismic velocity distribution (i.e., chemical composition) along the transect by combining surface geology, elevation, bouguer anomaly, geoid height, surface heat flow and mantle xenoliths data. I apply the integrated geophysical-petrological modeling tool, LitMod2D\_2.0, described in Chapter 2. The tectonic setting of the region and data used are described in Chapters 1 and 2, respectively.

The crustal and lithospheric structures obtained in this study are compared with previous interpretations and discussed in terms of the geodynamic evolution of studied tectonic domains within the complex and long-term evolving Alpine-Mediterranean mobile belt. Lastly, the contribution of deep geodynamic processes in the build-up of present orogenic topographic relief is discussed.

### Results from this chapter have been published as:

Zhang, W., Jiménez-Munt, I., Torne, M., Vergés, J., Bravo-Gutiérrez, E., Negredo, A. M., Carminati, E., García-Castellanos, D., & Fernàndez, M. (2022). Geophysical-Petrological Model for Bidirectional Mantle Delamination of the Adria Microplate Beneath the Northern Apennines and Dinarides Orogenic Systems. Journal of Geophysical Research: Solid Earth, 127(12), e2022JB024800. https://doi.org/10.1029/2022JB024800

### 3.1. Crustal structure from previous studies

During the last three decades, a large amount of geologic and geophysical investigation has been carried out to image the crustal structure of the study region (Figures 1.3, 3.1 and 3.2). Along the transect, geophysical data come from deep nearvertical reflection (e.g., Scrocca et al., 2003) and wide-angle reflection/refraction seismic experiments (e.g., Cassinis et al., 2005), seismic receiver functions (RF) analyses (e.g., Mele and Sandvol, 2003) and gravity modeling (e.g., Sumanovac, 2010). Additional data come from seismicity distribution at crustal and subcrustal levels (e.g., Chiarabba et al., 2004; De Luca et al., 2009). These studies show that shallow seismicity is mainly concentrated along a narrow band along the backbone of the Apennines while a diffuse activity characterizes the Adriatic region. At crustal levels, focal mechanisms evidence normal faulting below the central part of the Apennines belt and thrust/reverse faulting mechanisms at the outer fronts of the Apennines (e.g., De Luca et al., 2009; Chiarabba et al., 2014). Seismicity between 25 and 70 km is widespread in the Adriatic region with a tendency to cluster below the Apennines while no deep earthquakes were recorded below the Tyrrhenian Sea (profile E-F in Figures 8 of De Luca et al., 2009). The west dipping seismicity, registered down to 70 km depth, is interpreted as the evidence of the subduction of the Adriatic lithosphere beneath the Apennines (De Luca et al., 2009).

Figure 3.1 shows the location of the transect and previous studies about the crustal structure, which are projected onto the transect. In the Tyrrhenian basin, the crustal structure is constrained by the CROP line M-12A, while the onshore CROP 03 was used to constrain the crustal geometry of the Apennines and the western region of the Adriatic Sea (Barchi et al., 1998, 2006; Liotta et al., 1998; Finetti et al., 2001; Pauselli et al., 2006; Piana Agostinetti et al., 2011; Piana Agostinetti and Faccenna, 2018). In the Adriatic Sea I used the results of the CROP M-16 seismic line (Finetti et al., 2001; Finetti, 2005) and seismic cross-sections from Fantoni and Franciosi. (2010). For the Dinarides and the western Pannonian Basin, I used the Alp07 profile (Šumanovac et al., 2016) and the earthquake tomography analysis of Kapuralić et al. (2019). In addition to these profiles, I also projected onto the transect (Figure 3.2) the Moho depth data from EUNAseis (Artemieva and Thybo, 2013), CRUST1.0 (Laske et al., 2013) and EPcrust (Molinari and Morelli, 2011) models and the Eurasian Moho data set of Tesauro et al. (2008) and Grad et al. (2009). For the Dinarides and Pannonian Basin, additional information comes from seismicity distribution (e.g., Kuk et al., 2000 and Bondár et al., 2018, respectively).

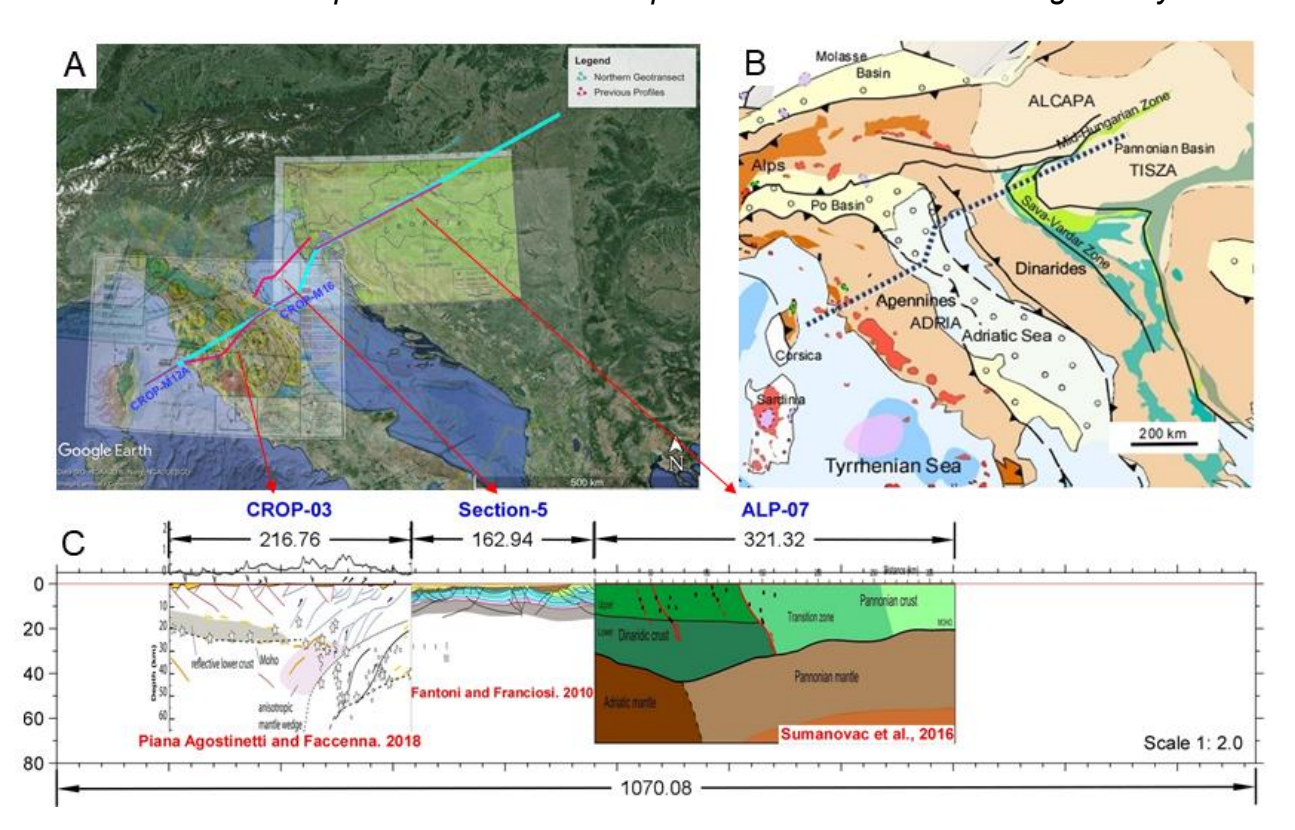


**Figure 3.1** Location of the northern transect and previous studies on the crustal structure. A: Topographic map from Google Earth with the location of the transect (Cyan solid line) and previous works (Red solid lines); B: Tectonic map (from Figure 1.4) with the location of the transect (black dash line). C: Crustal structure along the transect from previous studies, including CROP 03 (Piana Agostinetti and Faccenna, 2018), seismic section 5 (Fantoni and Franciosi, 2010) and Alp07 (Šumanovac et al., 2016). The section 5 is projected onto the northern transect. Vertical scale is exaggerated 2 times with respect to the horizontal scale.

There is agreement on the broad features of the crustal structure; however, important discrepancies arise when entering into the details of its internal structure and density distribution. All studies agree that the Moho lies at shallow depths (20-25 km) in the Tyrrhenian Sea and below western Italy, at intermediate depth (30-35 km) along the Adriatic coast, deepening under the Apennines (down to 50 km) and Dinarides (down to 45 km) mountain belts (Figure 3.2; e.g., Molinari et al., 2015; Kapuralić et al., 2019; Stipčević et al., 2020). In the Apennines, the complex internal crustal structure, the possible presence of a mantle wedge and the top of the subducting slab are reflected in the RFs results where differences in the Moho depth may be as large as 30 km from one study to another (Mele and Sandvol, 2003; Chiarabba et al., 2014; Piana Agostinetti and Faccenna, 2018). Major discrepancies are also observed in the interpretations of multichannel seismic reflection profiles about the internal structure of the crust and the exact location and geometry of the top of the subducting slab (Figure 3.2). Finetti et al. (2001), based on the interpretation of onshore CROP-03 profile, favor a complex thrust

system with thrust faults and shear planes that extend at low angle from the crust to the upper mantle offsetting the Moho. These authors also favor a westward location of the top of the subducting slab, compared to the location proposed by Pauselli et al. (2006) and Piana Agostinetti and Faccenna (2018) who place it right below the External Apennines (Figure 3.1 and 3.2). This latter interpretation is more in line with RFs and seismicity results of Mele and Sandvol (2003) and Chiarabba et al. (2014, 2020).

Receiver functions and seismic tomography indicate that beneath the Internal Apennines the shallowest mantle is characterized by about 5% lower shear wave velocity anomaly and 3% higher Vp/Vs ratio than the reference values for these depths (Chiarabba et al., 2020). These authors interpreted these anomalies as mantle upwelling with the presence of melts at the base of the crust, extending from the Tyrrhenian to the central Apennines. Below the Dinarides, Kapuralić et al. (2019) using local earthquake tomography inferred Moho depths between 40 and 45 km, similar to those obtained by Šumanovac et al. (2016) using RFs. A quite flat Moho around 25 km depth is observed underneath the back-arc Pannonian Basin (Šumanovac et al., 2016; Kapuralić et al., 2019). From local earthquake tomography, Kapuralić et al. (2019) found high velocities below the northern Dinarides at depths shallower than 10 km, but low velocities in the Pannonian Basin associated with a deep local depression. They also imaged a high-velocity body at 5-15 km depth between the Dinarides and the Pannonian Basin. The Dinaridic crust has been interpreted as two-layered, while the Pannonian crust is interpreted as single-layered (Šumanovac et al., 2016; Kapuralić et al., 2019).

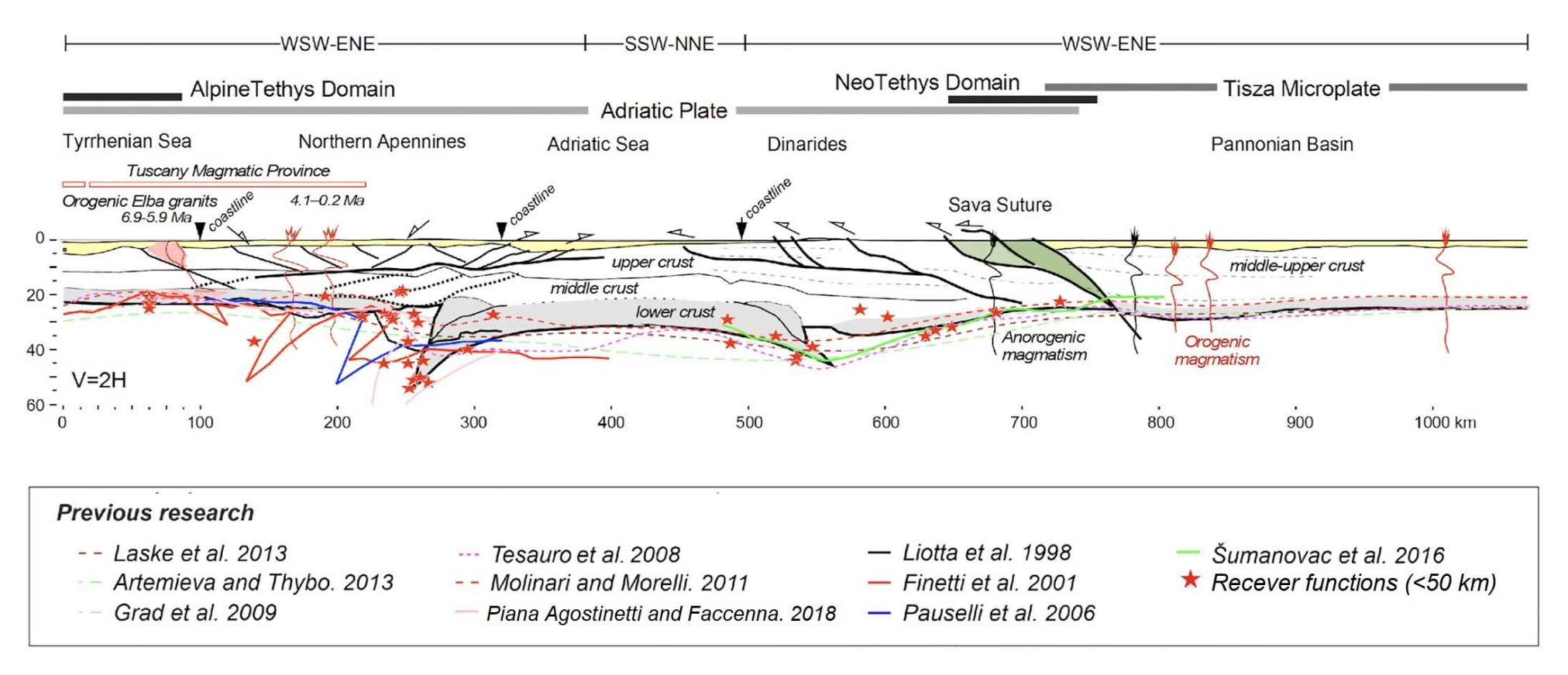
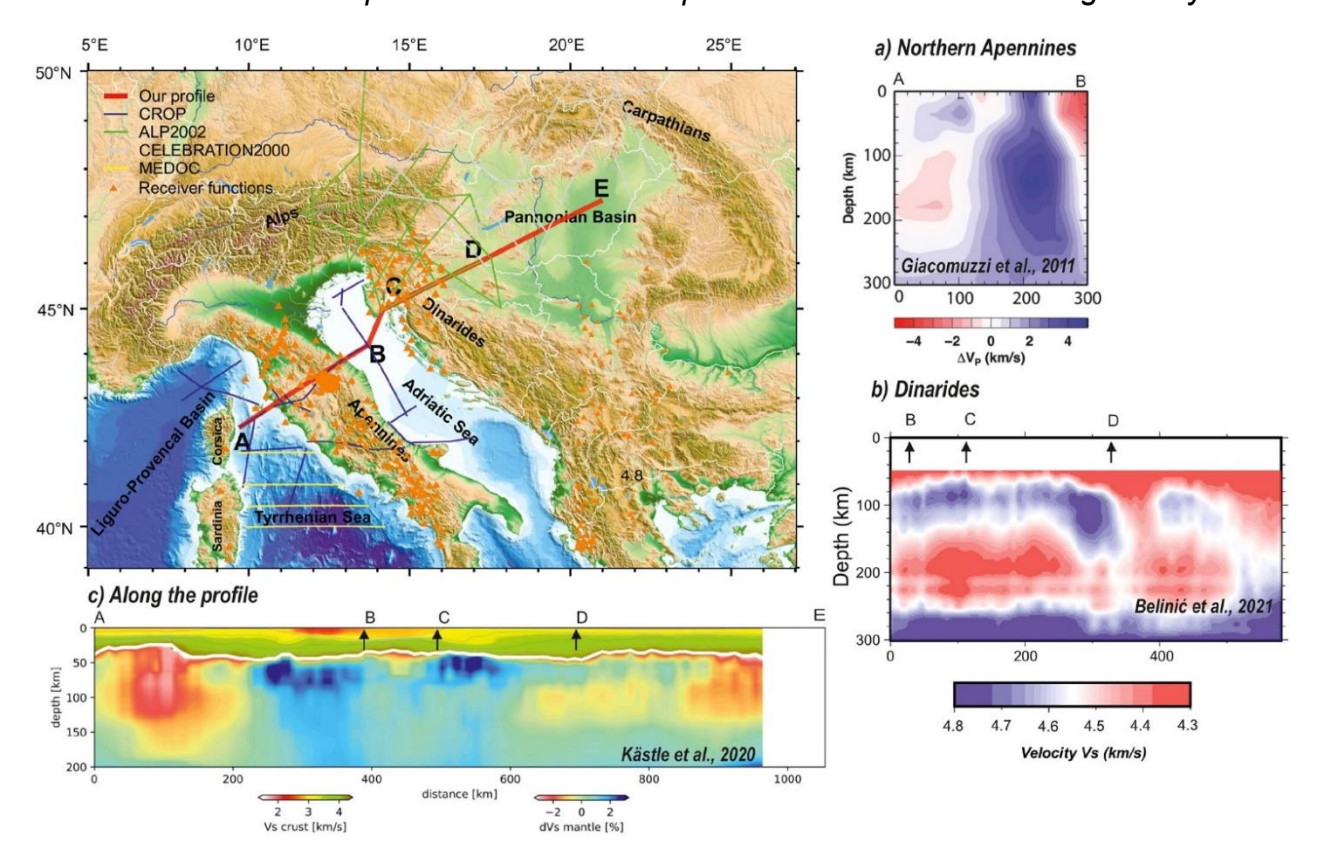


Figure 3.2 Crustal structure from the best fitting model constrained from the available geological and geophysical information listed in the text and in the panel legend. Yellow color is the sediment layer. Moho depths from previous studies and receiver functions (Mele and Sandvol, 2003; Piana Agostinetti and Amato, 2009; Chiarabba et al., 2014; Šumanovac et al., 2016; Piana Agostinetti and Faccenna, 2018; Diaferia et al., 2019; Stipčević et al., 2020) are shown for comparison. See Figure 3.1 for location.

### 3.2. Mantle characterisation from previous studies

In the study area a number of RF studies have focused on the LAB (Geissler et al., 2010; Miller and Piana Agostinetti, 2012; Belinić et al., 2018). Tomography, mainly based on teleseismic body-wave (e.g., Lippitsch et al., 2003; Piromallo and Morelli, 2003; Koulakov et al., 2009), P and surface wave tomography (e.g., Giacomuzzi et al., 2011; Kästle et al., 2018, 2022; El-Sharkawy et al., 2020; Belinić et al., 2021) and full-wave inversion of body and surface waves (e.g., Zhu et al., 2015; Beller et al., 2018; Blom et al., 2020) have provided images of the upper mantle down to the transition zone (Figure 2.12 and 3.3). All of them show strong lateral heterogeneities, where the different depths of the discontinuities, and the various shapes and lengths of the imaged slabs highlight the complexity of the region. Although comparison of tomography images is not forthright because mismatch in the location of the anomalies may be partly due to the different methods and sensitivities of the modeled wave types, the 3D structural complexity of the region adds a degree of uncertainty that is reflected in the variety of models proposed so far.

Comparison of available seismic LAB depths shows a high degree of variability between the main tectonic domains. Below the northern Apennines, Miller and Piana Agostinetti (2012), based on S-RFs, highlighted a complex lithospheric structure with two different S-velocity jumps, located at about 90 and 180 km depth. The shallowest one is interpreted as the LAB of the upper plate while the deepest jump is proposed to be associated with the LAB of the subducting lithosphere. This interpretation in terms of subducted/delaminated Adriatic lithosphere below the Apennines agrees with the location and distribution of the west-dipping seismicity down to about 70 km (e.g., Chiarabba et al., 2005; De Luca et al., 2009). Underneath the Dinarides discrepancies of the seismic LAB may reach up to 20 km, from 120 to 100 km depth, shallowing up toward the Adriatic Sea (90 km depth) and Pannonian Basin, where the LAB is placed at a rather constant depth of 70 km (e.g., Belinić et al., 2018). These studies also highlight the variability of the LAB depth encountered along the Dinarides, with deep LABs in the northern and southern regions (100-120 and 90 km depth, respectively) that contrast with the much shallower LAB (~50 km depth) in the central Dinaric region (Šumanovac et al., 2017; Belinić et al., 2018).



**Figure 3.3** Upper mantle characterization from previous studies. (a) P-wave teleseismic tomography from Giacomuzzi et al. (2011). (b) Shear-wave velocity structure beneath the Dinarides from the inversion of Rayleigh-wave dispersion after Belinić et al. (2021) that have been used to constrain the sub-continental lithospheric mantle anomaly (SCLM) below the Dinarides. (c) Crustal S-wave velocity, Moho depth (white line) and mantle Vs anomaly from Kästle et al. (2020) model along the transect.

As mentioned, tomography images differ substantially depending on the methods used (see Figure 2.12). While global models (e.g., Amaru, 2007 or Zhu et al., 2015) are not conclusive due to their low resolution, regional and local models show a high variability with the presence of subducted slabs, attached slabs of variable lengths and detached slabs (Blom et al., 2020; El-Sharkawy et al., 2020). These studies, based on a high-resolution shear-wave velocity model, find the presence of slab segments in the northern Apennines, beneath the Dinarides and in the central Alps. Below the Apennines, Hua et al. (2017), based on P-wave anisotropic tomography, image a vertically oriented slab extending down to ~300 km, a result that is coincident with that obtained by Benoit et al. (2011), who combined teleseismic P- and S-wave arrival time data. Studies based on P-wave teleseismic tomography find that the slab reaches depths of 400-500 km (Giacomuzzi et al., 2011) and 350-400 km (Spakman and Wortel, 2004; Hua et al., 2017). This result is coincident with that obtained by Koulakov et al. (2015), who, based on bodywaves analysis, find a steeply dipping high-velocity anomaly down to 400 km, that they interpret as composed of the continental lithospheric mantle of Adria. Overall, these

studies image shallower slab depths than previous models with less resolution (e.g., Lucente et al., 1999; Piromallo and Morelli, 2003), which predicted that the slab penetrates well into the transition zone.

Inversion of Rayleigh-wave dispersion by Belinić et al. (2021) shows a high-velocity anomaly reaching depths of 160 km beneath the northern Dinarides and more than 200 km beneath the southern regions (Figure 2.12b). These results differ slightly from those obtained by Šumanovac and Dudjak (2016) and Šumanovac et al. (2017), who, based on teleseismic tomography, conclude that in the northern Dinarides the pronounced fast anomaly reaches 250 km depth. The observed NE dipping fast anomalies in the northern region extend underneath the entire Dinarides fold-thrust belt, indicating the sinking of cold and rigid material of the Adria microplate. Belinić et al. (2021) imaged low velocity zones under the southwestern Pannonian Basin and beneath the central part of Adria, which they interpreted as results of lithospheric thinning and/or upwelling of hot asthenospheric material.

### 3.3. Results

Here, I summarize the main results of the crustal structure (Table 3.1 and Figure 3.2) and the physical properties of the lithospheric and sublithospheric mantle resulting from the best fit model (Figures 3.4 and 3.5). The obtained lithospheric model is defined by a series of crustal and mantle bodies, with the crustal physical parameters and the chemical composition of the mantle shown in Tables 3.1 and 3.2, respectively. The boundaries of the mantle domains shown in Figure 3.4f must be understood as transitional (with physical properties changing gradually) and not abrupt, as drawn for simplicity in the figure.

### 3.3.1. Crustal structure

Figure 3.2 shows the modeled crustal structure, which has been constrained by available seismic data and geological-cross sections and slightly modified to match the surface observables, after modifying the geometry and composition of the less constrained mantle bodies. Modifications of the crustal structure are always within the uncertainties of available data. Crustal density values have been taken from previous gravity modeling (Šumanovac, 2010) and calculated by empirical velocity-density relationships (Brocher, 2005), considering the crustal velocity models (e.g., Kapuralić et al., 2019; Molinari et al., 2015). Thermal conductivities and radiogenic heat production come from previous studies (e.g., Norden and Förster, 2006; Trumpy and Manzella, 2017)

### Chapter 3. The Northern Apennines and Dinarides Orogenic Systems

and from the global compilation by Vilà et al. (2010). Moreover, I consider specific thermal parameters for the Tuscany region and Internal Apennines, where SHF (Figure 3.4) shows high values probably related to active hydrothermal flow and magmatism, as indicated by the presence of active hydrothermal systems and recent volcanic and magmatic activity (e.g., Pandeli et al., 2013; Sani et al., 2016). I modeled the high SHF within the Tuscany Magmatic Province by high conductivity and radiogenic heat production, which correlates with a crust with magmatic intrusions and the presence of granitoids (Norden and Förster, 2006), cropping out and reached by drill holes in the area (e.g., Dini et al., 2005). In contrast, lower heat flow values (<60 mW/m²) are found in the Internal Apennines and Dinarides, whereas in the Pannonian Basin heat flow values are above 70 mW/m².

Table 3.1 Thermo-physical properties of the crustal tectonic units along the profile

Crustal Domains		Density (kg/m³)	Thermal conductivity (W/K m)	Radiogenic heat production (µW/m³)
	Sediment	2450	2.4	1
Adria Microplate	Elba granits	2750	3.1	3.5
	Apennines UC / Tuscany MP	2750-2800 (a)	2.7 / 3.1	1.3 / 3.8
	Apennines MC / Tuscany MP	2820	2.7 / 3.1	0.8 / 3.0
	Apennines LC / Tuscany MP	2920	2.1 / 3.1	0.6 / 1.0
	Dinarides UC-MC	2850	2.7	0.8
	Dinarides LC	2920	2.1	0.6
	Apennines / Dinarides duplicated LC	2950	2.1	0.6
Tisza Microplate	Sava Suture	2850	2.7	1.3
	Pannonian Basin UC	2750-2860 (a)	2.9	2
	Pannonian Basin LC	2950	2.1	0.6

*Note*. UC: Upper crust; MP: Magmatic Province; MC: Middle Crust; LC: Lower Crust. (a) Calculated as a function of pressure.

According to geological and geophysical information and the best fit of geophysical observables, I distinguish the Adria microplate, extending from the Tyrrhenian basin to the Dinarides, and the Tisza microplate, which in the modeled transect encompasses the western half of the Pannonian Basin. These two microplates are separated by the Sava Suture Zone (a remnant of the formerly intervening oceanic domain; Figures 3.2 and 3.4) and differ in their internal crustal structure and average densities.

The Moho lies at variable depths, deepening slightly from  $\sim \! 23$  km under the Tyrrhenian basin to  $\sim \! 25$  km under the Internal Apennines. The Moho depth in the External Apennines increases from ca. 35 km in the east to ca. 52 km in the west. Beneath the Adriatic Sea, the Moho remains at a rather constant depth (>30 km) deepening underneath the External Dinarides, where it is locally found at 45 km. East of the Sava Suture Zone, the Tisza microplate shows very little crustal thickness variation, with values decreasing from 30 km in the west to 25 km in the easternmost part of the Pannonian Basin.

In my favored model, three crystalline layers (Figure 3.2) characterize the crust of the Adria microplate. Crustal densities range from 2750 kg/m³ for the upper crust, 2820-2850 kg/m³ for the middle crust and 2920-2950 kg/m³ for the lower crust. However, I cannot rule out a two-layered crust, with upper-middle and lower crust with an average density of 2800 kg/m³ for the upper-middle part. These crystalline layers are covered by a sedimentary layer of variable thickness with an average density of 2450 kg/m³. In terms of crustal average density, within the Adria microplate I distinguish the Tuscany Magmatic Province with values ~2780 kg/m³ and the External Apennines, Adriatic Sea and Dinarides ~2830 kg/m³. The temperature at Moho depth is ~430 °C in the Adriatic Sea, gradually increasing with the crustal deepening below the Apennines (~700 °C) and the Dinarides (~500 °C). The Tuscany Magmatic Province is characterized by high temperatures at shallow levels with values around 100 °C at 2 km depth. The Moho temperature increases from 400 °C in the western part of the profile in the Tyrrhenian Sea to 530 °C in the Internal Apennines. These higher values in an area with thin crust are probably related to upwelling of hot sublithospheric material.

The modeled crustal structure of the Pannonian Basin is characterized by a two-layer crystalline crust, covered by a 4-6 km thick sedimentary layer (Figure 3.2). The upper-middle crust with an average density of 2750 kg/m³ extends down to 20 km depth, slightly deepening in its western termination. The lower crust is rather thin all along the basin (5 km) with an average density of 2950 kg/m³. Therefore, the average density of the crust in the Pannonian Basin is between 2790 and 2800 kg/m³. The model-predicted temperature at Moho levels beneath the Pannonian Basin varies from 500 °C in the west to 450 °C in

Figure 3.4 (see next page) Best fitting model. Surface observables (red dots): (a) Surface Heat flow, (b) Geoid height, (c) Bouguer anomaly and (d) absolute elevation, are projected onto the transect at 5 km sampling interval within a strip of 25 km half-width to account for lateral variations perpendicular to the strike. Standard deviations are shown as error bars. Blue and black lines show calculated values with and without sublithospheric anomalies, respectively. In (d) blue and black lines show thermal isostatic elevation (with and without mantle anomalies), and green lines are the calculated flexural elevation with elastic thickness  $T_e = 10$  km and dashed line  $T_e = 20$  km. Panel (e) shows the temperature distribution for the whole lithosphere. Panel (f) shows the density distribution within the lithospheric mantle along the modeled transect. See Figure 1.4 or 3.1 for location.

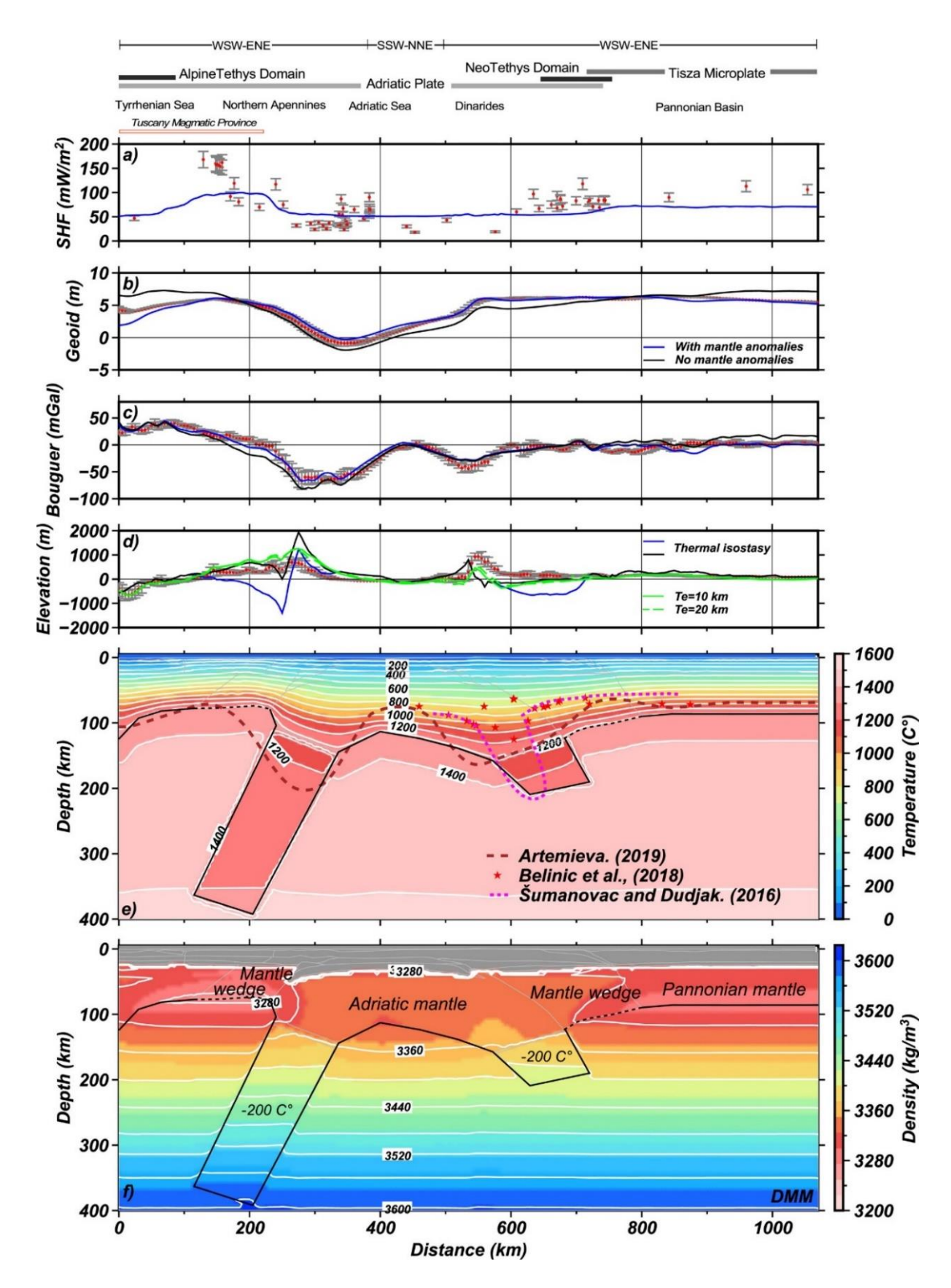
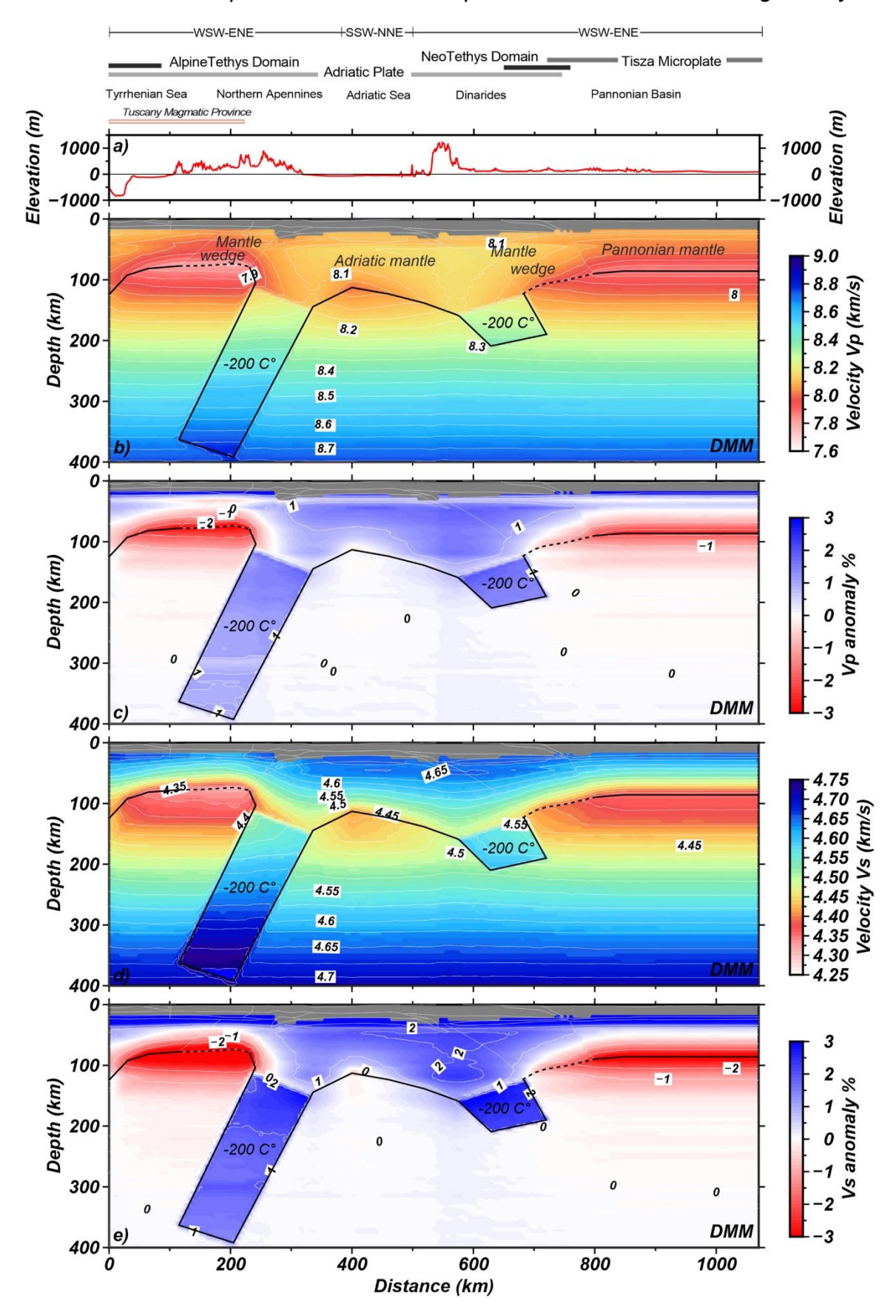


Figure 3.4 (see page 63)



**Figure 3.5** Mantle seismic velocities and synthetic seismic velocity anomaly along the transect. Panel (a) elevation profile, (b) and (d) absolute P- and S-wave velocities and (c) and (e) synthetic P and S-wave anomalies, respectively.

### 3.3.2. The LAB and upper mantle physical properties and composition

In the best fit model, I distinguish three lithospheric mantle compositions (Figure 3.4). Beneath the Adria microplate (Adriatic mantle, Table 3.2 and Figure 3.4f) the lithospheric mantle composition corresponds to a slightly depleted mantle (Tc 2 of Griffin et al., 2009) with a mean Mg# of 89.5. In the Pannonian Basin (Tisza microplate) the composition of the mantle is the same as obtained by Alasonati Tašárová et al. (2016) and Downes et al. (1992) from the analysis of 20 xenoliths (Pannonian mantle, Table 3.2 and Figure 3.4f). Its mean Mg# is 90.4, which indicates the presence of a fertile mantle. The densities and seismic velocities resulting from these two lithospheric mantle compositions are very similar (with maximum differences of ~10 kg/m<sup>3</sup> between densities and ~0.01 km/s for Vp and Vs). However, I preferred maintaining the distinction between these different compositions to highlight the different tectonic history between the Adria and Tisza microplates. The third lithospheric mantle composition used is a residual DMM-3% composition (Mantle wedge, Table 3.2 and Figure 3.4f) beneath the External Apennines, Dinarides and Sava suture zone. This composition is the residual composition after 3% aggregate meting from DMM (see Section 2.2.4). It accounts for the presence of a mantle wedge and potential melting of the depleted asthenosphere (DMM) following rollback of the western (hereinafter Apenninic) and the eastern (hereinafter Dinaric) segments of the Adriatic slab. The sublithospheric mantle has been modeled using the DMM composition of Workman and Hart (2005) that is a reference model for an average, non-melted, depleted MORB mantle (more details in Kumar et al., 2020).

The LAB along the Adria microplate domain (Figure 3.4) is shallow (about 75 km depth) underneath the Tyrrhenian and Tuscany extended terrains and deeper (125-150 km depth) between the External Apennines and the Dinarides. In contrast to the Adriatic domain, the Tisza domain is characterized by a rather flat LAB (~90 km), slightly deeper than the thermal LAB obtained by Artemieva (2019). Figure 3.4e compares the calculated LAB depth to the thermal LAB of Artemieva (2019) and to the S-RF and P-wave teleseismic LAB of Belinić et al. (2018) and Šumanovac and Dudjak (2016), respectively.

The resulting modeled densities and Vp and Vs seismic velocities for the assumed mantle compositions are shown in Figures 3.4 and 3.5. Under the same PT conditions, the density of the Adriatic mantle is slightly higher than that of the Pannonian mantle. Comparing the mantle density profiles of the Adriatic and Pannonian Basin I see that the density of the Adriatic mantle, for example, at 80 km depth, is higher, as much as 50 kg/m<sup>3</sup> than that of the Pannonian mantle (Figure 3.4). The lower values of mantle density are located at the base of the lithosphere in the Tuscany Magmatic Province (<3280 kg/m<sup>3</sup>) and in the Pannonian Basin (~3300 kg/m<sup>3</sup>). Similarly, there is also a decrease of Vp and

Vs from the Adria microplate to the Pannonian Basin (Figure 3.5) as observed also by Belinić et al. (2021) at similar depths (Figure 3.5, panel b). The lowest seismic velocity is obtained in the lithospheric mantle of the Tuscany Magmatic Province with Vp and Vs values from 8.01 to 4.62 km/s below Moho depth to 7.8 and 4.32 km/s at LAB. The highest values of these velocities are found in the lithospheric mantle beneath the Adriatic Sea, with Vp between 8.15 and 8 km/s and Vs from 4.66 to 4.43 km/s. These differences in density and seismic velocity are mainly related to the LAB changes and, then, temperature distribution, more than to compositional changes.

**Table 3.2** Major oxides composition in % of weight percent in the NCFMAS system used for the lithospheric and sublithospheric mantle

	Sublithospheric mantle	Mantle wedge	Lithospheric mantle		
Composition	<b>DMM</b> (Workman and Hart., 2005)	<b>DMM - 3%</b> (Kumar et al., 2021)	Adriatic mantle (Tc_2) Av. Tecton peridotite (Griffin et al., 2009)	Pannonian Mantle (PB_mant) (Alasonati Tašárová et al., 2016; Downes et al., 1992)	
SiO <sub>2</sub>	44.7	44.59	45	44.6	
$Al_2O_3$	3.98	3.51	3.9	2.9	
FeO	8.18	8.21	8.1	8.8	
MgO	38.73	39.63	38.7	40.8	
CaO	3.17	3.02	3.2	2.6	
Na <sub>2</sub> O	0.13	0.082	0.28	0.18	
Mg#	89.4	89.58	89.5	90.4	
(100*MgO/[MgO + FeO])					

*Note:* DMM, Depleted Mid-Oceanic Ridge Mantle; Tc\_2, Average Phanerozoic Mantle; PB\_mant, Pannonian Basin mantle

The resulting density of the DMM-3% composition of the mantle wedge is much higher underneath the Dinarides/western Pannonian Basin area than underneath the Tyrrhenian-Tuscany region where the lithospheric thinning results in an increase of the thermal gradient and consequently a decrease in density and seismic velocities.

Furthermore, to better fit the geoid height and Bouguer anomaly (Figures 3.4b and c) and considering seismic tomographic results, I have modeled two sublithospheric thermo-

compositional anomalies with an Adriatic mantle composition extending down to 400 km underneath the Apennines and to 250 km below the Dinarides. I keep the same chemical composition (Adriatic mantle) for both slabs considering that geophysical and geological data point to the same Adriatic origin. The positive seismic velocity anomaly (2%-3%) beneath the northern Apennines (Figure 3.3 profile A-B of panel A) (Giacomuzzi et al., 2011) and the increase of Vp (8.2-8.4 km/s) and Vs (4.6-4.8 km/s) velocities proposed by Belinić et al. (2021) underneath the Dinarides are both modeled as sublithospheric negative thermal mantle anomalies (-200 °C) that extend down to 400 and 250 km, respectively. The modeling shows that within the sublithospheric anomalies there is a 20 kg/m³ increase in density (Figure 3.4f) and an increase of ~1.5% for Vp and ~2% for Vs. These thermo-compositional sublithospheric anomalies allow for a better adjustment not just with the seismic tomographic models but also with the geoid height and Bouguer anomaly (Figures 3.4b and 3.4c, blue and black lines).

### 3.3.3. Isostatic and dynamic topography

Based on the principle of isostasy (see Section 2.2.7), I calculated two end-member thermal isostatic models, represented by the black and blue lines in Figure 3.4d, with and without considering the effect of the sublithospheric anomalies (slabs). The comparison shows that the slabs beneath the Apennines and Dinarides deflect the elevation by as much as 1500 m. Ignoring the effects of slabs, the local isostatic elevation shows remarkable misfits of ~500 m in the northern Apennines, and ~200 m in the Adriatic Sea and the northern Dinarides (Figure 3.4d).

Then, I consider the flexural rigidity of the lithosphere, calculating the flexural elevation with two values of effective elastic thickness ( $T_e$ ), 10 km and 20 km (green solid line and dashed line, Figure 3.4d). An effective elastic thickness of 20 km provides a better fit to the elevation along most of the transect, although minor misfits (less than 200 m) remain in the Apennines and Dinarides.

Furthermore, based on the results of the transect, 2D numerical models are used to study dynamic topography with a heterogeneous lithosphere (Figure 3.6). The methodology used is described in Chapter 2, Section 2.2.7. The model setup includes the geometry of the crust and lithosphere, and the density and temperature distribution modeled along the transect (Figure 3.4). The numerical model uses a uniform rectangular numerical grid with a resolution of 2 × 2 km. To avoid boundary effects, I applied a "sticky air" layer at the top of the model and homogeneous "extension" of 200 km at the bottom, left and right of the model. Crameri et al. (2012) found that for the

stability of the model it has to satisfy the condition  $\frac{\eta_{st}}{\eta_{ch}}(\frac{L}{h_{st}})^3 \ll 1$ , where  $\eta_{st}$  and  $h_{st}$  are the viscosity and thickness of the "sticky air" layer, and  $\eta_{ch}$  and L are the characteristic viscosity and length scale of the model. Then, the top 20 km "sticky air" layer is fixed to 1000 kg/m³ density and  $10^{18}$  Pa·s viscosity. This top layer allows the surface of the model to move as a real free surface (Crameri et al., 2012; Gerya, 2019).

The viscosities of the crust and lithospheric mantle are considered constant, at 10<sup>21</sup> and 10<sup>22</sup> Pa·s, respectively. The viscosity of the sublithospheric mantle is temperature and pressure dependent and it is controlled by a combination of diffusion and dislocation creep viscous flow laws (Table 2.2, Hirth and Kohlstedt, 2003). The numerical models assume free slip for all velocity boundary condition.

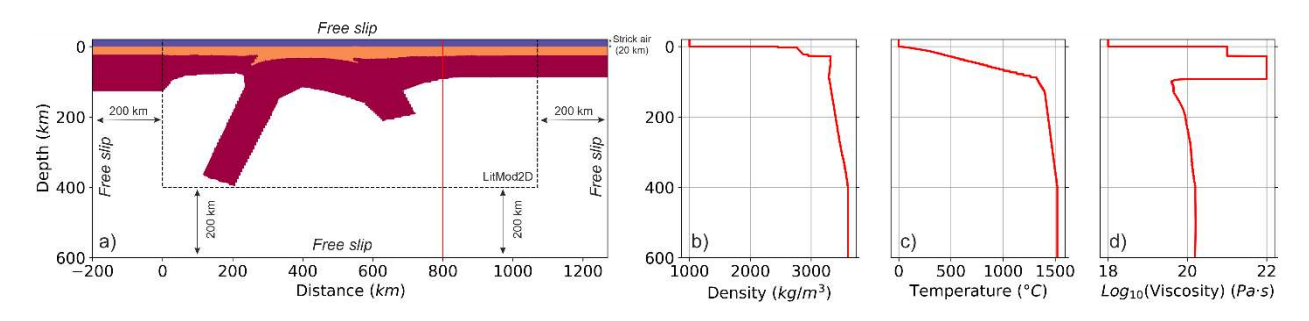


**Figure 3.6** Model setup and boundary conditions. (a) The top blue layer is the 20 km thick sticky air. The crustal body is shown in orange. The red body represents the lithospheric mantle. The bottom layer is a 200 km thick homogeneous layer. The left and right layers are 200 km extending homogeneous layers. The density and temperature are the results obtained from LitMod\_2D. Free slip is imposed at all boundaries. (b, c and d) The red lines represent the density, temperature and viscosity profiles at the position of red vertical line in the panel a, respectively.

The lithosphere and sublithospheric variations along the transect will induce a mantle flow and buoyancy variations which will result in vertical stress and dynamic topography at surface (Equation 2.34, Chapter 2). I consider two end-member models, with and without considering the effect of the sublithospheric anomalies (slabs). Figure 3.7 shows the calculated mantle flow and the resulting dynamic topography with these two scenarios: considering mantle anomalies (with two slabs, Figure 3.7b) and ignoring mantle anomalies (no slabs, Figure 3.7c). The maximum value of the dynamic topography of the no slab model (black line in Figure 3.7a) is about 230 m and it is located in the northern Apennines; meanwhile in the model with slabs it is ~200 m (blue line in Figure 3.7a) and located in the northern Tyrrhenian basin. Both models show negative dynamic topography along the Adriatic Sea, caused by the thicker lithosphere. The two denser slabs beneath the northern Apennines and Dinarides, pull down the lithosphere and generate a high velocity flow (Figure 3.7b), which also caused faster mantle upwelling beneath the Tyrrhenian

Basin and the Pannonian Basin. The pull-down effect of the denser North Apennines slab induces mantle downwelling, which in turn leads to upwelling beneath the Tyrrhenian Basin. However, the calculated dynamic topography with the two models shows little difference along the Pannonian Basin, and both show positive values (120-150 m). It should be mentioned that, due to the simplified assumed rheological structure (e.g., with a rheologically homogeneous crust), the lateral variations of dynamic topography are more representative of the buoyancy forces and mantle flow than the specific values themselves.

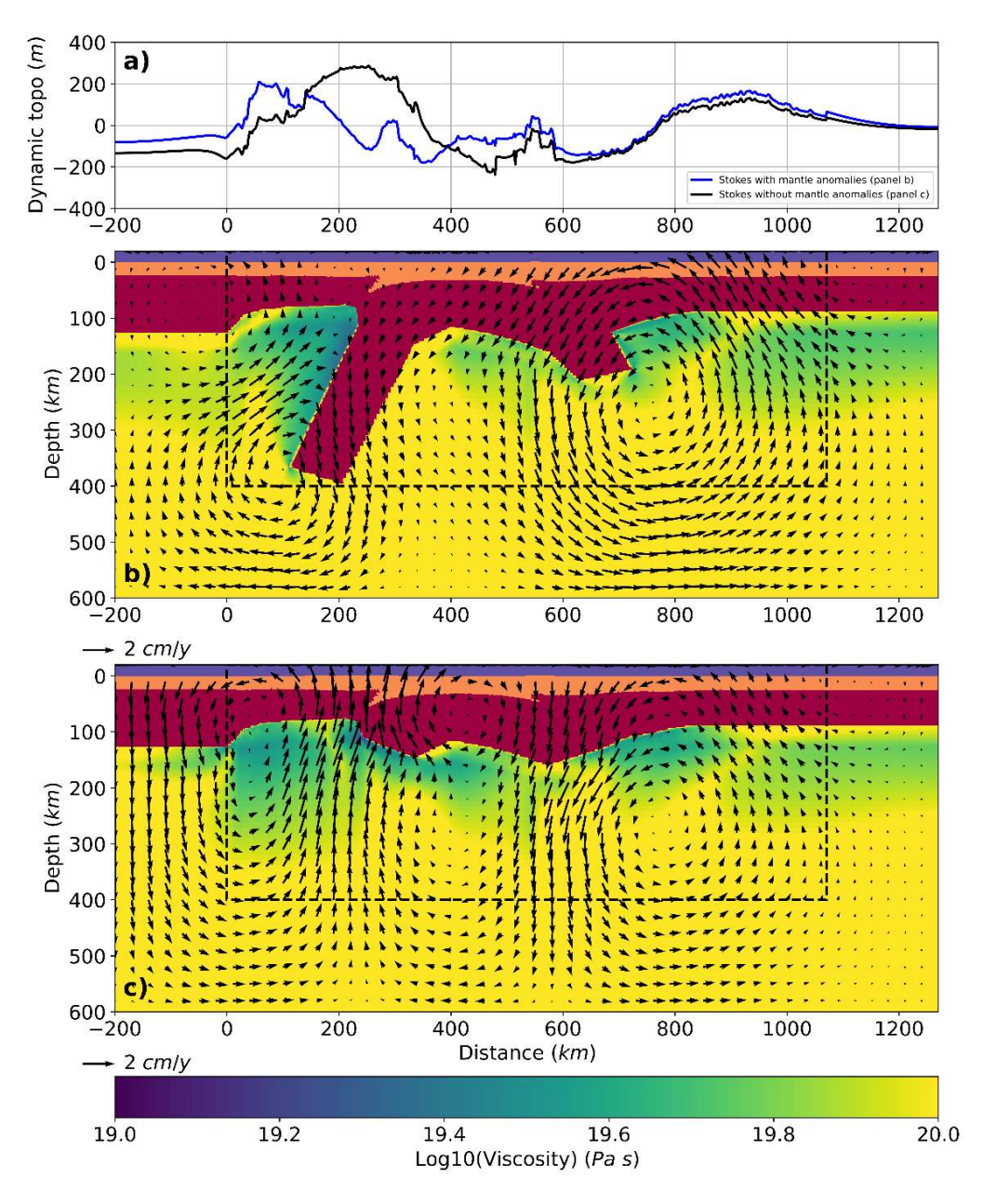


**Figure 3.7** Results of the models along the northern transect. (a) Calculated dynamic topography. Blue: considering two sublithospheric anomalies (Apenninic and Dinaric slabs are attached) Black: without sublithospheric denser anomalies. Panels b and c show the velocity field and effective viscosity distribution: (b) considering two sublithospheric anomalies; (c) without sublithospheric anomalies. Color legend is the same as in Figure 3.6. Black arrow length is proportional to velocity.

### 3.4. Discussion

### 3.4.1. Crustal and lithospheric structure

The numerous geophysical surveys carried out in the study region allowed me to have a good constraint on the Moho depth along the northern Apennines and Dinarides (Figure 3.2 and references therein). Along the transect, I distinguish two main microplates, Adria and Tisza, separated by the Sava Suture to the east of the Dinarides. The geometry of the crustal layers produces the density variations required to fit the observables (Bouguer anomaly, geoid height, and elevation) and it is consistent with the geodynamic context.

The structure of the northern Apennines is complex and the Moho depth differs noticeably in different studies (e.g., Liotta et al., 1998; Finetti et al., 2001; Pauselli et al., 2006). Along the External Apennines, the results agree with those obtained by RFs studies (see references in Figure 3.2), where the Moho locally reaches maximum depths of ~55 km, in an area where I modeled the top of the Apenninic slab (see next Section). Beneath the Adriatic Sea, the Moho remains at a rather constant depth, consistent with the results of Molinari and Morelli (2011) and Grad et al. (2009). The Adria crust is deepening underneath the External Dinarides, where it is locally found at 45 km, in agreement with RF data (Šumanovac et al., 2016; Stipčević et al., 2020) and local earthquake tomography (Kapuralić et al., 2019).

According to Pamić et al. (2002) the Sava Suture Zone developed as a back-arc basin during the Cretaceous-Early Paleogene and was subsequently affected by Eocene collisional deformation and metamorphism accompanied by synkinematic granite plutonism, generation of an ophiolite mélange and finally thrusting onto the Dinarides. The high average density that I found for the Sava Suture zone agrees with this geologic history and it also explains the high-velocity body imaged by Kapuralić et al. (2019) at the transition between the Dinarides and the Pannonian Basin.

Figure 3.4e compares the calculated LAB depths to those reported in other studies. Although there is coincidence with previous models in the regional pattern of lithospheric thickness variations and in the depth of the LAB in the Tyrrhenian and Pannonian basins, there are discrepancies along the External Apennines and Dinarides and in the Adriatic Sea. The predicted LAB is similar to that of Artemieva (2019), except below the Apennines and the Adriatic Sea, likely due to the regional low resolution of Artemieva's model. In addition, my results agree with those of Šumanovac and Dudjak (2016) and Belinić et al. (2018) below the Dinarides, although significant differences are observed below the Pannonian Basin where I find a deeper LAB. The precise determination of the LAB depth depends on the measuring parameters. However, the different definitions should show a

similar trend as all of them are imaging the rheological strong outer layer of the Earth. Jiménez-Munt et al. (2019) found than the seismic LAB roughly follows the  $1000^{\circ}\text{C} \pm 50^{\circ}\text{C}$  isotherm. Along my profile, the trends obtained with different methods are similar, with the thermal LAB deeper than the seismic LAB. The seismic LAB from Šumanovac and Dudjak (2016) roughly follows the isotherm 900-1000 °C, whereas below the Dinarides the seismic LAB largely departs from this isotherm, probably related to the presence of the subducted cold slab, which is not in thermal equilibrium (Jiménez-Munt et al., 2019).

### 3.4.2. Mantle composition and sublithospheric anomalies

It is challenging to identify mantle chemical composition based on density and seismic velocities, because of the non-linear nature of the problem and the lack of uniqueness (Kumar et al., 2020). Hence, the composition of the mantle must be compatible with the geological and geodynamic history of the area. The composition of lithospheric mantle wedges is related to their back-arc origin and to the degree of partial melting expected from the nature and volume of magmatic events. The space opened between the top of the slab and the upper plate during slab roll-back processes is replaced by a fertile sublithospheric mantle with DMM composition that will undergo partial melting by adiabatic decompression.

The best fitting model requires two negative thermal anomalies in the upper mantle below the Apennines and Dinarides in agreement with the interpretation of seismic tomography images (e.g., Benoit et al., 2011; Giacomuzzi et al., 2011; Koulakov et al., 2015; Šumanovac et al., 2017; El-Sharkawy et al., 2020; Belinić et al., 2021; Handy et al., 2021). Beneath the Apennines, the best-fit model indicates the presence of a west-dipping attached cold lithospheric body down to 400 km, in continuation with the west dipping seismicity observed down to 70-80 km below the northern Apennines (De Luca et al., 2009). This deep cold body is characterized by seismic velocities anomalies between 1% and 2%, which coincide with those observed from the seismic tomography (e.g., Figure 3.3; Giacomuzzi et al., 2011; Kästle et al., 2020). The modeled low mantle velocities around 100 km depth in the Tuscany Magmatic Province (Figure 3.4) agree with the values (<-2%) predicted by the seismic tomography (e.g., Figure 3.3).

Below the Dinarides, a much shorter 125 km-long and east-dipping mantle anomaly is required, resulting in a lithospheric slab down to 250 km. This result is in agreement with Šumanovac and Dudjak (2016), who image a pronounced fast velocity anomaly extending toward the NE direction to at least 250 km depth. The favored model includes a mantle wedge below the Dinarides and southwest of the Pannonian basin, which is

consistent with the S-wave low-velocity zone imaged from the inversion of Rayleigh-wave dispersion by Belinić et al. (2021) (Figure 3.3).

### 3.4.3. Geodynamic implications

The Tyrrhenian Sea and the onshore Tuscany Magmatic Province exhibit extensive igneous activity, evidenced by scattered islands and widespread volcanism (Dini et al., 2002; Pandeli et al., 2013; Sani et al., 2016). A prime example is the Elba Island, formed mainly from granitic intrusions like the Monte Capanne and Porto Azurro plutons (6.9 and 5.9 Ma old, Pandeli et al., 2013) (Figure 3.2). Orogenic events triggered lower crustal melting, leading to the formation of granitic intrusions (Serri et al., 1993; Peccerillo, 2005). In contrast, the large Tuscany Magmatic Province arose from about 4 to 0.2 Ma through extrusion along an extensional system of normal faults that thinned the Internal Apennines crust (Rossetti et al., 1999; Acocella and Rossetti, 2002).

This geological history aligns well with my findings where the Tyrrhenian Sea and western Apennines display high thermal gradients and thermal properties (thermal conductivity and heat production) characteristic of magmatic rocks. Provided that continental collision occurred at about 25-30 Ma (e.g., Carminati et al., 2012), these magmatic rocks can be related to either roll-back of a continental slab or to delamination of Adria lithospheric mantle. If, as proposed by some authors (e.g., Benoit et al., 2011), delamination of the mantle slab beneath Corsica began 15 million years ago, the remaining slab length should match the distance from western Corsica to the northern Apennines crest. This distance aligns with the model's predicted depth of 400 km for the slab.

Below the northern Tyrrhenian, the crust is relatively thin and it thickens toward the Internal-External Apennines boundary where west-dipping thrusts involve basement rocks. This simultaneous crustal thinning in the Tyrrhenian-Tuscan extended terrains and thickening in the External Apennines is consistent with eastward migrating continental subduction and with delamination, as acknowledged in the literature. The crust becomes thicker below the Adriatic foreland basin system along the Adriatic Sea, reaching maximum crustal thickness below the Internal Dinarides. This thick crust corresponds to the point of maximum bending of the eastern region of the Adria microplate.

The most interesting results, however, are the negative thermal anomalies required at the upper mantle below the Apennines and Dinarides. Beneath the Apennines, I find a west-dipping attached cold lithospheric body down to 400 km. I interpret this anomaly as the Apenninic slab, most likely generated by subduction rollback of oceanic and Adriatic

continental lithosphere in a first stage, followed by continental lithospheric mantle delamination, in agreement with previous interpretations (e.g., Benoit et al., 2011; Chiarabba et al., 2014). Subduction rollback of a long continental slab is considered less likely than delamination of the underlying mantle lithosphere. This is because continental crust is buoyant due to its lower density compared to the mantle. Therefore, a long continental slab would resist sinking deeply into the mantle, making subduction rollback less favorable.

Underlying the Dinarides and western Pannonian Basin, Šumanovac and Dudjak (2016) and Belinić et al. (2021) identified a fast velocity body penetrating sublithospheric depths and a low-velocity zone. These authors interpret the fast velocity as a subducting lithospheric slab sinking beneath the Dinarides, while the low-velocity zone is attributed to upwelling hot asthenospheric material. Similar to the findings in Western Adria, my results support the presence of a cold thermal anomaly extending to sublithospheric depths. Furthermore, the low-velocity zone imaged by Belinić et al. (2021) aligns with the modeled mantle wedge I found beneath the Dinarides and southwest of the Pannonian Basin.

The two mantle anomalies are located far from the Ligurian Tethys and Vardar (Neo-Tethys) subduction zones. Therefore, these anomalies most likely represent sinking of continental lithosphere. Here I provide a unified view for the origin of these anomalies, as resulting from bidirectional post-collisional delamination of the Adriatic lithospheric mantle below the Apennines and the Dinarides orogens (Figure 3.8). Delamination related to the Apenninic slab resulted in a near vertical deeper slab and caused crustal and lithospheric thinning and partial melting in the Tyrrhenian-Tuscany region. The shallower anomaly beneath the Dinarides is consistent with a shorter-lived delamination. On the basis of orogen-wide surface uplift of the Dinarides in Oligo-Miocene times and simultaneous emplacement of igneous rocks (33-22 Ma) in the Internal Dinarides, Balling et al. (2021) proposed post-collisional mantle delamination beginning at 28 Ma and terminated 22 Ma ago.

The thin lower crust below the Tuscany Magmatic Province and Dinarides and the current location of both slabs are compatible with their delamination once the continental collisions of Adria with Corsica Block and Tisza were accomplished with different ages and time lengths. The about 200 °C colder bodies with respect to the surrounding rocks, their present size, position and coupling with shallower lithosphere have important consequences for both the evolution of the Apennines and Dinarides orogenic systems and the contribution to their recent topography.

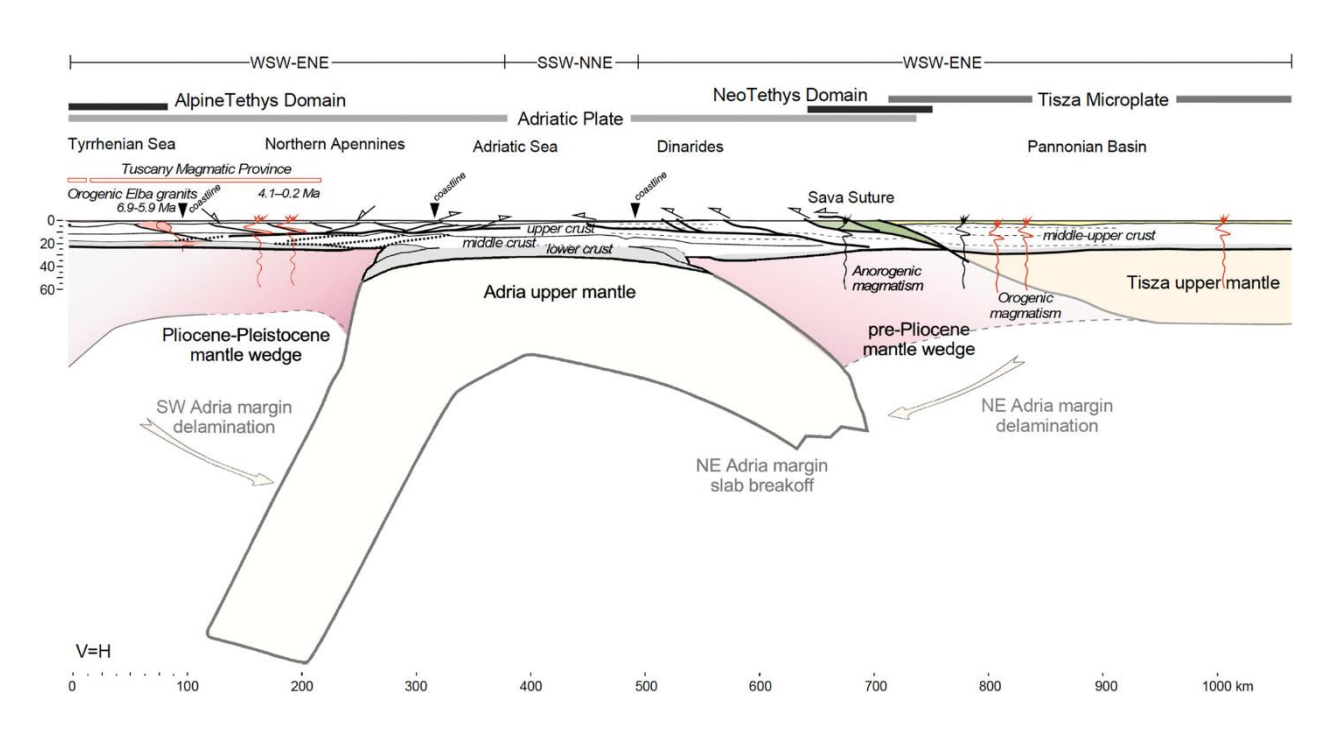


Figure 3.8 Modeled crust and upper mantle structure along the profile and its geodynamic interpretation.

High-amplitude and medium to long-wavelength elevation misfits are observed associated with the subducting slabs (Figure 3.4d). Calculation of two end-member thermal isostatic models, with and without considering the effect of the sublithospheric anomalies, shows that in the Apennines and Dinarides the slab deflects the elevation as much as 1500 m (Figure 3.4d). This effect is to be expected since the sublithospheric velocity anomalies (see Figure 3.3) are modeled as two thermal anomalies of −200°C (Figures 3.4 and 3.5) that result in a colder and higher density zone than the surrounding sublithospheric mantle.

Moreover, the thick lithosphere below the Adriatic Sea and the two deepening slabs at both edges pull down the topography of the Adriatic Sea below sea level. For most of the profile, assuming regional isostasy with an elastic thickness (T<sub>e</sub>) between 10 and 20 km considerably reduces the mismatch between observed and calculated elevation (Figure 3.4d). Tesauro et al. (2009) obtained similar values using thermal and rheological data.

Despite the application of regional isostasy, substantial misfits still persist, particularly in areas where high-amplitude and medium to long-wavelength topographic variations are present. As it will be assessed in the general discussion (see Chapter 5), the residual topography can be partly explained by the dynamic topography associated with the subducting slabs, thus indicating that the lithospheric structure alone cannot fully account for the observed topography.

### 3.5. Chapter conclusions

In this chapter, I present a geophysical-petrological model of the crust and upper mantle structure along a transect extending from the northern Tyrrhenian Sea to the Pannonian Basin, crossing the northern Apennines and the northern Dinarides fold-thrust belts. The model offers an integrated view of the complex structure of Adria and Tisza microplates and of the west- and east-dipping slabs occurring along both sides of the Adriatic foreland, building the Apennines and Dinarides orogenic systems. From the results I can draw the following conclusions:

- A better fit of the observations is obtained when Adria and Tisza microplates are distinguished by different densities. The best-fitting average density for the Adria crust is 2830 kg/m³, whereas the Tisza crust shows a lower average density between 2790 and 2800 kg/m³. This is partly because the lower crust of the Tisza plate is much thinner than that of Adria. The Tyrrhenian Sea and the Internal Apennines are characterized by the presence of elevated temperatures at shallow crustal levels, which is consistent with well-documented magmatic intrusions. I also observe that the crustal structure of the Adria microplate is more complex than that of the Tisza plate, particularly near the collisional zones showing that subduction/delamination in the area has mainly influenced the Adria domain. This is also observed at Moho levels, where major discrepancies between seismic data are found below the External Apennines and Dinarides. The modeling permits me to solve these discrepancies and conclude that along the Internal Apennines the Moho lies at depths <25 km while along the External Apennines the Moho is found a depth of 55 km.
- The LAB shows significant lateral variations mainly related to the two crustal domains, recording their different tectonic evolution from the Mesozoic onwards. Beneath the Tyrrhenian Sea the LAB is flat and shallow at ~75 km, slightly deepening toward the westernmost end of the transect. Below the Pannonian Basin the LAB remains quite flat although ~20 km deeper than the seismic one. Along the External Apennines and Dinarides I observe that the LAB deepens to 150 km depth but shallowing toward the Adriatic foreland basin reaching 125 km depth.
- Two thermo-compositional sublithospheric anomalies with a temperature anomaly of −200 °C relative to the surrounding mantle and with the same composition as the Adria lithospheric mantle are required to fit the geoid height and tomography studies. The presence of these thermal anomalies increases the density by 15-20

### Chapter 3. The Northern Apennines and Dinarides Orogenic Systems

kg/m³ allowing for a better fit of the geoid height and gravity anomaly and it is enough to reproduce the observed Vp and Vs anomalies. Below the Apennines, the west-dipping attached cold lithospheric slab reaches 400 km depth, which supports tomography models that favor the presence of a deep and cold anomaly as opposed to models that propose a shallower slab. Below the Dinarides, the east-dipping sublithospheric anomaly is shorter ending at 250 km depth, which agrees with seismic tomographic models.

- The lateral changes of Adria's LAB together with the bidirectional sublithospheric anomalies below the Apennines and Dinarides are responsible for the resulting elevation, with low values in the Adriatic Sea due to its thick lithospheric mantle and the pulling down effect of the sublithospheric anomalies. Most of the elevation along the profile is under thermal isostasy. In contrast, the dynamic topography represents a minor contribution to the actual elevation. The observed elevation in the External Apennines, Dinarides and Sava Suture Zone can be explained assuming regional isostasy with an elastic thickness between 10 and 20 km.
- The model is compatible with two different lithospheric mantle compositions, a reenriched basalt layer beneath the entire Adria microplate and a fertile mantle for the Tisza microplate lithospheric mantle. Moreover, the modeled lithospheric mantle composition below the Apennines and Dinarides is fertile compared to that of the rest of Adria and Tisza microplates. This is consistent with the presence of two sublithospheric mantle wedges, resulting from the bidirectional delamination of the Adria lithospheric mantle.



### **CHAPTER 4**

# Geophysical-Petrological Model of the Crust and Upper Mantle Beneath the Southern Apennines and Dinarides Orogenic Systems

## Chapter 4. Geophysical-Petrological Model of the Crust and Upper Mantle Beneath the Southern Apennines and Dinarides Orogenic Systems

In this Chapter 4, I present the crust and upper mantle structure along a ~1250 km SW-NE oriented transect, crossing the southern Tyrrhenian Sea, Apennines, Adriatic Sea and Dinarides and ending to the Carpathians-Balkanides. In Chapter 3, from modeling a profile crossing the northern Apennines and Dinarides I found a bidirectional subducting continental mantle delamination of the Adria microplate. Considering the longitudinal variations in plate-scale geometries that have been previously identified in various studies of the Apennines and Dinarides slabs, my primary goal is to investigate the southern continuity of the opposing Apennines and Dinarides slabs. Thus, in this chapter I am expanding my analysis to encompass the southern Apennines and Dinarides regions, using the same modeling approach as in the northern transect, the LitMod2D\_2.0 software, described in Chapter 2.

### Results from this chapter have been published as:

Zhang, W., Jiménez-Munt, I., Torne, M., Vergés, J., Bravo-Gutiérrez, E., Negredo, A. M., & García-Castellanos, D. (2024). The Lithosphere and Upper Mantle of the Western-Central Mediterranean Region From Integrated Geophysical-Geochemical Modeling. Journal of Geophysical Research: Solid Earth, 129(4), e2023JB028435. https://doi.org/10.1029/2023JB028435

### 4.1. Model parameters and constraints

The initial crustal geometry along the transect is constrained by previous works including seismic surveys, geological cross-sections, geological maps and combined geological-geophysical interpretations. Figure 4.1 shows the location of the transect and previous studies at crustal scale, which are projected into the transect with the same scale. The crustal structure in the central part of the southern Tyrrhenian Basin is mainly based on the MEDOC seismic profile from Prada et al. (2014, 2016). In the southern Apennines data come from the deep crustal seismic reflection (CROP-04) profile (e.g., Akimbekova et al., 2021; Finetti, 2005; Scrocca, 2010). In the Adriatic Sea I used the results of the seismic cross-sections from Fantoni and Franciosi. (2010). In the eastern section of the profile, the Dinarides and Carpathian-Balkanides crustal structure is mainly constrained by geological data (available crustal cross-sections) (Matenco and Radivojević, 2012; Schmid et al., 2008, 2020).

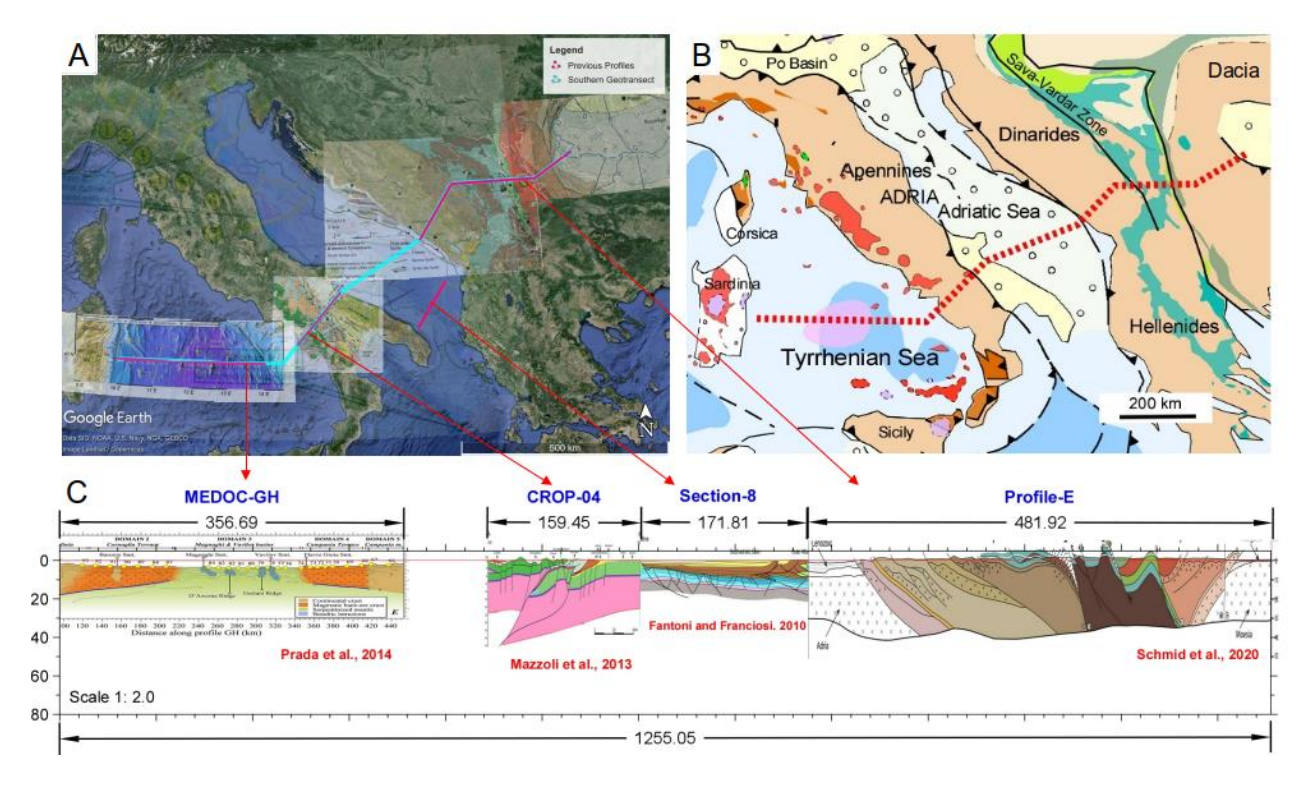


**Figure 4.1** Location of the southern transect and previous studies along the modeled profile. A: Topographic map from Google Earth with the location of the transect (Cyan solid line) and the previous profiles used in this study (Red solid lines); B: Tectonic map with the location of the transect (Red dash line). The transect crosses the Adria and Dacia microplates; C: Crustal structure from previous studies and locations of the profiles and data used to further constrain the crustal geometry, including MEDOC GH (Prada et al., 2014), CROP 04 (Mazzoli et al., 2013), seismic section 8 (Fantoni and Franciosi. 2010) and Profile-E (Schmid et al., 2020). The section 8 is projected onto the southern transect. Vertical scale is exaggerated 2 times the horizontal scale. Vertical scale is exaggerated 2 times with respect to the horizontal scale.

The Moho depth comes from seismic receiver functions (RF) analysis of Piana Agostinetti and Amato (2009); Stipčević et al. (2020) and Kalmár et al. (2021) and the regional crustal models of Mazzoli et al. (2013); Savastano and Piana Agostinetti (2019) and Akimbekova et al. (2021). The physical parameters for each crustal body are summarized in Table 4.1. Crustal density values are based on previous studies (e.g., Akimbekova et al., 2021; Prada et al., 2014; Savastano and Piana Agostinetti, 2019), that use the velocity-density relationship of Brocher (2005). The density of the sedimentary cover was deduced from the empirical relationships of Nafe and Drake (1963). Thermal conductivities are taken from Norden and Förster (2006) and Trumpy and Manzella (2017), and the radiogenic heat production data come from direct measurements in the Apennines (Verdoya et al., 2019) and from a global compilation of relevant crustal rocks (Hasterok and Webb, 2017; Vilà et al., 2010). Furthermore, the density and thermal conductivity of the exhumed mantle in the central Tyrrhenian Basin were estimated using a thermodynamic approach (Figure 4.2, Chapter 2), while its heat production was assumed to be 0.02 μW/m³ (Turcotte and Schubert, 2002).

I also consider the Moho depth from previous results: the global crustal model CRUST1.0 (Laske et al., 2013), regional crustal models of Europe based on various geophysical compilations (Tesauro et al., 2008; Grad et al., 2009; Molinari and Morelli, 2011; Di Stefano et al., 2011; Artemieva and Thybo, 2013), 3D model of seismic velocity constrained by surface wave tomography (Greve et al., 2014; Manu-Marfo et al., 2019; Magrini et al., 2020, 2022), density models derived from potential field modeling (Akimbekova et al., 2021; Kelemework et al., 2021), and crustal thickness derived from a combination of receiver function data (Stipčević et al., 2020; Kalmár et al., 2021). All this data has been projected along the southern transect (Figure 4.3).

For characterizing the lithospheric and sublithospheric mantle, I have considered the seismic velocities (both Vp and Vs, Figure 2.12) from the tomography studies of Amaru (2007), Benoit et al. (2011), Giacomuzzi et al. (2011), Koulakov et al. (2015), Šumanovac et al. (2017), El-Sharkawy et al. (2020), Belinić et al. (2021), Handy et al. (2021), and Rappisi et al. (2022).

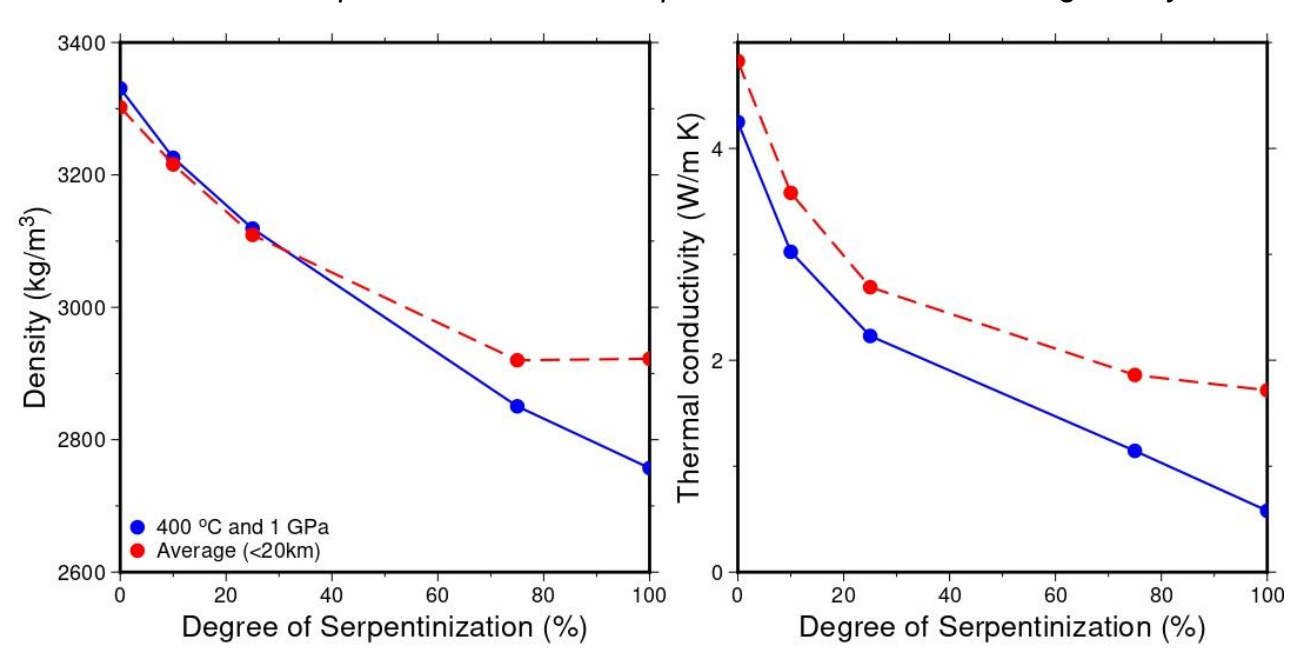
### Chapter 4. The Southern Apennines and Dinarides Orogenic Systems

Table 4.1 Thermo-physical properties of the crustal tectonic units and mantle domains along the transect

Tectonic un	its	Density (kg/m³)	Thermal conductivity (W/K m)	Radiogenic heat production (μW/m³)		
Sediment		2450	2.4	1		
	Tyrrhenian Basin Magmatic UC	2800	2.7	2		
	Tyrrhenian Basin Magmatic LC	2900	2.1	0.8		
	Tyrrhenian Basin EM75	2870 (a)	1.6	0.02		
	Tyrrhenian Basin EM25	2980 (a)	2.4	0.02		
Adria	Apennines UC	2780	2.7	2		
Microplate	Apennines LC	2850	2.1	0.6		
	Adriatic Sea UC	2780-2840 (b)	2.7	2		
	Adriatic Sea MC	2880	2.1	0.6		
	Adriatic Sea LC	3080	2.1	0.6		
	Dinarides UC	2750-2820 (b)	2.7	2		
	Dinarides LC	2880	2.1	0.6		
Dacia -	Sava Suture	2850	2.7	1.3		
	Balkanides UC	2750	2.9	2		
	Balkanides LC	2880	2.1	0.6		
Mantle -	Tyrrhenian LM		DMM-6% (Kumar et a	ıl., 2021)		
	Adriatic & Dacia LM	Tc_2 (Griffin et al., 2009)				
	Mantle wedge	DMM-3% (Kumar et al., 2021)				
	Sublithospheric mantle	DMM (Workman and Hart, 2005)				

UC: Upper Crust; MC: Middle Crust; LC: Lower Crust; EM75: Exhumed Mantle 75% serpentinized; EM25: Exhumed Mantle 25% serpentinized; LM: Lithospheric Mantle. The details of mantle composition are shown in table 4.2. (a) The density and thermal conductivity of the exhumed mantle of the central Tyrrhenian Basin is estimated using the thermodynamic approach presented in Figure 4.2. (b) Calculated as a function of pressure using isothermal compressibility.

Chapter 4. The Southern Apennines and Dinarides Orogenic Systems



**Figure 4.2** Estimated changes in density (left panel) and thermal conductivity (right panel) of exhumed mantle as a function of varying degrees of serpentinization. Blue line shows the values at 1000 MPa and 400°C. Red line shows the average values between 0 and 20 km.

**Table 4.2** Major oxides composition in % of weight percent in the NCFMAS system used in the different mantle domains

	Lithosphe	ric mantle	Exhumed mantle		Mantle wedge	Sublithospheric mantle
Composition	Tyrrhenian (DMM-6%) Kumar et al. (2021)	Adriatic (Tc_2) Av. Tecton peridotite Griffin et al. (2009)	Tyrrhenian Sea EM75 75 % serpentinization	Tyrrhenian Sea EM25 25 % serpentinization	<b>DMM - 3%</b> Kumar et al. (2021)	<b>DMM</b> Workman and Hart (2005)
SiO <sub>2</sub>	44.47	45	44.47	44.47	44.59	44.7
Al <sub>2</sub> O <sub>3</sub>	3.08	3.9	3.08	3.08	3.51	3.98
FeO	8.23	8.1	8.23	8.23	8.21	8.18
MgO	40.53	38.7	40.53	40.53	39.63	38.73
CaO	2.78	3.2	2.78	2.78	3.02	3.17
Na₂O	0.051	0.28	0.051	0.051	0.082	0.13
H <sub>2</sub> O	1	1	9.75	3.25	1	1
Mg#	89.72	89.5	89.72	89.72	89.58	89.4
(100*MgO/[Mg	gO + FeO])					

Note: DMM, Depleted Mid-Oceanic Ridge Mantle; Tc\_2, Average Phanerozoic Mantle; EM75, Exhumed Mantle 75 % Serpentinization; EM25, Exhumed Mantle 25 % Serpentinization

### 4.2. Results

Considering the previously mentioned geological cross-sections and seismic experiments, Figures 4.3 and 4.4 show the crustal and upper-mantle structure that best fit all observables (elevation, geoid height, Bouguer gravity anomaly, surface heat flow and mantle seismic velocities).

### 4.2.1. Crustal structure

Along the southern transect (Figure 4.3) I distinguish four main configurations of the crystalline crust that significantly differ in their internal structure and average densities. The westernmost domain consists of the Tyrrhenian Basin, composed in its central region of sediments and a basement that is fundamentally made of mantle rocks and subordinate oceanic crustal rocks. Moving to the east, in the Adria plain domain, from west to east, I find two more domains: the double-layered crust of the continental slope and the onshore western Apennines and the three-layered crust of the eastern Apennines and Adriatic Sea. To differentiate the Apennines, I define the southern western Apennines, adjacent to the Tyrrhenian Sea, and the southern eastern Apennines, bordering the Adriatic Sea. The first region encompasses both offshore and onshore domains in which the crust is thinned and under extension, while the second region is located above a thicker crust under a compressional regime. The best fitting model shows that the easternmost domain of the profile, including the internal Dinarides (Adria microplate) and the Carpathian-Balkanides (Dacia microplate) is characterized by a two-layered crust of variable thickness, covered by a thick sedimentary cover showing lateral thickness variations. The Adria and Dacia domains are separated by the Sava Suture Zone, exposing remnants of the former Vardar Ocean, which closed at the end of the Cretaceous (e.g., Schmid et al., 2020; Spahić and Gaudenyi, 2022).

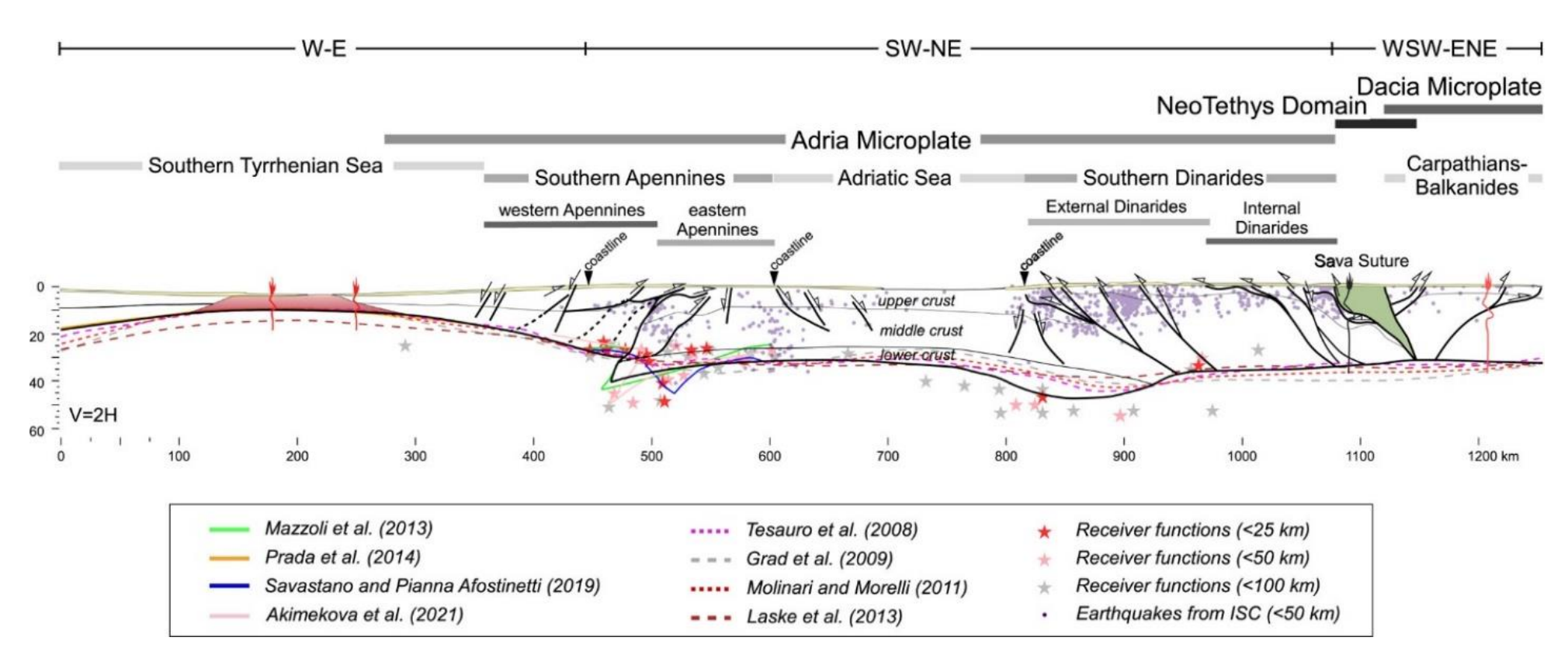


Figure 4.3 Crustal structure from the best fitting model, which was constrained using available geological and geophysical information as listed in the panel legend and in the main text. Yellow color represents the sediment layer. Degraded red in the central Tyrrhenian Basin shows the serpentinized mantle (75% top, 25% bottom). Moho depths from previous studies are shown with different colors, see bottom legend for color table and references. Stars show Moho locations from receiver function studies of Stipčević et al. (2020) and Piana Agostinetti and Amato (2009), with different color according to their distance to the profile (<25 km, <50 km, and <100 km). Earthquakes with a magnitude of Mb ≥ 3.0 between 2008 and 2021, as recorded in the ISC catalog, are plotted as gray circles projected at 50 km across the transect. Red arrows show the location of main volcanic edifices.

As depicted in Figure 4.3, significant variations in crustal structure and thickness are observed along the transect. Toward the west, seismic data and drilling results (e.g., Prada et al., 2014, 2016; Loreto et al., 2021) show that the southern Tyrrhenian Basin is characterized by a sedimentary cover with variable thickness and two exhumed mantle layers with different degrees of serpentinization. Following the interpretation from Prada et al. (2014, 2016), the best fitting results indicate that serpentinization reaches up to 75% in the upper layer and 25% in the lower layer (Table 4.1). Their densities have been calculated for different degrees of serpentinization using the thermodynamic approach (Figure 4.2), and ranging from 2870 to 2980 km/m³, respectively (Table 4.1 and Figure 4.3). Thus, the results are compatible with the central region of the Tyrrhenian Basin characterized by serpentinized mantle and subordinate oceanic rocks, surrounded by a magmatic crust at the western and eastern margins of the basin, where the crust thickens up to 20 km. The magmatic crust consists of two layers, an upper layer that is about 4 km thick, with a density of 2800 kg/m³, and a lower layer of variable thickness with a density of 2900 kg/m³ (Table 4.1 and Figure 4.3).

The magmatic crust of the eastern Tyrrhenian Basin passes laterally into a two-layered crust that extends from the continental slope to the onshore (Figures 4.3 and 4.4). The Moho depth varies from 20 km to almost 30 km with densities of 2780 kg/m³ for the upper crust and 2850 kg/m³, for the lower crust. Across the southern Apennines, Adriatic Sea and external Dinarides, the upper crust has a constant thickness of about 10 km, except in the western and eastern collisional fronts where a thickening of about 5 km is observed. A similar trend is observed in the middle crust, although on average, it is approximately 10 km thicker than the upper crust. Upper and middle crustal densities range from 2750 to 2820 kg/m³ for the upper crust and 2880 kg/m³ for the middle crust (Figure 4.3). It is worth noting that beneath the Apennines and external Dinarides, the Moho locally reaches depths of 40 and 55 km, respectively. The thickening of the Dinarides crust primarily occurs in the lower crust, which nearly doubles in thickness. A slight thickening is also observed in the upper and middle crust (Figure 4.3).

Crustal thickening underneath the central and southern external Dinarides is supported by seismic receiver functions (RF) data, which locate the Moho at a depth of 50-55 km (e.g., Šumanovac et al., 2017; Stipčević et al., 2020). Uncertainties found in RF's in this region could be an indication of a double or overlapping Moho (Stipčević et al., 2020). The presence of a high-density lower crust (3080 kg/m³) is mainly determined by the fitting of the geophysical observables (Figure 4.4), while also being consistent with the expected densities at those depths.

Figure 4.4 (see next page) Best fit model, see Figure 4.1 for location. (a) Surface heat flow. (b) Geoid height. (c) Bouguer gravity anomaly. (d) Elevation. Blue and black lines show modeled results, with and without sublithospheric anomalies, respectively. Red dots show measured data, and vertical bars show the standard deviation calculated across a swath of 25 km half width. (e) Temperature distribution for the entire lithosphere. Continuous black lines highlight the obtained Lithosphere-Asthenosphere boundary (LAB) depth and location of sublithospheric mantle anomalies. LAB depth from previous studies (red stars) are shown for comparison. Earthquake locations (International Seismological Centre, ISC) with a magnitude of mb ≥ 3.0 between 2008 and 2021, projected 50 km across the transect are shown as solid gray circles. (f) Mantle density distribution. The different compositional domains in the lithospheric mantle are separated by thin gray lines, and major oxide compositions are listed in Table 4.1 and 4.2. Data from Rappisi et al. (2022) have been taken from <a href="https://figshare.com/articles/dataset/iso-and\_aniNEWTON21\_tomographic\_models/19188950">https://figshare.com/articles/dataset/iso-and\_aniNEWTON21\_tomographic\_models/19188950</a> and projected onto the profile.

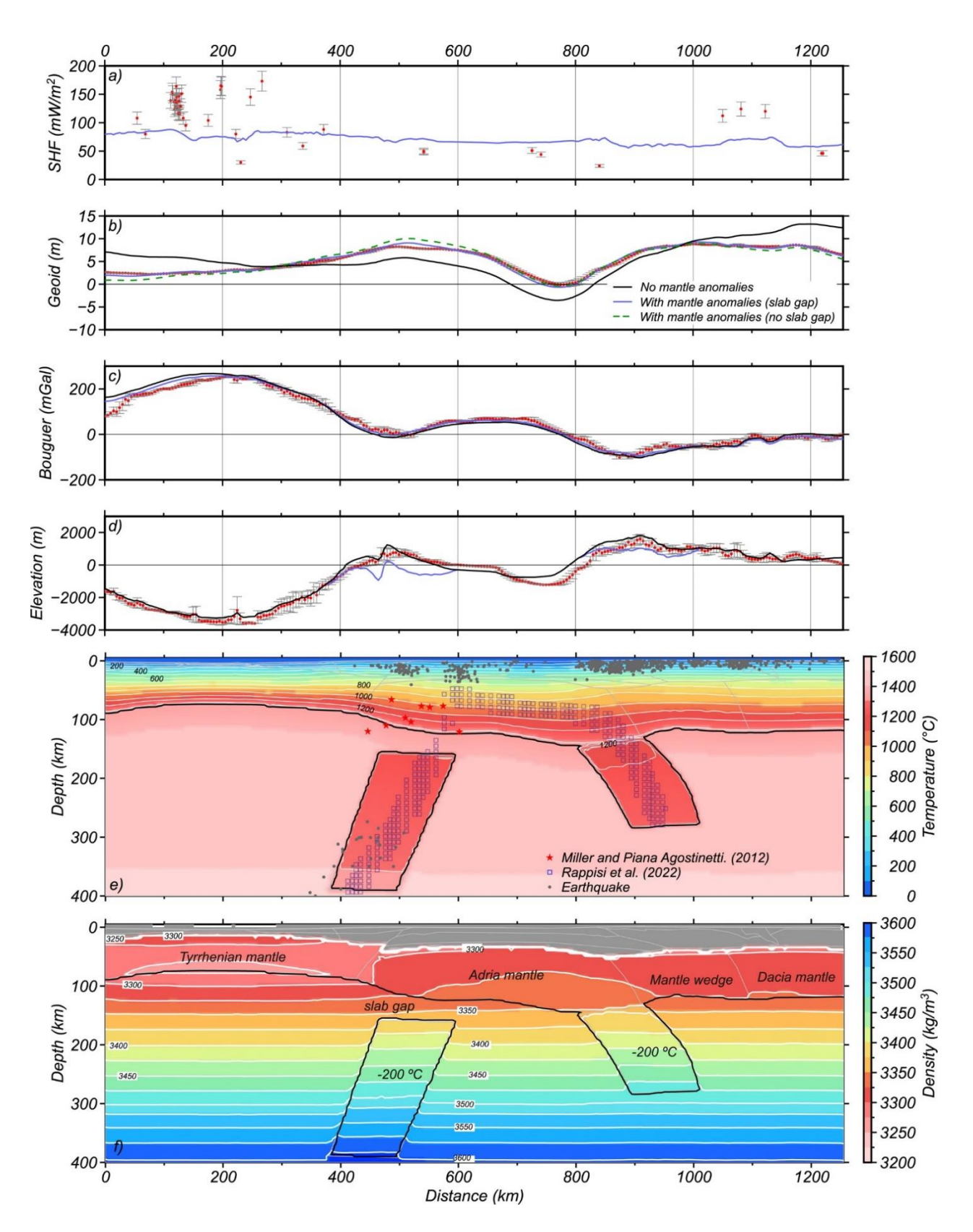


Figure 4.4 (see page 89)

To the east, the crust exhibits a relatively constant thickness, with the Moho located at 30-35 km depth, slightly deepening toward the internal Dinarides (35 km). The crust is composed of two distinct layers, namely the upper and the middle-lower crust, which have relatively lighter average densities than those observed in the western and central regions of Adria (Table 4.1). The upper crust, except in the areas surrounding the Sava Suture Zone, is relatively thin (~5 km) and has an average density of 2750 kg/m³. The middle-lower crust is significantly thicker and denser, with an average thickness of 25 km and a mean density of 2880 kg/m³ (Figure 4.3).

The Adria and Dacia domains are separated by the Sava Suture zone, which stretches from the eastern Alps in the northwest to the Dinarides in the southeast, encompassing a significant portion of the western Balkanides. The suture is mainly composed of a mélange of flysch, ophiolites and metamorphic rocks with densities ranging between 2200 and 2800 kg/m³ for the flysch sedimentary rocks and 2900-3500 kg/m³ for the metamorphic and ophiolitic rocks (Ustaszewski et al., 2010; Spahić and Gaudenyi, 2022). The best fitting model shows an average density of 2850 kg/m³ for the entire Sava Suture Zone complex (Table 4.1).

The thermal model results also indicate that the temperature at the Moho depth ranges from 300 to 420 °C in the western part of the Tyrrhenian Basin to 600-650 °C in the southern western Apennines. In the Adriatic Sea, temperatures are between 600 and 680 °C, and they increase rapidly as the base of the crust becomes deeper beneath the external Dinarides, reaching temperatures over 700 °C and 800 °C, respectively (Figure 4.4e).

Shallow seismic activity is mainly concentrated along a narrow and nested band along the southern Apennines and Dinarides (Figure 4.3). More diffuse activity, mainly located at upper/middle crustal levels (<20 km) is observed in the Sava Suture Zone and Carpathian-Balkanides region. In the inner southern Apennines normal faulting and thrust/reverse faulting mechanisms occur at the outer fronts of the chain (Chiarabba et al., 2014; De Luca et al., 2009). For most of the region, hypocenters are confined to the upper 20-25 km of the crust with the exception of onshore and offshore areas in the western Adriatic coast where earthquake depths reach the lower crust and uppermost mantle as deep as 40 km depth (Figure 1.5b and 4.3).

Recent seismic activity on the central Apennines and Adriatic Sea has a generally lower magnitude compared to the southern Apennines (Figure 1.5b), and it is typically associated with strike-slip and normal faults. In the southern Apennines, major destructive, high-magnitude earthquakes are due to extensional faults. In the Dinarides earthquakes are observed at shallow-intermediate crustal depths and predominantly contractional.

Notably, no recent shallow earthquakes have been recorded in the Tyrrhenian Basin where earthquakes primarily occur at depths exceeding 300 km and are related to the Calabrian Wadati-Benioff zone (Figure 1.5b).

## 4.2.2. The LAB and upper mantle physical properties and composition

In the best-fit model, I have identified three distinct lithospheric mantle compositions: the Tyrrhenian mantle, the Adria and Dacia mantle, and the Dinarides mantle wedge (Table 4.1 and 4.2 and Figure 4.4). For the sublithospheric mantle, I used a depleted midocean-ridge (DMM, or Depleted MORB Mantle) composition, as defined by Workman and Hart (2005), which is a reference model for an average, non-melted, depleted MORB mantle. For more details, refer to Chapter 2.

The lithospheric mantle composition beneath the southern Tyrrhenian Basin is characterized as DMM-6%, indicating approximately 6% melting of the sublithospheric mantle with a Mg# of 89.72. For the Adria and Dacia mantle, the results reveal a Tc\_2 composition (an average Tecton composition, defined in Griffin et al., 2009), which is a slightly depleted mantle with an average Mg# of 89.5. Below the Dinarides, the best-fit model indicates a DMM-3% composition, which is interpreted as due to the presence of a mantle wedge. This DMM composition with a variable degree of melting accounts for potential melting of both the lithospheric and sublithospheric mantle, likely attributed to the rollback of the Apennines and Dinarides slabs (see more discussion in Chapter 5).

The thermal LAB is defined by the depth of the 1320 °C isotherm, in agreement with the findings of numerical simulations employing realistic viscosities (e.g., Gerya, 2019). The LAB beneath the southern Tyrrhenian Basin reaches a minimum depth of  $\sim$ 70 km (Figure 4.4). Toward the southern Apennines and the external Dinarides, it gradually deepens, and in the Dinarides the lithospheric plate sinks about 280 km below Dacia. From the internal Dinarides to the Carpathian-Balkanides, the LAB is relatively flat at a depth of about 120 km.

These variations in lithosphere thickness along the profile also imply different temperatures between the domains at the same depth. The Tyrrhenian Basin exhibits the highest temperatures, reaching  $\sim\!970\,^{\circ}\text{C}$  at a depth of 50 km (Figure 4.4e and Figure 4.5), decreasing toward the margin, where the temperature below the Apennines becomes  $\sim\!900\,^{\circ}\text{C}$ . Meanwhile, in the Adriatic Sea and the Dinarides, the temperatures at 50 km depth are  $\sim\!780\,^{\circ}\text{C}$  and  $\sim\!870\,^{\circ}\text{C}$ , respectively. These lateral temperature variations are reflected in the calculated densities and seismic velocities.

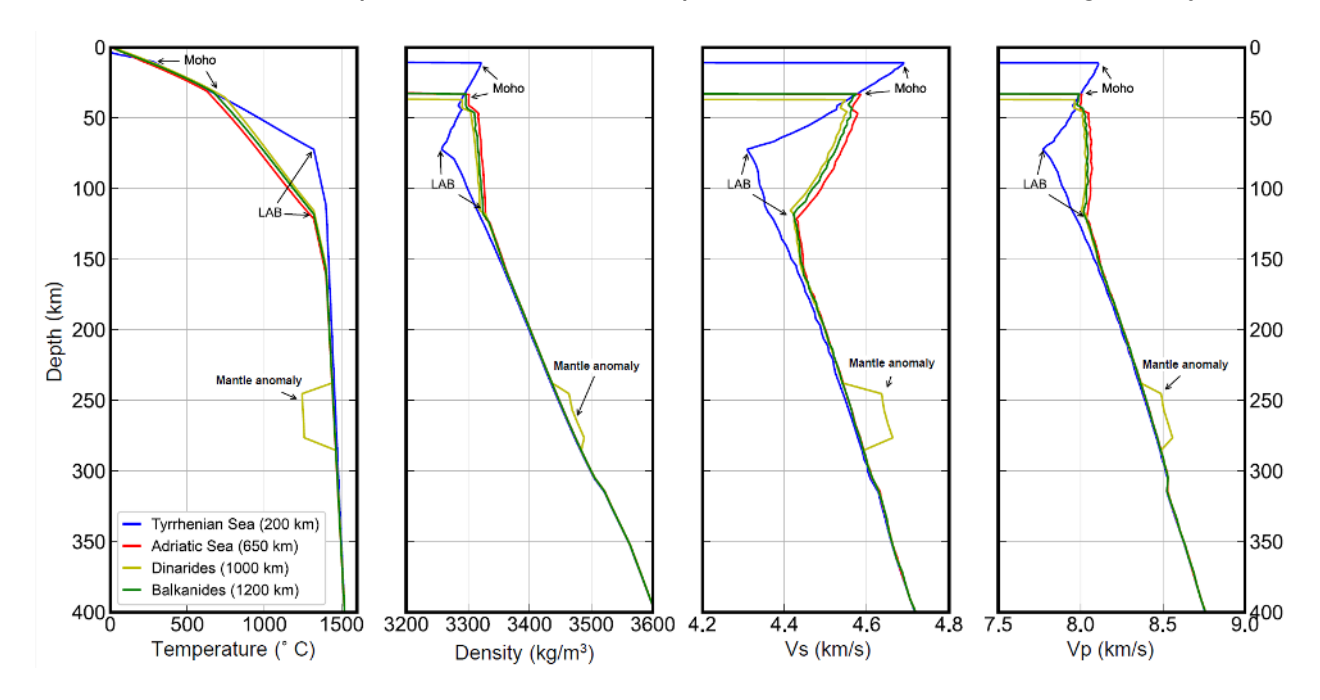


**Figure 4.5** Temperature, density, Vs and Vp along four selected lithospheric columns located in the Tyrrhenian Sea (200 km); Adriatic Sea (650 km); Dinarides (1000 km), and Dacia microplate (1200 km).

The density distribution of the upper mantle is shown in Figure 4.4f and Figure 4.5. In the 50-120 km depth range Adria's mantle has a slightly higher density (30 kg/m³) than farther to the east. Although the chemical composition of the mantle wedge and the Dacian mantle domain are different, the density differences between the two domains are very small, since they have a similar temperature distribution.

In the Tyrrhenian Basin, the presence of serpentinized mantle at shallow levels (<12 km) results in low densities of 2870 and 2980 kg/m³. Below that depth, the mantle is devoid of serpentinization and because of the elevated temperatures at shallower depths, the density distribution decreases from 3320 kg/m³ at 13 km to 3270 kg/m³ at the LAB (Figure 4.5). Akimbekova et al. (2021), using a compilation of available active and passive seismic data and gravity modeling, also distinguished between the older, colder and denser Adriatic lithospheric mantle, and the warmer and lighter Tyrrhenian mantle (Figure 4.5).

Seismic velocities below the Tyrrhenian Basin are higher at 15-30 km (Vs > 4.6 km/s and Vp  $\sim$  8.1 km/s) decreasing in depth to 4.3 km/s and 7.8 km/s at the LAB. At 50 km depth there is an increase in seismic velocities from the center of the Tyrrhenian Basin to the Adria microplate (Figures 4.6 and 4.7). The highest velocities are observed in the Adria block with Vp values of  $\sim$ 8.1 km/s and Vs values between 4.42 and 4.57 km/s (Figures 4.5 and 4.6) while lower values are obtained in the Dacia mantle, although the differences are relatively minor ( $\sim$ 0.5 km/s).

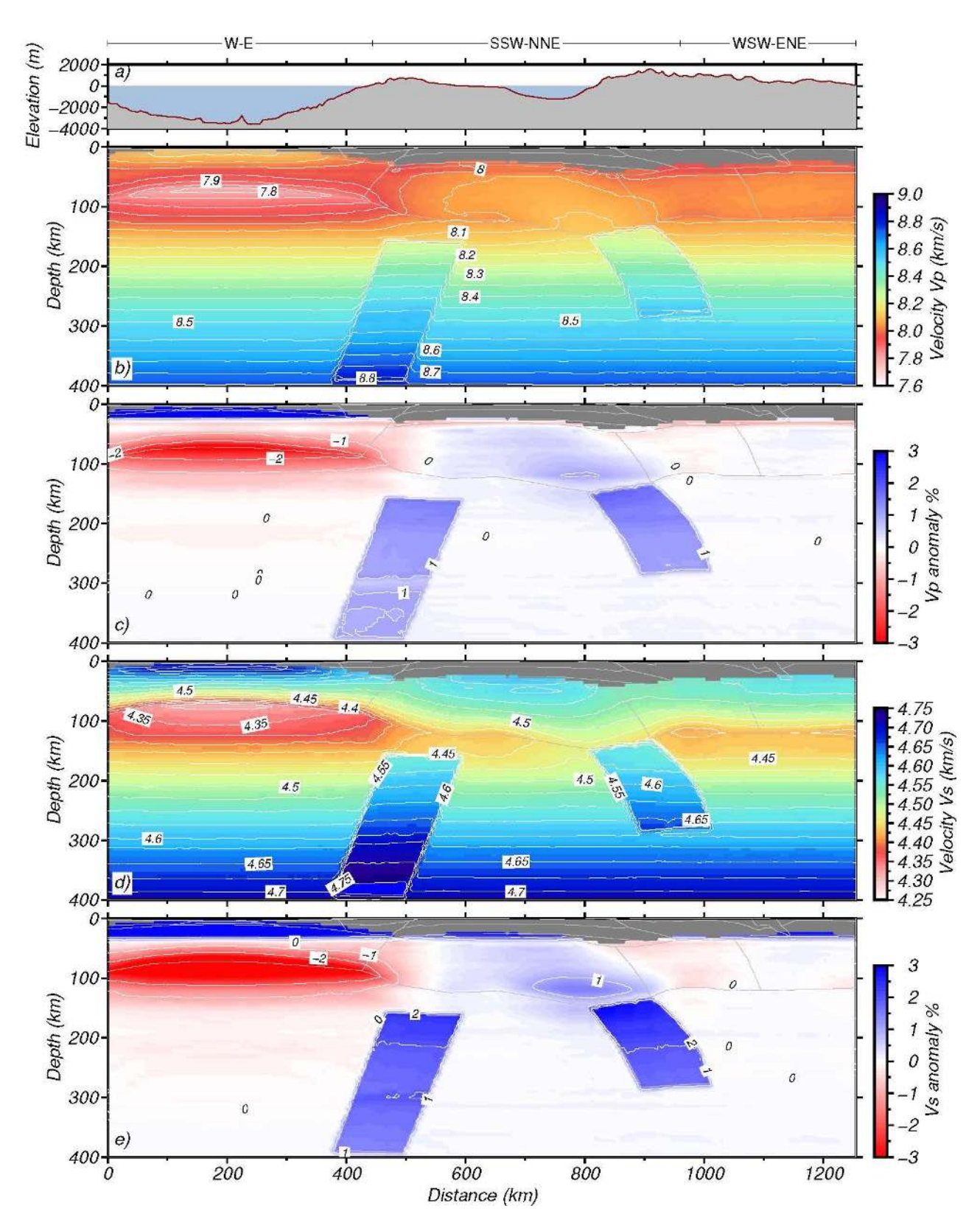


**Figure 4.6** Mantle seismic velocities and synthetic seismic velocity anomaly along the transect. Panel (a) elevation profile, (b) and (d) absolute P- and S-wave velocities and (c) and (e) synthetic P and S-wave anomalies, respectively. Note that the color scale used in the synthetic models, (c) and (e), saturates in areas where the Moho depth is less than 35 km. This saturation occurs due to the reference model employed, which incorporates a 35 km thick crust (Kumar et al., 2020) and highlights areas with crustal thinning.

Chapter 4. The Southern Apennines and Dinarides Orogenic Systems

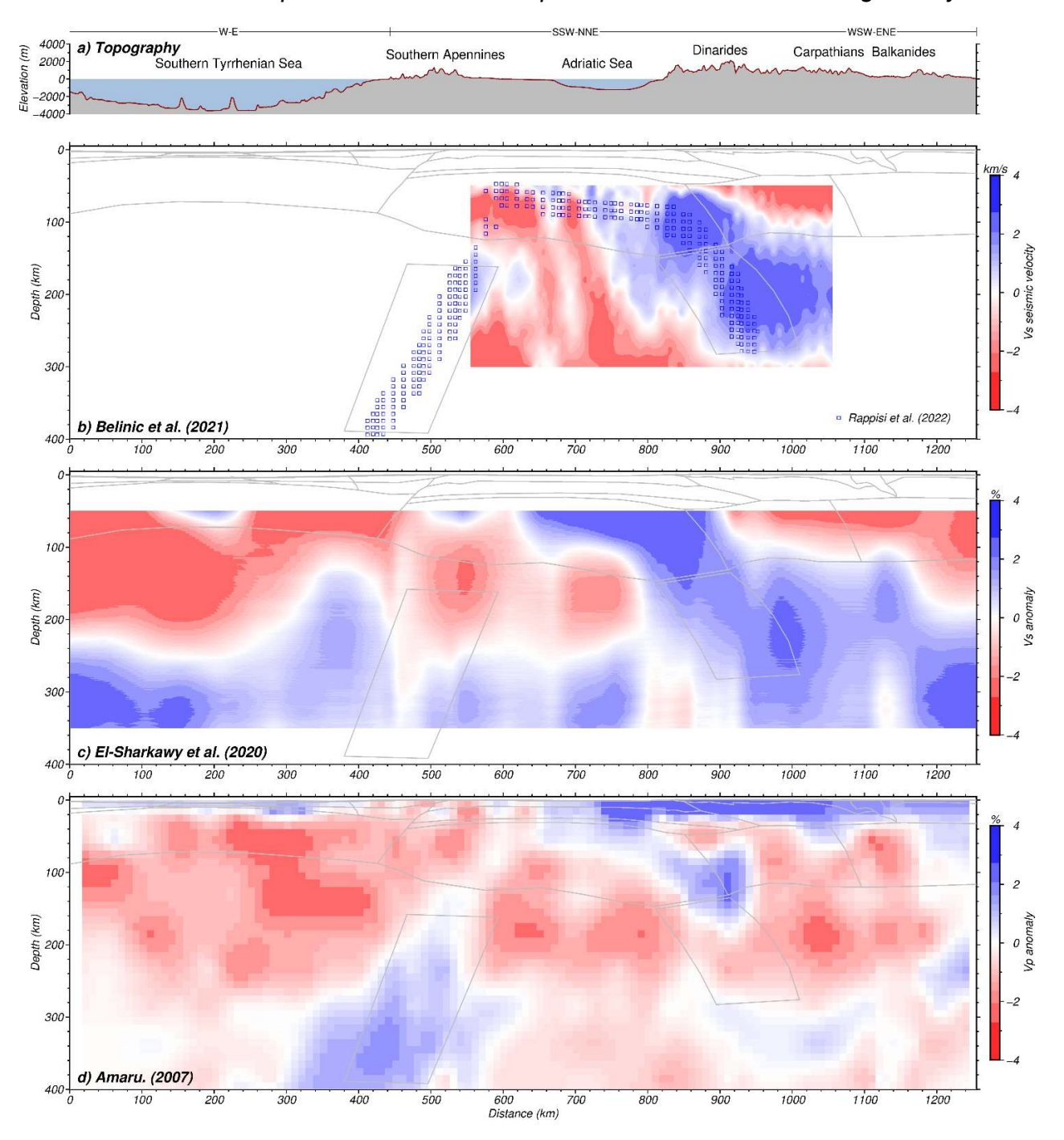


**Figure 4.7** Tomography data used along the modeled transect. a) Elevation profile. b) Blue empty squares show slab model identified by Rappisi et al. (2022). Tomography data has been projected onto the modeled transect from b) Belinić et al. (2021); c) El-Sharkawy et al. (2020) and d) Amaru (2007).

Tomography studies show that the sublithospheric mantle at depth between 100 and 160-200 km (Figure 2.12) below the southern Apennines is characterized by negative Vp anomalies (e.g., Amaru, 2007; Rappisi et al., 2022) and negative Vs anomalies (e.g., Belinić et al., 2021; El-Sharkawy et al., 2020) whereas positive Vp and Vs anomalies are observed at greater depths (Figure 4.7). In contrast, beneath the southern Dinarides,

positive Vp and Vs anomalies extend continuously from the LAB to 280-300 km depth (e.g., Belinić et al., 2021; El-Sharkawy et al., 2020; Rappisi et al., 2022) (Figure 4.7).

Based on the 3D anisotropic teleseismic P-wave tomographic model of Rappisi et al. (2022) and the high-resolution shear-wave velocity model of El-Sharkawy et al. (2020) and in order to fit the observed geoid height and elevation data (Figure 4.4), I have modeled two sublithospheric thermo-compositional anomalies beneath the southern Apennines and Dinarides. Both anomalies are set to 200 °C lower than the surrounding mantle, but with different geometries and extensions. The southwestern anomaly is detached from the overlying plate and extends from 160 to 400 km below the southern Apennines, whereas the northeastern one is attached and extends to 280 km below the southern Dinarides. Since both anomalies are related to the sinking of Adria continental lithosphere, I have used the same chemical composition as for the Adria mantle. The results show that the two sublithospheric anomalies have an increase in density of 20 kg/m³, as well as an increase in Vp and Vs of 1.5% and 2%, respectively (Figure 4.4 and Figure 4.6) with respect to the surrounding lithosphere.

Along the profile seismic activity in the sublithospheric mantle occurs primarily within the Apennines slab and its immediate surroundings at depths ≥250 km (Figure 4.4b).

# 4.2.3. Isostatic and dynamic topography

In Figure 4.8, I calculate local isostatic elevations considering different scenarios, which include: ignoring the Apennines and Dinarides slabs (black line); the Apennines slab is detached (blue solid line, Figure 4.8b); or both Apennines and Dinarides slabs are attached (green dashed line, Figure 4.8c) to the continental lithosphere. The local isostatic elevation without both slabs shows higher misfits of about 400 m in the Adriatic Sea and 300 m in the southern Apennines and Dinarides. However, the local isostatic elevation with both slabs attached shows higher misfits (> 900 m) in the southern Apennines and better adjustment (~200 m) in the Dinarides. I also calculate the flexural elevation with an elastic thickness of 30 km (dark blue dashed line), resulting from the detached Apennines and Dinarides slabs scenario (best-fit model, Figure 4.8b). The flexural elevation shows better fit with the measured topography, but the minor misfits (<200 m) still exist in the Adriatic Sea and Dinarides.

Chapter 4. The Southern Apennines and Dinarides Orogenic Systems

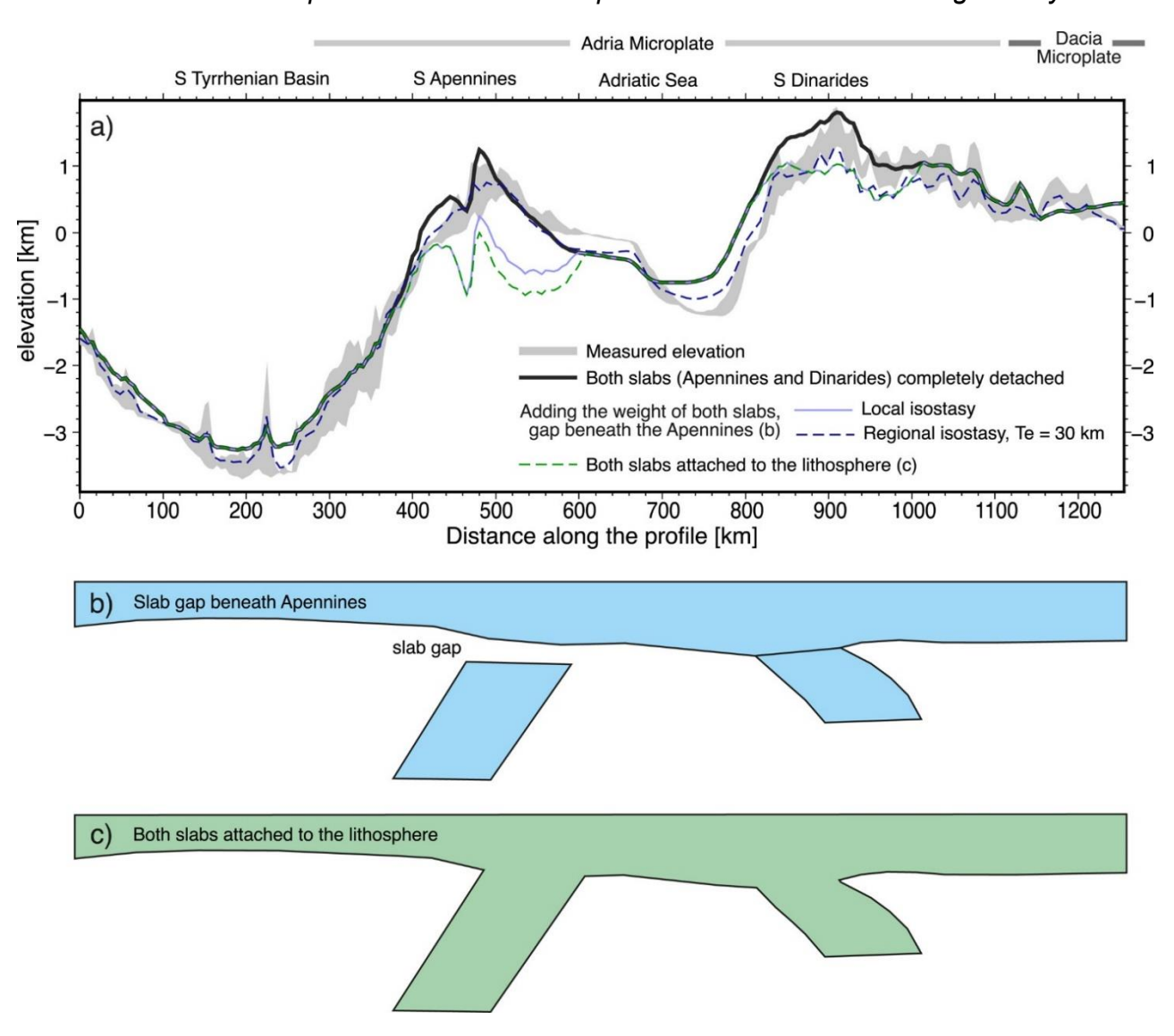


**Figure 4.8** Observed and modeled elevation along the transect (a) Gray: standard deviation of the observed elevation across a 50 - km - wide swath. Black: local isostasy ignoring the sublithospheric denser anomalies (Apenninic and Dinaric slabs completely detached). Blue: local isostasy considering the weight of the two sublithospheric anomalies, with as slab gap beneath Apennines (b) Dark blue dashed: regional isostasy with an elastic thickness of 30 km, resulting from model (b). Green dashed: local isostasy considering the weight of the two sublithospheric anomalies, with no slab gap beneath Apennines, both slabs attached (c).

Using the same approach as in the northern transect, I calculate the 2D mantle flow and the dynamic topography along the southern transect (see Chapter 3 for details on model setting) (Figure 4.9). This is computed solving the Stokes flow and resulting vertical stresses at the crust surface (Equation 2.34, Chapter 2). Figure 4.9 shows the geometry of the different layers and the density, temperature and resulting viscosity along a selected column.

# Chapter 4. The Southern Apennines and Dinarides Orogenic Systems

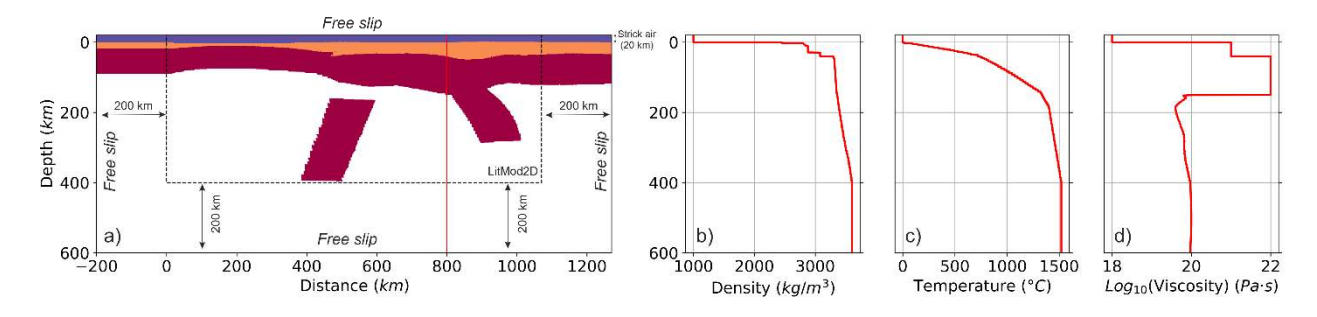


**Figure 4.9** Model setup and boundary condition. (a) The top blue layer is the 20 km thick sticky air. The crustal body is shown in orange. The red body represents the lithospheric mantle material, with the slabs. The extended bottom layer is a 200 km thick homogeneous layer. The left and right layers are 200 km extending homogeneous layers. The density and temperature are the results obtained from LitMod\_2D (Figure 4.4). Free slip is imposed at all boundaries. (b, c and d) The red lines represent the density, temperature and viscosity profiles at the position of red vertical line in the panel a, respectively.

Figure 4.10 shows the three different scenarios considered to evaluate the dynamic topography and mantle flow along the southern transect: 1) Figure 4.10b, including the modeled sublithospheric mantle anomalies with the Apenninic slab detached, as in Figure 4.4; 2) Figure 4.10c, excluding sublithospheric mantle anomalies; and 3) Figure 4.10d considering both slabs attached to the lithosphere. The three models exhibit near-zero dynamic topography along the southern Tyrrhenian Sea and larger negative dynamic topography (~200 m) along the Adriatic Sea. This large-scale negative value could be related to a thicker lithosphere. The model without anomalies (black line) shows the largest positive dynamic topography in the southern Apennines and Dinarides, ~140 m and ~360 m, respectively. The model considering two attached slabs (orange line) shows the lowest negative dynamic topography (-180 m) in the southern Apennines. The results show the maximum differences, ~180 m, between the model with detached slab in the southern Apennines. The results also show that the effective viscosity within the sublithospheric mantle is between 10<sup>19</sup> and 10<sup>20</sup> Pa·s. However, the velocity flow of the mantle from these models are different. The detached Apennines slab generates faster downward flow (Figure 4.10b), which weakens the viscosity of sublithosphere mantle within the slab gap. The model without slabs shows lower mantle flow (Figure 4.10c).

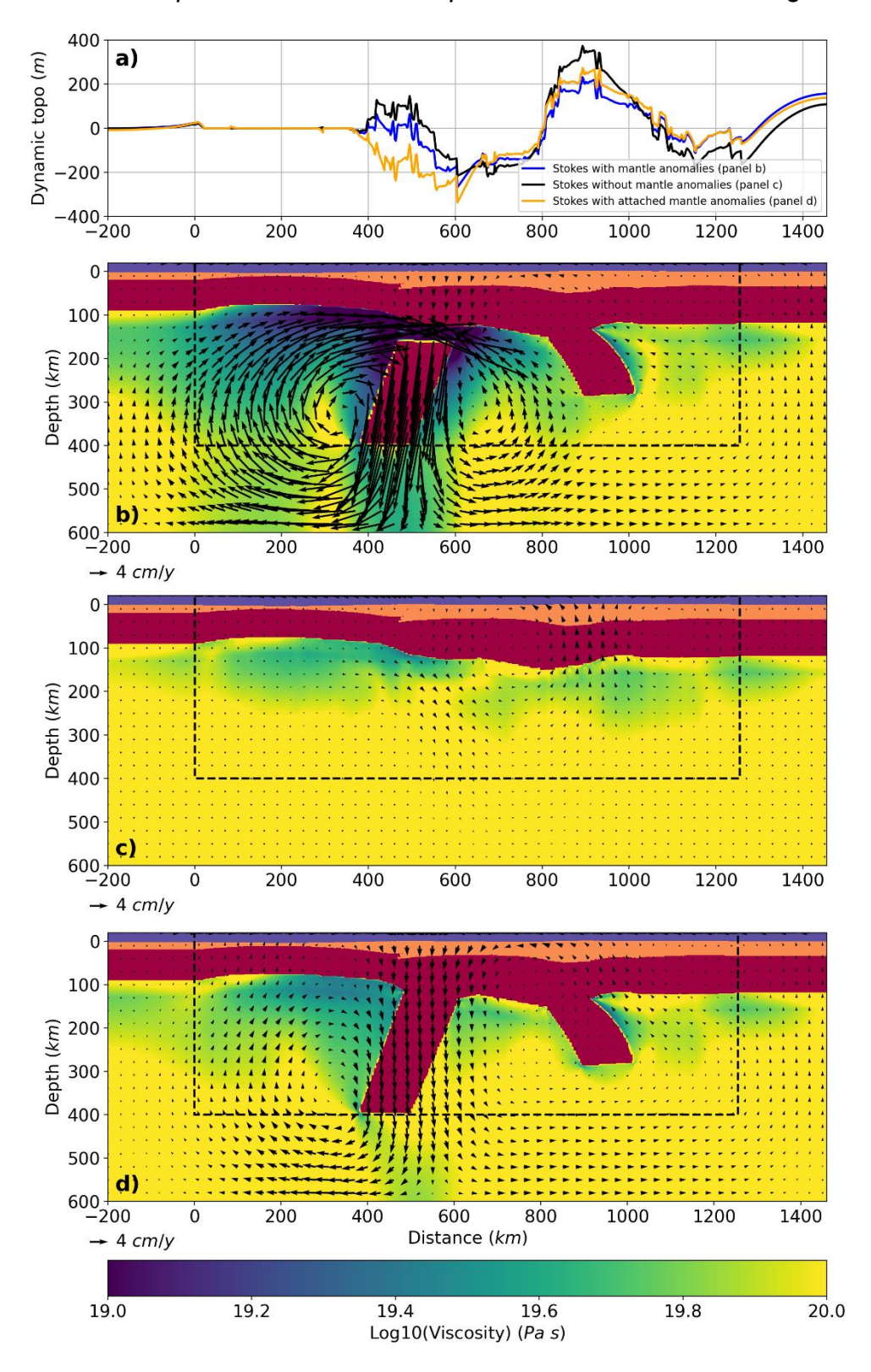


**Figure 4.10** Results of the models along the southern transect. (a) Calculated dynamic topography. Blue: geometry from Figure 4.4, with the slab gap within the Apenninic slab (panel b). Black: without the sublithospheric denser anomalies (panel c). Orange: both slabs attached to the lithosphere (panel d). (b, c and d) Velocity field and effective viscosity distribution considering b) a slab gap beneath the Apennines; (c) without the two sublithospheric anomalies; (d) both slabs attached to the lithosphere. The colors of rock materials are the same than in Figure 4.9a. Black arrow length proportional to velocity.

#### 4.3. Discussion

# 4.3.1. Crustal and lithospheric structure

Based on the numerous geological studies and seismic surveys carried out in the study region, I have been able to obtain a well-constrained estimate of the main crustal tectonic units and of the Moho depth for most of the study profile (Figure 4.3). However, in regions with limited availability of deep seismic data such as the Carpathians and Balkanides, and in regions where there is some uncertainty in the Moho depth estimates, I have refined the depth estimate based on fitting the geophysical observables (Figure 4.4). This uncertainty is evident along the southern Apennines and Dinarides, where the 3D complexity of the crustal structure results in notable differences between the seismic Moho depth and that obtained by regional crustal models (Figure 4.3).

Although there is coincidence for most of the profile between the results and those obtained from the regional models and seismic data (Figure 4.3), there are certain discrepancies. In the Tyrrhenian Basin, the main discrepancy is observed with the models proposed by Laske et al. (2013), as these authors suggest a crust that is 5-10 km thicker. The way the Tyrrhenian crust thickens to the west varies among different regional models and my results. Prada et al. (2014, 2016) interpreted anomalously high P-wave velocities as exhumed mantle with variable degrees of serpentinization from 100% below the sedimentary layer to 0% at about 10 km depth. This is compatible with the model results, where I infer a 4 km thick upper layer with 75% serpentinization, and a 2 km thick lower layer with a 25% serpentinized mantle.

To the east, the crustal structure below the southern Apennines and Dinarides is complex and published estimates of the Moho depth differ noticeably. Below the Apennines, teleseismic RF data from Steckler et al. (2008), Piana Agostinetti et al. (2008), Piana Agostinetti and Amato (2009) as well as from ambient-noise surface wave dispersion (Molinari et al., 2015) show local differences in Moho depth in the order of 10 km and the presence of a double Moho beneath the western Apennines (Piana Agostinetti and Amato, 2009). From the compilation of active and passive seismic data along the CROP-04 crustal reflection seismic profile, Savastano and Piana Agostinetti (2019) concluded that the local crustal thickening is slightly displaced to the east (~50 km) and deeper than that obtained from my results. However, my results are consistent with those of Akimbekova et al. (2021), both in terms of the western location and depth of the crustal thickening (Figure 4.3). These authors, after a compelling review of the published Moho geometries from both active and passive seismic methods, performed gravity modeling along CROP-04 (onshore) and M-6B (offshore) multichannel deep seismic profiles. My

results also agree with the geological crustal model of Mazzoli et al. (2013) based on the integration of surface geological data and the CROP-04 deep seismic reflection profile.

Previous crustal models agree on a generic crustal thickening below the southern Dinarides but, there is no consensus on its absolute values. My findings align closely with the Moho map presented by Zailac et al. (2023) and the RF results of Stipčević et al. (2020). These authors conclude that in the southern external Dinarides, the Moho is located at  $\sim 50$  km, whereas in the northern Dinarides it is at  $\sim 40$  km (e.g., Stipčević et al., 2020). They also report that the uncertainty of the RF data could be indicating the presence of a double or overlapping Moho likely related to the collisional front.

In good agreement with the available regional models my results show a relatively constant Moho depth of 35-40 km depth throughout the Dacia crustal domain, the only difference being a slight crustal thinning in the Sava Suture Zone region (Figure 4.3). The high average density (2850 kg/m³) obtained in the suture zone agrees with the high-velocity body imaged by Kapuralić et al. (2019). Subduction and gradual closure of the Vardar Ocean from the Late Cretaceous to the Paleogene resulted in the emplacement of the high density ophiolitic rocks imaged in my modeling results. In the northern transect, Chapter 3, I also found the same average density at the suture zone between the Adria and Tisza microplates. RF results from Miller and Piana Agostinetti (2012) show some local coincidence with the predicted LAB, which is located at about 120 km depth, in the Apennines. However, the majority of seismic studies predict a shallower seismic LAB than the modeled thermal LAB (Figure 4.4e). The uncertainties in the RF data, which predict the seismic LAB depth ranging from 60 to 120 km, may be associated with the complexity and 3D crustal structure in the subduction front.

In the southern Tyrrhenian Basin, surface waves dispersion curves constrain the seismic LAB at about 50 km depth (Pontevivo and Panza, 2002; Pontevivo, 2003; Panza et al., 2003, 2007), much shallower than my thermal LAB, at 70 km depth. This is a widely recognized yet unresolved issue, with the seismic LAB -particularly that obtained from surface waves-usually shallower than the thermal LAB. Jiménez-Munt et al. (2019) found that the seismic LAB roughly follows the 1000 °C ± 50 °C isotherm. As observed in Figure 4.4e, the seismic LAB obtained by surface wave dispersion roughly follows the 950 °C isotherm, which would explain the differences obtained from my study.

#### 4.3.2. Mantle composition and sublithospheric anomalies

Although the relationships between mantle chemical composition, density, and elastic properties is not straightforward due to their non-linear nature and the lack of uniqueness

(Kumar et al., 2021), I can still relate the composition of the lithospheric mantle to the primary geodynamic processes. Geoid height and elevation, and to a lesser extent, gravity anomalies should reflect the density anomalies resulting from these processes.

In the Central Mediterranean, the predominant geodynamic processes are extension in the back-arc basins and compression along the front of the subduction-related orogenic system on the SW margins of Adria. Both processes determine by far the type of magmatism and changes in composition of the lithospheric mantle (Peccerillo, 2005, 2017; Lustrino et al., 2011, 2022).

In the study profile, significant magmatism beneath the Tyrrhenian Basin and southern Apennines and Dinarides, coupled with geophysical observations, suggest variations in the lithospheric mantle composition and degrees of mantle melting. Subduction processes can chemically enrich the mantle through metasomatism. Subduction accompanied by slab retreat and/or continental delamination, may induce partial melting via adiabatic decompression, leading to mantle depletion. Additionally, regional extensional stresses in the back-arc region can thin the lithosphere, allowing the underlying mantle to rise. Adiabatic decompression and the presence of fluids released by the descending slab may facilitate melting of a partially depleted mantle from the back-arc to the mantle wedge (Peccerillo, 2005, 2017).

The composition of the Tyrrhenian lithospheric mantle is closely linked to its back-arc origin and degree of partial melting, which can be inferred from the nature and volume of the magmatic events in the area. Based on seismic (surface waves) and petrological modeling, Panza et al. (2007) concluded that the thin crust of southern Tyrrhenian Basin is underlain by a soft mantle with partial melting reaching 10%, as shown by low velocities (3.0-3.15 km/s) in the uppermost mantle and the presence of mafic tholeiitic-to-transitional volcanic rocks with low-to-moderate abundance of incompatible elements.

In the central region of the southern Tyrrhenian Basin, my best fit model shows exhumed mantle with a degree of serpentinization that decreases with depth, surrounded by a thin magmatic crust toward its margin, which is underlain by a DMM with 6% of partial melting (DMM-6%) (Table 4.2), in agreement with the results of Panza et al. (2007). From the best fit model, the depleted and partially melted mantle extends laterally to the onshore carbonate platform, where abundant vulcanism is recorded a little farther to the north, for example, Ischia, Vesuvio, Roccamonfina (Peccerillo, 2005). Additionally, surface wave studies indicate a low velocity zone at the base of the crust ranging from 3.00 to 3.15 km/s below the central southern Tyrrhenian Basin to 3.85-4.15 km/s below the onshore carbonate platform (Panza et al., 2007).

Beneath the southern external Dinarides, my modeling suggests a mantle wedge with a DMM composition having 3% of melting, based on the fitting of the geophysical observables and considering that the area has undergone continental delamination. The low mantle wedge velocity predicted by my model is also consistent with the low seismic velocity zone proposed by Amaru (2007), Blom et al. (2020) and Belinić et al. (2021). The lithospheric mantle below the remaining Adria and Dacia plates corresponds to a slightly depleted mantle of Tc\_2 composition (Table 4.2).

To enhance the fit with geoid height and elevation data, and considering seismic tomography results (e.g., Amaru, 2007; Benoit et al., 2011; Giacomuzzi et al., 2011; Koulakov et al., 2015; Šumanovac et al., 2017; Blom et al., 2020; El-Sharkawy et al., 2020; Belinić et al., 2021; Handy et al., 2021; Rappisi et al., 2022), I have modeled two sublithospheric thermo-compositional anomalies with an Adriatic mantle composition. My best fitting model shows that the western anomaly, situated below the southern Apennines, is a west-dipping detached cold (-200 °C) anomaly, extending from 160 km down to 400 km.

Figure 4.8 compares the observed and calculated isostatic elevations under different scenarios, focusing on whether the Apennines slab is detached (Figure 4.8b) or attached (Figure 4.8c) to the continental lithosphere. I conclude that the Apennine elevation fits well without considering the slab weight (black line), suggesting detachment. Conversely, the elevation of the Dinarides is consistent with a fully attached slab. Similar observations are seen for the geoid height in Figure 4.4b (green dashed line), with a mismatch of about 1 m when I consider that the slab is attached to the continental lithosphere. Combining these findings with seismic tomography results (Figure 4.7) supports the hypothesis of a slab gap beneath the southern Apennines. This deep cold body is characterized by seismic anomalies between +1% and +1.5%, which agree with tomography results (e.g., Amaru, 2007; El-Sharkawy et al., 2020; Rapissi et al., 2022) as shown in Figures 4.6 and 4.7.

Below the southern Dinarides, a much shorter attached east-dipping anomaly is observed, resulting in a lithospheric slab down to 280 km. These results agree with Rappisi et al. (2022), who observed a pronounced fast velocity anomaly extending along the northern and southern Dinarides in a NW-SE direction down to 280 km depth. By contrast, along the Apennines the fast velocity anomaly is mapped down to 400 km.

Deep seismicity, occurring at depths greater than 100 km within the study region, is concentrated in the southern half of the southern Apennines, southern Tyrrhenian and Calabrian Arc basins (at depths exceeding 300 km). In contrast, no deep earthquakes have been recorded along the northern-Central Apennines and Dinarides (Figure 1.5b).

The deep earthquakes observed along the study profile are plausibly linked to the interaction between the deepest segment of the southern Apennines slab and the Calabria slab (Figure 1.5b).

## 4.3.3. Geodynamic implications

At difference with the northern profile, the Tyrrhenian Sea is characterized by a very thin crust at its margins. This crust thins further towards the central parts of the basin, becoming quasi-oceanic. In the central regions of the basin, a variable thin sedimentary layer lies directly on top of a serpentinized mantle. The degree of serpentinization varies from 75% to 25%, indicating that extension has been much higher in the southern than in the northern Tyrrhenian.

As in the northern region, volcanism is widespread extending to the onshore Campanian Plain. Magmatism in the central Tyrrhenian Basin is triggered by both extension-induced melting (back-arc basin magmatism) and continental delamination-related processes (e.g., Chiarabba et al., 2014). Moreover, the offshore and onshore continental platform is characterized by volcanic arc-type magmatism. Peccerillo (2017) concludes that magmatism from the Tuscany Province of the northern Apennines to the Aeolian Arc northwest of Calabria exhibits geochemical markers of source regions that have undergone metasomatism related to subduction processes (involving fluids and subducted sediments). These processes are superimposed upon original mantle components ranging from compositions akin to MORBs to Ocean Island Basalts (OIBs).

As I fully discuss in Chapter 5, in the southern Adria region, the deep crustal and lithospheric structure is more complex, primarily due to the nearly 90-degree change in tectonic directions between the southern Apennines and the Calabrian Arc and their respective slabs, as already proposed by Edwards and Grasemann (2009) and Faccenna et al. (2014).

Regarding the lithospheric mantle composition, in the northern profile I propose the existence of two distinct mantle wedges. These wedges are inferred to have a DMM (Depleted MORB Mantle) composition with an additional 3% melting. This composition likely results from the rollback of the Ligurian-Tethys oceanic slab along the SW margin of Adria and the Vardar-Neo-Tethys oceanic slab along its NE margin. In contrast, the southern profile and the Tyrrhenian Basin itself reveal a different degree of melting. Here, based on the age and type of magmatism and my best-fitting model, I propose a DMM composition with a higher degree of melting, around 6%. This anomalous mantle composition extends beneath the entire Tyrrhenian Basin, the thinned continental margin

onshore, and the western Apennines. Interestingly, modeling in the Dinarides region suggests a DMM mantle wedge with 3% melting, similar to the northern transect (see Chapter 3).

As in the northern profile, the most intriguing finding is the presence of two negative thermal anomalies at sublithospheric depths, located beneath the Apennines and Dinarides. Beneath the southern Apennines, I identify a westward-dipping, cold lithospheric body extending down to 400 km. However, unlike the northern profile, most seismic tomography studies and my best-fitting model show a discontinuity or rupture at depths between 120 and 160 km (Figures 4.1 and 4.2). Consequently, in the southern profile, the anomaly is detached from the corresponding lithosphere, exhibiting a gap whose origin will be fully discussed in Chapter 5. Here, however, I can offer a preliminary explanation: the gap might be related to a sub-horizontal tear detachment.

Subducting a long continental slab entirely through rollback is unlikely due to the positive buoyancy of the continental crust. This suggests a more complex process for the formation of the Apenninic slab. My interpretation proposes a two-stage model: initial subduction rollback followed by continental lithospheric mantle delamination. This aligns with previous interpretations (e.g., Benoit et al., 2011; Chiarabba et al., 2014).

Eastern Adria shows a distinct slab configuration compared to the west. The Dinarides anomaly, while deeper than the north, reaches shallower depths than in western margin (Figures 3.8 and 4.11). This difference suggests variations in subduction and delamination history. As I will fully argue in chapter 5 Eastern Adria experienced earlier subduction (Jurassic) than the west (Oligocene) (Carminati et al., 2012; Gawlick and Missoni, 2019). Consequently, the eastern slab may be more detached or thermally equilibrated, potentially due to earlier continental delamination (Schefer et al., 2010).

Regarding the elevation, high-amplitude, medium to long-wavelength misfits are evident in areas associated with the subducting slabs (Figure 4.4d). These misfits likely represent deflections in the Earth's surface caused by the slabs. Thermal isostatic models that consider these anomalies show the subduction slabs can cause up to 1000 meters of deflection in the Apennines and Dinarides (Figure 4.4d). This is unsurprising because the modeled sublithospheric velocity anomalies (Figure 4.6) represent colder, denser zones (around 200 °C colder) compared to the surrounding mantle (Figure 4.4 and 4.6).

The combined effect of the thick Adriatic lithosphere and the deepening slabs on both sides is likely to depress the Adria microplate's topography below sea level. Assuming regional isostasy with an elastic thickness (T<sub>e</sub>) of 30 km reduces significantly elevation

# Chapter 4. The Southern Apennines and Dinarides Orogenic Systems

misfits across most of the profile, but still leaves noticeable residuals along the southern Apennines (-250 m) and Dinarides (-400 m).

Along both transects, regional isostasy consistently reduced the mismatch between observed and calculated elevations but fails to eliminate the high-amplitude, medium to long-wavelength topographic misfits. In order to evaluate if these denser slabs are the primary drivers of these misfits, I will perform in Chapter 5 a comparison between residual topography (the difference between actual elevation and modeled isostatic topography) and the dynamic topography associated with the denser slab.

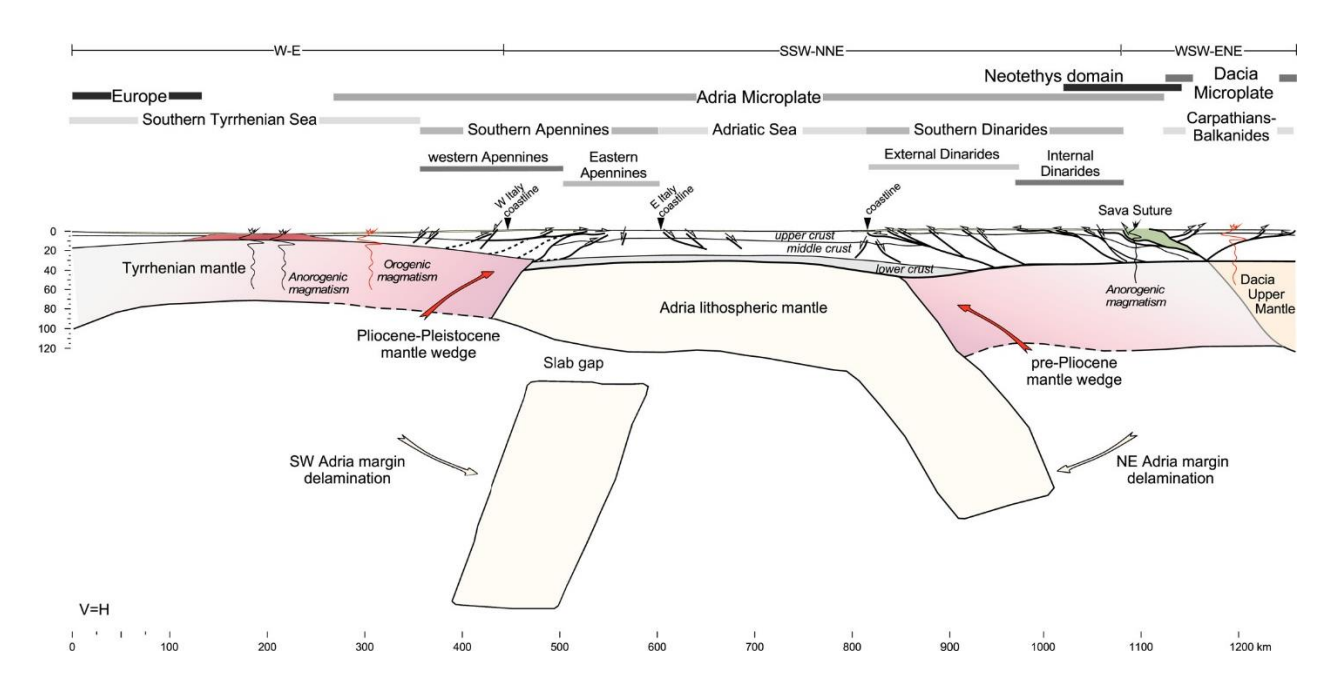


**Figure 4.11** Geodynamic interpretation of the lithospheric structure along the southern transect presented in this chapter.

# 4.4. Chapter conclusions

In this chapter, I present the findings of a geophysical-petrological model of the lithosphere and uppermost sublithospheric mantle, spanning from the southern Tyrrhenian Basin to the Carpathians-Balkanides in a roughly SW-NE direction, crossing the southern Apennines and Dinarides fold-thurst belts. The modeled transect offers an integrated view of the deep structure of Adria and Dacia microplates. It also reveals the west- and east-dipping slabs occurring along both sides of the Adriatic foreland, responsible for building the Apennines and Dinarides orogenic systems. Based on this study I can draw the following conclusions:

- In the southern Tyrrhenian Basin, the obtained results confirm the presence of a variable-thickness sedimentary layer overlying serpentinized mantle rocks. The degree of serpentinization in the mantle rocks decreases from 75% to 25% with depth, transitioning laterally to a two-layered magmatic crust.
- In the southern Adria domain, my modeling reveals a transition in crustal structure from west to east. A double-layered crust underlies the western Apennines, laterally transitioning to a thicker, three-layered crust characteristic of the eastern Apennines, Adriatic Sea, and southern Dinarides. The Moho depth varies from 40 km beneath the Apennines to 50 km beneath the Dinarides. Crustal thickening primarily occurs at the expense of the lower crust, which nearly doubles its thickness. In the internal Dinarides (Adria microplate) and the Carpathian-Balkanides (Dacia microplate), the crust has a relatively constant thickness of 30-35 km.
- The thermal LAB shows significant lateral variations recording the different tectonic evolution since the Mesozoic. Beneath the southern Tyrrhenian Basin, the LAB is shallow, reaching a depth of ~70 km. Toward the southern Apennines and Dinarides, the lithosphere gradually thickens, reaching ~280 km in the Dinarides below the Dacia microplate. From the internal Dinarides to the Carpathians-Balkanides, the LAB is relatively flat at a depth of about 120 km.
- The thermo-geochemical model shows two different mantle compositions: a slightly depleted mantle with an average Mg# of 89.5 for the Adria and Dacia microplates, and a more fertile mantle below the southern Tyrrhenian and Apennines (DMM-6%) and Dinarides (DMM-3%). This is consistent with the presence of two sublithospheric mantle wedges, attributed to the rollback of the Apennines and Dinaric slabs.

# Chapter 4. The Southern Apennines and Dinarides Orogenic Systems

- My results also reveal the presence of two thermo-compositional anomalies beneath the southern Apennines and Dinarides. These anomalies exhibit a temperature anomaly of -200 °C compared to the surrounding mantle and share the same composition as the Adria lithospheric mantle. The anomalies beneath the southern Apennines and Dinarides differ significantly. In the Dinarides, a short, east-dipping anomaly suggests a lithospheric slab ending at 280 km depth. However, below the Apennines, the best fitting model indicates the presence of a slab gap. This gap separates the west-dipping cold anomaly from the lithosphere, extending from 160 km to 400 km depth. The presence of this slab gap could potentially indicate a horizontal tearing of the subducted slab.
- As observed in the northern transect, the model results allow for two distinct lithospheric mantle compositions beneath the study area. Beneath the entire Adria microplate, a re-enriched basalt layer may be present. In contrast, the Dacia microplate likely has a more fertile mantle composition. Interestingly, the modeling suggests a fertile mantle composition beneath the Apennines and Dinarides compared to the rest of Adria and Dacia. As already pointed out in the northern transect, this finding aligns with the presence of two sublithospheric mantle wedges, potentially caused by the bidirectional delamination of the Adria lithospheric mantle.

# CHAPTER 5 General Discussion

# **Chapter 5. General Discussion**

In this Chapter, I integrate the results from the geophysical-geochemical models along the northern and southern Adria transects with independent geological, and geophysical data to investigate the role of the Adria Microplate in the geodynamic evolution of the Central Mediterranean region. Since both transects have been modeled using the same methodology (Kumar et al., 2020), the comparison is straightforward.

I also analyze and discuss the main structural features of the crust and lithospheric mantle observed in the northern Tyrrhenian-Apennines and Dinarides based on the results of Chapter 3, and compare them with those obtained in the southern transect crossing the southern Tyrrhenian-Apennines and Dinarides from Chapter 4. Additionally, I compare the distinct mantle compositions and sublithospheric mantle anomalies obtained from the thermal approach, in relation to oxide compositions (lithospheric mantle) and velocity/thermal anomalies (sublithospheric mantle). Finally, I explore the geodynamic consequences that can be inferred from the resulting lateral variations of the lithosphere across the southern transect.

# 5.1. Present-day crustal and lithospheric structure

Numerous geological, geophysical, and interdisciplinary investigations have been carried out in the study region (Figure 1.3), providing great constraints on the detailed crustal structure along the modeled transects. However, the Adriatic Sea region remains less constrained due to the scarcity of Deep Seismic Soundings (DDS) and Multichanel Seismic Data (MCS). When comparing the crustal structure of the northern and southern profiles (Figure 5.1), the most significant differences are observed in the Tyrrhenian Basin. The Adria crust, between the Apennines and the Dinarides, has been modeled as a three-layer structure, comprising the upper, middle, and lower crust with relatively similar densities, while beneath the internal Dinarides my results show a two-layer crust (uppermiddle and lower crust). Although the best fitting model and geological data indicate a two-layer crust below the internal Dinarides, I cannot rule out the presence of a three-layer crust. The resolution of the geophysical data used is not accurate enough to distinguish between two or three layers, as the response will be the same if the distribution of average density in depth is similar.

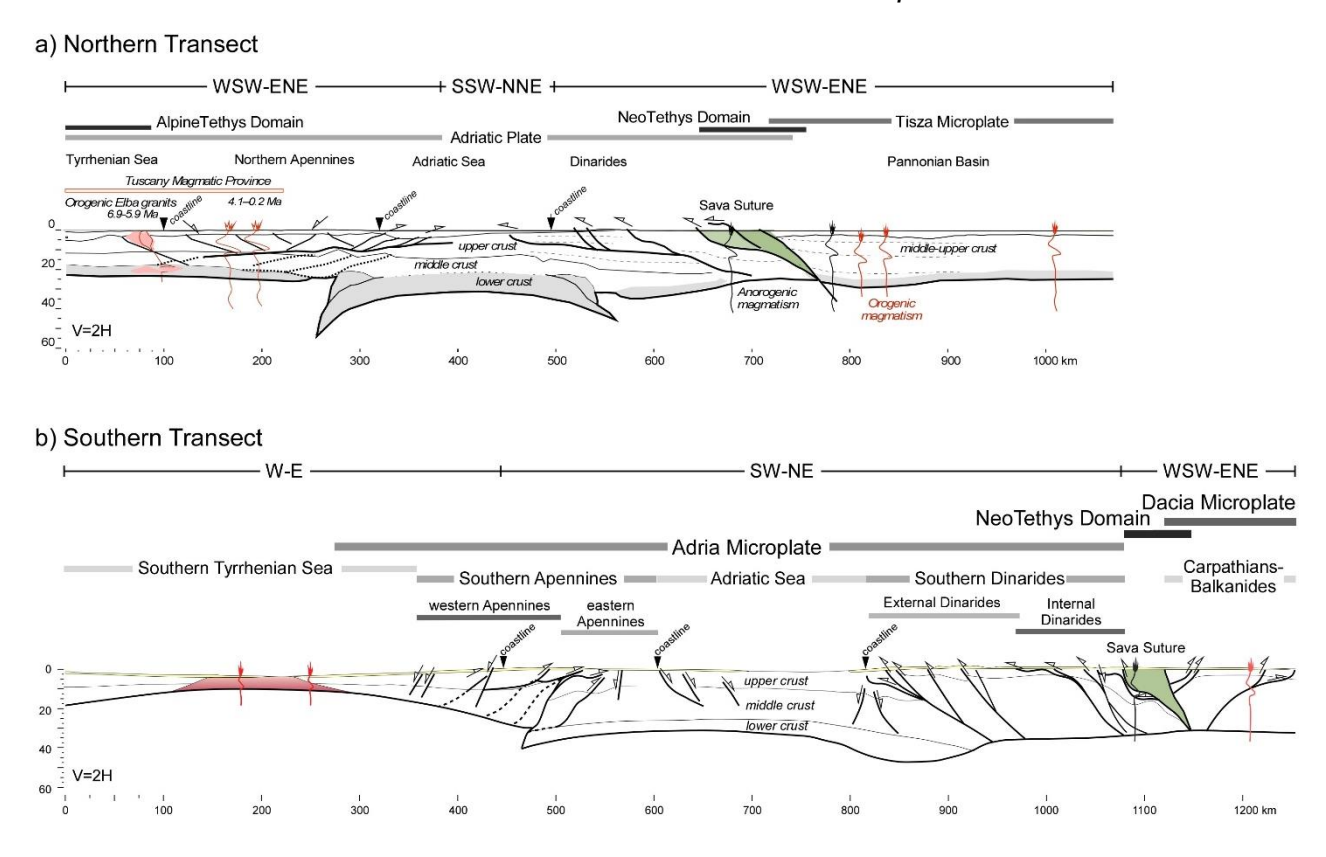


**Figure 5.1** Crustal structure along the northern (Chapter 3) and southern transects (Chapter 4). To facilitate comparison between the two transects, their origins have been aligned with the coastline of Corsica and Sardinia, respectively. See Figure 1.4 for their respective locations.

Slightly higher densities for the upper-middle crust are obtained along the southern transect, although they are not large enough to be considered significant. Regarding the base of the crust, the comparison between the northern and southern transects shows a crustal thickening along the eastern Adriatic Sea and southern external Dinarides (Figure 5.1). The southern external Dinarides have a crust that is about 10 km thicker than in the northern profile, which agrees with the teleseismic data results of Stipčević et al. (2020). Furthermore, the density of the lower crust is slightly higher, which is coherent with its increasing depth.

To the west, the Tyrrhenian Basin shows a very distinct organization north and south of 41 °N latitude (Faccenna et al., 2001; Peccerillo, 2017). In the northern Tyrrhenian Basin, the obtained density-depth distribution and crustal structure corresponds to that of a thin continental crust with widespread volcanism, extending to the Tuscany Magmatic Province (e.g., Dini et al., 2002; Pandeli et al., 2013; Sani et al., 2016).

My results along the northern transect, Chapter 3, show that the western Apennines and northern Tyrrhenian Basin are characterized by high thermal gradient and thermal properties (thermal conductivity and heat production, 3.1 W/(m·K) and 3.8-1.0  $\mu$ W/m³, respectively) characteristic of magmatic rocks. Assuming that the continental collision

between the Corsica-Sardinia Block and the Adria microplate took place at 30-25 Ma (Carminati et al., 2012; Molli and Malavieille, 2011; Romagny et al., 2020; Turco et al., 2021), these magmatic rocks could be associated with either the retreat of a continental slab or the continental delamination of the Adria lithospheric mantle, possibly initiated ca. 15 Ma, as proposed by Benoit et al. (2011).

For the southern transect, I have modeled a thin sedimentary cover and two exhumed mantle layers that display varying degrees of serpentinization, in agreement with the results of Prada et al. (2014). As in the northern region, volcanism is widespread extending to the onshore Campanian Plain. Magmatism in the central Tyrrhenian Basin is triggered by both extension-induced melting (back-arc basin magmatism) and continental delamination-related processes. Moreover, the offshore and onshore continental platform is characterized by volcanic arc-type magmatism. Peccerillo (2017) concludes that magmatism from the Tuscany Province of the northern Apennines to the Aeolian Arc northwest of Calabria exhibits geochemical markers of source regions that have undergone metasomatism related to subduction processes (involving fluids and subducted sediments). These processes are superimposed upon original mantle components ranging from compositions akin to MORBs to Ocean Island Basalts (OIBs).

Regarding the differences in crustal structure of the orogenic belts, in the northern Apennines, the crust is thicker and less dense compared to the southern Apennines. The northern Apennines are mainly composed of sedimentary and metamorphic rocks, which are folded and thrust-faulted due to the collision of the African and Eurasian plates. In contrast, the southern Apennines have a thinner crust that is denser and highly metamorphosed (Montone and Mariucci, 2023). In addition, the northern Dinarides have a thicker and more stable crust with a simpler structure, while the southern Dinarides have a thinner and more complex crust with a more varied structure, including ophiolite complexes (e.g., Balling et al., 2021). These differences in crustal structure are likely related to the different geological histories and tectonic processes that have occurred in the two regions. Similarly, receiver-function (Bianchi et al., 2010, Piana Agostinetti et al., 2011) and seismic tomography (Chiarabba et al., 2009) support that the Tyrrhenian Moho represents a detachment surface with its leading edge beneath the Apennines crest, beneath which the lower crust and continental lithosphere of the Adria microplate separate from the upper crust.

For both the northern and southern transects, the calculated LAB depths show varying degrees of agreement and discrepancy with previous studies. In the northern transect (Figure 3.4e), results are consistent with Artemieva (2019), except below the Apennines and Adriatic Sea. Additionally, the findings are consistent with Šumanovac and Dudjak

(2016) and Belinić et al. (2018) below the Dinarides, but I observe a deeper LAB beneath the Pannonian Basin.

In the southern transect (Figure 4.4e), the RF results from Miller and Piana Agostinetti (2012) partially coincide with my LAB predictions in the Apennines, where the thermal LAB is about 120 km deep. However, most seismic studies suggest a shallower seismic LAB compared to the thermal LAB (Figure 4.4e). In the southern Tyrrhenian Basin, surface wave dispersion curves suggest a seismic LAB at about 50 km depth (Pontevivo and Panza, 2002; Pontevivo 2003; Panza et al., 2007), which is shallower than our thermal LAB at 70 km depth. This systematic discrepancy between the seismic and the thermal LAB was also found in previous studies (e.g., Jiménez-Munt et al., 2019 and Fullea et al., 2021). In this study I find that the 950°C isotherm provides the best fit of the seismic LAB. This result is in close agreement with the 1000 °C  $\pm$  50 °C isotherm found for the seismic LAB by Jiménez-Munt et al. (2019)

# 5.2. Mantle composition and anomalies

Figure 5.2 shows the results of the two transects and their locations in a 3D view. My results clearly identify the presence of several lithospheric mantle domains with distinct composition. Due to the absence of xenolith samples or other petrological data available from the Adriatic Sea and Balkanides, the representative Tecton lithospheric mantle composition (Tc 2) is used for the entire Adria and Dacia mantle, based on the tectonothermal age of the overlying crust, as suggested by Griffin et al. (2009). This composition has also been proposed by Alasonati Tašárová et al. (2016) for the eastern Alpine slabs or beneath young extensional areas (Griffin et al., 1999; O'Reilly and Griffin, 2006). The Tc 2 composition is only slightly depleted compared with the Primitive Upper Mantle (PUM) and depleted MOR basalt mantle (DMM), but less fertile than other Tectons compositions (Figure 5.3). Along the Pannonian Basin, the PB mant composition proposed by Downes et al. (1992), based on the analysis of 20 xenolith samples and further confirmed by the best-fitting model results of Alasonati Tašárová et al. (2016), fits well with my modeling approach. The Mg# of most of these xenolith samples from the western Pannonian Basin mainly falls between 89 and 91, with an average value of 90.4 (Downes et al., 1992).

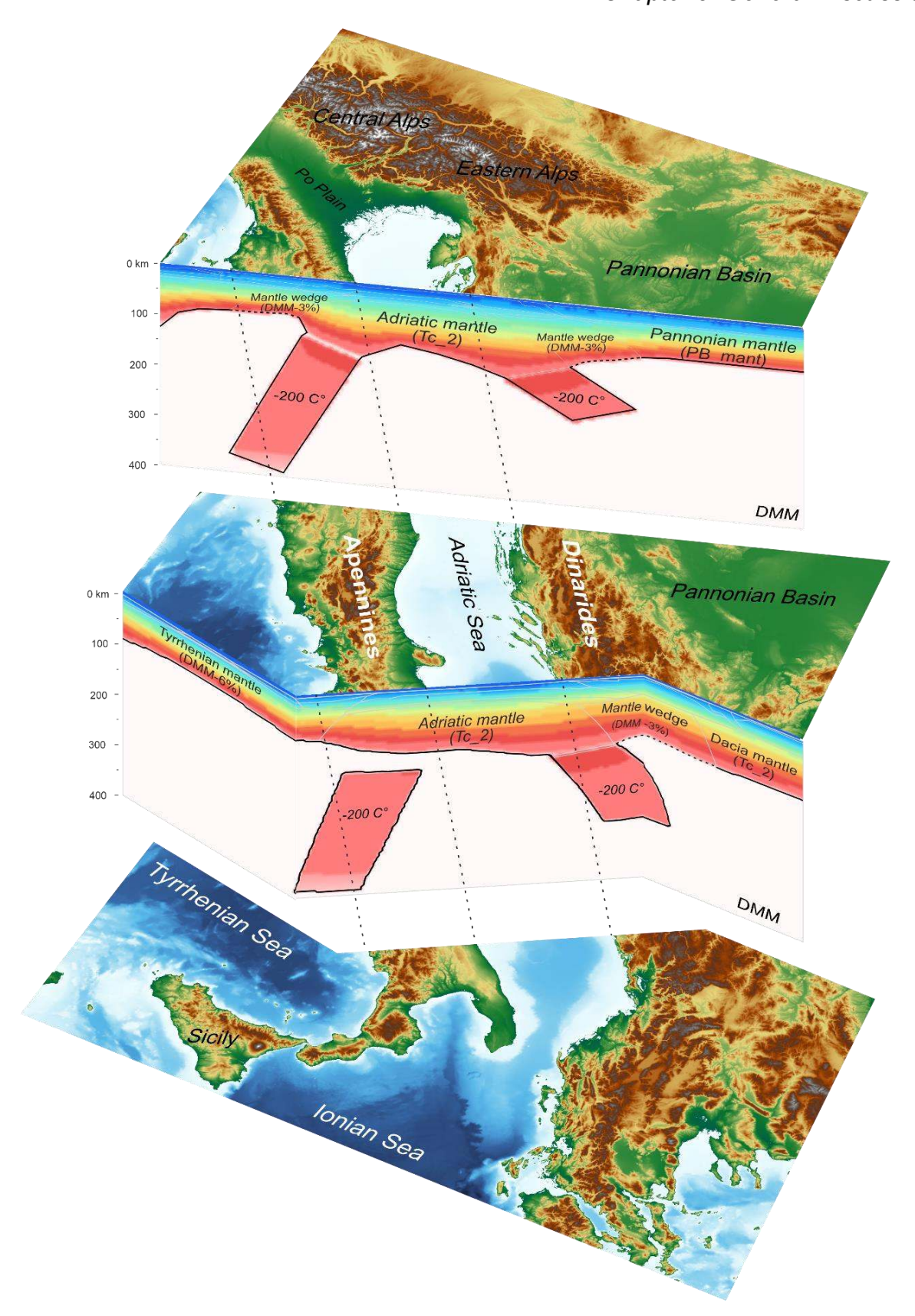


**Figure 5.2** 3D top view showing the location and main results along the two modeled transects. The vertical cross sections show the temperature distribution for the whole lithosphere and mantle anomalies. The dashed black lines project the locations of the coastlines.

My results also show the existence of mantle wedges with a slight degree of melting beneath the northern Apennines and Dinarides (Figure 5.2). Along the northern transect, I propose two mantle wedges with a DMM-3% composition resulting from the rollback of the Ligurian-Tethys oceanic slab in the SW margin of Adria, and from the Vardar-Neo-Tethys oceanic slabs in its NE margin. The two opposite and asynchronous subduction rollback processes were followed by continental mantle delamination of the southwestern and northeastern distal margins of the Adria Microplate.

In the southern Tyrrhenian Basin, considering the age and type of the magmatism and my best-fitting model, the lithospheric-mantle wedge is compatible with a DMM composition with 6% of melting. The higher melting composition is probably associated with its back-arc origin, and degree of partial melting that can be inferred from the characteristics of the volcanic activity within the region (Panza et al., 2007). This mantle composition encompasses the Tyrrhenian Basin, the thinned onshore continental margin and the western Apennines. In the Dinarides region, along both transects, modeling results show a DMM mantle wedge with 3% of melting. The primary difference lies in its length; however, it aligns with the distance between the Sava suture zone and the subduction hinge.

Along both transects, the density of the lithospheric mantle underneath the Dinarides is significantly greater than beneath the Tyrrhenian region. This difference arises due to lithospheric thinning in the Tyrrhenian region, leading to an increase of the thermal gradient and, consequently, a decrease in density and seismic velocities.

Regarding the sublithospheric mantle I find thermal anomalies with different extent and geometry along the Adria margins. Several seismic velocity anomalies in the sublithospheric mantle, especially beneath Adria's margins, have been imaged by seismic tomography models (e.g., Amaru, 2007; Šumanovac et al., 2017; El-Sharkawy et al., 2020; Belinić et al., 2021; Handy et al., 2021; Rappisi et al., 2022), which I have modeled as sublithospheric thermo-compositional anomalies (Figure 5.2). Having no other data or evidence, I have assumed that its composition is the same as Adria mantle (Tc\_2), thereby ignoring the effect of possible mantle transformations that may be related to the subduction processes.

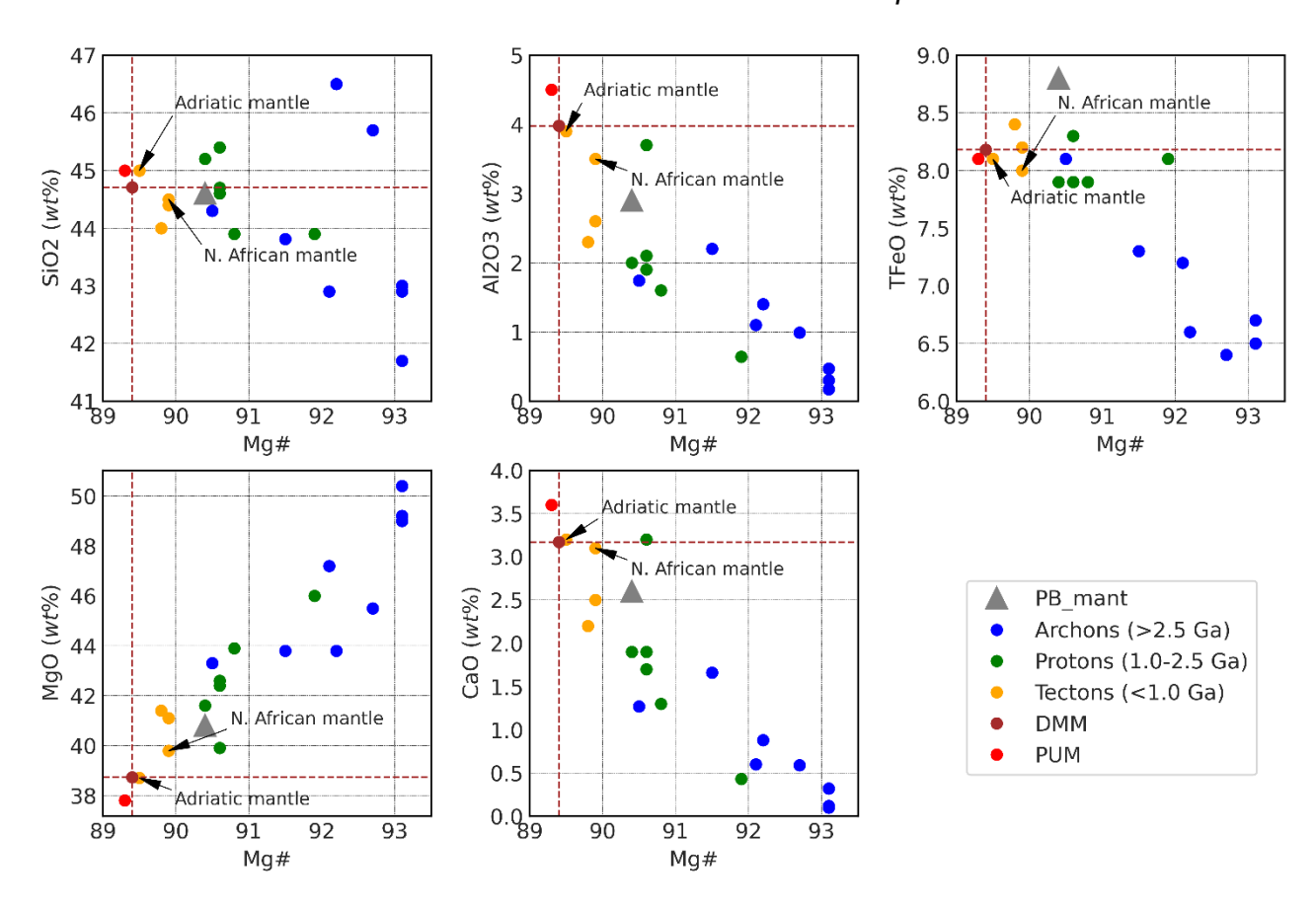


**Figure 5.3** Major element oxide weight percentages of mantle compositions are plotted as a function of Magnesium number Mg#. Gray triangle represents the composition of Pannonian mantle (PB\_mant, Downes et al., 1992; Alasonati Tašárová et al., 2016). Colored dots represent the classification of the lithospheric mantle composition by Griffin et al. (2009) based on the tectonothermal age of the overlying crust: Archons (2.5 - 1.0 Ga) in blue, Protons (1.0 Ga) in green, and Tectons (<1.0 Ga) in yellow. DMM is the sublithospheric mantle composition assumed in this Thesis (Workman and Hart, 2005), in dark red. PUM (light red) is the primitive upper mantle from McDonough and Sun (1995). I also marked the Adriatic mantle composition (Tc\_2), and the composition of northern African mantle (N. African mantle) used in Kumar et al., (2021).

My results show the presence of two slabs in the western and eastern margin of Adria (Figure 5.2), although their shape, continuity and extend at depth are still in debate (e.g., Šumanovac et al., 2017; El-Sharkawy et al., 2020; Handy et al., 2021). In the western margin of Adria, my results show that the slab beneath the northern Apennines is west-dipping and attached to the continental lithosphere, reaching to 400 km depth while the southern slab beneath the southern Apennines is detached, extending from 160 km to 400 km. This detached slab possibly is the result of a slab horizontal tearing, and I am discussing it in Section 5.4. The length of the slab should be taken with caution since my model is limited to a depth of 400 km and some studies have suggested that the slab in the northern Apennines may extend to greater depths (Figure 5.4), possibly reaching into the transition zone (e.g., Lucente and Speranza, 2001; Amaru, 2007).

In the eastern margin of Adria, the anomalies below the northern and southern Dinarides are east-dipping and shorter than those observed at the western margin of Adria. The slabs beneath the Dinarides reach about 200 km depth in the north and 280 km in the south (Figure 5.2), in agreement with Belinić et al. (2021) and Rappisi et al. (2022). The variations in depth of the eastern Adria slabs may be caused by differences between the North and South subduction and continental delamination histories. Their length greatly fits the distance from the Sava suture zone to the subduction hinge (Figure 5.2), which supports the delamination process beneath the Dinarides after continental collision.

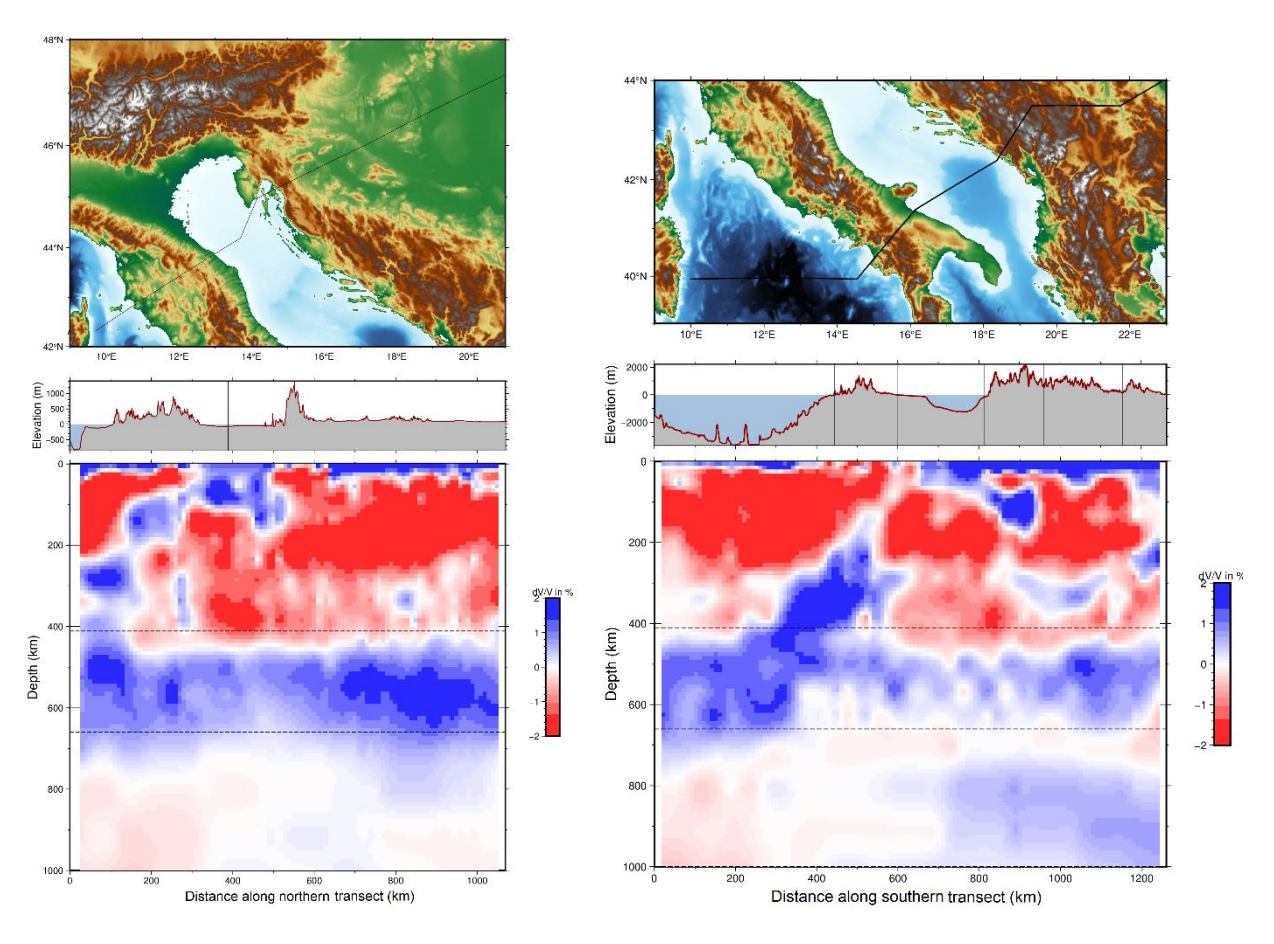


**Figure 5.4** Lower panels show mantle seismic tomography along northern and southern transects (Amaru, 2007). Upper panels show the topography maps and elevation profile along the transects (black lines).

# 5.3. Dynamic topography

Following the classical definition by Braun (2010), the dynamic topography is the vertical deflection caused by viscous stresses generated by flow within the sublithospheric mantle. The study of dynamic topography provides valuable information about the interaction between mantle flow and surface deformation, contributing to a deeper

understanding of Earth's geodynamic processes. However, the amplitudes of dynamic topography in the Mediterranean region are still debated (Boschi et al., 2010; Carminati et al., 2009; Faccenna et al., 2014; Molnar et al., 2015; Gvirtzman et al., 2016; Faccenna and Becker, 2020), and this is in part due to the uncertainties on the determination of the isostatically compensated/residual topography component (e.g., Becker et al., 2014; Levandowski et al., 2014; Guerri et al., 2015).

Figure 5.5 compares the isostatic topography and dynamic topography along the northern transect. The isostatic elevation is the result of three different scenarios: 1) local isostasy including sublithospheric anomalies; 2) local isostasy without sublithospheric anomalies and an elastic thickness of 20 km (Figure 5.5a, see Chapter 3). Following the definition from Faccenna and Becker (2020), the residual topography is the subtraction between the isostatic component and the observed topography. Residual topography (Figure 5.5b) shows large variations, with values exceeding 1 km in the Apennines. Regional isostasy considerably reduces the residual topography to less than 500 m, with higher values observed in the northern Apennines, Dinarides, and the Sava suture zone. These calculations disregard vertical movements induced by mantle flow, which can be significant, particularly in areas with deep slabs where phenomena such as viscous pulling or suction may occur. The residual topography could be associated with a dynamic contribution of the mantle flow.

The dynamic topography calculated with Equation 2.34 from Stokes flow in Chapter 2, accounts for vertical movements due to mantle flow, as well as buoyancy forces arising from lateral density contrasts (Figure 3.7). Although this 'dynamic topography' is conceptually different from the classical definition of topography associated with mantle flow, I prefer to retain this terminology as it is standard in the literature. The values of this dynamic topography are less than 400 m (Figures 3.7 and 5.5c). To identify the topography resulting just from the flow due to mantle anomalies, it is necessary to eliminate the lithosphere component. Therefore, the dynamic topography caused solely by mantle anomalies (red line from Figure 5.5c) is obtained by subtracting the dynamic topography without mantle anomalies (model Figure 3.7c, black line Figure 5.5c) from the dynamic tomography with mantle anomalies (Figure 3.7b, blue line Figure 5.5c). Finally, in Figure 5.5d, I compare the dynamic topography (caused by mantle anomalies) with the residual topography derived from regional isostasy.

Figure 5.5d shows that most of the residual topography in the northern Apennines can be attributed to the dynamic response to mantle anomalies. In contrast, since the dynamic response to the mantle anomaly below the Dinarides is negligible, the high residual topography (up to 400 m) is likely to be attributed to local effects, such as short-wavelength density variations not accounted for in the modeling presented in Chapter 3.

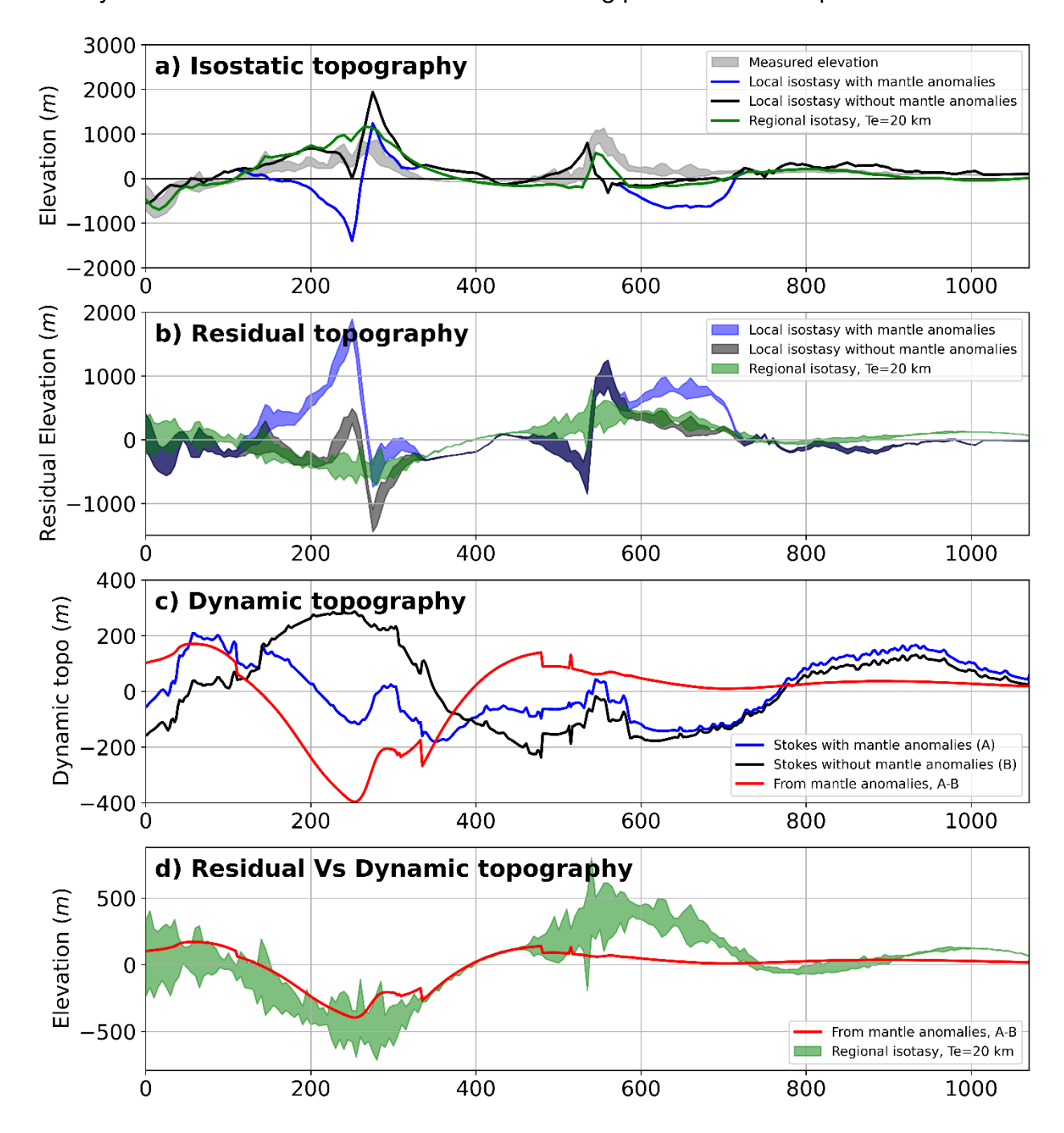


**Figure 5.5** Isostatic, residual and dynamic topography along the northern transect. In blue, including the two sublithospheric anomalies; In dark-gray, without the two sublithospheric denser anomalies; In green, regional isostasy (T<sub>e</sub> = 20 km) without the two sublithospheric denser anomalies. (a) Standard deviation of the observed elevation across a 50-km-wide swath (light-gray); modeled local (blue and dark-gray) and regional (green) isostatic elevation form LitMod\_2D (Chapter 3). (b) Standard deviation of the residual topography, according to (a). (c) Dynamic topography (Figure 3.7). (d) Standard deviation of the residual regional isostasy (green); dynamic topography attributed to the dynamic response to mantle anomalies (red line).

In the southern transect, I followed the same procedure described for the northern transect, Figure 5.6. In this case, I considered three mantle anomalies distribution (see Chapter 4, Figure 4.9) and their corresponding topographic response (Figure 5.6c). The dynamic topography, just caused by the mantle anomalies, is the difference between the topographic response of model with the Apenninic slab gap (Figure 4.9b) and the model without anomalies (Figure 4.9c).

The isostatic model that shows smaller residual topography is the regional isostasy with a 30 km elastic thickness (green line, Figure 5.6b and d). However, it also shows some misfit in the southern Apennines (-250 m) and Dinarides (-400 m). In contrast, the maximum contribution of the dynamic topography (associated to mantle anomalies) is between 100-150 m (Figure 5.6d), being the amplitude of the dynamic contribution much lower than the residual topography. The dynamic contribution of the mantle anomalies to the southern profile is very small. Therefore, the residual topography amplitudes up to 400 m found in the western Adriatic and external Dinarides should be attributed to local structural variations not included in the modeling of the southern transect (Chapter 4).

The dynamic topography beneath the southern Apennines is about 120 m, which is three times lower than that in the northern Apennines. This difference is attributed to slab geometry: in the northern Apennines, the topography is controlled by the pulling effect of the attached slab, whereas in the southern Apennines, it results from the suction of the detached slab. In other words, the detached slab in the southern Apennines is less effective in producing topographic undulations compared to the continuous slab beneath the northern Apennines. Conversely, on the eastern margin of Adria, the dynamic contribution is greater in the southern Dinarides (around 150 m) than in the northern Dinarides, where it is practically negligible. This is due to the increasing slab length from north to south.

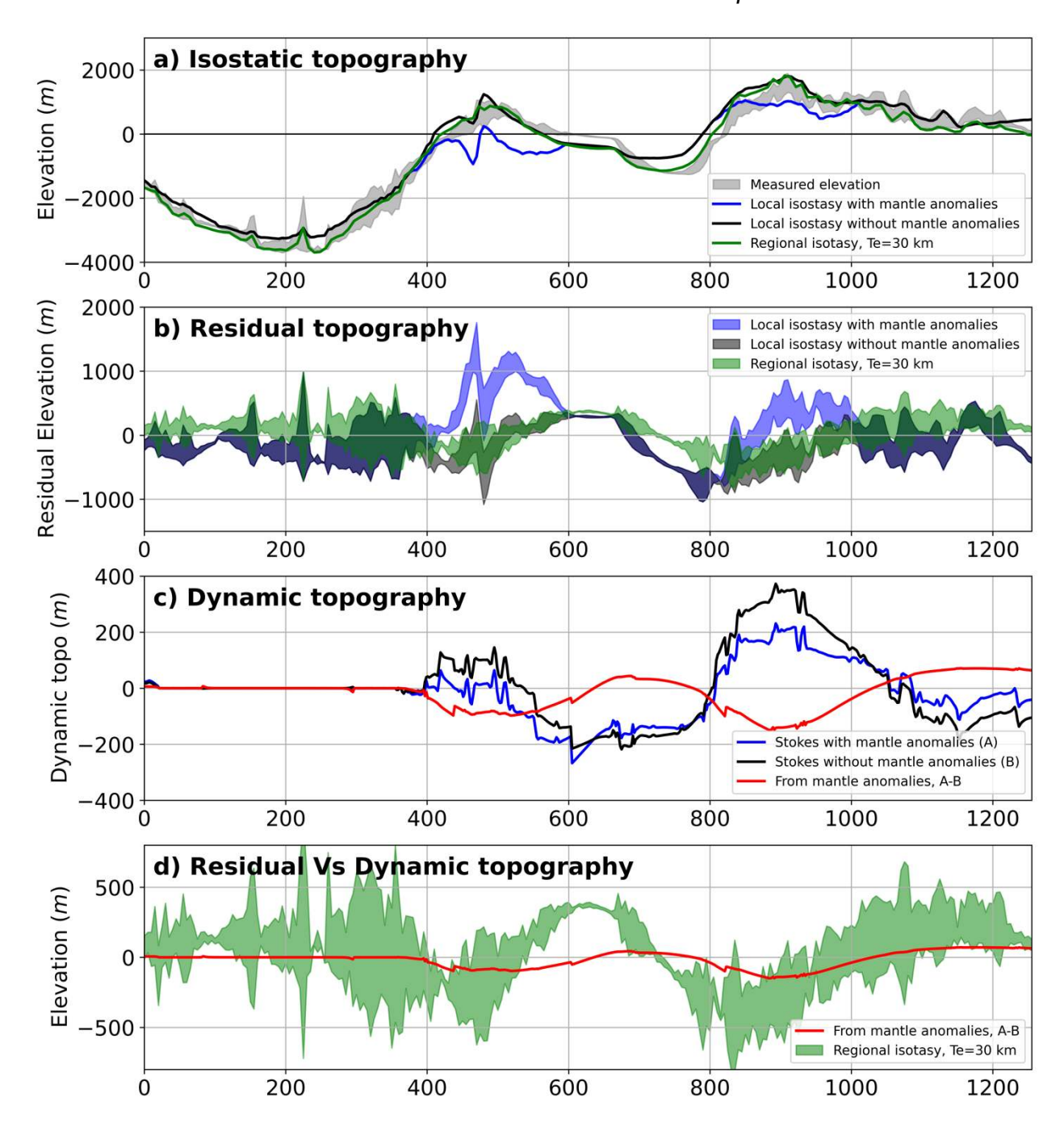


**Figure 5.6** Isostatic, residual and dynamic topography along the southern transect. In blue, including the two sublithospheric anomalies, with the slab gap beneath the Apennines; In dark-gray, without the two sublithospheric denser anomalies; In green, regional isostasy (T<sub>e</sub>= 30 km) without the two sublithospheric denser anomalies. (a) Standard deviation of the observed elevation across a 50-km-wide swath (light-gray); modeled local (blue and dark-black) and regional (green) isostatic elevation form LitMod\_2D (Chapter 4). (b) Standard deviation of the residual topography, according to (a). (c) Dynamic topography. (d) Standard deviation of the residual regional isostasy (green); dynamic topography attributed to the dynamic response to mantle anomalies (red line).

# 5.4. Geodynamic implications

Results from the two modeled transects support an initial configuration consisting of a main microplate, Adria, and two smaller microplates or, as some authors refer to them, continental blocks: Tisza, to the North and Dacia to the South (e.g., Schmid et al., 2020; Bravo-Gutiérrez et al., 2024). The Tisza and Dacia microplates, separated from the Adria microplate by the N-S oriented Vardar Ocean (a branch of the Neo-Tethys Ocean), interacted through subduction processes during Mesozoic and Cenozoic time within the framework of the Africa and Eurasia convergence, which also led to the development of a SE-dipping Alpine-Tethys subduction system responsible for the formation of the Alps.

The Adria microplate shows the most complex crustal structure since it encompasses both the Apennines and Dinarides fold-thrust belts that show opposing vergence and are separated by the Adriatic Sea foreland. The Apennines orogenic system was built from Oligocene onwards by the deformation of the thinned western continental margin of Adria, after the consumption of the Ligurian-Alpine Tethys in a NW- and W-dipping subduction (Figure 3.8). I interpret the sublithospheric anomaly observed in the model, extending down to 400 km beneath the Apennines, as the remnant of the slab following these processes. The eastern margin of Adria microplate was deformed over a much longer period spanning the Mesozoic and Cenozoic building of the Dinarides orogenic system (Schmid et al., 2008, 2020; Van Unen et al., 2019).

The Apennines thrust system geometry is still debated, since thin- and thick-skinned models have been proposed (e.g., Butler et al., 2004). Several studies suggest that its most recent Neogene evolution is associated with east-directed rollback and subsequent delamination processes (e.g., Benoit et al., 2011; Chiarabba et al., 2014; D'Acquisto et al., 2020). The Internal Dinarides are composed by thrusted tectonic domains, including the Western Vardar Ophiolite Unit (e.g., Schmid et al., 2008), involving Mesozoic cover rocks belonging to the NE distal margin of Adria (Tari, 2002; Tomljenović et al., 2008). Jurassic obduction of Vadar oceanic crust is well preserved and well imaged in my crustal profile by a high-density body about 50 km wide and extending down to the base of the crust.

In summary, the present-day structure of the crust and lithospheric mantle in the study region is the result of a prolonged tectonic evolution. This includes the subduction and delamination of the Adria microplate, as well as the lithospheric breakup and seafloor spreading in the southern Tyrrhenian basin, and continental extension and rifting of the Pannonian back-arc basins. The analyzed transects show the present-day lithosphere mostly formed during the pervasive Cenozoic northern Africa convergence triggering the

building of the subduction-related orogenic systems. However, the deep mantle structure is the result of the bidirectional delamination of the Adria lithosphere.

In the northern Adria region, the coexistence of crustal thinning in the Tyrrhenian domain and thickening toward the forefront of the northern Apennines fold belt may be explained by northeastward rollback of the SW Adria slab and its subsequent continental mantle delamination (see Chapter 3). In the southern Adria region, the deep structure is more complex, primarily due to the nearly 90-degree change in tectonic directions between the southern Apennines and the Calabrian Arc and their respective slabs (Edwards and Grasemann, 2009; Faccenna et al., 2014). Wadati-Benioff zone earthquakes and local earthquake tomography studies have unveiled the geometry and position of the Calabrian slab, along with its role in the tectonic evolution of the region (e.g., Scarfi et al., 2018; Presti et al., 2019; Neri et al., 2020), showing that the slab might extend to depths of 300-450 km with an approximate northern dip ranging from 60 to 70°, thus reaching the central region of the southern Tyrrhenian Basin (e.g., Giardini and Velonà, 1991; Chiarabba et al., 2005, 2008; Neri et al., 2020).

Underneath the Apennines, the integrated modeling points to a significant cold thermal anomaly ( $-200\,^{\circ}$ C) that extends to depths of at least to 400 km, reaching the lower boundary of the model. The main difference is that in the northern profile, the slab is attached to the continental lithosphere. Conversely, in the southern profile, most seismic tomography studies and the results of the best-fit model show a discontinuity or rupture at depths 120 and 160 km (Figure 5.2 and 5.7).

One possible hypothesis is that the southern transect intersects a slab gap likely linked to a vertical tear fault that would have favored the initiation of a slab tear, as depicted by the modeled profile (Figure 5.7 and 5.8). This gap has been commonly interpreted as the detachment of the southern Apennines slab. It has been explained by different models (Spakman and Wortel, 2004; Rosenbaum et al., 2008; Neri et al., 2009), all of them involving a sub-horizontal or vertical lateral tear detachment, with the broken slab dipping like the northern and Central Apennines slab segments (Figure 5.8). The slab tear direction would therefore be sub-parallel to the direction of the Apennines rather than sub-perpendicular if it is related to a transform fault defining the segments of the SW Adria margin. From this viewpoint, the modeled slab gap could be the result of incipient slab break-off at the corner of this collision zone (bordered by the transform fault), similar to the 3D numerical model by Li et al. (2013) and Boonma et al. (2023). In an alternative view, Carminati and Chiarabba (2023) compare two cross-sections across the southern Apennines and Calabrian arc and identify similar slab necking structures that they interpreted as slab damage zones. This process of slab weakening would be caused by

brittle-ductile damage in the outer rise (Gerya et al., 2021). According to this interpretation, slab weakening would be characterized by low viscosity zones leading slab break-off processes. While I agree with the interpretation of slab damage for deep necking features in both cross sections, the best fitting model, particularly geoid and elevation, suggests that the shallower low seismic velocity anomaly in the southern Apennines is a small slab gap that could be related to the initiation of a slab break-off process.

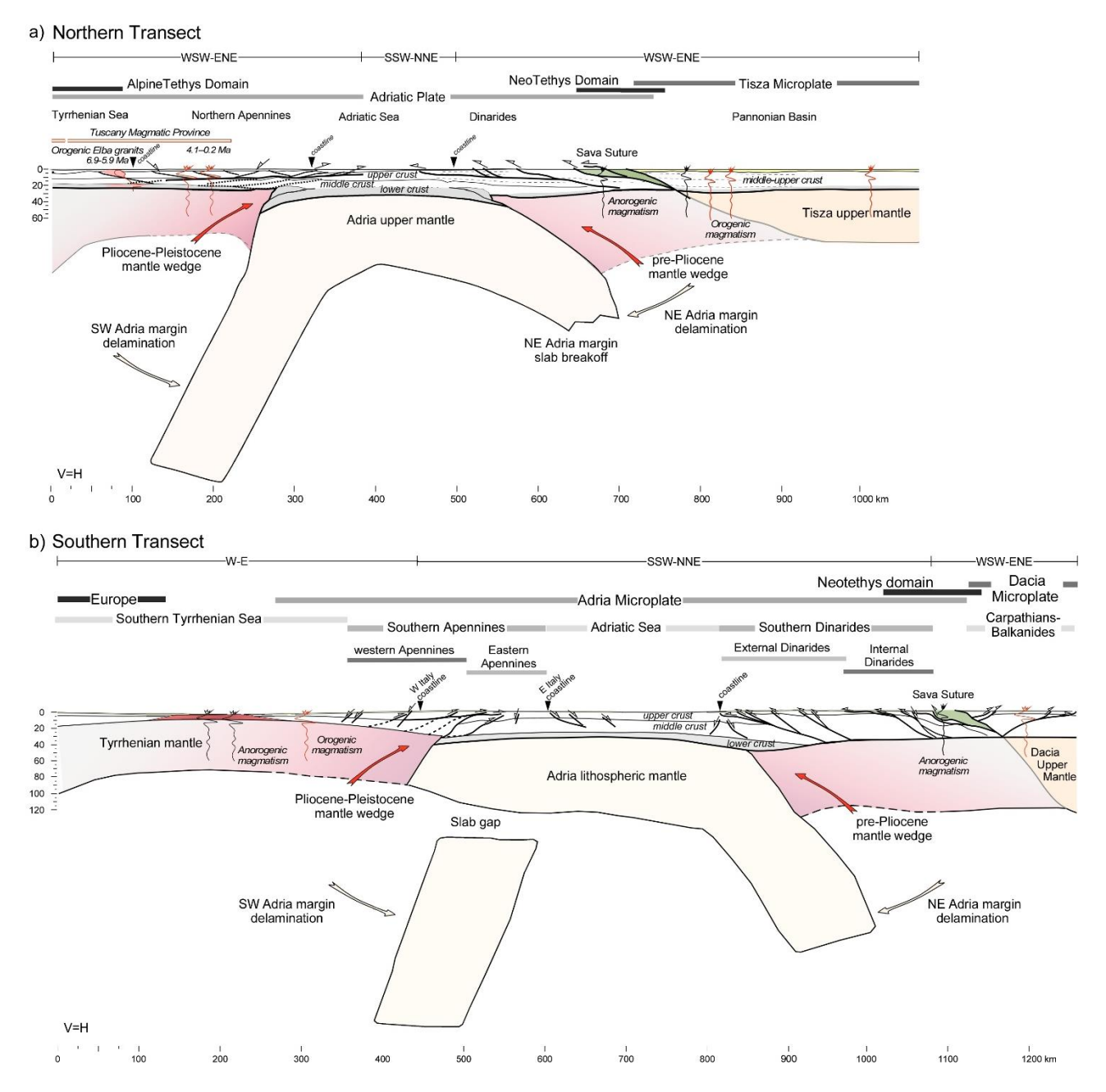


**Figure 5.7** Geodynamic interpretation of the lithospheric structure along the northern and southern transects. To facilitate comparison, the origins of both transects have been aligned with the coastlines of Corsica and Sardinia.

Vertical tears due to differential retreat have already been proposed by several authors to explain characteristic features observed in the Tyrrhenian-Apennines system (Doglioni, 1991; Doglioni et al., 1994, 2001; Scrocca, 2006; D'Orazio et al., 2007; Rosenbaum et al., 2008; Petricca et al., 2013; Chiarabba et al., 2016; Pierantoni et al., 2020; De Gori et al., 2022). Pierantoni et al. (2020) following other authors (e.g., Doglioni et al., 1994; Rosenbaum et al., 2008) and based on kinematic reconstructions, postulate that the subduction of the continental part of the slab initiated in the North and progressed toward the South. This could lead to different sinking velocities and, as a result, in the segmentation of the slab along slab tear faults. These tear faults might propagate along the trend of fracture zones and transform faults inherited from the break-up of Pangea.

Segmented margins have been proposed for other areas within the Western Mediterranean where slab asymmetry and geometric variations were inferred from seismic tomography and lithospheric modeling. For example, the existence of segments of the Jurassic Ligurian-Tethyan lithosphere along the Gulf of Cádiz-Gibraltar Arc region and in the Algerian basin is suggested to explain the observed lithospheric and upper mantle structure, and the double polarity of the subducting slabs (Fernàndez et al., 2019; Kumar et al., 2021).

A different slab configuration is modeled in the eastern margin of Adria. In the Dinarides the cold thermal anomaly reaches depths of about 200 km in the northern profile and 280 in the southern profile, shallower than those observed at the western margin of Adria (Figure 5.8). The variations currently observed in the geometry and depth of the western and eastern Adria slabs may potentially stem from differences in subduction and continental delamination histories. The initiation of oceanic subduction along the eastern Adria margin dates back to the Jurassic period, whereas subduction along the western Adria margin commenced during the Oligocene (e.g., Schmid et al., 2008; Carminati et al., 2012; Gawlick and Missoni, 2019; van Hinsbergen et al., 2020). Consequently, the eastern margin seems more evolved as the slab is either largely detached or is partially, if not completely, thermally re-equilibrated with the underlying sub-lithospheric mantle. Based on fission-track ages and isotope geochemistry, Schefer et al. (2010) concluded that (a) following the closure of the Neotethys in the Eocene, the north-eastward Adriatic slab had initiated continental delamination and retreat, and (b) slab break-off may have taken place shortly after the onset of continental delamination. This could explain the depth of the eastern slab, as determined through tomography and the thermal approach.

Adria is encompassed by significantly deformed convergent margins entailing three plate subductions with distinct polarities. One remarkable characteristic of these subducted and delaminated slabs is their diverse geometry and segmentation, as

observed in tomographic studies and being compatible with the thermal modeling results presented herein. These segments are divided by lithospheric gaps, which have often been interpreted as having formed during subduction (Faccenna et al., 2014). On the other hand, most of the paleogeographic maps depict a segmentation of the Adria margins, featuring segments separated by transform faults. These segments could indeed be remnants of the Mesozoic Adria plate margins, emphasizing the necessity for a more thorough and comprehensive investigation.

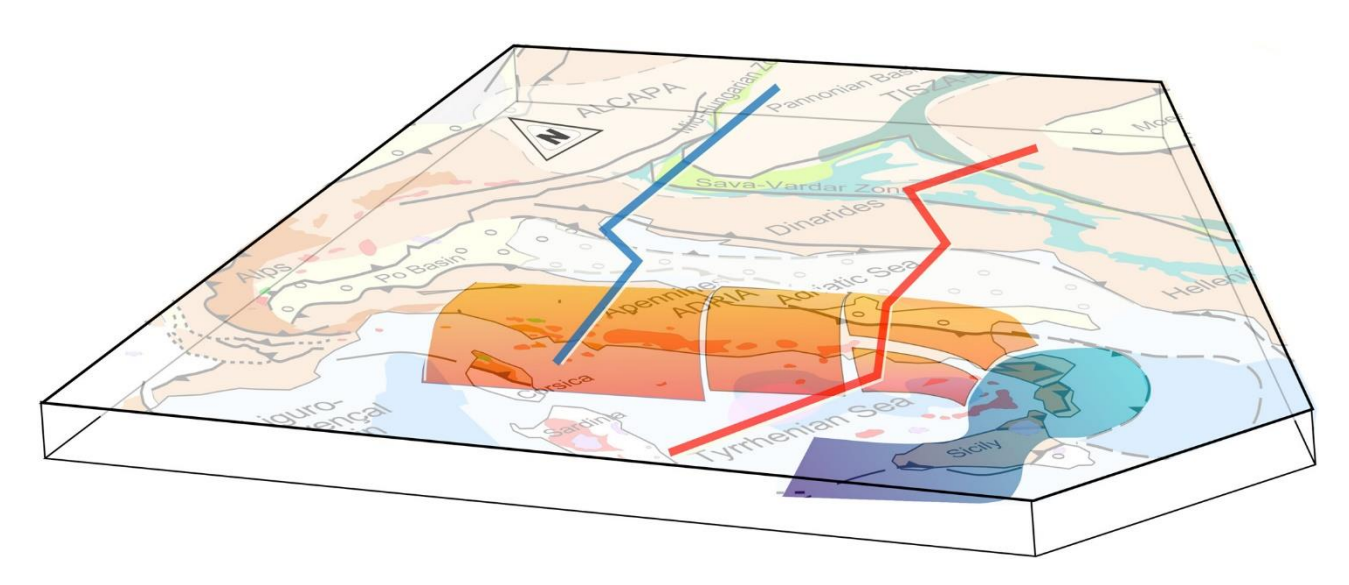


**Figure 5.8** Diagram illustrating a simplified view of the slab geometry underneath the western Adriatic margin. The slab geometry is based on integrated lithospheric modeling (northern transect, blue line and southern transect, red line) as well as geological and geophysical interpretations, for example, Spakman and Wortel (2004); Rosenbaum et al. (2008); Carminati et al. (2012); Faccenna et al. (2014); Sun et al. (2019); Pierantoni et al. (2020); Rappisi et al. (2022).

### Chapter 5. General Discussion

# CHAPTER 6 Conclusions, limitations and future work



## Chapter 6. Conclusions, limitations and future work

This thesis presents the findings of a geophysical-petrological model of the lithosphere and uppermost sublithospheric mantle along two transects spanning from the Tyrrhenian Basin to the Carpathians-Balkanides region, in a roughly SW-NE direction. The northern profile is approximately 1000 km, running from the Tyrrhenian Sea, the northern Apennines, the Adriatic Sea, the Dinarides and the Pannonian Basin. The southern profile is about 1250 km long and spans from the southern Tyrrhenian Basin, trough the southern Apennines, the Adriatic Sea, to the Carpathian-Balkanides region. Modeling these geotransects provides an integrated view of the deep structure of the Adria and Dacia microplates, as well as of the slabs located along the western and eastern Adria margins.

In particular, the geophysical-petrological model, further constrained by additional geological and seismological data, has allowed me to present the present-day crust and upper mantle structure (down to a depth of 400 km) of the Adria microplate and its margins. Furthermore, the model has allowed for the distinction of different mantle domains, the mapping of the geometry and extent of the slabs at depth, and the evaluation of the implications of deep mantle anomalies on surface dynamic topography.

Based on the results of the thesis I draw the following conclusions:

#### 1) Crustal and Lithospheric structure

The crustal structure of the Adria microplate is more complex than that of the Tisza microplate, particularly near collisional zones. This complexity suggests that subduction and delamination primarily affect the Adria domain. These differences are also evident at the Moho level, with variations observed beneath the Internal and External zones of the Apennines and Dinarides. The complexity of the external zones is highlighted in seismic data, where discrepancies arise between the Moho depths obtained using different seismic methods, such as Receiver Functions (RF) and Deep Seismic Soundings (DSS). The modeling resolves these discrepancies, indicating that the Moho lies at depths of less than 25 km and 35 km along the Internal Apennines and Dinarides, respectively, while it is found at depths greater than 50 km along the external zones of both orogens. In the internal Dinarides (Adria microplate) and the Carpathian-Balkanides (Dacia microplate), the crust has a relatively constant thickness of 30-35 km.

The Adria and Tisza microplates have different densities. The Adria crust has an average density of 2830 kg/m³, while the Tisza crust is between 2790 and 2800 kg/m³.

The lower average density of the Tisza plate is partly because the lower crust of the Tisza plate is thinner than that of Adria.

The density distribution and crustal structure of the northern Tyrrhenian Basin, corresponds to a thin continental crust with widespread volcanism, which extends to the Tuscany Magmatic Province. In contrast, in the southern Tyrrhenian Basin, the crust is oceanic, with the presence of serpentinized mantle at crustal depths.

The Tyrrhenian Sea and the Internal Apennines are characterized by the presence of elevated temperatures at shallow crustal levels, which is consistent with well-documented magmatic intrusions and volcanism.

The LAB shows significant lateral variations, reflecting different tectonic evolutions since the Mesozoic. Beneath the Tyrrhenian Sea, the LAB is flat and shallow at approximately 70-75 km, deepening slightly to the east, below the Internal Apennines. A significant thickening is observed beneath the External Apennines and Dinarides, reaching depths around 125 km in the Adriatic foreland basin. From the Internal Dinarides to the Carpathian-Balkanides region, the LAB is relatively flat at around 120 km.

#### 2) Mantle Composition and Anomalies:

The thermo-geochemical model shows two different mantle compositions: a slightly depleted mantle with an average Mg# of 89.5 for the Adria microplate, and a more fertile mantle below the southern Tyrrhenian and Apennines (DMM-6%) and Dinarides (DMM-3%). This is consistent with the presence of two sublithospheric mantle wedges, attributed to the rollback of the Apennines and Dinaric slabs.

The model also indicates two lithospheric mantle compositions: a re-enriched basalt layer beneath Adria and a fertile mantle below the Tisza microplate. The lithospheric mantle composition below the Apennines and Dinarides is more fertile, which aligns with the presence of sublithospheric mantle wedges caused by the delamination of the Adria lithospheric mantle.

I also find that along the western margin of Adria, a cold thermal sublithospheric anomaly extends down to depths of at least 400 km, while in the eastern margin, the anomaly is much shallower. In the northern Dinarides, the anomaly penetrates to ~200 km, and in the southern Dinarides, it extends around 280 km. Beneath the northern Apennines, the sublithospheric anomaly is connected to the shallower lithosphere, whereas in the southern Apennines, a small slab gap is observed.

#### 3) Geodynamic Implications

Most elevation along the transects is due to thermal isostasy. Elevations in the External Apennines, Dinarides, and Sava Suture Zone can be explained by regional isostasy with an elastic thickness of 20-30 km. Residual topography in the northern Apennines can be explained by the flow created by the cold thermal anomaly associated with the Apennines slab. The rest of mantle anomalies produce a negligible dynamic topography, either because their reduced size below the Dinarides, or because of being detached from the surface beneath the southern Apennines.

In the northern Adria region, thinning of the lithosphere in the Tyrrhenian domain and thickening toward the forefront of the northern Apennines fold belt can be attributed to the northeastward rollback of the SW Adria slab and the resulting continental delamination. In the southern Adria region, variably oriented lithospheric slabs determine a more complex deep structure, primarily due to the nearly 90-degree shift in tectonic directions between the southern Apennines, the Calabrian Arc, and their respective slabs. The small slab gap observed in the southern Apennines, it is likely the result of a slab horizontal tearing.

#### **Limitations and future work**

A significant limitation of the numerical method I have used to model Adria and its margins is the assumption of thermal steady-state and conductive heat transfer, making it insensitive to mantle flow and thermal recovery associated with ongoing mantle deformation. The results I present here are constrained by the simultaneous fitting of density-dependent observables, including gravity, geoid, and elevation, at a point in time. Therefore, these results should be viewed as a snapshot of the current density distribution related to active tectonic processes.

Transitioning form steady-state to transient models in Earth sciences presents several key challenges. A major difficulty lies in the availability and quality of data. Transient models require detailed past and high-resolution geological data to accurately represent how thermal properties and conditions have changed over time. However, such data are often incomplete, of varying quality, or simply unavailable, especially for processes occurring deep within the Earth. This limitation complicates the ability to model time-dependent processes with high precision. Furthermore, transient models are more

computationally intensive than steady-state models, necessitating sophisticated numerical techniques and high-performance computing resources. Additionally, the inherent uncertainty in thermal parameters, which can vary with temperature, pressure, and composition, further complicates modeling efforts.

Moreover, transient models must account for interconnected geological processes like mantle convection, plate tectonics, and magmatism, which often have nonlinear interactions affecting thermal evolution. Accurately capturing these phenomena requires multiscale modeling across the wide range of spatial and temporal scales involved. Coupling thermal evolution with mechanical processes, such as stress and strain distribution, and understanding material behavior under changing thermal conditions further complicates modeling. Finally, defining accurate initial and boundary conditions, especially over long timescales, remains a significant challenge. These difficulties highlight the need for advances in data collection, computational methods, and our understanding of Earth's thermal and geological processes to effectively develop and utilize transient thermal models.

In this thesis, I modeled two profiles crossing the Apennines and Dinarides, allowing for a discussion of the current lithospheric and uppermost mantle structure. By integrating these models with available geological data, I examined the geodynamic implications for the SW and NE Adria plate margins and their interactions with the surrounding microplates and terrains. A next step would be to study the physical properties and structure of the crust and upper mantle of Adria's northern (crossing the Alps) and southern margins (through the Calabrian arc). I propose modeling two additional lithospheric profiles, crossing the northern and the southern margins of Adria, along the Alps and the Calabrian arc. These new profiles would provide a comprehensive and integrated image of the microplate and its deformed margins, aiding in identifying upper mantle heterogeneities to determine the geometry of subducting plates, to infer the geodynamics of the region and relating sublithospheric heterogeneities to the current topography. Nonetheless, the final goal should be integrating Adria and its margins as a whole, which will help to better understand how Adria has accommodated between the two major plates, Africa and Eurasia.

As a final step I propose to test numerically the proposed geodynamic evolution through numerical simulations. Using thermo-mechanical, time-evolving modeling, one can reconstruct the subduction, rollback, and delamination processes of the Apennines and Dinarides fold belts. This approach will allow for determining the timing and thermal and geometric conditions of each of these processes. By accurately simulating these dynamics, deeper insights can be gained into the evolution of the region, refining our

#### Chapter 6. Conclusions, limitations and future work

understanding of the underlying mechanisms driving these geological phenomena. Importantly, steady-state integrated models as presented in this thesis are a good starting point for time-evolving geodynamic models since the final stage of the latter should be consistent with the present-day lithosphere and upper mantle structure determined from the kind of modeling developed in this thesis.

## Chapter 6. Conclusions, limitations and future work

# **List of Figures and Tables**

# **List of Figures**

<b>Figure 1.1</b> Topography map of the Alpine-Himalayan collision zone. The area inside the blue box locates the study region (Figure 1.3)
<b>Figure 1.2</b> Collection of images of the Adriatic slab beneath the Apennines according to different interpretations: a) Spakman and Wortel (2004), b) Zhao et al. (2016), c) Hua et al. (2017), d) Kästle et al. (2020), e) Pierantoni et al. (2020), f) Handy et al. (2021)5
Figure 1.3 Elevation map of the Central Mediterranean featuring the main orogenic belts and foreland basins. The red lines show the locations of the northern and southern transects (Chapter 3, Zhang et al., 2022; and Chapter 4, Zhang et al., 2024, respectively). The seismic profiles and receiver functions (RF) data used to constrain the crustal structure are also shown, according to the color legend displayed in the lower right inset.
<b>Figure 1.4</b> Simplified tectonic map of the Central Mediterranean region with the main orogenic belts and foreland basins (based on Vergés and Sàbat, 1999; Melchiorre et al., 2017; Schmid et al., 2020). The blue dashed line shows the location of the northern transect. The red dashed line shows the location of the southern transect. The gray dashed area shows the location of Adria microplate
Figure 1.5 (a) Distribution of the active faults in the study region. The faults are colored by their kinematics; red faults are normal, black faults are reverse and blue faults are strike-slip. The data are taken from Global Active Faults Database (Styron and Pagani, 2020). Red trigangles show the location of main volcanoes (Pierantoni et al., 2020). The dashed line represents the 41° Parallel Line. (b) Distribution of the earthquake epicenters, M>3.0, in the same region between 2008 and 2021. The data are taken from the International Seismological Centre (ISC). Colored circles mark the hypocentral depths (color scale is shown at the bottom left inset). Blue and red dashed lines indicate the locations of the study transects.
<b>Figure 2.1</b> Two views of the internal structure of the Earth (modified from Palin et al., 2020). Not to scale. The Moho discontinuity separates the crust and mantle. The LAB separates the lithosphere and sublithospheric mantle (i.e., asthenosphere)
Figure 2.2 Schematic definition of the lithosphere and common geophysical proxies

Figure 2.3 A. Estimates of the mean CaO and Al <sub>2</sub> O <sub>3</sub> contents in continental lithospheric mantle of different tectonothermal age based on the compositions of garnet xenocryst populations (circles) and xenolith populations (crosses) in volcanic rocks (modified from Griffin et al., 2009). B. Interpretation of the data in (A) in terms of depletion-refertilization processes
<b>Figure 2.4</b> Examples of processes producing dynamic topography and mechanisms causing evolving vertical motion. Taken from Hoggard et al. (2021). (a) lithospheric isostasy (both oceans and continents); (b) isostasy within the mantle (asthenosphere and deeper); (c) mantle flow.
Figure 2.5 Simplified scheme of the LitMod2D_2.030
Figure 2.6 Simplified flowchart indicating the general modeling procedure used in LitMod 2D.
Figure 2.7 Density, seismic velocities (Vs and Vp) changes with depth due to temperature and pressure variations for different lithospheric mantle compositions. The results are calculated with a model considering the Moho and the LAB discontinuities at depth of 35 km and 150 km, respectively. Here this model adopts a constant grain size (10 mm) and constant oscillation period (75 s) for the mantle with a modified version of the thermodynamic database from Holland and Powell (1998), revised by Afonso and Zlotnik (2011). Compositions of lithospheric mantle are taken from Griffin et al. (2009), and the depleted mid-ocean ridge basalt mantle (DMM, Workman and Hart, 2005) is assumed for the sublithospheric mantle
<b>Figure 2.8</b> Topography and bathymetry map of the study area. Elevation data comes from topo_19.1.img (Smith and Sandwell, 1997, updated 2019). The blue and red lines show the locations of the northern and southern transects. Red trigangles show the location of three seamounts in the Tyrrennian Sea
<b>Figure 2.9</b> Bouguer gravity anomaly was obtained by applying the complete Bouguer correction to the free air gravity anomaly data (Sandwell et al., 2014, updated 2019) using the software FA2BOUG (Fullea et al., 2008) with a density reduction of 2670 kg/m <sup>3</sup> . The blue and red lines show the locations of the northern and southern transects44
<b>Figure 2.10</b> Geoid height data were derived from the global gravitational model GECO (Gilardoni et al., 2016), filtered up to degree and order 10 for removing deep signals (>400

45
<b>Figure 2.11</b> Surface heat flow data from the Global Heat Flow Database (Fuchs et al., 2021) and completed with the Italian National Geothermal Database (Trumpy and Manzella, 2017; Pauselli et al., 2019). The blue and red lines show the locations of the northern and southern transects
<b>Figure 2.12</b> Horizontal cross-sections of representative P and S wave tomographic models at depths of 100 km and 300 km within the upper mantle. All the images use the same color palette, which represents the velocity perturbation with respect to the reference model.
Figure 3.1 Location of the northern transect and previous studies on the crustal structure. A: Topographic map from Google Earth with the location of the transect (Cyan solid line) and previous works (Red solid lines); B: Tectonic map (from Figure 1.4) with the location of the transect (black dash line). C: Crustal structure along the transect from previous studies, including CROP 03 (Piana Agostinetti and Faccenna, 2018), seismic section 5 (Fantoni and Franciosi, 2010) and Alp07 (Šumanovac et al., 2016). The section 5 is projected onto the northern transect. Vertical scale is exaggerated 2 times with respect to the horizontal scale.
<b>Figure 3.2</b> Crustal structure from the best fitting model constrained from the available geological and geophysical information listed in the text and in the panel legend. Yellow color is the sediment layer. Moho depths from previous studies and receiver functions (Mele and Sandvol, 2003; Piana Agostinetti and Amato, 2009; Chiarabba et al., 2014; Šumanovac et al., 2016; Piana Agostinetti and Faccenna, 2018; Diaferia et al., 2019; Stipčević et al., 2020) are shown for comparison. See Figure 3.1 for location
geological and geophysical information listed in the text and in the panel legend. Yellow color is the sediment layer. Moho depths from previous studies and receiver functions (Mele and Sandvol, 2003; Piana Agostinetti and Amato, 2009; Chiarabba et al., 2014; Šumanovac et al., 2016; Piana Agostinetti and Faccenna, 2018; Diaferia et al., 2019;

projected onto the transect at 5 km sampling interval within a strip of 25 km half-width to

account for lateral variations perpendicular to the strike. Standard deviations are shown as error bars. Blue and black lines show calculated values with and without sublithospheric anomalies, respectively. In (d) blue and black lines show thermal isostatic elevation (with and without mantle anomalies), and green lines are the calculated flexural elevation with elastic thickness  $T_e = 10$  km and dashed line  $T_e = 20$  km. Panel (e) shows the temperature distribution for the whole lithosphere. Panel (f) shows the density distribution within the lithospheric mantle along the modeled transect. See Figure 1.4 or 3.1 for location. ......63

**Figure 4.1** Location of the southern transect and previous studies along the modeled profile. A: Topographic map from Google Earth with the location of the transect (Cyan solid line) and the previous profiles used in this study (Red solid lines); B: Tectonic map with the location of the transect (Red dash line). The transect crosses the Adria and Dacia microplates; C: Crustal structure from previous studies and locations of the profiles and data used to further constrain the crustal geometry, including MEDOC GH (Prada et al., 2014), CROP 04 (Mazzoli et al., 2013), seismic section 8 (Fantoni and Franciosi. 2010) and Profile-E (Schmid et al., 2020). The section 8 is projected onto the southern transect.

Vertical scale is exaggerated 2 times the	e horizontal	scale. Vertical	scale is exaggera	ated 2
times with respect to the horizontal scal	e			82

Figure 4.4 (see next page) Best fit model, see Figure 4.1 for location. (a) Surface heat flow. (b) Geoid height. (c) Bouguer gravity anomaly. (d) Elevation. Blue and black lines show modeled results, with and without sublithospheric anomalies, respectively. Red dots show measured data, and vertical bars show the standard deviation calculated across a swath of 25 km half width. (e) Temperature distribution for the entire lithosphere. Continuous black lines highlight the obtained Lithosphere-Asthenosphere boundary (LAB) depth and location of sublithospheric mantle anomalies. LAB depth from previous studies (red stars) are shown for comparison. Earthquake locations (International Seismological Centre, ISC) with a magnitude of mb ≥ 3.0 between 2008 and 2021, projected 50 km across the transect are shown as solid gray circles. (f) Mantle density distribution. The different compositional domains in the lithospheric mantle are separated by thin gray lines, and major oxide compositions are listed in Table 4.1 and 4.2. Data from Rappisi et al. (2022)have been taken from https://figshare.com/articles/dataset/isoand aniNEWTON21 tomographic models/19188950 and projected onto the profile.89

 **Figure 4.6** Mantle seismic velocities and synthetic seismic velocity anomaly along the transect. Panel (a) elevation profile, (b) and (d) absolute P- and S-wave velocities and (c) and (e) synthetic P and S-wave anomalies, respectively. Note that the color scale used in the synthetic models, (c) and (e), saturates in areas where the Moho depth is less than 35 km. This saturation occurs due to the reference model employed, which incorporates a 35 km thick crust (Kumar et al., 2020) and highlights areas with crustal thinning......94

Figure 4.11 Geodynamic interpretation of the lithospheric structure along the southern
transect presented in this chapter106
Figure 5.1 Crustal structure along the northern (Chapter 3) and southern transects (Chapter 4). To facilitate comparison between the two transects, their origins have been
aligned with the coastline of Corsica and Sardinia, respectively. See Figure 1.4 for their
respective locations112
Figure 5.2 3D top view showing the location and main results along the two modeled
transects. The vertical cross sections show the temperature distribution for the whole
lithosphere and mantle anomalies. The dashed black lines project the locations of the
coastlines
<b>Figure 5.3</b> Major element oxide weight percentages of mantle compositions are plotted as a function of Magnesium number Mg#. Gray triangle represents the composition of Pannonian mantle (PB_mant, Downes et al., 1992; Alasonati Tašárová et al., 2016). Colored dots represent the classification of the lithospheric mantle composition by Griffin et al. (2009) based on the tectonothermal age of the overlying crust: Archons (2.5 - 1.0 Ga) in blue, Protons (1.0 Ga) in green, and Tectons (<1.0 Ga) in yellow. DMM is the sublithospheric mantle composition assumed in this Thesis (Workman and Hart, 2005), in dark red. PUM (light red) is the primitive upper mantle from McDonough and Sun (1995). I also marked the Adriatic mantle composition (Tc_2), and the composition of northern African mantle (N. African mantle) used in Kumar et al., (2021)
Amcan manue (N. Amcan manue) useu in Kumai et al., (2021)
Figure 5.4 Lower panels show mantle seismic tomography along northern and
southern transects (Amaru, 2007). Upper panels show the topography maps and elevation
profile along the transects (black lines)
Figure 5.5 Isostatic, residual and dynamic topography along the northern transect. In
blue, including the two sublithospheric anomalies; In dark-gray, without the two
sublithospheric denser anomalies; In green, regional isostasy (T <sub>e</sub> = 20 km) without the two
sublithospheric denser anomalies. (a) Standard deviation of the observed elevation
across a 50-km-wide swath (light-gray); modeled local (blue and dark-gray) and regional
(green) isostatic elevation form LitMod_2D (Chapter 3). (b) Standard deviation of the
residual topography, according to (a). (c) Dynamic topography (Figure 3.7). (d) Standard
deviation of the residual regional isostasy (green); dynamic topography attributed to the
dynamic response to mantle anomalies (red line)

Figure 5.6 Isostatic, residual and dynamic topography along the southern transect. In
blue, including the two sublithospheric anomalies, with the slab gap beneath the
Apennines; In dark-gray, without the two sublithospheric denser anomalies; In green,
regional isostasy ( $T_e$ = 30 km) without the two sublithospheric denser anomalies. (a)
Standard deviation of the observed elevation across a 50-km-wide swath (light-gray);
modeled local (blue and dark-black) and regional (green) isostatic elevation form
LitMod_2D (Chapter 4). (b) Standard deviation of the residual topography, according to
(a). (c) Dynamic topography. (d) Standard deviation of the residual regional isostasy
(green); dynamic topography attributed to the dynamic response to mantle anomalies (red
line)122

## **List of Tables**

Table 2.1 Bulk compositions and characteristics of different lithospheric mantle
compositions which come from Griffin et al., 2009. DMM: Depleted mid-ocean ridge basalt
mantle (Workman and Hart, 2005; Kumar et al., 2020) is the composition attributed to the
sublithospheric mantle
Table 2.2 Rheological parameters and viscosities used in this thesis42
Table 3.1 Thermo-physical properties of the crustal tectonic units along the profile 61
Table 3.2 Major oxides composition in % of weight percent in the NCFMAS system           used for the lithospheric and sublithospheric mantle         67
Table 4.1 Thermo-physical properties of the crustal tectonic units and mantle domains         along the transect       84
Table 4.2 Major oxides composition in % of weight percent in the NCFMAS system
used in the different mantle domains85



# References



#### References

- Acocella, V., & Rossetti, F. (2002). The role of extensional tectonics at different crustal levels on granite ascent and emplacement: An example from Tuscany (Italy). *Tectonophysics*, *354*(1), 71–83. <a href="https://doi.org/10.1016/S0040-1951(02)00290-1">https://doi.org/10.1016/S0040-1951(02)00290-1</a>
- Afonso, J. C., Fernàndez, M., Ranalli, G., Griffin, W. L., & Connolly, J. a. D. (2008). Integrated geophysical-petrological modeling of the lithosphere and sublithospheric upper mantle: Methodology and applications. *Geochemistry, Geophysics, Geosystems*, 9(5). <a href="https://doi.org/10.1029/2007GC001834">https://doi.org/10.1029/2007GC001834</a>
- Afonso, J. C., & Zlotnik, S. (2011). The Subductability of Continental Lithosphere: The Before and After Story. In D. Brown & P. D. Ryan (Eds.), *Arc-Continent Collision* (pp. 53–86). Springer. https://doi.org/10.1007/978-3-540-88558-0 3
- Akimbekova A., Mancinelli P., Pauselli C., Minelli G., & Barchi M. R. (2021). Forward modelling of Bouguer anomalies along a transect of the Southern Apennines and the Southern Tyrrhenian Sea (Italy). *Italian Journal of Geosciences*, *140*(3), 411–421. https://doi.org/10.3301/IJG.2021.03
- Alasonati Tašárová, Z., Fullea, J., Bielik, M., & Środa, P. (2016). Lithospheric structure of Central Europe: Puzzle pieces from Pannonian Basin to Trans-European Suture Zone resolved by geophysical-petrological modeling: GEOPHYSICAL-PETROLOGICAL MODELING. *Tectonics*, *35*(3), 722–753. <a href="https://doi.org/10.1002/2015TC003935">https://doi.org/10.1002/2015TC003935</a>
- Amaru, M. L. (2007). Global travel time tomography with 3-D reference models [Utrecht University]. http://dspace.library.uu.nl/handle/1874/19338
- Anderson, D. L. (2007). New Theory of the Earth. Cambridge University Press.
- Artemieva, I. (2011). The Lithosphere: An Interdisciplinary Approach. In *The Lithosphere:* An Interdisciplinary Approach. <a href="https://doi.org/10.1017/CBO9780511975417">https://doi.org/10.1017/CBO9780511975417</a>
- Artemieva, I. M. (2019). Lithosphere thermal thickness and geothermal heat flux in Greenland from a new thermal isostasy method. *Earth-Science Reviews*, *188*, 469–481. <a href="https://doi.org/10.1016/j.earscirev.2018.10.015">https://doi.org/10.1016/j.earscirev.2018.10.015</a>
- Artemieva, I. M., & Thybo, H. (2013). EUNAseis: A seismic model for Moho and crustal structure in Europe, Greenland, and the North Atlantic region. *Tectonophysics*, *609*, 97–153. <a href="https://doi.org/10.1016/j.tecto.2013.08.004">https://doi.org/10.1016/j.tecto.2013.08.004</a>

- Asimow, P. D., Hirschmann, M. M., & Stolper, E. M. (2001). Calculation of Peridotite Partial Melting from Thermodynamic Models of Minerals and Melts, IV. Adiabatic Decompression and the Composition and Mean Properties of Mid-ocean Ridge Basalts. Journal of Petrology, 42(5), 963–998. <a href="https://doi.org/10.1093/petrology/42.5.963">https://doi.org/10.1093/petrology/42.5.963</a>
- Bache, F., Olivet, J. L., Gorini, C., Aslanian, D., Labails, C., & Rabineau, M. (2010). Evolution of rifted continental margins: The case of the Gulf of Lions (Western Mediterranean Basin). *Earth and Planetary Science Letters*, 292(3), 345–356. <a href="https://doi.org/10.1016/j.epsl.2010.02.001">https://doi.org/10.1016/j.epsl.2010.02.001</a>
- Bada, G., Horváth, F., Dövényi, P., Szafián, P., Windhoffer, G., & Cloetingh, S. (2007). Present-day stress field and tectonic inversion in the Pannonian basin. *Global and Planetary Change*, *58*(1), 165–180. <a href="https://doi.org/10.1016/j.gloplacha.2007.01.007">https://doi.org/10.1016/j.gloplacha.2007.01.007</a>
- Balling, P., Grützner, C., Tomljenović, B., Spakman, W., & Ustaszewski, K. (2021). Post-collisional mantle delamination in the Dinarides implied from staircases of Oligo-Miocene uplifted marine terraces. *Scientific Reports*, *11*(1), Article 1. https://doi.org/10.1038/s41598-021-81561-5
- Balling, P., Tomljenović, B., Schmid, S. M., & Ustaszewski, K. (2021). Contrasting along-strike deformation styles in the central external Dinarides assessed by balanced cross-sections: Implications for the tectonic evolution of its Paleogene flexural foreland basin system. *Global and Planetary Change*, 205, 103587. https://doi.org/10.1016/j.gloplacha.2021.103587
- Bally, A. W. (1987). Balanced Sections and Seismic Reflection Profiles Across the Central Apennines, Italy. *Mem. Soc. Geol. It.*, 29(8), 11–12.
- Barchi, M., Minelli, G., Magnani, B., & Mazzotti, A. (2003). Line CROP 03: Northern Apennines. *Mem. Descr. Carta Geol. d'Italia LXII*, 62, 127–136.
- Barchi, M., Minelli, G., & Pialli, G. (1998). The Crop 03 Profile: A Synthesis of Results on Deep Structures of the Northern Apennines. *Memorie Della Società Geologica Italiana*, *52*, 383–400.
- Barchi, M., Pauselli, C., Chiarabba, C., Di Stefano, R., Federico, C., & Minelli, G. (2006). Crustal structure, tectonic evolution and seismogenesis in the Northern Apennines (Italy). *Bollettino Di Geofisica Teorica Ed Applicata*, *47*, 249–270.

- Basili, R., & Barba, S. (2007). Migration and shortening rates in the northern Apennines, Italy: Implications for seismic hazard. *Terra Nova*, 19(6), 462–468. <a href="https://doi.org/10.1111/j.1365-3121.2007.00772.x">https://doi.org/10.1111/j.1365-3121.2007.00772.x</a>
- Becker, T. W., Faccenna, C., Humphreys, E. D., Lowry, A. R., & Miller, M. S. (2014). Static and dynamic support of western United States topography. *Earth and Planetary Science Letters*, 402, 234–246. https://doi.org/10.1016/j.epsl.2013.10.012
- Belinić, T., Kolínský, P., & Stipčević, J. (2021). Shear-wave velocity structure beneath the Dinarides from the inversion of Rayleigh-wave dispersion. *Earth and Planetary Science Letters*, *555*, 116686. https://doi.org/10.1016/j.epsl.2020.116686
- Belinić, T., Stipčević, J., & Živčić, M. (2018). Lithospheric thickness under the Dinarides. *Earth and Planetary Science Letters*, 484, 229–240. <a href="https://doi.org/10.1016/j.epsl.2017.12.030">https://doi.org/10.1016/j.epsl.2017.12.030</a>
- Beller, S., Monteiller, V., Operto, S., Nolet, G., Paul, A., & Zhao, L. (2018). Lithospheric architecture of the South-Western Alps revealed by multiparameter teleseismic full-waveform inversion. *Geophysical Journal International*, 212(2), 1369–1388. <a href="https://doi.org/10.1093/gji/ggx216">https://doi.org/10.1093/gji/ggx216</a>
- Benoit, M. H., Torpey, M., Liszewski, K., Levin, V., & Park, J. (2011). P and S wave upper mantle seismic velocity structure beneath the northern Apennines: New evidence for the end of subduction. *Geochemistry, Geophysics, Geosystems*, 12(6). https://doi.org/10.1029/2010GC003428
- Bernstein, S., Kelemen, P. B., & Hanghøj, K. (2007). Consistent olivine Mg# in cratonic mantle reflects Archean mantle melting to the exhaustion of orthopyroxene. *Geology*, 35(5), 459–462. https://doi.org/10.1130/G23336A.1
- Bianchi, I., Park, J., Piana Agostinetti, N., & Levin, V. (2010). Mapping seismic anisotropy using harmonic decomposition of receiver functions: An application to Northern Apennines, Italy. *Journal of Geophysical Research: Solid Earth*, 115(B12). <a href="https://doi.org/10.1029/2009JB007061">https://doi.org/10.1029/2009JB007061</a>
- Bijwaard, H., & Spakman, W. (1999). Tomographic evidence for a narrow whole mantle plume below Iceland. *Earth and Planetary Science Letters*, *166*(3), 121–126. https://doi.org/10.1016/S0012-821X(99)00004-7
- Billi, A., Presti, D., Faccenna, C., Neri, G., & Orecchio, B. (2007). Seismotectonics of the Nubia plate compressive margin in the south Tyrrhenian region, Italy: Clues for

- subduction inception. *Journal of Geophysical Research: Solid Earth*, *112*(B8). https://doi.org/10.1029/2006JB004837
- Blom, N., Gokhberg, A., & Fichtner, A. (2020). Seismic waveform tomography of the central and eastern Mediterranean upper mantle. *Solid Earth*, *11*(2), 669–690. <a href="https://doi.org/10.5194/se-11-669-2020">https://doi.org/10.5194/se-11-669-2020</a>
- Boccaletti, M., Ciaranfi, N., Cosentino, D., Deiana, G., Gelati, R., Lentini, F., Massari, F., Moratti, G., Pescatore, T., Ricci Lucchi, F., & Tortorici, L. (1990). Palinspastic restoration and paleogeographic reconstruction of the peri-Tyrrhenian area during the Neogene. *Palaeogeography, Palaeoclimatology, Palaeoecology*, 77(1), 41-IN13. https://doi.org/10.1016/0031-0182(90)90097-Q
- Bodur, Ö. F., & Rey, P. F. (2019). The impact of rheological uncertainty on dynamic topography predictions. *Solid Earth*, *10*(6), 2167–2178. <a href="https://doi.org/10.5194/se-10-2167-2019">https://doi.org/10.5194/se-10-2167-2019</a>
- Bondár, I., Mónus, P., Czanik, C., Kiszely, M., Gráczer, Z., Wéber, Z., & the AlpArrayWorking Group. (2018). Relocation of Seismicity in the Pannonian Basin Using a Global 3D Velocity Model. Seismological Research Letters, 89(6), 2284–2293. https://doi.org/10.1785/0220180143
- Boonma, K., García-Castellanos, D., Jiménez-Munt, I., & Gerya, T. (2023). Thermomechanical modelling of lithospheric slab tearing and its topographic response. *Frontiers in Earth Science*, *11*. https://doi.org/10.3389/feart.2023.1095229
- Boschi, L., Faccenna, C., & Becker, T. W. (2010). Mantle structure and dynamic topography in the Mediterranean Basin. *Geophysical Research Letters*, *37*(20). <a href="https://doi.org/10.1029/2010GL045001">https://doi.org/10.1029/2010GL045001</a>
- Braun, J. (2010). The many surface expressions of mantle dynamics. *Nature Geoscience*, 3(12), Article 12. <a href="https://doi.org/10.1038/ngeo1020">https://doi.org/10.1038/ngeo1020</a>
- Braun, J., Robert, X., & Simon-Labric, T. (2013). Eroding dynamic topography. *Geophysical Research Letters*, *40*(8), 1494–1499. <a href="https://doi.org/10.1002/grl.50310">https://doi.org/10.1002/grl.50310</a>
- Braun, J., Simon-Labric, T., Murray, K. E., & Reiners, P. W. (2014). Topographic relief driven by variations in surface rock density. *Nature Geoscience*, 7(7), 534–540. <a href="https://doi.org/10.1038/ngeo2171">https://doi.org/10.1038/ngeo2171</a>
- Bravo-Gutiérrez, E., Vergés, J., Torne, M., García-Castellanos, D., Negredo, A. M., Zhang, W., Cruset, D., Viaplana-Muzas, M., & Jiménez-Munt, I. (2024). Pre-shortening

- reconstruction of the adria microplate: Balanced and restored cross-sections through the Southern Apennines–Dinarides (Central Mediterranean Sea). *Marine and Petroleum Geology*, 169, 107055. <a href="https://doi.org/10.1016/j.marpetgeo.2024.107055">https://doi.org/10.1016/j.marpetgeo.2024.107055</a>
- Brocher, T. M. (2005). Empirical Relations between Elastic Wavespeeds and Density in the Earth's Crust. *Bulletin of the Seismological Society of America*, *95*(6), 2081–2092. https://doi.org/10.1785/0120050077
- Burgess & Moresi. (1999). Modelling rates and distribution of subsidence due to dynamic topography over subducting slabs: Is it possible to identify dynamic topography from ancient strata? *Basin Research*, *11*(4), 305–314. <a href="https://doi.org/10.1046/j.1365-2117.1999.00102.x">https://doi.org/10.1046/j.1365-2117.1999.00102.x</a>
- Burgess, P. M., Gurnis, M., & Moresi, L. (1997). Formation of sequences in the cratonic interior of North America by interaction between mantle, eustatic, and stratigraphic processes. *GSA Bulletin*, 109(12), 1515–1535. <a href="https://doi.org/10.1130/0016-7606(1997)109<1515:FOSITC>2.3.CO;2">https://doi.org/10.1130/0016-7606(1997)109<1515:FOSITC>2.3.CO;2</a>
- Burov, E. (2011). Lithosphere, Mechanical Properties. In H. K. Gupta (Ed.), *Encyclopedia of Solid Earth Geophysics* (pp. 693–701). Springer Netherlands. <a href="https://doi.org/10.1007/978-90-481-8702-7">https://doi.org/10.1007/978-90-481-8702-7</a> 147
- Burrus, J. (1984). Contribution to a geodynamic synthesis of the Provençal Basin (North-Western Mediterranean). *Marine Geology*, *55*(3), 247–269. https://doi.org/10.1016/0025-3227(84)90071-9
- Butler, R. W. H., Mazzoli, S., Corrado, S., Donatis, M. D., Bucci, D. D., Gambini, R., Naso, G., Nicolai, C., Scrocca, D., Shiner, P., & Zucconi, V. (2004). Applying Thick-skinned Tectonic Models to the Apennine Thrust Belt of Italy—Limitations and Implications. 647–667.
- Cammarano, F., Goes, S., Vacher, P., & Giardini, D. (2003). Inferring upper-mantle temperatures from seismic velocities. *Physics of the Earth and Planetary Interiors*, 138(3), 197–222. <a href="https://doi.org/10.1016/S0031-9201(03)00156-0">https://doi.org/10.1016/S0031-9201(03)00156-0</a>
- Carballo, A., Fernandez, M., Torne, M., Jiménez-Munt, I., & Villaseñor, A. (2015). Thermal and petrophysical characterization of the lithospheric mantle along the northeastern lberia geo-transect. *Gondwana Research*, 27(4), 1430–1445. <a href="https://doi.org/10.1016/j.gr.2013.12.012">https://doi.org/10.1016/j.gr.2013.12.012</a>

- Carlson, R. W., Pearson, D. G., & James, D. E. (2005). Physical, chemical, and chronological characteristics of continental mantle. *Reviews of Geophysics*, *43*(1). https://doi.org/10.1029/2004RG000156
- Carminati, E., & Chiarabba, C. (2023). Slab damage and the pulsating retreat of the Ionian-Apennines subduction. *Geology*, *51*(3), 227–232. https://doi.org/10.1130/G50676.1
- Carminati, E., Cuffaro, M., & Doglioni, C. (2009). Cenozoic uplift of Europe. *Tectonics*, 28(4). https://doi.org/10.1029/2009TC002472
- Carminati, E., & Doglioni, C. (2012). Alps vs. Apennines: The paradigm of a tectonically asymmetric Earth. *Earth-Science Reviews*, *112*(1), 67–96. https://doi.org/10.1016/j.earscirev.2012.02.004
- Carminati, E., Lustrino, M., & Doglioni, C. (2012). Geodynamic evolution of the central and western Mediterranean: Tectonics vs. Igneous petrology constraints. *Tectonophysics*, *579*, 173–192. <a href="https://doi.org/10.1016/j.tecto.2012.01.026">https://doi.org/10.1016/j.tecto.2012.01.026</a>
- Carminati, E., Petricca, P., & Doglioni, C. (2020). Mediterranean Tectonics. In D. Alderton & S. A. Elias (Eds.), *Encyclopedia of Geology (Second Edition)* (pp. 408–419). Academic Press. <a href="https://doi.org/10.1016/B978-0-08-102908-4.00010-2">https://doi.org/10.1016/B978-0-08-102908-4.00010-2</a>
- Cassinis, R., Scarascia, S., Lozej, A., & Finetti, I. R. (2005). Review of seismic wide-angle reflection–refraction (WARR) results in the Italian region (1956–1987). In *CROP PROJECT: Deep seismic exploration of the central Mediterranean and Italy* (pp. 31–55). Elsevier Amsterdam, The Netherlands.
- Cavazza, W., Roure, F., Spakman, W., Stampfli, G. M., & Ziegler, P. A. (Eds.). (2004). *The TRANSMED Atlas. The Mediterranean Region from Crust to Mantle*. Springer. https://doi.org/10.1007/978-3-642-18919-7
- Cavinato, G. P., & De Celles, P. G. (1999). Extensional basins in the tectonically bimodal central Apennines fold-thrust belt, Italy: Response to corner flow above a subducting slab in retrograde motion. *Geology*, 27(10), 955–958. <a href="https://doi.org/10.1130/0091-7613(1999)027<0955:EBITTB>2.3.CO;2">https://doi.org/10.1130/0091-7613(1999)027<0955:EBITTB>2.3.CO;2</a>
- Channell, J. E. T., Tüysüz, O., Bektas, O., & Sengör, A. M. C. (1996). Jurassic-Cretaceous paleomagnetism and paleogeography of the Pontides (Turkey). *Tectonics*, *15*(1), 201–212. <a href="https://doi.org/10.1029/95TC02290">https://doi.org/10.1029/95TC02290</a>

- Chiarabba, C., Agostinetti, N. P., & Bianchi, I. (2016). Lithospheric fault and kinematic decoupling of the Apennines system across the Pollino range. *Geophysical Research Letters*, *43*(7), 3201–3207. <a href="https://doi.org/10.1002/2015GL067610">https://doi.org/10.1002/2015GL067610</a>
- Chiarabba, C., Bianchi, I., De Gori, P., & Agostinetti, N. P. (2020). Mantle upwelling beneath the Apennines identified by receiver function imaging. *Scientific Reports*, 10(1), Article 1. https://doi.org/10.1038/s41598-020-76515-2
- Chiarabba, C., De Gori, P., & Speranza, F. (2008). The southern Tyrrhenian subduction zone: Deep geometry, magmatism and Plio-Pleistocene evolution. *Earth and Planetary Science Letters*, 268(3), 408–423. <a href="https://doi.org/10.1016/j.epsl.2008.01.036">https://doi.org/10.1016/j.epsl.2008.01.036</a>
- Chiarabba, C., De Gori, P., & Speranza, F. (2009). Deep geometry and rheology of an orogenic wedge developing above a continental subduction zone: Seismological evidence from the northern-central Apennines (Italy). *Lithosphere*, *1*(2), 95–104. <a href="https://doi.org/10.1130/L34.1">https://doi.org/10.1130/L34.1</a>
- Chiarabba, C., Giacomuzzi, G., Bianchi, I., Agostinetti, N. P., & Park, J. (2014). From underplating to delamination-retreat in the northern Apennines. *Earth and Planetary Science Letters*, 403, 108–116. https://doi.org/10.1016/j.epsl.2014.06.041
- Chiarabba, C., Jovane, L., & DiStefano, R. (2005). A new view of Italian seismicity using 20 years of instrumental recordings. Tectonophysics, 395(3), 251–268. https://doi.org/10.1016/j.tecto.2004.09.013
- Chiarabba, C., Pino, N. A., Ventura, G., & Vilardo, G. (2004). Structural features of the shallow plumbing system of Vulcano Island Italy. *Bulletin of Volcanology*, *66*(6), 477–484. https://doi.org/10.1007/s00445-003-0331-9
- Chiari, M., Djerić, N., Garfagnoli, F., Hrvatović, H., Krstić, M., Levi, N., Malasoma, A., Marroni, M., Menna, F., Nirta, G., Pandolfi, L., Principi, G., Saccani, E., Stojadinović, U., & Trivić, B. (2011). THE GEOLOGY OF THE ZLATIBOR-MALJEN AREA (WESTERN SERBIA): A GEOTRAVERSE ACROSS THE OPHIOLITES OF THE DINARIC-HELLENIC COLLISIONAL BELT. *Ofioliti*, 36(2), Article 2. <a href="https://doi.org/10.4454/OFIOLITI.V36.I2.3">https://doi.org/10.4454/OFIOLITI.V36.I2.3</a>
- Christensen, N. I., & Mooney, W. D. (1995). Seismic velocity structure and composition of the continental crust: A global view. *Journal of Geophysical Research: Solid Earth*, 100(B6), 9761–9788. https://doi.org/10.1029/95JB00259

- Connolly, J. A. D. (2005). Computation of phase equilibria by linear programming: A tool for geodynamic modeling and its application to subduction zone decarbonation. *Earth and Planetary Science Letters*, 236(1), 524–541. <a href="https://doi.org/10.1016/j.epsl.2005.04.033">https://doi.org/10.1016/j.epsl.2005.04.033</a>
- Connolly, J. a. D. (2009). The geodynamic equation of state: What and how. *Geochemistry, Geophysics, Geosystems*, 10(10). https://doi.org/10.1029/2009GC002540
- Cosentino, D., Cipollari, P., Marsili, P., & Scrocca, D. (2010). Geology of the central Apennines: A regional review. *Journal of the Virtual Explorer*, *36*. https://doi.org/10.3809/jvirtex.2010.00223
- Crameri, F., Schmeling, H., Golabek, G. J., Duretz, T., Orendt, R., Buiter, S. J. H., May, D. A., Kaus, B. J. P., Gerya, T. V., & Tackley, P. J. (2012). A comparison of numerical surface topography calculations in geodynamic modelling: An evaluation of the 'sticky air' method: Modelling topography in geodynamics. *Geophysical Journal International*, 189(1), 38–54. <a href="https://doi.org/10.1111/j.1365-246X.2012.05388.x">https://doi.org/10.1111/j.1365-246X.2012.05388.x</a>
- Csontos, L., & Nagymarosy, A. (1998). The Mid-Hungarian line: A zone of repeated tectonic inversions. *Tectonophysics*, 297(1), 51–71. <a href="https://doi.org/10.1016/S0040-1951(98)00163-2">https://doi.org/10.1016/S0040-1951(98)00163-2</a>
- Czarnota, K., Hoggard, M. J., White, N., & Winterbourne, J. (2013). Spatial and temporal patterns of Cenozoic dynamic topography around Australia. *Geochemistry, Geophysics, Geosystems*, *14*(3), 634–658. <a href="https://doi.org/10.1029/2012GC004392">https://doi.org/10.1029/2012GC004392</a>
- Czarnota, K., Roberts, G. G., White, N. J., & Fishwick, S. (2014). Spatial and temporal patterns of Australian dynamic topography from River Profile Modeling. *Journal of Geophysical Research: Solid Earth*, 119(2), 1384–1424. https://doi.org/10.1002/2013JB010436
- D'Acquisto, M., Dal Zilio, L., Molinari, I., Kissling, E., Gerya, T., & van Dinther, Y. (2020). Tectonics and seismicity in the Northern Apennines driven by slab retreat and lithospheric delamination. *Tectonophysics*, 789, 228481. https://doi.org/10.1016/j.tecto.2020.228481
- Dalton, C. A., Langmuir, C. H., & Gale, A. (2014). Geophysical and Geochemical Evidence for Deep Temperature Variations Beneath Mid-Ocean Ridges. *Science*, *344*(6179), 80–83. <a href="https://doi.org/10.1126/science.1249466">https://doi.org/10.1126/science.1249466</a>

- Davies, D. R., Valentine, A. P., Kramer, S. C., Rawlinson, N., Hoggard, M. J., Eakin, C. M., & Wilson, C. R. (2019). Earth's multi-scale topographic response to global mantle flow. *Nature Geoscience*, *12*(10), 845–850. <a href="https://doi.org/10.1038/s41561-019-0441-4">https://doi.org/10.1038/s41561-019-0441-4</a>
- De Gori, P., Lucente, F. P., Govoni, A., Margheriti, L., & Chiarabba, C. (2022). Seismic swarms in the Pollino seismic gap: Positive fault inversion within a popup structure. *Frontiers in Earth Science*, *10*, 968187. https://doi.org/10.3389/feart.2022.968187
- De Luca, G., Cattaneo, M., Monachesi, G., & Amato, A. (2009). Seismicity in Central and Northern Apennines integrating the Italian national and regional networks. *Tectonophysics*, *476*(1), 121–135. https://doi.org/10.1016/j.tecto.2008.11.032
- Dewey, J. F., Helman, M. L., Knott, S. D., Turco, E., & Hutton, D. H. W. (1989). Kinematics of the western Mediterranean. *Geological Society, London, Special Publications*, *45*(1), 265–283. https://doi.org/10.1144/GSL.SP.1989.045.01.15
- Di Stefano, R., Bianchi, I., Ciaccio, M. G., Carrara, G., & Kissling, E. (2011). Three-dimensional Moho topography in Italy: New constraints from receiver functions and controlled source seismology. *Geochemistry, Geophysics, Geosystems*, *12*(9). <a href="https://doi.org/10.1029/2011GC003649">https://doi.org/10.1029/2011GC003649</a>
- Diaferia, G., Cammarano, F., Piana Agostinetti, N., Gao, C., Lekic, V., Molinari, I., & Boschi, L. (2019). Inferring Crustal Temperatures Beneath Italy From Joint Inversion of Receiver Functions and Surface Waves. *Journal of Geophysical Research: Solid Earth*, 124(8), 8771–8785. https://doi.org/10.1029/2019JB018340
- Ding, X., Salles, T., Flament, N., Mallard, C., & Rey, P. F. (2019). Drainage and Sedimentary Responses to Dynamic Topography. *Geophysical Research Letters*, 46(24), 14385–14394. https://doi.org/10.1029/2019GL084400
- Dini, A., Gianelli, G., Puxeddu, M., & Ruggieri, G. (2005). Origin and evolution of Pliocene–Pleistocene granites from the Larderello geothermal field (Tuscan Magmatic Province, Italy). *Lithos*, *81*(1), 1–31. <a href="https://doi.org/10.1016/j.lithos.2004.09.002">https://doi.org/10.1016/j.lithos.2004.09.002</a>
- Dini, A., Innocenti, F., Rocchi, S., Tonarini, S., & Westerman, D. S. (2002). The magmatic evolution of the late Miocene laccolith–pluton–dyke granitic complex of Elba Island, Italy. *Geological Magazine*, 139(3), 257–279. <a href="https://doi.org/10.1017/S0016756802006556">https://doi.org/10.1017/S0016756802006556</a>
- Doglioni, C. (1991). A proposal for the kinematic modelling of W-dipping subductions— Possible applications to the Tyrrhenian-Apennines system. Terra Nova, 3(4), 423–434. https://doi.org/10.1111/j.1365-3121.1991.tb00172.x

- Doglioni, C., Gueguen, E., Sàbat, F., & Fernandez, M. (1997). The Western Mediterranean extensional basins and the Alpine orogen. *Terra Nova*, 9(3), 109–112. <a href="https://doi.org/10.1046/j.1365-3121.1997.d01-18.x">https://doi.org/10.1046/j.1365-3121.1997.d01-18.x</a>
- Doglioni, C., Harabaglia, P., Martinelli, G., Mongelli, F., & Zito, G. (1996). A geodynamic model of the Southern Apennines accretionary prism. *Terra Nova*, *8*(6), 540–547. https://doi.org/10.1111/j.1365-3121.1996.tb00783.x
- Doglioni, C., Innocenti, F., & Mariotti, G. (2001). Why Mt Etna? *Terra Nova*, *13*(1), 25–31. https://doi.org/10.1046/j.1365-3121.2001.00301.x
- Doglioni, C., Mongelli, F., & Pieri, P. (1994). The Puglia uplift (SE Italy): An anomaly in the foreland of the Apenninic subduction due to buckling of a thick continental lithosphere. *Tectonics*, *13*(5), 1309–1321. https://doi.org/10.1029/94TC01501
- D'Orazio, M., Innocenti, F., Tonarini, S., & Doglioni, C. (2007). Carbonatites in a subduction system: The Pleistocene alvikites from Mt. Vulture (southern Italy). *Lithos*, 98(1), 313–334. https://doi.org/10.1016/j.lithos.2007.05.004
- Downes, H., Embey-Isztin, A., & Thirlwall, M. F. (1992). Petrology and geochemistry of spinel peridotite xenoliths from the western Pannonian Basin (Hungary): Evidence for an association between enrichment and texture in the upper mantle. *Contributions to Mineralogy and Petrology*, 109(3), 340–354. <a href="https://doi.org/10.1007/BF00283323">https://doi.org/10.1007/BF00283323</a>
- Eaton, D. W., Darbyshire, F., Evans, R. L., Grütter, H., Jones, A. G., & Yuan, X. (2009). The elusive lithosphere–asthenosphere boundary (LAB) beneath cratons. *Lithos*, 109(1–2), 1–22. <a href="https://doi.org/10.1016/j.lithos.2008.05.009">https://doi.org/10.1016/j.lithos.2008.05.009</a>
- Edwards, M. A., & Grasemann, B. (2009). Mediterranean snapshots of accelerated slab retreat: Subduction instability in stalled continental collision. *Geological Society, London, Special Publications*, *311*(1), 155–192. https://doi.org/10.1144/SP311.6
- El-Sharkawy, A., Meier, T., Lebedev, S., Behrmann, J. H., Hamada, M., Cristiano, L., Weidle, C., & Köhn, D. (2020). The Slab Puzzle of the Alpine-Mediterranean Region: Insights From a New, High-Resolution, Shear Wave Velocity Model of the Upper Mantle. *Geochemistry, Geophysics, Geosystems*, 21(8), e2020GC008993. https://doi.org/10.1029/2020GC008993
- Faccenna, C., & Becker, T. W. (2010). Shaping mobile belts by small-scale convection. *Nature*, *465*(7298), Article 7298. <a href="https://doi.org/10.1038/nature09064">https://doi.org/10.1038/nature09064</a>

- Faccenna, C., & Becker, T. W. (2020). Topographic expressions of mantle dynamics in the Mediterranean. *Earth-Science Reviews*, 209, 103327. https://doi.org/10.1016/j.earscirev.2020.103327
- Faccenna, C., Becker, T. W., Auer, L., Billi, A., Boschi, L., Brun, J. P., Capitanio, F. A., Funiciello, F., Horvàth, F., Jolivet, L., Piromallo, C., Royden, L., Rossetti, F., & Serpelloni, E. (2014). Mantle dynamics in the Mediterranean. *Reviews of Geophysics*, 52(3), 283–332. https://doi.org/10.1002/2013RG000444
- Faccenna, C., Becker, T. W., Lucente, F. P., Jolivet, L., & Rossetti, F. (2001). History of subduction and back arc extension in the Central Mediterranean. *Geophysical Journal International*, *145*(3), 809–820. https://doi.org/10.1046/j.0956-540x.2001.01435.x
- Fantoni, R., & Franciosi, R. (2010). Tectono-sedimentary setting of the Po Plain and Adriatic foreland. RENDICONTI LINCEI, 21(1), 197–209. <a href="https://doi.org/10.1007/s12210-010-0102-4">https://doi.org/10.1007/s12210-010-0102-4</a>
- Fernàndez, M., Afonso, J. C., & Ranalli, G. (2010). The deep lithospheric structure of the Namibian volcanic margin. *Tectonophysics*, *481*(1–4), 68–81. <a href="https://doi.org/10.1016/j.tecto.2009.02.036">https://doi.org/10.1016/j.tecto.2009.02.036</a>
- Fernàndez, M., Torne, M., Vergés, J., Casciello, E., & Macchiavelli, C. (2019). Evidence of Segmentation in the Iberia–Africa Plate Boundary: A Jurassic Heritage? *Geosciences*, 9(8), Article 8. https://doi.org/10.3390/geosciences9080343
- Finetti, I. R. (2005). CROP Project: Deep Seismic Exploration of the Central Mediterranean and Italy. Elsevier.
- Finetti, I. R., Boccaletti, M., Bonini, M., Del Ben, A., Geletti, R., Pipan, M., & Sani, F. (2001). Crustal section based on CROP seismic data across the North Tyrrhenian–Northern Apennines–Adriatic Sea. *Tectonophysics*, 343(3), 135–163. <a href="https://doi.org/10.1016/S0040-1951(01)00141-X">https://doi.org/10.1016/S0040-1951(01)00141-X</a>
- Flament, N., Gurnis, M., & Müller, R. D. (2013). A review of observations and models of dynamic topography. *Lithosphere*, *5*(2), 189–210. <a href="https://doi.org/10.1130/L245.1">https://doi.org/10.1130/L245.1</a>
- Flament, N., Gurnis, M., Williams, S., Seton, M., Skogseid, J., Heine, C., & Dietmar Müller, R. (2014). Topographic asymmetry of the South Atlantic from global models of mantle flow and lithospheric stretching. *Earth and Planetary Science Letters*, 387, 107–119. <a href="https://doi.org/10.1016/j.epsl.2013.11.017">https://doi.org/10.1016/j.epsl.2013.11.017</a>

- Fuchs, S., Norden, B., & International Heat Flow Commission. (2021). The Global Heat Flow Database: Release 202. *GFZ Data Services*, 73. <a href="https://doi.org/10.5880/fidgeo.2021.014">https://doi.org/10.5880/fidgeo.2021.014</a>
- Fullea, J., Fernàndez, M., & Zeyen, H. (2008). FA2BOUG—A FORTRAN 90 code to compute Bouguer gravity anomalies from gridded free-air anomalies: Application to the Atlantic-Mediterranean transition zone. *Computers & Geosciences*, *34*(12), 1665–1681. <a href="https://doi.org/10.1016/j.cageo.2008.02.018">https://doi.org/10.1016/j.cageo.2008.02.018</a>
- Fullea, J., Lebedev, S., Martinec, Z., & Celli, N. L. (2021). WINTERC-G: mapping the upper mantle thermochemical heterogeneity from coupled geophysical—petrological inversion of seismic waveforms, heat flow, surface elevation and gravity satellite data. *Geophysical Journal International*, 226(1), 146–191. <a href="https://doi.org/10.1093/gji/ggab094">https://doi.org/10.1093/gji/ggab094</a>
- Gailler, A., Klingelhoefer, F., Olivet, J.-L., & Aslanian, D. (2009). Crustal structure of a young margin pair: New results across the Liguro–Provencal Basin from wide-angle seismic tomography. *Earth and Planetary Science Letters*, *286*(1), 333–345. <a href="https://doi.org/10.1016/j.epsl.2009.07.001">https://doi.org/10.1016/j.epsl.2009.07.001</a>
- Gale, A., Langmuir, C. H., & Dalton, C. A. (2014). The Global Systematics of Ocean Ridge Basalts and their Origin. *Journal of Petrology*, *55*(6), 1051–1082. https://doi.org/10.1093/petrology/equ017
- Gallhofer, D., von Quadt, A., Schmid, S. M., Guillong, M., Peytcheva, I., & Seghedi, I. (2017). Magmatic and tectonic history of Jurassic ophiolites and associated granitoids from the South Apuseni Mountains (Romania). *Swiss Journal of Geosciences*, *110*(2), Article 2. <a href="https://doi.org/10.1007/s00015-016-0231-6">https://doi.org/10.1007/s00015-016-0231-6</a>
- Garcia-Castellanos, D., Fernàndez, M., & Torne, M. (1997). Numerical modeling of foreland basin formation: A program relating thrusting, flexure, sediment geometry and lithosphere rheology. *Computers & Geosciences*, 23(9), 993–1003. https://doi.org/10.1016/S0098-3004(97)00057-5
- Gattacceca, J., Deino, A., Rizzo, R., Jones, D. S., Henry, B., Beaudoin, B., & Vadeboin, F. (2007). Miocene rotation of Sardinia: New paleomagnetic and geochronological constraints and geodynamic implications. *Earth and Planetary Science Letters*, *258*(3), 359–377. https://doi.org/10.1016/j.epsl.2007.02.003

- Gaul, O. F., Griffin, W. L., O'Reilly, S. Y., & Pearson, N. J. (2000). Mapping olivine composition in the lithospheric mantle. *Earth and Planetary Science Letters*, *182*(3), 223–235. <a href="https://doi.org/10.1016/S0012-821X(00)00243-0">https://doi.org/10.1016/S0012-821X(00)00243-0</a>
- Gawlick, H.-J., & Missoni, S. (2019). Middle-Late Jurassic sedimentary mélange formation related to ophiolite obduction in the Alpine-Carpathian-Dinaridic Mountain Range. *Gondwana Research*, 74, 144–172. https://doi.org/10.1016/j.gr.2019.03.003
- Geissler, W. H., Sodoudi, F., & Kind, R. (2010). Thickness of the central and eastern European lithosphere as seen by S receiver functions. *Geophysical Journal International*, *181*(2), 604–634. https://doi.org/10.1111/j.1365-246X.2010.04548.x
- Gerya, T. (2019). *Introduction to Numerical Geodynamic Modelling* (2nd ed.). Cambridge University Press. https://doi.org/10.1017/9781316534243
- Gerya, T. V., Bercovici, D., & Becker, T. W. (2021). Dynamic slab segmentation due to brittle–ductile damage in the outer rise. *Nature*, *599*(7884), Article 7884. <a href="https://doi.org/10.1038/s41586-021-03937-x">https://doi.org/10.1038/s41586-021-03937-x</a>
- Giacomuzzi, G., Chiarabba, C., & De Gori, P. (2011). Linking the Alps and Apennines subduction systems: New constraints revealed by high-resolution teleseismic tomography. *Earth and Planetary Science Letters*, 301(3), 531–543. <a href="https://doi.org/10.1016/j.epsl.2010.11.033">https://doi.org/10.1016/j.epsl.2010.11.033</a>
- Giacomuzzi, G., Civalleri, M., De Gori, P., & Chiarabba, C. (2012). A 3D Vs model of the upper mantle beneath Italy: Insight on the geodynamics of central Mediterranean. *Earth and Planetary Science Letters*, 335–336, 105–120. https://doi.org/10.1016/j.epsl.2012.05.004
- Giacomuzzi, G., De Gori, P., & Chiarabba, C. (2022). How mantle heterogeneities drive continental subduction and magmatism in the Apennines. *Scientific Reports*, *12*(1), 13631. https://doi.org/10.1038/s41598-022-17715-w
- Giardini, D., & Velonà, M. (1991). The deep seismicity of the tyrrhenian sea\*. Terra Nova, 3(1), 57–64. <a href="https://doi.org/10.1111/j.1365-3121.1991.tb00844.x">https://doi.org/10.1111/j.1365-3121.1991.tb00844.x</a>
- Gilardoni, M., Reguzzoni, M., & Sampietro, D. (2016). GECO: A global gravity model by locally combining GOCE data and EGM2008. *Studia Geophysica et Geodaetica*, *60*(2), 228–247. <a href="https://doi.org/10.1007/s11200-015-1114-4">https://doi.org/10.1007/s11200-015-1114-4</a>

- Godey, S., Bossu, R., & Guilbert, J. (2013). Improving the Mediterranean seismicity picture thanks to international collaborations. *Physics and Chemistry of the Earth, Parts A/B/C*, 63, 3–11. <a href="https://doi.org/10.1016/j.pce.2013.04.012">https://doi.org/10.1016/j.pce.2013.04.012</a>
- Grad, M., Tiira, T., & ESC Working Group. (2009). The Moho depth map of the European Plate. *Geophysical Journal International*, 176(1), 279–292. https://doi.org/10.1111/j.1365-246X.2008.03919.x
- Greve, S., Paulssen, H., Goes, S., & van Bergen, M. (2014). Shear-velocity structure of the Tyrrhenian Sea: Tectonics, volcanism and mantle (de)hydration of a back-arc basin. *Earth and Planetary Science Letters*, 400, 45–53. https://doi.org/10.1016/j.epsl.2014.05.028
- Griffin, W. L., O'Reilly, S., & Ryan, C. G. (1999). The composition and origin of sub-continental lithospheric mantle. *Mantle Petrology: Field Observations and High Pressure Experimentation, A Tribute to Francis R.(Joe) Boyd*, 13–45.
- Griffin, W. L., O'Reilly, S. Y., Afonso, J. C., & Begg, G. C. (2009). The Composition and Evolution of Lithospheric Mantle: A Re-evaluation and its Tectonic Implications. *Journal of Petrology*, *50*(7), 1185–1204. https://doi.org/10.1093/petrology/egn033
- Grose, C. J., & Afonso, J. C. (2013). Comprehensive plate models for the thermal evolution of oceanic lithosphere. *Geochemistry, Geophysics, Geosystems*, *14*(9), 3751–3778. https://doi.org/10.1002/ggge.20232
- Guerri, M., Cammarano, F., & Connolly, J. A. D. (2015). Effects of chemical composition, water and temperature on physical properties of continental crust. *Geochemistry, Geophysics, Geosystems*, *16*(7), 2431–2449. <a href="https://doi.org/10.1002/2015GC005819">https://doi.org/10.1002/2015GC005819</a>
- Guidoboni, E., Ferrari, G., Mariotti, D., Comastri, A., Tarabusi, G., & Valensise, G. (2007). CFTI4Med, Catalogue of strong earthquakes in Italy (461 B.C.-1997) and Mediterranean area (760 B.C.-1500).
- Gurnis, M., Mitrovica, J. X., Ritsema, J., & van Heijst, H.-J. (2000). Constraining mantle density structure using geological evidence of surface uplift rates: The case of the African Superplume. *Geochemistry, Geophysics, Geosystems*, 1(7). https://doi.org/10.1029/1999GC000035
- Gvirtzman, Z., Faccenna, C., & Becker, T. W. (2016). Isostasy, flexure, and dynamic topography. *Tectonophysics*, 683, 255–271. <a href="https://doi.org/10.1016/j.tecto.2016.05.041">https://doi.org/10.1016/j.tecto.2016.05.041</a>

- Gvirtzman, Z., & Nur, A. (2001). Residual topography, lithospheric structure and sunken slabs in the central Mediterranean. *Earth and Planetary Science Letters*, *187*(1), 117–130. <a href="https://doi.org/10.1016/S0012-821X(01)00272-2">https://doi.org/10.1016/S0012-821X(01)00272-2</a>
- Handy, M. R., M. Schmid, S., Bousquet, R., Kissling, E., & Bernoulli, D. (2010). Reconciling plate-tectonic reconstructions of Alpine Tethys with the geological—geophysical record of spreading and subduction in the Alps. *Earth-Science Reviews*, 102(3), 121–158. https://doi.org/10.1016/j.earscirev.2010.06.002
- Handy, M. R., Schmid, S. M., Paffrath, M., Friederich, W., & the AlpArray Working Group. (2021). Orogenic lithosphere and slabs in the greater Alpine area interpretations based on teleseismic P-wave tomography. *Solid Earth*, *12*(11), 2633–2669. https://doi.org/10.5194/se-12-2633-2021
- Handy, M. R., Ustaszewski, K., & Kissling, E. (2015). Reconstructing the Alps–Carpathians–Dinarides as a key to understanding switches in subduction polarity, slab gaps and surface motion. *International Journal of Earth Sciences*, 104(1), 1–26. <a href="https://doi.org/10.1007/s00531-014-1060-3">https://doi.org/10.1007/s00531-014-1060-3</a>
- Hasterok, D., & Webb, J. (2017). On the radiogenic heat production of igneous rocks. *Geoscience Frontiers*, *8*(5), 919–940. <a href="https://doi.org/10.1016/j.gsf.2017.03.006">https://doi.org/10.1016/j.gsf.2017.03.006</a>
- Hayes, G. P., Moore, G. L., Portner, D. E., Hearne, M., Flamme, H., Furtney, M., & Smoczyk, G. M. (2018). Slab2, a comprehensive subduction zone geometry model. *Science*, *362*(6410), 58–61. <a href="https://doi.org/10.1126/science.aat4723">https://doi.org/10.1126/science.aat4723</a>
- Heller, P. L., & Liu, L. (2016). Dynamic topography and vertical motion of the U.S. Rocky Mountain region prior to and during the Laramide orogeny. *GSA Bulletin*, *128*(5–6), 973–988. https://doi.org/10.1130/B31431.1
- Hetényi, G., Molinari, I., Clinton, J., Bokelmann, G., Bondár, I., Crawford, W. C., Dessa, J.-X., Doubre, C., Friederich, W., Fuchs, F., Giardini, D., Gráczer, Z., Handy, M. R., Herak, M., Jia, Y., Kissling, E., Kopp, H., Korn, M., Margheriti, L., ... AlpArray Working Group. (2018). The AlpArray Seismic Network: A Large-Scale European Experiment to Image the Alpine Orogen. Surveys in Geophysics, 39(5), 1009–1033. <a href="https://doi.org/10.1007/s10712-018-9472-4">https://doi.org/10.1007/s10712-018-9472-4</a>
- Hetényi, G., Ren, Y., Dando, B., Stuart, G. W., Hegedűs, E., Kovács, A. C., & Houseman, G. A. (2015). Crustal structure of the Pannonian Basin: The AlCaPa and Tisza Terrains and the Mid-Hungarian Zone. *Tectonophysics*, 646, 106–116. <a href="https://doi.org/10.1016/j.tecto.2015.02.004">https://doi.org/10.1016/j.tecto.2015.02.004</a>

- Hill, R. (1952). The Elastic Behaviour of a Crystalline Aggregate. *Proceedings of the Physical Society. Section A*, 65(5), 349. <a href="https://doi.org/10.1088/0370-1298/65/5/307">https://doi.org/10.1088/0370-1298/65/5/307</a>
- Hirth, G., & Kohlstedt, D. (2003). Rheology of the upper mantle and the mantle wedge: A view from the experimentalists. *Geophysical Monograph Series*, *138*, 83–105. https://doi.org/10.1029/138GM06
- Hofmann, A. W. (1988). Chemical differentiation of the Earth: The relationship between mantle, continental crust, and oceanic crust. *Earth and Planetary Science Letters*, 90(3), 297–314. <a href="https://doi.org/10.1016/0012-821X(88)90132-X">https://doi.org/10.1016/0012-821X(88)90132-X</a>
- Hofmann, A. W. (1997). Mantle geochemistry: The message from oceanic volcanism. *Nature*, 385(6613), 219–229. <a href="https://doi.org/10.1038/385219a0">https://doi.org/10.1038/385219a0</a>
- Hofmann, A. W., Class, C., & Goldstein, S. L. (2022). Size and Composition of the MORB+OIB Mantle Reservoir. *Geochemistry, Geophysics, Geosystems*, 23(8), e2022GC010339. https://doi.org/10.1029/2022GC010339
- Hoggard, M., Austermann, J., Randel, C., & Stephenson, S. (2021). Observational Estimates of Dynamic Topography Through Space and Time. In H. Marquardt, M. Ballmer, S. Cottaar, & J. Konter (Eds.), *Geophysical Monograph Series* (1st ed., pp. 371–411). Wiley. <a href="https://doi.org/10.1002/9781119528609.ch15">https://doi.org/10.1002/9781119528609.ch15</a>
- Holland, T. J. B., & Powell, R. (1998). An internally consistent thermodynamic data set for phases of petrological interest. *Journal of Metamorphic Geology*, *16*(3), 309–343. <a href="https://doi.org/10.1111/j.1525-1314.1998.00140.x">https://doi.org/10.1111/j.1525-1314.1998.00140.x</a>
- Horváth, F. (1995). Phases of compression during the evolution of the Pannonian Basin and its bearing on hydrocarbon exploration. *Marine and Petroleum Geology*, *12*(8), 837–844. https://doi.org/10.1016/0264-8172(95)98851-U
- Horváth, F., Bada, G., Szafián, P., Tari, G., Ádám, A., & Cloetingh, S. (2006). Formation and deformation of the Pannonian Basin: Constraints from observational data. *Geological Society, London, Memoirs*, 32(1), 191–206. <a href="https://doi.org/10.1144/GSL.MEM.2006.032.01.11">https://doi.org/10.1144/GSL.MEM.2006.032.01.11</a>
- Horváth, F., Musitz, B., Balázs, A., Végh, A., Uhrin, A., Nádor, A., Koroknai, B., Pap, N., Tóth, T., & Wórum, G. (2015). Evolution of the Pannonian basin and its geothermal resources. *Geothermics*, 53, 328–352. <a href="https://doi.org/10.1016/j.geothermics.2014.07.009">https://doi.org/10.1016/j.geothermics.2014.07.009</a>

- Hu, J., Liu, L., Faccenda, M., Zhou, Q., Fischer, K. M., Marshak, S., & Lundstrom, C. (2018). Modification of the Western Gondwana craton by plume–lithosphere interaction. *Nature Geoscience*, 11(3), Article 3. <a href="https://doi.org/10.1038/s41561-018-0064-1">https://doi.org/10.1038/s41561-018-0064-1</a>
- Hua, Y., Zhao, D., & Xu, Y. (2017). P wave anisotropic tomography of the Alps. *Journal of Geophysical Research: Solid Earth*, 122(6), 4509–4528. https://doi.org/10.1002/2016JB013831
- Husson, L. (2006). Dynamic topography above retreating subduction zones. *Geology*, 34(9), 741–744. https://doi.org/10.1130/G22436.1
- Ito, E., & Katsura, T. (1989). A temperature profile of the mantle transition zone. *Geophysical Research Letters*, 16(5), 425–428. <a href="https://doi.org/10.1029/GL016i005p00425">https://doi.org/10.1029/GL016i005p00425</a>
- Jackson, I., & Faul, U. H. (2010). Grainsize-sensitive viscoelastic relaxation in olivine: Towards a robust laboratory-based model for seismological application. *Physics of the Earth and Planetary Interiors*, 183(1), 151–163. <a href="https://doi.org/10.1016/j.pepi.2010.09.005">https://doi.org/10.1016/j.pepi.2010.09.005</a>
- Jarchow, C. M., & Thompson, G. A. (1989). The Nature of the Mohorovicic Discontinuity. *Annual Review of Earth and Planetary Sciences*, *17*(1), 475–506. https://doi.org/10.1146/annurev.ea.17.050189.002355
- Jiménez-Munt, I., Fernàndez, M., Vergés, J., Afonso, J. C., Garcia-Castellanos, D., & Fullea, J. (2010). Lithospheric structure of the Gorringe Bank: Insights into its origin and tectonic evolution. Tectonics, 29(5). https://doi.org/10.1029/2009TC002458
- Jiménez-Munt, I., Torne, M., Fernàndez, M., Vergés, J., Kumar, A., Carballo, A., & García-Castellanos, D. (2019). Deep seated density anomalies across the iberia-africa plate boundary and its topographic response. *Journal of Geophysical Research: Solid Earth*, 124(12), 13310–13332. https://doi.org/10.1029/2019JB018445
- Johnson, T. E., Benedix, G. K., & Bland, P. A. (2016). Metamorphism and partial melting of ordinary chondrites: Calculated phase equilibria. *Earth and Planetary Science Letters*, 433, 21–30. https://doi.org/10.1016/j.epsl.2015.10.035
- Jolivet, L. (2023). Tethys and Apulia (Adria), 100 years of reconstructions. *Comptes Rendus. Géoscience*, 355(S2), 1–20. <a href="https://doi.org/10.5802/crgeos.198">https://doi.org/10.5802/crgeos.198</a>

- Jolivet, L., & Faccenna, C. (2000). Mediterranean extension and the Africa-Eurasia collision. *Tectonics*, *19*(6), 1095–1106. <a href="https://doi.org/10.1029/2000TC900018">https://doi.org/10.1029/2000TC900018</a>
- Jones, A. G., & Craven, J. A. (2004). Area selection for diamond exploration using deep-probing electromagnetic surveying. *Lithos*, 77(1), 765–782. <a href="https://doi.org/10.1016/j.lithos.2004.03.057">https://doi.org/10.1016/j.lithos.2004.03.057</a>
- Kalmár, D., Hetényi, G., Balázs, A., Bondár, I., & Group, A. W. (2021). Crustal Thinning From Orogen to Back-Arc Basin: The Structure of the Pannonian Basin Region Revealed by P-to-S Converted Seismic Waves. *Journal of Geophysical Research:* Solid Earth, 126(7), e2020JB021309. https://doi.org/10.1029/2020JB021309
- Kapuralić, J., Šumanovac, F., & Markušić, S. (2019). Crustal structure of the northern Dinarides and southwestern part of the Pannonian basin inferred from local earthquake tomography. *Swiss Journal of Geosciences*, *112*(1), 181–198. <a href="https://doi.org/10.1007/s00015-018-0335-2">https://doi.org/10.1007/s00015-018-0335-2</a>
- Karlstrom, K. E., Coblentz, D., Dueker, K., Ouimet, W., Kirby, E., Van Wijk, J., Schmandt, B., Kelley, S., Lazear, G., Crossey, L. J., Crow, R., Aslan, A., Darling, A., Aster, R., MacCarthy, J., Hansen, S. M., Stachnik, J., Stockli, D. F., Garcia, R. V., ... and the CREST Working Group. (2012). Mantle-driven dynamic uplift of the Rocky Mountains and Colorado Plateau and its surface response: Toward a unified hypothesis. *Lithosphere*, *4*(1), 3–22. https://doi.org/10.1130/L150.1
- Kastens, K., Mascle, J., Auroux, C., Bonatti, E., Broglia, C., Channell, J., Curzi, P., Emeis, K.-C., Glaçon, G., Hasegawa, S., Hieke, W., Mascle, G., McCoy, F., McKenzie, J., Mendelson, J., Müller, C., Réhault, J.-P., Robertson, A., Sartori, R., ... Torii, M. (1988).
  ODP Leg 107 in the Tyrrhenian Sea: Insights into passive margin and back-arc basin evolution. GSA Bulletin, 100(7), 1140–1156. <a href="https://doi.org/10.1130/0016-7606(1988)100<1140:OLITTS>2.3.CO;2">https://doi.org/10.1130/0016-7606(1988)100<1140:OLITTS>2.3.CO;2</a>
- Kästle, E. D., El-Sharkawy, A., Boschi, L., Meier, T., Rosenberg, C., Bellahsen, N., Cristiano, L., & Weidle, C. (2018). Surface Wave Tomography of the Alps Using Ambient-Noise and Earthquake Phase Velocity Measurements. *Journal of Geophysical Research: Solid Earth*, 123(2), 1770–1792. <a href="https://doi.org/10.1002/2017JB014698">https://doi.org/10.1002/2017JB014698</a>
- Kästle, E. D., Molinari, I., Boschi, L., Kissling, E., & and the AlpArray Working Group. (2022). Azimuthal anisotropy from eikonal tomography: Example from ambient-noise measurements in the AlpArray network. *Geophysical Journal International*, 229(1), 151–170. <a href="https://doi.org/10.1093/gji/ggab453">https://doi.org/10.1093/gji/ggab453</a>

- Kästle, E. D., Rosenberg, C., Boschi, L., Bellahsen, N., Meier, T., & El-Sharkawy, A. (2020). Slab break-offs in the Alpine subduction zone. *International Journal of Earth Sciences*, 109(2), 587–603. <a href="https://doi.org/10.1007/s00531-020-01821-z">https://doi.org/10.1007/s00531-020-01821-z</a>
- Katsura, T., Yamada, H., Nishikawa, O., Song, M., Kubo, A., Shinmei, T., Yokoshi, S., Aizawa, Y., Yoshino, T., Walter, M. J., Ito, E., & Funakoshi, K. (2004). Olivine-wadsleyite transition in the system (Mg,Fe)2SiO4. *Journal of Geophysical Research: Solid Earth*, 109(B2). <a href="https://doi.org/10.1029/2003JB002438">https://doi.org/10.1029/2003JB002438</a>
- Kelemework, Y., Milano, M., La Manna, M., de Alteriis, G., Iorio, M., & Fedi, M. (2021). Crustal structure in the Campanian region (Southern Apennines, Italy) from potential field modelling. *Scientific Reports*, *11*(1), Article 1. <a href="https://doi.org/10.1038/s41598-021-93945-8">https://doi.org/10.1038/s41598-021-93945-8</a>
- Keller, J. V. A., & Coward, M. P. (1996). The structure and evolution of the Northern Tyrrhenian Sea. *Geological Magazine*, 133(1), 1–16. <a href="https://doi.org/10.1017/S0016756800007214">https://doi.org/10.1017/S0016756800007214</a>
- Kennett, J. P. (with Internet Archive). (1982). *Marine geology*. Englewood Cliffs, N.J.: Prentice-Hall. http://archive.org/details/marinegeology0000kenn
- Király, Á., Holt, A. F., Funiciello, F., Faccenna, C., & Capitanio, F. A. (2018). Modeling Slab-Slab Interactions: Dynamics of Outward Dipping Double-Sided Subduction Systems. *Geochemistry, Geophysics, Geosystems*, 19(3), 693–714. <a href="https://doi.org/10.1002/2017GC007199">https://doi.org/10.1002/2017GC007199</a>
- Klein, E. M., & Langmuir, C. H. (1987). Global correlations of ocean ridge basalt chemistry with axial depth and crustal thickness. *Journal of Geophysical Research: Solid Earth*, 92(B8), 8089–8115. https://doi.org/10.1029/JB092iB08p08089
- Korbar, T. (2009). Orogenic evolution of the External Dinarides in the NE Adriatic region:

  A model constrained by tectonostratigraphy of Upper Cretaceous to Paleogene carbonates. *Earth-Science Reviews*, 96(4), 296–312. <a href="https://doi.org/10.1016/j.earscirev.2009.07.004">https://doi.org/10.1016/j.earscirev.2009.07.004</a>
- Koroknai, B., Wórum, G., Tóth, T., Koroknai, Z., Fekete-Németh, V., & Kovács, G. (2020). Geological deformations in the Pannonian Basin during the neotectonic phase: New insights from the latest regional mapping in Hungary. *Earth-Science Reviews*, 211, 103411. <a href="https://doi.org/10.1016/j.earscirev.2020.103411">https://doi.org/10.1016/j.earscirev.2020.103411</a>

- Koulakov, I., Jakovlev, A., Zabelina, I., Roure, F., Cloetingh, S., El Khrepy, S., & Al-Arifi, N. (2015). Subduction or delamination beneath the Apennines? Evidence from regional tomography. *Solid Earth*, *6*(2), 669–679. <a href="https://doi.org/10.5194/se-6-669-2015">https://doi.org/10.5194/se-6-669-2015</a>
- Koulakov, I., Kaban, M. K., Tesauro, M., & Cloetingh, S. (2009). P- and S-velocity anomalies in the upper mantle beneath Europe from tomographic inversion of ISC data. *Geophysical Journal International*, 179(1), 345–366. <a href="https://doi.org/10.1111/j.1365-246X.2009.04279.x">https://doi.org/10.1111/j.1365-246X.2009.04279.x</a>
- Kovács, I., Csontos, L., Szabó, Cs., Bali, E., Falus, Gy., Benedek, K., & Zajacz, Z. (2007).
   Paleogene–early Miocene igneous rocks and geodynamics of the Alpine-Carpathian-Pannonian-Dinaric region: An integrated approach. In L. Beccaluva, G. Bianchini, & M. Wilson, *Cenozoic Volcanism in the Mediterranean Area*. Geological Society of America. <a href="https://doi.org/10.1130/2007.2418(05)">https://doi.org/10.1130/2007.2418(05)</a>
- Kuk, V., Prelogović, E., & Dragičević, I. (2000). Seismotectonically Active Zones in the Dinarides. *Geologia Croatica*, *53*(2), 295–303.
- Kumar, A., Fernàndez, M., Jiménez-Munt, I., Torne, M., Vergés, J., & Afonso, J. C. (2020). LitMod2D\_2.0: An Improved Integrated Geophysical-Petrological Modeling Tool for the Physical Interpretation of Upper Mantle Anomalies. *Geochemistry, Geophysics, Geosystems*, 21(3), e2019GC008777. https://doi.org/10.1029/2019GC008777
- Kumar, A., Fernàndez, M., Vergés, J., Torne, M., & Jiménez-Munt, I. (2021). Opposite Symmetry in the Lithospheric Structure of the Alboran and Algerian Basins and Their Margins (Western Mediterranean): Geodynamic Implications. *Journal of Geophysical Research:* Solid Earth, 126(7), e2020JB021388. <a href="https://doi.org/10.1029/2020JB021388">https://doi.org/10.1029/2020JB021388</a>
- Lacombe, O., & Jolivet, L. (2005). Structural and kinematic relationships between Corsica and the Pyrenees-Provence domain at the time of the Pyrenean orogeny. *Tectonics*, 24(1). https://doi.org/10.1029/2004TC001673
- Langmuir, C. H., Klein, E. M., & Plank, T. (1992). Petrological Systematics of Mid-Ocean Ridge Basalts: Constraints on Melt Generation Beneath Ocean Ridges. In J. P. Morgan, D. K. Blackman, & J. M. Sinton (Eds.), *Geophysical Monograph Series* (pp. 183–280). American Geophysical Union. https://doi.org/10.1029/GM071p0183
- Laske, G., Masters, G., Ma, Z., & Pasyanos, M. (2013). *Update on CRUST1.0—A 1-degree Global Model of Earth's Crust.* 15, 2658.

- Le Breton, E., Handy, M. R., Molli, G., & Ustaszewski, K. (2017). Post-20 Ma Motion of the Adriatic Plate: New Constraints From Surrounding Orogens and Implications for Crust-Mantle Decoupling. *Tectonics*, 36(12), 3135–3154. <a href="https://doi.org/10.1002/2016TC004443">https://doi.org/10.1002/2016TC004443</a>
- Lee, C.-T. A., Luffi, P., & Chin, E. J. (2011). Building and Destroying Continental Mantle. Annual Review of Earth and Planetary Sciences, 39(Volume 39, 2011), 59–90. https://doi.org/10.1146/annurev-earth-040610-133505
- Levandowski, W., Jones, C. H., Shen, W., Ritzwoller, M. H., & Schulte-Pelkum, V. (2014). Origins of topography in the western U.S.: Mapping crustal and upper mantle density variations using a uniform seismic velocity model. *Journal of Geophysical Research: Solid Earth*, 119(3), 2375–2396. https://doi.org/10.1002/2013JB010607
- Li, Z.-H., Xu, Z., Gerya, T., & Burg, J.-P. (2013). Collision of continental corner from 3-D numerical modeling. *Earth and Planetary Science Letters*, *380*, 98–111. <a href="https://doi.org/10.1016/j.epsl.2013.08.034">https://doi.org/10.1016/j.epsl.2013.08.034</a>
- Liao, J., Gerya, T., & Wang, Q. (2013). Layered structure of the lithospheric mantle changes dynamics of craton extension. *Geophysical Research Letters*, *40*(22), 5861–5866. https://doi.org/10.1002/2013GL058081
- Liotta, D., Cernobori, L., & Nicolich, R. (1998). Restricted rifting and its consistence with compressional structures: Results from CROP 3 traverse (Northern Apenninies, Italy). *Terra Nova*, *10*, 16–20.
- Lippitsch, R., Kissling, E., & Ansorge, J. (2003). Upper mantle structure beneath the Alpine orogen from high-resolution teleseismic tomography. *Journal of Geophysical Research: Solid Earth*, *108*(B8). https://doi.org/10.1029/2002JB002016
- Lithgow-Bertelloni, C., & Silver, P. G. (1998). Dynamic topography, plate driving forces and the African superswell. *Nature*, 395(6699), Article 6699. <a href="https://doi.org/10.1038/26212">https://doi.org/10.1038/26212</a>
- Liu, L., & Gurnis, M. (2010). Dynamic subsidence and uplift of the Colorado Plateau. *Geology*, 38(7), 663–666. <a href="https://doi.org/10.1130/G30624.1">https://doi.org/10.1130/G30624.1</a>
- Lo Bue, R., Faccenda, M., & Yang, J. (2021). The Role of Adria Plate Lithospheric Structures on the Recent Dynamics of the Central Mediterranean Region. *Journal of Geophysical Research: Solid Earth*, 126(10), e2021JB022377. <a href="https://doi.org/10.1029/2021JB022377">https://doi.org/10.1029/2021JB022377</a>

- Loreto, M. F., Zitellini, N., Ranero, C. R., Palmiotto, C., & Prada, M. (2021). Extensional tectonics during the Tyrrhenian back-arc basin formation and a new morpho-tectonic map. *Basin Research*, *33*(1), 138–158. <a href="https://doi.org/10.1111/bre.12458">https://doi.org/10.1111/bre.12458</a>
- Lucente, F. P., Chiarabba, C., Cimini, G. B., & Giardini, D. (1999). Tomographic constraints on the geodynamic evolution of the Italian region. *Journal of Geophysical Research: Solid Earth*, *104*(B9), 20307–20327. https://doi.org/10.1029/1999JB900147
- Lucente, F. P., & Speranza, F. (2001). Belt bending driven by lateral bending of subducting lithospheric slab: Geophysical evidences from the northern Apennines (Italy). *Tectonophysics*, 337(1), 53–64. <a href="https://doi.org/10.1016/S0040-1951(00)00286-9">https://doi.org/10.1016/S0040-1951(00)00286-9</a>
- Lustrino, M., Chiarabba, C., & Carminati, E. (2022). Igneous activity in central-southern Italy: Is the subduction paradigm still valid? In *In the footsteps of warren b. Hamilton:*New ideas in earth science. Geological Society of America.

  <a href="https://doi.org/10.1130/2021.2553(28)">https://doi.org/10.1130/2021.2553(28)</a>
- Lustrino, M., Duggen, S., & Rosenberg, C. L. (2011). The Central-Western Mediterranean: Anomalous igneous activity in an anomalous collisional tectonic setting. *Earth-Science Reviews*, *104*(1), 1–40. <a href="https://doi.org/10.1016/j.earscirev.2010.08.002">https://doi.org/10.1016/j.earscirev.2010.08.002</a>
- Maclennan, J., MKenzie, D., & Gronvöld, K. (2001). Plume-driven upwelling under central lceland. *Earth and Planetary Science Letters*, 194(1), 67–82. https://doi.org/10.1016/S0012-821X(01)00553-2
- Maffione, M., & van Hinsbergen, D. J. J. (2018). Reconstructing Plate Boundaries in the Jurassic Neo-Tethys From the East and West Vardar Ophiolites (Greece and Serbia). *Tectonics*, *37*(3), 858–887. <a href="https://doi.org/10.1002/2017TC004790">https://doi.org/10.1002/2017TC004790</a>
- Magrini, F., Diaferia, G., El-Sharkawy, A., Cammarano, F., van der Meijde, M., Meier, T., & Boschi, L. (2022). Surface-Wave Tomography of the Central-Western Mediterranean: New Insights Into the Liguro-Provençal and Tyrrhenian Basins. *Journal of Geophysical Research:* Solid Earth, 127(3), e2021JB023267. <a href="https://doi.org/10.1029/2021JB023267">https://doi.org/10.1029/2021JB023267</a>
- Magrini, F., Diaferia, G., Fadel, I., Cammarano, F., van der Meijde, M., & Boschi, L. (2020). 3-D shear wave velocity model of the lithosphere below the Sardinia–Corsica continental block based on Rayleigh-wave phase velocities. *Geophysical Journal International*, 220(3), 2119–2130. https://doi.org/10.1093/gji/ggz555

- Malinverno, A., & Ryan, W. B. F. (1986). Extension in the Tyrrhenian Sea and shortening in the Apennines as result of arc migration driven by sinking of the lithosphere. *Tectonics*, *5*(2), 227–245. <a href="https://doi.org/10.1029/TC005i002p00227">https://doi.org/10.1029/TC005i002p00227</a>
- Mantovani, E., Viti, M., Tamburelli, C., & Babbucci, D. (2022). Generation and Disruption of Subducted Lithosphere in the Central-Western Mediterranean Region and Time-Space Distribution of Magmatic Activity Since the Late Miocene. *International Journal of Geosciences*, *13*(9), Article 9. <a href="https://doi.org/10.4236/ijg.2022.139041">https://doi.org/10.4236/ijg.2022.139041</a>
- Manu-Marfo, D., Aoudia, A., Pachhai, S., & Kherchouche, R. (2019). 3D shear wave velocity model of the crust and uppermost mantle beneath the Tyrrhenian basin and margins. *Scientific Reports*, *9*(1), 3609. <a href="https://doi.org/10.1038/s41598-019-40510-z">https://doi.org/10.1038/s41598-019-40510-z</a>
- Mascle, J., & Rehault, J.-P. (1990). A REVISED SEISMIC STRATIGRAPHY OF THE TYRRHENIAN SEA: IMPLICATIONS FOR THE BASIN EVOLUTION. *Proceedings of the Ocean Drilling Program*, 107, 617–636.
- Massoli, D., Koyi, H. A., & Barchi, M. R. (2006). Structural evolution of a fold and thrust belt generated by multiple décollements: Analogue models and natural examples from the Northern Apennines (Italy). *Journal of Structural Geology*, *28*(2), 185–199. <a href="https://doi.org/10.1016/j.jsg.2005.11.002">https://doi.org/10.1016/j.jsg.2005.11.002</a>
- Matenco, L., & Radivojević, D. (2012). On the formation and evolution of the Pannonian Basin: Constraints derived from the structure of the junction area between the Carpathians and Dinarides. *Tectonics*, *31*(6). https://doi.org/10.1029/2012TC003206
- Matthews, K. J., Hale, A. J., Gurnis, M., Müller, R. D., & DiCaprio, L. (2011). Dynamic subsidence of Eastern Australia during the Cretaceous. *Gondwana Research*, *19*(2), 372–383. <a href="https://doi.org/10.1016/j.gr.2010.06.006">https://doi.org/10.1016/j.gr.2010.06.006</a>
- Mazzoli, S., Ascione, A., S., C., Iannace, A., Megna, A., Santini, S., & Vitale, S. (2013). Subduction and continental collision events in the southern Apennines: Constraints from two crustal cross-sections. RENDICONTI ONLINE DELLA SOCIETÀ GEOLOGICA ITALIANA, 25, 78–84. <a href="https://doi.org/10.3301/ROL.2013.07">https://doi.org/10.3301/ROL.2013.07</a>
- Mazzoli, S., Pierantoni, P. P., Borraccini, F., Paltrinieri, W., & Deiana, G. (2005). Geometry, segmentation pattern and displacement variations along a major Apennine thrust zone, central Italy. *Journal of Structural Geology*, 27(11), 1940–1953. <a href="https://doi.org/10.1016/j.jsg.2005.06.002">https://doi.org/10.1016/j.jsg.2005.06.002</a>
- McDonough, W. F., & Sun, S. -s. (1995). The composition of the Earth. *Chemical Geology*, 120(3), 223–253. https://doi.org/10.1016/0009-2541(94)00140-4

- Melchiorre, M., Vergés, J., Fernàndez, M., Coltorti, M., Torne, M., & Casciello, E. (2017). Evidence for mantle heterogeneities in the westernmost Mediterranean from a statistical approach to volcanic petrology. *Lithos*, 276, 62–74. <a href="https://doi.org/10.1016/j.lithos.2016.11.018">https://doi.org/10.1016/j.lithos.2016.11.018</a>
- Mele, G., & Sandvol, E. (2003). Deep crustal roots beneath the northern Apennines inferred from teleseismic receiver functions. *Earth and Planetary Science Letters*, 211(1), 69–78. https://doi.org/10.1016/S0012-821X(03)00185-7
- Miller, M. S., & Piana Agostinetti, N. (2012). Insights into the evolution of the Italian lithospheric structure from S receiver function analysis. *Earth and Planetary Science Letters*, *345*–348, 49–59. https://doi.org/10.1016/j.epsl.2012.06.028
- Molinari, I., & Morelli, A. (2011). EPcrust: A reference crustal model for the European Plate. *Geophysical Journal International*, 185(1), 352–364. <a href="https://doi.org/10.1111/j.1365-246X.2011.04940.x">https://doi.org/10.1111/j.1365-246X.2011.04940.x</a>
- Molinari, I., Verbeke, J., Boschi, L., Kissling, E., & Morelli, A. (2015). Italian and Alpine three-dimensional crustal structure imaged by ambient-noise surface-wave dispersion. *Geochemistry, Geophysics, Geosystems*, 16(12), 4405–4421. <a href="https://doi.org/10.1002/2015GC006176">https://doi.org/10.1002/2015GC006176</a>
- Molli, G. (2008). Northern Apennine–Corsica orogenic system: An updated overview. Geological Society, London, Special Publications, 298(1), 413–442. https://doi.org/10.1144/SP298.19
- Molli, G., Crispini, L., Malusà, M. G., Mosca, P., Piana, F., & Federico, L. (2010). Geology of the Western Alps-Northern Apennine junction area: A regional review. *Journal of the Virtual Explorer*, *36*. https://doi.org/10.3809/jvirtex.2010.00215
- Molli, G., & Malavieille, J. (2011). Orogenic processes and the Corsica/Apennines geodynamic evolution: Insights from Taiwan. *International Journal of Earth Sciences*, 100(5), 1207–1224. <a href="https://doi.org/10.1007/s00531-010-0598-y">https://doi.org/10.1007/s00531-010-0598-y</a>
- Molnar, P., England, P. C., & Jones, C. H. (2015). Mantle dynamics, isostasy, and the support of high terrain. *Journal of Geophysical Research: Solid Earth*, *120*(3), 1932–1957. https://doi.org/10.1002/2014JB011724
- Montone, P., & Mariucci, M. T. (2023). Lateral Variations of P-Wave Velocity from Deep Borehole Data in the Southern Apennines, Italy. *Pure and Applied Geophysics*. <a href="https://doi.org/10.1007/s00024-023-03248-4">https://doi.org/10.1007/s00024-023-03248-4</a>

- Mostardini, F., & Merlini, S. (1986). Appennino centro-meridionale: Sesioni geologiche e proposta di modello strutturale. *Memorie della Società Geologica Italiana*, 35, 177–202.
- Moucha, R., & Forte, A. M. (2011). Changes in African topography driven by mantle convection. *Nature Geoscience*, *4*(10), 707–712. <a href="https://doi.org/10.1038/ngeo1235">https://doi.org/10.1038/ngeo1235</a>
- Moucha, R., Forte, A. M., Rowley, D. B., Mitrovica, J. X., Simmons, N. A., & Grand, S. P. (2009). Deep mantle forces and the uplift of the Colorado Plateau. *Geophysical Research Letters*, *36*(19). <a href="https://doi.org/10.1029/2009GL039778">https://doi.org/10.1029/2009GL039778</a>
- Nafe, J. E., & Drake, C. L. (1963). Physical properties of marine sediments. *The Sea v. 3:* New York, John Wiley & Sons, 794–815.
- Negredo, A. M., Mancilla, F. d L., Clemente, C., Morales, J., & Fullea, J. (2020). Geodynamic Modeling of Edge-Delamination Driven by Subduction-Transform Edge Propagator Faults: The Westernmost Mediterranean Margin (Central Betic Orogen) Case Study. Frontiers in Earth Science, 8. <a href="https://doi.org/10.3389/feart.2020.533392">https://doi.org/10.3389/feart.2020.533392</a>
- Neri, G., Orecchio, B., Scolaro, S., & Totaro, C. (2020). Major Earthquakes of Southern Calabria, Italy, Into the Regional Geodynamic Context. *Frontiers in Earth Science*, *8*, 579846. <a href="https://doi.org/10.3389/feart.2020.579846">https://doi.org/10.3389/feart.2020.579846</a>
- Neri, G., Orecchio, B., Totaro, C., Falcone, G., & Presti, D. (2009). Subduction Beneath Southern Italy Close the Ending: Results from Seismic Tomography. *Seismological Research Letters*, *80*(1), 63–70. <a href="https://doi.org/10.1785/gssrl.80.1.63">https://doi.org/10.1785/gssrl.80.1.63</a>
- Niu, Y. (1997). Mantle Melting and Melt Extraction Processes beneath Ocean Ridges: Evidence from Abyssal Peridotites. *Journal of Petrology*, *38*(8), 1047–1074. https://doi.org/10.1093/petroj/38.8.1047
- Niu, Y. (2021). Lithosphere thickness controls the extent of mantle melting, depth of melt extraction and basalt compositions in all tectonic settings on Earth A review and new perspectives. *Earth-Science Reviews*, 217, 103614. <a href="https://doi.org/10.1016/j.earscirev.2021.103614">https://doi.org/10.1016/j.earscirev.2021.103614</a>
- Noguera, A. M., & Rea, G. (2000). Deep structure of the Campanian–Lucanian Arc (Southern Apennine, Italy). *Tectonophysics*, 324(4), 239–265. <a href="https://doi.org/10.1016/S0040-1951(00)00137-2">https://doi.org/10.1016/S0040-1951(00)00137-2</a>

- Norden, B., & Förster, A. (2006). Thermal conductivity and radiogenic heat production of sedimentary and magmatic rocks in the Northeast German Basin. *AAPG Bulletin*, 90(6), 939–962. <a href="https://doi.org/10.1306/01250605100">https://doi.org/10.1306/01250605100</a>
- O'Reilly, S. Y., & Griffin, W. L. (2006). Imaging global chemical and thermal heterogeneity in the subcontinental lithospheric mantle with garnets and xenoliths: Geophysical implications. *Tectonophysics*, 416(1–4), 289–309. <a href="https://doi.org/10.1016/j.tecto.2005.11.014">https://doi.org/10.1016/j.tecto.2005.11.014</a>
- O'Reilly, S. Y., & Griffin, W. L. (2010). The continental lithosphere–asthenosphere boundary: Can we sample it? *Lithos*, *120*(1), 1–13. <a href="https://doi.org/10.1016/j.lithos.2010.03.016">https://doi.org/10.1016/j.lithos.2010.03.016</a>
- O'Reilly, S. Y., Griffin, W. L., Djomani, Y. H. P., & Morgan, P. (2001). Are lithospheres forever? Tracking changes in subcontinental lithospheric mantle through time. *GSA Today*, *11*(4), 4–10.
- Paffrath, M., Friederich, W., Schmid, S. M., Handy, M. R., & the AlpArray and AlpArray-Swath D Working Group. (2021). Imaging structure and geometry of slabs in the greater Alpine area a P-wave travel-time tomography using AlpArray Seismic Network data. *Solid Earth*, *12*(11), 2671–2702. <a href="https://doi.org/10.5194/se-12-2671-2021">https://doi.org/10.5194/se-12-2671-2021</a>
- Palin, R. M., Santosh, M., Cao, W., Li, S.-S., Hernández-Uribe, D., & Parsons, A. (2020). Secular change and the onset of plate tectonics on Earth. *Earth-Science Reviews*, 207, 103172. <a href="https://doi.org/10.1016/j.earscirev.2020.103172">https://doi.org/10.1016/j.earscirev.2020.103172</a>
- Pamić, J., Balen, D., & Herak, M. (2002). Origin and geodynamic evolution of Late Paleogene magmatic associations along the Periadriatic-Sava-Vardar magmatic belt. Geodinamica Acta, 15(4), 209–231. https://doi.org/10.1080/09853111.2002.10510755
- Pamić, J., Gušić, I., & Jelaska, V. (1998). Geodynamic evolution of the Central Dinarides. *Tectonophysics*, 297(1), 251–268. <a href="https://doi.org/10.1016/S0040-1951(98)00171-1">https://doi.org/10.1016/S0040-1951(98)00171-1</a>
- Pandeli, E., Principi, G., Bortolotti, V., Benvenuti, M., Fazzuoli, M., Dini, A., Fanucci, F., Menna, F., & Nirta, G. (2013). The Elba Island: An intriguing geological puzzle in the Northern Tyrrhenian Sea. *ISPRA and Soc. Geol. It., Geol. Field Trips*, *5*(2.1).
- Panza, G. F., Pontevivo, A., Chimera, G., Raykova, R., & Aoudia, A. (2003). The lithosphere-asthenosphere: Italy and surroundings. *Episodes Journal of International Geoscience*, *26*(3), 169–174. https://doi.org/10.18814/epiiugs/2003/v26i3/003

- Panza, G., Peccerillo, A., Aoudia, A., & Farina, B. (2007). Geophysical and petrological modelling of the structure and composition of the crust and upper mantle in complex geodynamic settings: The Tyrrhenian Sea and surroundings. *Earth-Science Reviews*, 80(1–2), 1–46. <a href="https://doi.org/10.1016/j.earscirev.2006.08.004">https://doi.org/10.1016/j.earscirev.2006.08.004</a>
- Patacca, E., R., S., & Scandone, P. (1990). Tyrrhenian Basin and Apenninic Arcs: Kinematic relations since late Tortonian times. *Mem. Soc. Geol. It.*, *45*, 425–451.
- Patacca, E., & Scandone, P. (2001). Late thrust propagation and sedimentary response in the thrust-belt—Foredeep system of the Southern Apennines (Pliocene-Pleistocene). In G. B. Vai & I. P. Martini (Eds.), *Anatomy of an Orogen: The Apennines and Adjacent Mediterranean Basins* (pp. 401–440). Springer Netherlands. https://doi.org/10.1007/978-94-015-9829-3 23
- Patacca, E., & Scandone, P. (2007). Geological interpretation of the CROP-04 seismic line (Southern Apennines, Italy). *Boll.Soc.Geol.It.* (Ital.J.Geosci.), 7, 297–315.
- Pauselli, C., Barchi, M. R., Federico, C., Magnani, M. B., & Minelli, G. (2006). The crustal structure of the northern apennines (Central Italy): An insight by the crop03 seismic line. *American Journal of Science*, 306(6), 428–450. https://doi.org/10.2475/06.2006.02
- Pauselli, C., Gola, G., Mancinelli, P., Trumpy, E., Saccone, M., Manzella, A., & Ranalli, G. (2019). A new surface heat flow map of the Northern Apennines between latitudes 42.5 and 44.5 N. *Geothermics*, 81, 39–52. <a href="https://doi.org/10.1016/j.geothermics.2019.04.002">https://doi.org/10.1016/j.geothermics.2019.04.002</a>
- Peccerillo, A. (2005). *Plio-Quaternary volcanism in Italy: Petrology, geochemistry, geodynamics*. Springer.
- Peccerillo, A. (2017). *Cenozoic Volcanism in the Tyrrhenian Sea Region*. Springer International Publishing. <a href="https://doi.org/10.1007/978-3-319-42491-0">https://doi.org/10.1007/978-3-319-42491-0</a>
- Pedreira, D., Afonso, J. C., Pulgar, J. A., Gallastegui, J., Carballo, A., Fernàndez, M., Garcia-Castellanos, D., Jiménez-Munt, I., Semprich, J., & García-Moreno, O. (2015). Geophysical-petrological modeling of the lithosphere beneath the Cantabrian Mountains and the North-Iberian margin: Geodynamic implications. *Lithos*, *230*, 46–68. https://doi.org/10.1016/j.lithos.2015.04.018
- Pekeris, C. L. (1935). Thermal Convection in the Interior of the Earth. *Geophysical Supplements to the Monthly Notices of the Royal Astronomical Society*, *3*(8), 343–367. https://doi.org/10.1111/j.1365-246X.1935.tb01742.x

- Petricca, P., Carafa, M. M. C., Barba, S., & Carminati, E. (2013). Local, regional, and plate scale sources for the stress field in the Adriatic and Periadriatic region. *Marine and Petroleum Geology*, 42, 160–181. <a href="https://doi.org/10.1016/j.marpetgeo.2012.08.005">https://doi.org/10.1016/j.marpetgeo.2012.08.005</a>
- Piana Agostinetti, N., & Amato, A. (2009). Moho depth and Vp/Vs ratio in peninsular Italy from teleseismic receiver functions. *Journal of Geophysical Research: Solid Earth*, 114(B6). https://doi.org/10.1029/2008JB005899
- Piana Agostinetti, N., Bianchi, I., Amato, A., & Chiarabba, C. (2011). Fluid migration in continental subduction: The Northern Apennines case study. *Earth and Planetary Science Letters*, *302*(3), 267–278. https://doi.org/10.1016/j.epsl.2010.10.039
- Piana Agostinetti, N., & Faccenna, C. (2018). Deep Structure of Northern Apennines Subduction Orogen (Italy) as Revealed by a Joint Interpretation of Passive and Active Seismic Data. *Geophysical Research Letters*, *45*(9), 4017–4024. <a href="https://doi.org/10.1029/2018GL077640">https://doi.org/10.1029/2018GL077640</a>
- Piana Agostinetti, N., Park, J., & Lucente, F. P. (2008). Mantle wedge anisotropy in Southern Tyrrhenian Subduction Zone (Italy), from receiver function analysis. *Tectonophysics*, *462*(1–4), 35–48. <a href="https://doi.org/10.1016/j.tecto.2008.03.020">https://doi.org/10.1016/j.tecto.2008.03.020</a>
- Pierantoni, P. P., Penza, G., Macchiavelli, C., Schettino, A., & Turco, E. (2020). Kinematics of the Tyrrhenian-Apennine system and implications for the origin of the Campanian magmatism. In *Vesuvius, Campi Flegrei, and Campanian Volcanism* (pp. 33–56). Elsevier. https://doi.org/10.1016/B978-0-12-816454-9.00003-1
- Piromallo, C., & Morelli, A. (2003). P wave tomography of the mantle under the Alpine-Mediterranean area. *Journal of Geophysical Research: Solid Earth*, 108(B2). https://doi.org/10.1029/2002JB001757
- Placer, L., Vrabec, M., & Celarc, B. (2010). The bases for understanding of the NW Dinarides and Istria Peninsula tectonics. *Geologija*, 53(1), 55–86. <a href="https://doi.org/10.5474/geologija.2010.005">https://doi.org/10.5474/geologija.2010.005</a>
- Plomerová, J., & Babuška, V. (2010). Long memory of mantle lithosphere fabric— European LAB constrained from seismic anisotropy. *Lithos*, *120*(1), 131–143. https://doi.org/10.1016/j.lithos.2010.01.008
- Pontevivo, A. (2003). Surface-wave tomography and non-linear inversion in Italy and surrounding areas. University of Trieste.

- Pontevivo, A., & Panza, G. F. (2002). Group velocity tomography and regionalization in Italy and bordering areas. *Physics of the Earth and Planetary Interiors*, *134*(1), 1–15. https://doi.org/10.1016/S0031-9201(02)00079-1
- Prada, M., Ranero, C. R., Sallarès, V., Zitellini, N., & Grevemeyer, I. (2016). Mantle exhumation and sequence of magmatic events in the Magnaghi–Vavilov Basin (Central Tyrrhenian, Italy): New constraints from geological and geophysical observations. Tectonophysics, 689, 133–142. https://doi.org/10.1016/j.tecto.2016.01.041
- Prada, M., Sallares, V., Ranero, C. R., Vendrell, M. G., Grevemeyer, I., Zitellini, N., & de Franco, R. (2014). Seismic structure of the Central Tyrrhenian basin: Geophysical constraints on the nature of the main crustal domains. *Journal of Geophysical Research: Solid Earth*, 119(1), 52–70. https://doi.org/10.1002/2013JB010527
- Prada, M., Sallares, V., Ranero, C. R., Vendrell, M. G., Grevemeyer, I., Zitellini, N., & de Franco, R. (2015). The complex 3-D transition from continental crust to backarc magmatism and exhumed mantle in the Central Tyrrhenian basin. *Geophysical Journal International*, 203(1), 63–78. https://doi.org/10.1093/gji/ggv271
- Presti, D., Totaro, C., Neri, G., & Orecchio, B. (2019). New Earthquake Data in the Calabrian Subduction Zone, Italy, Suggest Revision of the Presumed Dynamics in the Upper Part of the Subducting Slab. *Seismological Research Letters*, *90*(5), 1994–2004. https://doi.org/10.1785/0220190024
- Rappisi, F., VanderBeek, B. P., Faccenda, M., Morelli, A., & Molinari, I. (2022). Slab Geometry and Upper Mantle Flow Patterns in the Central Mediterranean From 3D Anisotropic P-Wave Tomography. *Journal of Geophysical Research: Solid Earth*, 127(5), e2021JB023488. <a href="https://doi.org/10.1029/2021JB023488">https://doi.org/10.1029/2021JB023488</a>
- Ravikumar, M., Singh, B., Pavan Kumar, V., Satyakumar, A. V., Ramesh, D. S., & Tiwari, V. M. (2020). Lithospheric Density Structure and Effective Elastic Thickness Beneath Himalaya and Tibetan Plateau: Inference From the Integrated Analysis of Gravity, Geoid, and Topographic Data Incorporating Seismic Constraints. Tectonics, 39(10), e2020TC006219. https://doi.org/10.1029/2020TC006219
- Robertson, A., Karamata, S., & Šarić, K. (2009). Overview of ophiolites and related units in the Late Palaeozoic–Early Cenozoic magmatic and tectonic development of Tethys in the northern part of the Balkan region. *Lithos*, *108*(1), 1–36. <a href="https://doi.org/10.1016/j.lithos.2008.09.007">https://doi.org/10.1016/j.lithos.2008.09.007</a>

- Romagny, A., Jolivet, L., Menant, A., Bessière, E., Maillard, A., Canva, A., Gorini, C., & Augier, R. (2020). Detailed tectonic reconstructions of the Western Mediterranean region for the last 35 Ma, insights on driving mechanisms. *Bulletin de La Société Géologique de France*, 191(1), 37. <a href="https://doi.org/10.1051/bsgf/2020040">https://doi.org/10.1051/bsgf/2020040</a>
- Rosenbaum, G., Gasparon, M., Lucente, F. P., Peccerillo, A., & Miller, M. S. (2008). Kinematics of slab tear faults during subduction segmentation and implications for Italian magmatism: KINEMATICS OF SLAB TEAR FAULTS. *Tectonics*, 27(2), n/a-n/a. https://doi.org/10.1029/2007TC002143
- Rossetti, F., Faccenna, C., Jolivet, L., Funiciello, R., Tecce, F., & Brunet, C. (1999). Synversus post-orogenic extension: The case study of Giglio Island (Northern Tyrrhenian Sea, Italy). *Tectonophysics*, 304(1), 71–93. <a href="https://doi.org/10.1016/S0040-1951(98)00304-7">https://doi.org/10.1016/S0040-1951(98)00304-7</a>
- Royden, L. H. (1993). The tectonic expression slab pull at continental convergent boundaries. *Tectonics*, *12*(2), 303–325. <a href="https://doi.org/10.1029/92TC02248">https://doi.org/10.1029/92TC02248</a>
- Sandiford, M. (2007). The tilting continent: A new constraint on the dynamic topographic field from Australia. *Earth and Planetary Science Letters*, 261(1), 152–163. <a href="https://doi.org/10.1016/j.epsl.2007.06.023">https://doi.org/10.1016/j.epsl.2007.06.023</a>
- Sandwell, D. T., Müller, R. D., Smith, W. H. F., Garcia, E., & Francis, R. (2014). New global marine gravity model from CryoSat-2 and Jason-1 reveals buried tectonic structure. *Science*, 346(6205), 65–67. https://doi.org/10.1126/science.1258213
- Sani, C., Sanfilippo, A., Peyve, A. A., Genske, F., & Stracke, A. (2023). Earth Mantle's Isotopic Record of Progressive Chemical Depletion. *AGU Advances*, *4*(2), e2022AV000792. https://doi.org/10.1029/2022AV000792
- Sani, F., Bonini, M., Montanari, D., Moratti, G., Corti, G., & Ventisette, C. D. (2016). The structural evolution of the Radicondoli–Volterra Basin (southern Tuscany, Italy): Relationships with magmatism and geothermal implications. *Geothermics*, *59*, 38–55. <a href="https://doi.org/10.1016/j.geothermics.2015.10.008">https://doi.org/10.1016/j.geothermics.2015.10.008</a>
- Sartori, R. (1990). The main results of ODP Leg 107 in the frame of Neogene to Recent geology of peri Tyrrhenian areas. *Proc., Scientific Results, ODP, Leg 107, Tyrrhenian Sea*, 715–730. https://doi.org/10.2973/odp.proc.sr.107.183.1990
- Sartori, R., Carrara, G., Torelli, L., & Zitellini, N. (2001). Neogene evolution of the southwestern Tyrrhenian Sea (Sardinia Basin and western Bathyal plain). *Marine Geology*, 175(1), 47–66. https://doi.org/10.1016/S0025-3227(01)00116-5

- Sartori, R., Torelli, L., Zitellini, N., Carrara, G., Magaldi, M., & Mussoni, P. (2004). Crustal features along a W–E Tyrrhenian transect from Sardinia to Campania margins (Central Mediterranean). *Tectonophysics*, 383(3), 171–192. <a href="https://doi.org/10.1016/j.tecto.2004.02.008">https://doi.org/10.1016/j.tecto.2004.02.008</a>
- Savastano, L., & Piana Agostinetti, N. (2019). Deep structure of the Southern Apennines as imaged by active and passive seismic data along the CROP-04 (crustal) reflection seismic profile. *Journal of the Geological Society*, *176*(6), 1284–1290. https://doi.org/10.1144/jgs2018-201
- Scarfì, L., Barberi, G., Barreca, G., Cannavò, F., Koulakov, I., & Patanè, D. (2018). Slab narrowing in the Central Mediterranean: The Calabro-Ionian subduction zone as imaged by high resolution seismic tomography. *Scientific Reports*, 8(1), Article 1. <a href="https://doi.org/10.1038/s41598-018-23543-8">https://doi.org/10.1038/s41598-018-23543-8</a>
- Schefer, S., Egli, D., Missoni, S., Bernoulli, D., Fügenschuh, B., Gawlick, H.-J., Jovanović, D., Krystyn, L., Lein, R., Schmid, S., & Sudar, M. (2010). Triassic metasediments in the internal Dinarides (Kopaonik area, southern Serbia): Stratigraphy, paleogeographic and tectonic significance. *Geologica Carpathica*, *61*(2), 89–109. https://doi.org/10.2478/v10096-010-0003-6
- Schmid, S. M., Bernoulli, D., Fügenschuh, B., Matenco, L., Schefer, S., Schuster, R., Tischler, M., & Ustaszewski, K. (2008). The Alpine-Carpathian-Dinaridic orogenic system: Correlation and evolution of tectonic units. *Swiss Journal of Geosciences*, 101(1), Article 1. <a href="https://doi.org/10.1007/s00015-008-1247-3">https://doi.org/10.1007/s00015-008-1247-3</a>
- Schmid, S. M., Fügenschuh, B., Kissling, E., & Schuster, R. (2004). Tectonic map and overall architecture of the Alpine orogen. *Eclogae Geologicae Helvetiae*, 97(1), Article 1. https://doi.org/10.1007/s00015-004-1113-x
- Schmid, S. M., Fügenschuh, B., Kounov, A., Maţenco, L., Nievergelt, P., Oberhänsli, R., Pleuger, J., Schefer, S., Schuster, R., Tomljenović, B., Ustaszewski, K., & van Hinsbergen, D. J. J. (2020). Tectonic units of the Alpine collision zone between Eastern Alps and western Turkey. *Gondwana Research*, 78, 308–374. <a href="https://doi.org/10.1016/j.gr.2019.07.005">https://doi.org/10.1016/j.gr.2019.07.005</a>
- Scrocca, D. (2006). Thrust front segmentation induced by differential slab retreat in the Apennines (Italy). *Terra Nova*, *18*(2), 154–161. <a href="https://doi.org/10.1111/j.1365-3121.2006.00675.x">https://doi.org/10.1111/j.1365-3121.2006.00675.x</a>

- Scrocca, D. (2010). Southern Apennines: Structural setting and tectonic evolution. *Journal of the Virtual Explorer*, 36. <a href="https://doi.org/10.3809/jvirtex.2010.00225">https://doi.org/10.3809/jvirtex.2010.00225</a>
- Scrocca, D., Doglioni, C., Innocenti, F., Manetti, P., MAZZOTTI, A., Bertelli, L., Burbi, L., & D'offizi, S. (2003). *CROP Atlas—Seismic Reflection Profiles of the Italian Crust*. Ist. Poligrafico e Zecca dello Stato.
- Seghedi, I., & Downes, H. (2011). Geochemistry and tectonic development of Cenozoic magmatism in the Carpathian–Pannonian region. *Gondwana Research*, 20(4), 655–672. <a href="https://doi.org/10.1016/j.gr.2011.06.009">https://doi.org/10.1016/j.gr.2011.06.009</a>
- Selvaggi, G., & Chiarabba, C. (1995). Seismicity and P-wave velocity image of the Southern Tyrrhenian subduction zone. *Geophysical Journal International*, *121*(3), 818–826. https://doi.org/10.1111/j.1365-246X.1995.tb06441.x
- Serpelloni, E., Bürgmann, R., Anzidei, M., Baldi, P., Mastrolembo Ventura, B., & Boschi, E. (2010). Strain accumulation across the Messina Straits and kinematics of Sicily and Calabria from GPS data and dislocation modeling. *Earth and Planetary Science Letters*, 298(3), 347–360. https://doi.org/10.1016/j.epsl.2010.08.005
- Serpelloni, E., Vannucci, G., Pondrelli, S., Argnani, A., Casula, G., Anzidei, M., Baldi, P., & Gasperini, P. (2007). Kinematics of the Western Africa-Eurasia plate boundary from focal mechanisms and GPS data. *Geophysical Journal International*, *169*(3), 1180–1200. https://doi.org/10.1111/j.1365-246X.2007.03367.x
- Serri, G., Innocenti, F., & Manetti, P. (1993). Geochemical and petrological evidence of the subduction of delaminated Adriatic continental lithosphere in the genesis of the Neogene-Quaternary magmatism of central Italy. *Tectonophysics*, *223*(1), 117–147. https://doi.org/10.1016/0040-1951(93)90161-C
- Shankland, T. J., O'Connell, R. J., & Waff, H. S. (1981). Geophysical constraints on partial melt in the upper mantle. *Reviews of Geophysics*, *19*(3), 394–406. <a href="https://doi.org/10.1029/RG019i003p00394">https://doi.org/10.1029/RG019i003p00394</a>
- Smith, W. H. F., & Sandwell, D. T. (1997). Global Sea Floor Topography from Satellite Altimetry and Ship Depth Soundings. *Science*, 277(5334), 1956–1962. <a href="https://doi.org/10.1126/science.277.5334.1956">https://doi.org/10.1126/science.277.5334.1956</a>
- Spahić, D., & Gaudenyi, T. (2022). On the Sava Suture Zone: Post-Neotethyan oblique subduction and the origin of the Late Cretaceous mini-magma pools. *Cretaceous Research*, *131*, 105062. https://doi.org/10.1016/j.cretres.2021.105062

- Spakman, W., & Wortel, R. (2004). A Tomographic View on Western Mediterranean Geodynamics. In W. Cavazza, F. Roure, W. Spakman, G. M. Stampfli, & P. A. Ziegler (Eds.), The TRANSMED Atlas. The Mediterranean Region from Crust to Mantle: Geological and Geophysical Framework of the Mediterranean and the Surrounding Areas (pp. 31–52). Springer. <a href="https://doi.org/10.1007/978-3-642-18919-7">https://doi.org/10.1007/978-3-642-18919-7</a> 2
- Stampfli, G. M., & Borel, G. D. (2002). A plate tectonic model for the Paleozoic and Mesozoic constrained by dynamic plate boundaries and restored synthetic oceanic isochrons. *Earth and Planetary Science Letters*, 196(1), 17–33. https://doi.org/10.1016/S0012-821X(01)00588-X
- Steckler, M. S., Agostinetti, N. P., Wilson, C. K., Roselli, P., Seeber, L., Amato, A., & Lerner-Lam, A. (2008). Crustal structure in the Southern Apennines from teleseismic receiver functions. *Geology*, *36*(2), 155–158. <a href="https://doi.org/10.1130/G24065A.1">https://doi.org/10.1130/G24065A.1</a>
- Stipčević, J., Herak, M., Molinari, I., Dasović, I., Tkalčić, H., & Gosar, A. (2020). Crustal Thickness Beneath the Dinarides and Surrounding Areas From Receiver Functions. *Tectonics*, *39*(3), e2019TC005872. <a href="https://doi.org/10.1029/2019TC005872">https://doi.org/10.1029/2019TC005872</a>
- Stracke, A. (2021). Composition of Earth's Mantle. In *Encyclopedia of Geology* (pp. 164–177). Elsevier. https://doi.org/10.1016/B978-0-08-102908-4.00043-6
- Styron, R., & Pagani, M. (2020). The GEM Global Active Faults Database. *Earthquake Spectra*, *36*(1 suppl), 160–180. <a href="https://doi.org/10.1177/8755293020944182">https://doi.org/10.1177/8755293020944182</a>
- Šumanovac, F. (2010). Lithosphere structure at the contact of the Adriatic microplate and the Pannonian segment based on the gravity modelling. *Tectonophysics*, *485*(1), 94–106. <a href="https://doi.org/10.1016/j.tecto.2009.12.005">https://doi.org/10.1016/j.tecto.2009.12.005</a>
- Šumanovac, F., & Dudjak, D. (2016). Descending lithosphere slab beneath the Northwest Dinarides from teleseismic tomography. *Journal of Geodynamics*, *102*, 171–184. <a href="https://doi.org/10.1016/j.jog.2016.09.007">https://doi.org/10.1016/j.jog.2016.09.007</a>
- Šumanovac, F., Hegedűs, E., Orešković, J., Kolar, S., Kovács, A. C., Dudjak, D., & Kovács, I. J. (2016). Passive seismic experiment and receiver functions analysis to determine crustal structure at the contact of the northern Dinarides and southwestern Pannonian Basin. *Geophysical Journal International*, 205(3), 1420–1436. https://doi.org/10.1093/gji/ggw101
- Šumanovac, F., Markušić, S., Engelsfeld, T., Jurković, K., & Orešković, J. (2017). Shallow and deep lithosphere slabs beneath the Dinarides from teleseismic tomography as

- the result of the Adriatic lithosphere downwelling. *Tectonophysics*, *712–713*, 523–541. https://doi.org/10.1016/j.tecto.2017.06.018
- Sun, W., Zhao, L., Malusà, M. G., Guillot, S., & Fu, L.-Y. (2019). 3-D Pn tomography reveals continental subduction at the boundaries of the Adriatic microplate in the absence of a precursor oceanic slab. *Earth and Planetary Science Letters*, *510*, 131–141. https://doi.org/10.1016/j.epsl.2019.01.012
- Talwani, M., Worzel, J. L., & Landisman, M. (1959). Rapid gravity computations for two-dimensional bodies with application to the Mendocino submarine fracture zone. *Journal of Geophysical Research (1896-1977)*, 64(1), 49–59. https://doi.org/10.1029/JZ064i001p00049
- Tari, V. (2002). Evolution of the northern and western Dinarides: A tectonostratigraphic approach. *Stephan Mueller Special Publication Series*, 1, 223–236. <a href="https://doi.org/10.5194/smsps-1-223-2002">https://doi.org/10.5194/smsps-1-223-2002</a>
- Tesauro, M., Kaban, M. K., & Cloetingh, S. A. P. L. (2008). EuCRUST-07: A new reference model for the European crust. *Geophysical Research Letters*, *35*(5). https://doi.org/10.1029/2007GL032244
- Tesauro, M., Kaban, M. K., & Cloetingh, S. A. P. L. (2009). A new thermal and rheological model of the European lithosphere. *Tectonophysics*, *476*(3), 478–495. https://doi.org/10.1016/j.tecto.2009.07.022
- Thybo, H., Artemieva, I. M., & Kennett, B. (2013). Moho: 100 years after Andrija Mohorovičić. *Tectonophysics*, 609, 1–8. <a href="https://doi.org/10.1016/j.tecto.2013.10.004">https://doi.org/10.1016/j.tecto.2013.10.004</a>
- Tomljenović, B., Csontos, L., Márton, E., & Márton, P. (2008). Tectonic evolution of the northwestern Internal Dinarides as constrained by structures and rotation of Medvednica Mountains, North Croatia. *Geological Society, London, Special Publications*, 298(1), 145–167. <a href="https://doi.org/10.1144/SP298.8">https://doi.org/10.1144/SP298.8</a>
- Tommasi, A., & Vauchez, A. (2015). Heterogeneity and anisotropy in the lithospheric mantle. *Tectonophysics*, *661*, 11–37. <a href="https://doi.org/10.1016/j.tecto.2015.07.026">https://doi.org/10.1016/j.tecto.2015.07.026</a>
- Trincardi, F., & Zitellini, N. (1987). The rifting of the Tyrrhenian Basin. *Geo-Marine Letters*, 7, 1–6. <a href="https://doi.org/10.1007/BF02310459">https://doi.org/10.1007/BF02310459</a>
- Trumpy, E., & Manzella, A. (2017). Geothopica and the interactive analysis and visualization of the updated Italian National Geothermal Database. *International*

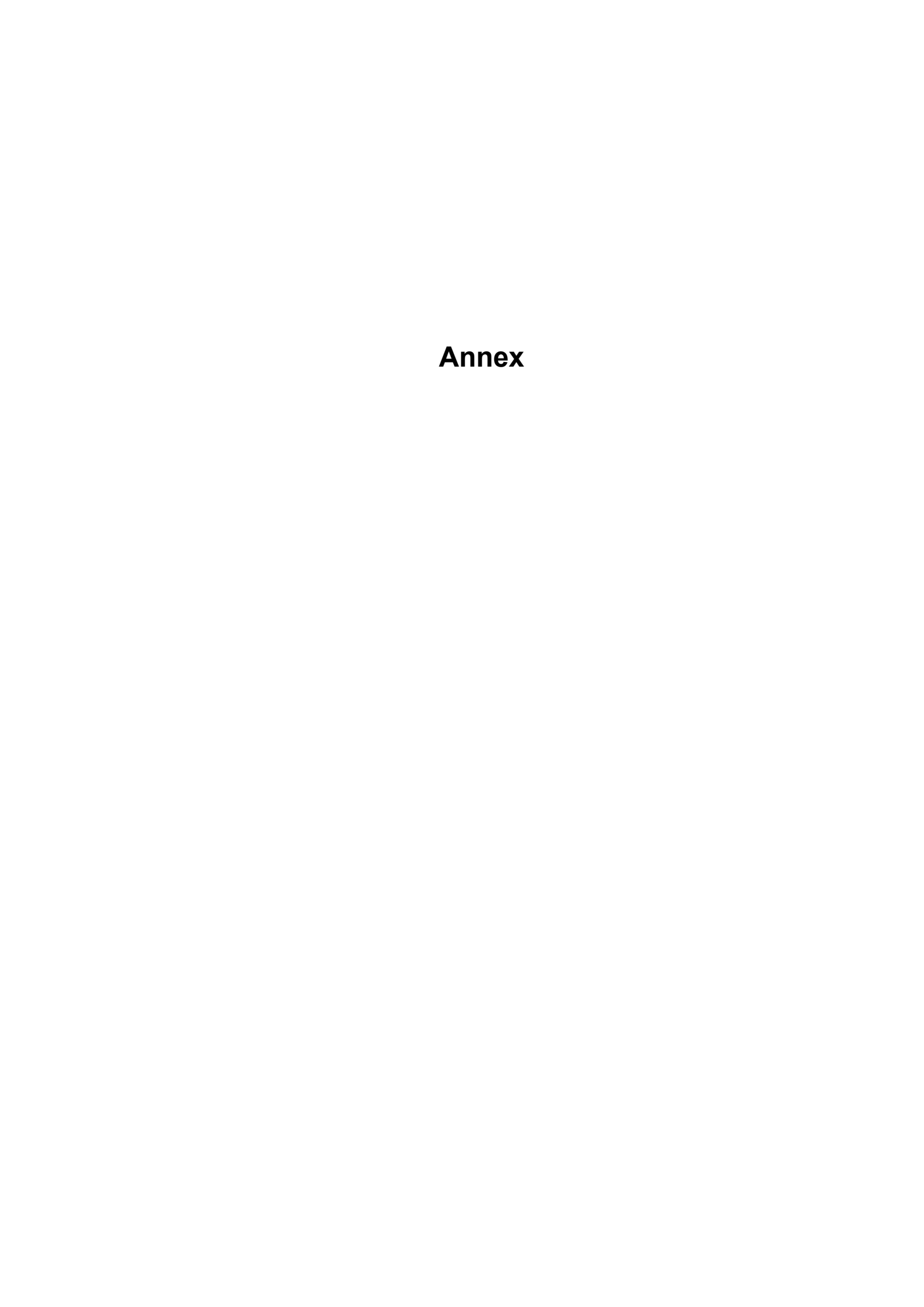
- Journal of Applied Earth Observation and Geoinformation, 54, 28–37. <a href="https://doi.org/10.1016/j.jag.2016.09.004">https://doi.org/10.1016/j.jag.2016.09.004</a>
- Tumanian, M., Frezzotti, M. L., Peccerillo, A., Brandmayr, E., & Panza, G. F. (2012). Thermal structure of the shallow upper mantle beneath Italy and neighbouring areas: Correlation with magmatic activity and geodynamic significance. *Earth-Science Reviews*, 114(3), 369–385. <a href="https://doi.org/10.1016/j.earscirev.2012.07.002">https://doi.org/10.1016/j.earscirev.2012.07.002</a>
- Tunini, L., Jiménez-Munt, I., Fernandez, M., Vergés, J., & Villaseñor, A. (2015). Lithospheric mantle heterogeneities beneath the Zagros Mountains and the Iranian Plateau: A petrological-geophysical study. *Geophysical Journal International*, 200(1), 596–614. <a href="https://doi.org/10.1093/gji/ggu418">https://doi.org/10.1093/gji/ggu418</a>
- Turco, E., Macchiavelli, C., Mazzoli, S., Schettino, A., & Pierantoni, P. P. (2012). Kinematic evolution of Alpine Corsica in the framework of Mediterranean mountain belts. *Tectonophysics*, *579*, 193–206. <a href="https://doi.org/10.1016/j.tecto.2012.05.010">https://doi.org/10.1016/j.tecto.2012.05.010</a>
- Turco, E., Macchiavelli, C., Penza, G., Schettino, A., & Pierantoni, P. P. (2021). Kinematics of Deformable Blocks: Application to the Opening of the Tyrrhenian Basin and the Formation of the Apennine Chain. *Geosciences*, 11(4), Article 4. <a href="https://doi.org/10.3390/geosciences11040177">https://doi.org/10.3390/geosciences11040177</a>
- Turcotte, D. L., & Schubert, G. (2002). *Geodynamics* (2nd ed.). Cambridge University Press. https://doi.org/10.1017/CBO9780511807442
- Turcotte, D., & Schubert, G. (2014). *Geodynamics* (3rd ed.). Cambridge University Press. <a href="https://doi.org/10.1017/CBO9780511843877">https://doi.org/10.1017/CBO9780511843877</a>
- Ustaszewski, K., Kounov, A., Schmid, S. M., Schaltegger, U., Krenn, E., Frank, W., & Fügenschuh, B. (2010). Evolution of the Adria-Europe plate boundary in the northern Dinarides: From continent-continent collision to back-arc extension. *Tectonics*, *29*(6). <a href="https://doi.org/10.1029/2010TC002668">https://doi.org/10.1029/2010TC002668</a>
- van Hinsbergen, D. J. J., Maffione, M., Koornneef, L. M. T., & Guilmette, C. (2019). Kinematic and paleomagnetic restoration of the Semail ophiolite (Oman) reveals subduction initiation along an ancient Neotethyan fracture zone. *Earth and Planetary Science Letters*, *518*, 183–196. https://doi.org/10.1016/j.epsl.2019.04.038
- van Hinsbergen, D. J. J., Torsvik, T. H., Schmid, S. M., Maţenco, L. C., Maffione, M., Vissers, R. L. M., Gürer, D., & Spakman, W. (2020). Orogenic architecture of the Mediterranean region and kinematic reconstruction of its tectonic evolution since the Triassic. *Gondwana Research*, *81*, 79–229. https://doi.org/10.1016/j.gr.2019.07.009

- van Unen, M., Matenco, L., Nader, F. H., Darnault, R., Mandic, O., & Demir, V. (2019). Kinematics of Foreland-Vergent Crustal Accretion: Inferences From the Dinarides Evolution. *Tectonics*, *38*(1), 49–76. <a href="https://doi.org/10.1029/2018TC005066">https://doi.org/10.1029/2018TC005066</a>
- Vannucci, G., Pondrelli, S., Argnani, A., Morelli, A., Gasperini, P., & Boschi, E. (2004). *An Atlas of Mediterranean seismicity*. <a href="https://cris.unibo.it/handle/11585/18668">https://cris.unibo.it/handle/11585/18668</a>
- Verdoya, M., Chiozzi, P., Gola, G., & Jbeily, E. E. (2019). Conductive heat flow pattern of the central-northern Apennines, Italy. *International Journal of Terrestrial Heat Flow and Applied Geothermics*, 2(1), Article 1. <a href="https://doi.org/10.31214/ijthfa.v2i1.33">https://doi.org/10.31214/ijthfa.v2i1.33</a>
- Vergés, J., & Sàbat, F. (1999). Constraints on the Neogene Mediterranean kinematic evolution along a 1000 km transect from Iberia to Africa. *Geological Society, London, Special Publications*, *156*(1), 63–80. https://doi.org/10.1144/GSL.SP.1999.156.01.05
- Vezzani, L., Festa, A., & Ghisetti, F. C. (2010). Geology and Tectonic Evolution of the Central-southern Apennines, Italy. Geological Society of America.
- Vignaroli, G., Faccenna, C., Jolivet, L., Piromallo, C., & Rossetti, F. (2008). Subduction polarity reversal at the junction between the Western Alps and the Northern Apennines, Italy. *Tectonophysics*, *450*(1), 34–50. <a href="https://doi.org/10.1016/j.tecto.2007.12.012">https://doi.org/10.1016/j.tecto.2007.12.012</a>
- Vignaroli, G., Faccenna, C., Rossetti, F., & Jolivet, L. (2009). Insights from the Apennines metamorphic complexes and their bearing on the kinematics evolution of the orogen. *Geological Society, London, Special Publications*, 311(1), 235–256. <a href="https://doi.org/10.1144/SP311.9">https://doi.org/10.1144/SP311.9</a>
- Vilà, M., Fernández, M., & Jiménez-Munt, I. (2010). Radiogenic heat production variability of some common lithological groups and its significance to lithospheric thermal modeling. *Tectonophysics*, 490(3), 152–164. <a href="https://doi.org/10.1016/j.tecto.2010.05.003">https://doi.org/10.1016/j.tecto.2010.05.003</a>
- Wang, Y., Cao, Z., Peng, L., Liu, L., Chen, L., Lundstrom, C., Peng, D., & Yang, X. (2023). Secular craton evolution due to cyclic deformation of underlying dense mantle lithosphere. *Nature Geoscience*, 1–9. <a href="https://doi.org/10.1038/s41561-023-01203-5">https://doi.org/10.1038/s41561-023-01203-5</a>
- Watts, A. (2001). Isostasy and Flexure of the Lithosphere (Vol. 458).
- Workman, R. K., & Hart, S. R. (2005). Major and trace element composition of the depleted MORB mantle (DMM). *Earth and Planetary Science Letters*, 231(1), 53–72. <a href="https://doi.org/10.1016/j.epsl.2004.12.005">https://doi.org/10.1016/j.epsl.2004.12.005</a>

- Wortel, M. J. R., & Spakman, W. (2000). Subduction and Slab Detachment in the Mediterranean-Carpathian Region. *Science*, 290(5498), 1910–1917. <a href="https://doi.org/10.1126/science.290.5498.1910">https://doi.org/10.1126/science.290.5498.1910</a>
- Wrigley, R., Hodgson, N., & Esestime, P. (2015). Petroleum Geology and Hydrocarbon Potential of the Adriatic Basin, Offshore Croatia. *Journal of Petroleum Geology*, *38*(3), 301–316. https://doi.org/10.1111/jpg.12612
- Zailac, K., Matoš, B., Vlahović, I., & Stipčević, J. (2023). Reference seismic crustal model of the Dinarides. *Solid Earth*, *14*(11), 1197–1220. <a href="https://doi.org/10.5194/se-14-1197-2023">https://doi.org/10.5194/se-14-1197-2023</a>
- Zeyen, H., Ayarza, P., Fernàndez, M., & Rimi, A. (2005). Lithospheric structure under the western African-European plate boundary: A transect across the Atlas Mountains and the Gulf of Cadiz. Tectonics, 24(2). <a href="https://doi.org/10.1029/2004TC001639">https://doi.org/10.1029/2004TC001639</a>
- Zhang, W., Jiménez-Munt, I., Torne, M., Vergés, J., Bravo-Gutiérrez, E., Negredo, A. M., Carminati, E., García-Castellanos, D., & Fernàndez, M. (2022). Geophysical-Petrological Model for Bidirectional Mantle Delamination of the Adria Microplate Beneath the Northern Apennines and Dinarides Orogenic Systems. *Journal of Geophysical Research: Solid Earth*, 127(12), e2022JB024800. <a href="https://doi.org/10.1029/2022JB024800">https://doi.org/10.1029/2022JB024800</a>
- Zhang, W., Jiménez-Munt, I., Torne, M., Vergés, J., Bravo-Gutiérrez, E., Negredo, A. M., & García-Castellanos, D. (2024). The Lithosphere and Upper Mantle of the Western-Central Mediterranean Region From Integrated Geophysical-Geochemical Modeling. *Journal of Geophysical Research: Solid Earth*, 129(4), e2023JB028435. https://doi.org/10.1029/2023JB028435
- Zhao, L., Paul, A., Malusà, M. G., Xu, X., Zheng, T., Solarino, S., Guillot, S., Schwartz, S., Dumont, T., Salimbeni, S., Aubert, C., Pondrelli, S., Wang, Q., & Zhu, R. (2016). Continuity of the Alpine slab unraveled by high-resolution P wave tomography. *Journal of Geophysical Research: Solid Earth*, 121(12), 8720–8737. <a href="https://doi.org/10.1002/2016JB013310">https://doi.org/10.1002/2016JB013310</a>
- Zhu, H., Bozdağ, E., & Tromp, J. (2015). Seismic structure of the European upper mantle based on adjoint tomography. *Geophysical Journal International*, 201(1), 18–52. https://doi.org/10.1093/gji/gqu492

## References

Zitellini, N., Ranero, C. R., Loreto, M. F., Ligi, M., Pastore, M., D'Oriano, F., Sallares, V., Grevemeyer, I., Moeller, S., & Prada, M. (2019). Recent inversion of the Tyrrhenian Basin. *Geology*, *48*(2), 123–127. <a href="https://doi.org/10.1130/G46774.1">https://doi.org/10.1130/G46774.1</a>





# **JGR** Solid Earth

## <del>-</del>

### RESEARCH ARTICLE

10.1029/2022JB024800

#### **Key Points:**

- A new thermochemical structure of the crust and uppermost mantle is obtained along the northern Apennines, Dinarides, and Pannonian Basin
- The model distinguishes Adria and Tisza microplates with different crustal structures and lithosphere mantle compositions
- Two mantle wedges occur below the northern Apennines and Dinarides, resulting from the mantle delamination of Adria beneath its margins

#### Correspondence to:

I. Jiménez-Munt, ivone@geo3bcn.csic.es

#### Citation:

Zhang, W., Jiménez-Munt, I., Torne, M., Vergés, J., Bravo-Gutiérrez, E., Negredo, A. M., et al. (2022). Geophysical-petrological model for bidirectional mantle delamination of the Adria microplate beneath the northern Apennines and Dinarides orogenic systems. *Journal of Geophysical Research: Solid Earth*, 127, e2022JB024800. https://doi.org/10.1029/2022JB024800

Received 19 MAY 2022 Accepted 1 DEC 2022

#### **Author Contributions:**

Conceptualization: Ivone Jiménez-Munt, Montserrat Torne, Jaume Vergés, Manel Fernàndez

Formal analysis: Wentao Zhang, Estefanía Bravo-Gutiérrez Funding acquisition: Ivone Jiménez-Munt, Daniel García-Castellanos Investigation: Wentao Zhang, Ivone Jiménez-Munt, Montserrat Torne, Jaume Vergés, Ana M. Negredo Methodology: Ivone Jiménez-Munt

Software: Ivone Jiménez-Munt

## © 2022 The Authors.

This is an open access article under the terms of the Creative Commons Attribution-NonCommercial License, which permits use, distribution and reproduction in any medium, provided the original work is properly cited and is not used for commercial purposes.

## Geophysical-Petrological Model for Bidirectional Mantle Delamination of the Adria Microplate Beneath the Northern Apennines and Dinarides Orogenic Systems

Wentao Zhang<sup>1,2</sup> , Ivone Jiménez-Munt<sup>1</sup> , Montserrat Torne<sup>1</sup> , Jaume Vergés<sup>1</sup> , Estefanía Bravo-Gutiérrez<sup>1</sup> , Ana M. Negredo<sup>3,4</sup> , Eugenio Carminati<sup>5</sup> , Daniel García-Castellanos<sup>1</sup> , and Manel Fernàndez<sup>1</sup>

<sup>1</sup>Geosciences Barcelona, Geo3BCN-CSIC, Barcelona, Spain, <sup>2</sup>Department of Earth and Ocean Dynamics, University of Barcelona, Barcelona, Spain, <sup>3</sup>Departmento de Física de la Tierra y Astrofísica, Universidad Complutense de Madrid, Madrid, Spain, <sup>4</sup>Instituto de Geociencias, IGEO-(CSIC, UCM), Madrid, Spain, <sup>5</sup>Dipartimento di Scienze della Terra, Sapienza Università di Roma, Roma, Italy

**Abstract** This study presents a geophysical-geochemical integrated model of the thermochemical structure of the lithosphere and uppermost mantle along a transect from the Northern Tyrrhenian Sea to the Pannonian Basin, crossing the northern Apennines, the Adriatic Sea, and the Dinarides fold-thrust belt. The objectives are to image crustal thickness variations and characterize the different mantle domains. In addition, we evaluate the topographic response of opposed subductions along this transect and discuss their implications in the evolution of the region. Results show a more complex structure and slightly higher average crustal density of Adria compared to Tisza microplate. Below the Tyrrhenian Sea and Western Apennines, Moho lays at <25 km depth while along the Eastern Apennines it is as deep as 55 km. The modeled lithosphere-asthenosphere boundary (LAB) below the Tyrrhenian Sea and Pannonian Basin is flat lying at ~75 and 90 km, respectively. Below the External Apennines and Dinarides the LAB deepens to 150 km, slightly shallowing toward the Adriatic foreland basin at 125 km depth. Our results are consistent with the presence of two mantle wedges, resulting from the rollback of the Ligurian-Tethys and Vardar-NeoTethys oceanic slabs followed by continental mantle delamination of the eastern and western distal margins of Adria. These two opposed slabs beneath the Apennines and Dinarides are modeled as two thermal sublithospheric anomalies of -200°C. Most of the elevation along the profile is under thermal isostasy and departures can be explained by regional isostasy with an elastic thickness between 10 and 20 km.

Plain Language Summary This study integrates a wide range of geological and geophysical observations (e.g., elevation, gravity, geoid, seismic tomography) to investigate the density and temperature variations down to 400 km along a transect that extends from the Tyrrhenian Sea and northern Apennines in Italy to the Dinarides and Pannonian Basin in southern Europe. The main objectives are to study the present-day structure and composition of the lithosphere and uppermost mantle, and to evaluate the resulting topography, and finally to discuss their implications in the tectonic evolution of the region. Our results show that the crust and the base of the lithosphere vary significantly in the study region, lying shallow below the basins to much deeper underneath the mountain belts where topography is higher. We also observe two cold and dense zones sitting in the distal margins of the Adria microplate, beneath the northern Apennines and Dinarides, that are interpreted as two opposed subducting slabs that have largely controlled the geodynamic evolution of the study region in the last 30 My.

## 1. Introduction

The N-S convergence between the African and Eurasian plates since the Late Cretaceous is recognized as the primary causal mechanism for the squeezing of intervening microplates, bounded by narrow branches of the Neo-Tethys Ocean (e.g., Dewey et al., 1989). In particular, it drove to the development of subduction and collision orogens in the Central-Western Mediterranean region, which is a part of the active Alpine-Mediterranean mobile belt. The Adria microplate plays a key role in this geodynamic puzzle since Jurassic times, when the Vardar ophiolitic obduction started, followed by continental collisions with the Tisza microplate and Eurasian plate (Schmid et al., 2020). Subsequently, the NW-SE trending Dinarides orogenic belt developed along the NE margin of Adria whereas the NW-SE trending Apennines fold-thrust belt evolved in its SW margin. The Adria-Eurasia

ZHANG ET AL. 1 of 24

Supervision: Ivone Jiménez-Munt, Montserrat Torne Writing – original draft: Wentao Zhang Writing – review & editing: Ivone Jiménez-Munt, Montserrat Torne, Jaume Vergés, Estefanía Bravo-Gutiérrez, Ana

M. Negredo, Eugenio Carminati, Daniel

García-Castellanos, Manel Fernàndez

convergence also produced the almost 1,000 km long ENE-WSW trending Alps orogenic belt (Figure 1) (e.g., Dewey et al., 1989; Handy et al., 2010; Stampfli & Borel, 2002).

The Western-Central Mediterranean region is a challenging area characterized by structural heterogeneity and tectonic complexity (e.g., Carminati et al., 2020; van Hinsbergen et al., 2020). The region has experienced a wide diversity of geodynamic processes, which include pre-orogenic rifting and oceanization, subduction and extinction of the Tethys oceanic lithosphere, counterclockwise rotation of the Adria microplate, back-arc spreading of the Tyrrhenian Sea and Pannonian Basin, and final continental collision and rapid uplift in the Apennines, Dinarides, Alps, and Carpathians (e.g., Carminati et al., 2012, 2020; Handy et al., 2015; Schmid et al., 2020; van Hinsbergen et al., 2019, 2020). All these deep geodynamic processes have a direct effect on the topography of the orogenic belts, producing the so-called dynamic topography (e.g., Faccenna et al., 2014; Kumar et al., 2021).

The structure and evolution of the Adria microplate is clearly described after decades of careful studies of its geology and geophysics. These studies reconstructed its crustal orogenic fold-belt structure and its upper mantle structure in three dimensions, interpreted as the result of subducted lithospheric slabs displaying abrupt changes in subduction polarity across transfer fault zones (e.g., Rosenbaum et al., 2008; Vignaroli et al., 2008). However, despite the wealth of data and research published about the study region (e.g., Artemieva & Thybo, 2013; Carminati & Doglioni, 2012; Kapuralić et al., 2019; Kästle et al., 2020), the current crustal and lithospheric structure and the topographic implications of the lithospheric anomalies are still under debate. Results on Moho depth show differences between deep seismic refraction profiles and receiver function (RF) results (Barchi et al., 2006; Finetti et al., 2001; Piana Agostinetti and Faccenna, 2018). Moreover, some tomographic models suggest that the Adriatic slab beneath the Apennines may be found nearby the mantle transition zone at  $\sim 300-400$  km depth (e.g., Giacomuzzi et al., 2011; Hua et al., 2017; Zhao et al., 2016), while others suggest that the slab terminates at much shallower depths (~250 km; e.g., Lippitsch et al., 2003). Additionally, there are also discrepancies on the lithosphere-asthenosphere boundary (LAB) between seismic anisotropy models (Plomerová & Babuška, 2010), RFs (Belinić et al., 2018), thermal isostasy analyses (Artemieva, 2019) and on the origin of the highly variable topography. Recently, numerous geophysical surveys have investigated into the lesser-known composition and structure of the lithospheric mantle (e.g., Belinić et al., 2021; Blom et al., 2020; El-Sharkawy et al., 2020; Kästle et al., 2020). The surveys have elucidated the geometry of subducted slabs beneath the northern Apennines and Dinarides although the results vary significantly depending on the methodology used.

The prerequisite for a good understanding of the geodynamic evolution of the Western-Central Mediterranean region is to reconcile the observations obtained from different data sets and methods. The main aim of this study is to derive the present-day crust and upper mantle structure (down to 400 km depth) along a ~1,000 km transect, crossing in a SW-NE direction the Tyrrhenian Sea, the northern Apennines, the Adriatic Sea, the Dinarides and the Pannonian Basin (Figure 2a). The transect is sufficiently far from the potential influence of the subducted Alpine slab to allow straightforward interpretation of mantle seismic anomalies in terms of Apennines and Dinarides slabs. To determine the lithospheric structure along the transect we applied an integrated geophysical-petrological modeling tool, which combines surface heat flow (SHF), Bouguer anomaly, geoid height, elevation and petrological data to produce the thermal, density, and seismic velocity structure of the crust and upper mantle as described in Kumar et al. (2020). A similar approach has been used to study the deep structure of the Gibraltar Arc region (Jiménez-Munt et al., 2019) and along the Algerian and Alboran basins of the Western Mediterranean (Kumar et al., 2021). Both studies demonstrated that the pull force of hanging lithospheric slabs is markedly different if the slab is still attached to the continental lithosphere or is detached after break-off processes. They also permitted to determine the up-down direction, amount and extent of the dynamic topography linked to the sub-lithospheric forces as well as its impact at the surface.

The crustal and lithospheric structures obtained in this study are compared with previous interpretations and discussed in terms of the geodynamic evolution of studied tectonic domains within the complex and long-term evolving Alpine-Mediterranean mobile belt. Lastly, the contribution of deep geodynamic processes in the build-up of present orogenic topographic relief is discussed.

ZHANG ET AL. 2 of 24

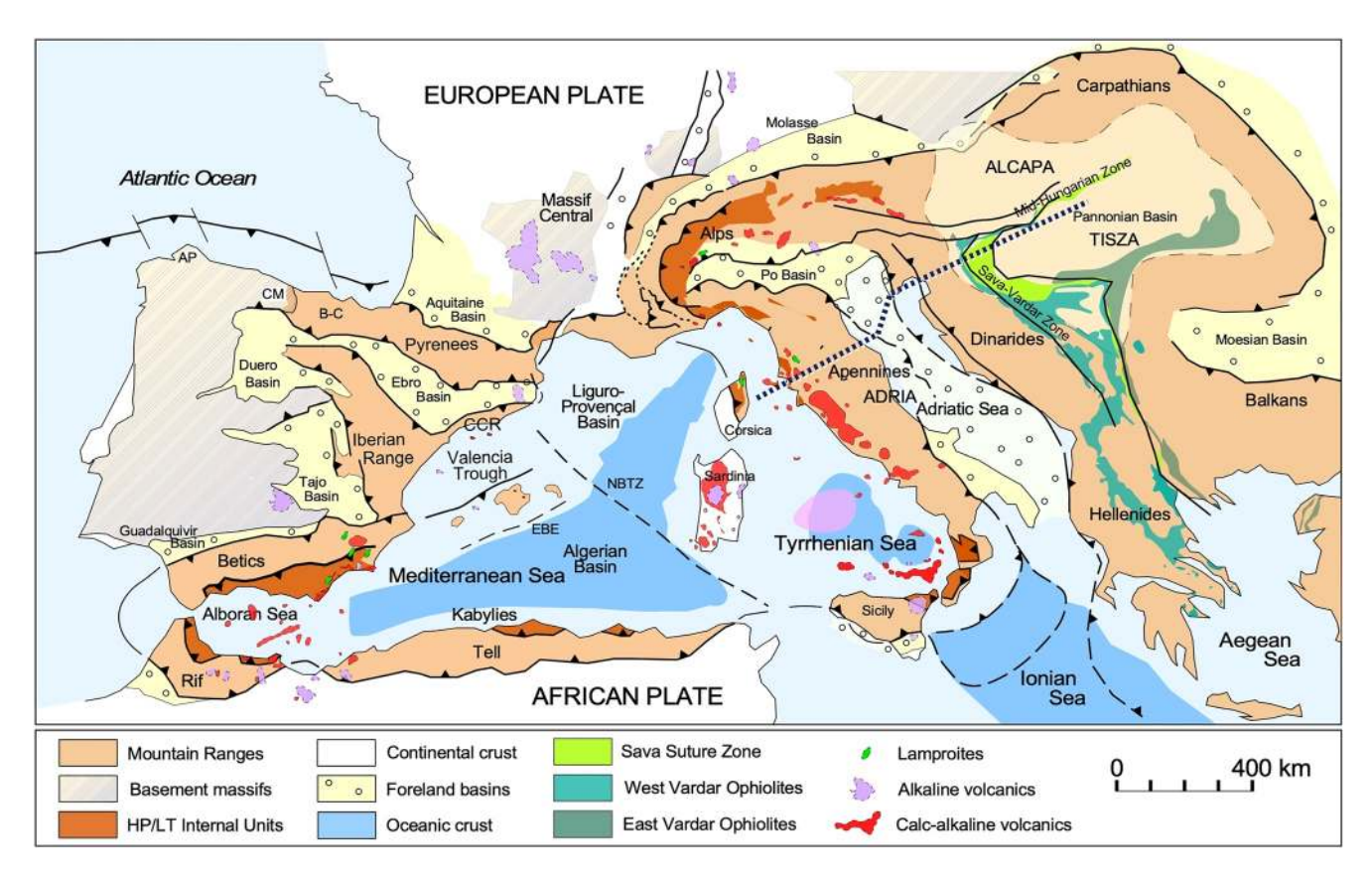


Figure 1. Tectonic map of the Western-Central Mediterranean region with the main orogenic belts and foreland basins.

### 2. Geological Setting

The Western-Central Alpine Mediterranean orogenic system is the result of the interplay between Eurasian plate and the Adria and Tisza microplates (originally separated by Vardar oceanic domain, a northern branch of the Neo-Tethys) in the framework of the Africa-Eurasia convergence. At upper crustal levels, the main tectonic domains that evolved on the Adria microplate are, from west to east, the NE-directed Apennines and the SW-directed Dinarides orogens with their common foreland basin along the entire Adriatic Sea. The Apennines mainly developed during the W- to SW-dipping subduction of the Alpine Tethys oceanic domain (that separated Adria microplate from Eurasian plate) and the following subduction of the Adria thinned margin (Doglioni, 1991; Faccenna et al., 2001; Molli, 2008), that drove to the deformation of cover rocks of the SW margin of Adria. The eastward retreat of the subducting-plate hinge generated the ENE-directed Apennines orogenic system and the development of a complex back-arc basin system (e.g., Doglioni et al., 1997; Lacombe & Jolivet, 2005; Le Breton et al., 2017; Malinverno & Ryan, 1986; Patacca et al., 1990; Romagny et al., 2020; Royden, 1993). The Corsica-Sardinia lithosphere was drifted from the southern Europe continental margin (Doglioni et al., 1997; Romagny et al., 2020), and it is located between the Liguro-Provencal and Tyrrhenian back-arc basins. The Dinarides lie along the deformed NE margin of Adria and have a longer and more complex history that includes subduction of the Vardar Ocean basin. This long-term subduction produced a first late Jurassic obduction of oceanic lithosphere and a later continental collision between Adria and Tisza microplates (Channell et al., 1996; Schmid et al., 2020), presently forming the thinned crust flooring the northern region of the Pannonian Basin along the easternmost segment of the transect. The Tisza crustal domain is welded to the Eurasian plate (Figure 1).

The Apennines orogenic system is characterized by two tectonic domains; the Internal (western) Apennines including the Ligurian-Tuscan-Tyrrhenian regions toward the WSW and the External (eastern) Apennines comprising the Apennines fold-thrust belt and the Adriatic foreland basin toward the ENE (e.g., Barchi et al., 1998, 2003; Cosentino et al., 2010; Molli, 2008; Scrocca, 2006). Evidence for oceanic and continental subduction is provided by metaophiolites and metasedimentary rocks of the Adria passive margin with late Cenozoic HP-LT metamorphism

ZHANG ET AL. 3 of 24

1 from https://agupubs.onlinelibrary.wiley.com/doi/10.1029/2022/B024800 by Csic Organización Central Om (Oficialia Mayor) (Urici), Wiley Online Library on [13/12/2022]. See the Terms

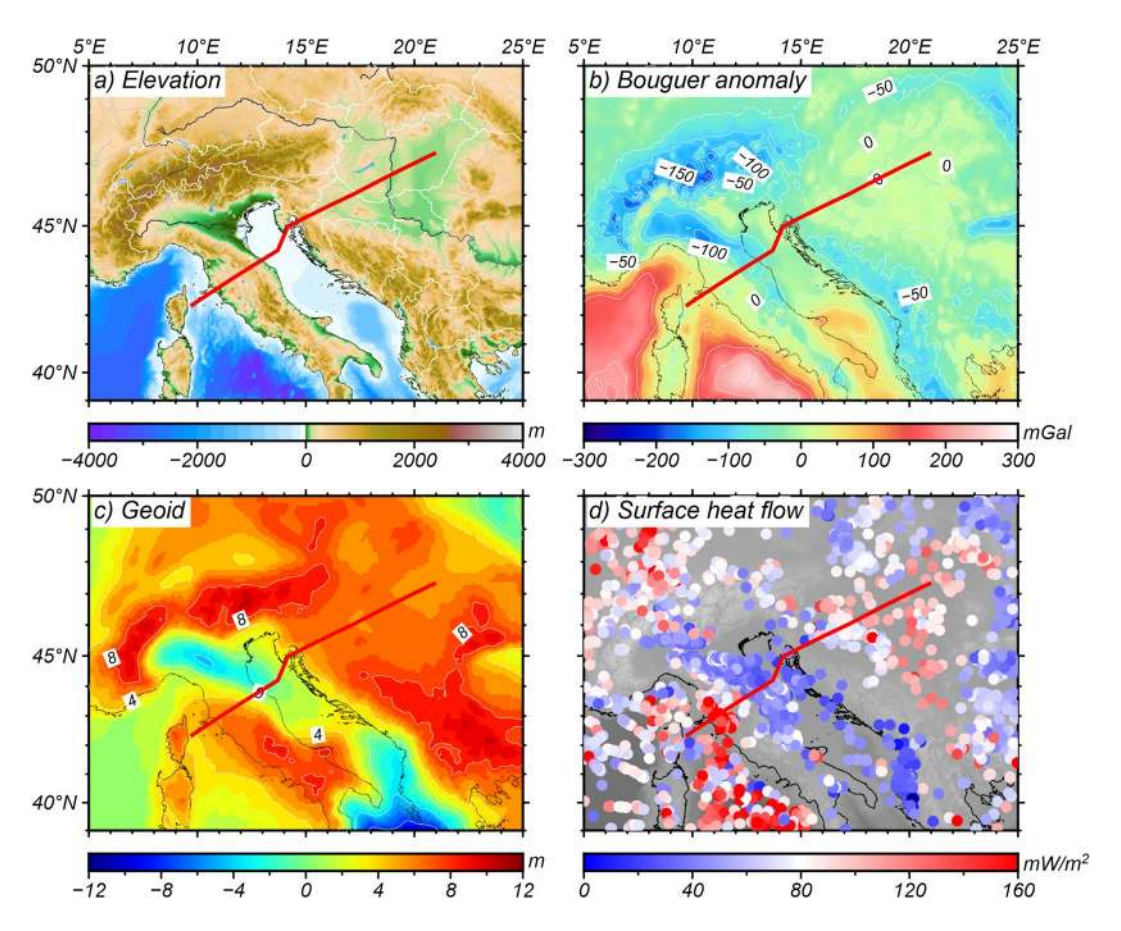


**Figure 2.** (a) Elevation data come from topo\_19.1.img (Smith & Sandwell, 1997, updated 2019). Major flat areas characterized the Pannonian Basin and the northern Adriatic Sea, which contrasts with the relief of the Dinarides and Apennines mountain belts. (b) Bouguer gravity anomaly has been obtained applying the complete Bouguer correction to the free air gravity anomaly data (Sandwell et al., 2014, updated 2019) using the software FA2BOUG (Fullea et al., 2008) with a density reduction of 2,670 kg/m³. Areas with high relief show gravity lows, while the basins are characterized by relative gravity highs. Note that most of the Pannonian Basin has near-zero Bouguer gravity values. A strongest positive Bouguer anomaly of 200–300 mGal marks the abyssal areas of the Tyrrhenian sea, whereas the Adriatic Sea show values between 0 and 60 mGal. (c) Geoid height data were derived from the global gravitational model GECO (Gilardoni et al., 2016), filtered up to degree and order 10. For most of the region, the geoid shows positive values, except for the Po plain and southern Adriatic Sea. The Alps, Apennines and southern Dinarides are characterized by relative highs (locally up to 10 m). (d) Surface heat flow data from the Global Heat Flow Database (Fuchs & Norden, 2021) and completed with the Italian National Geothermal Database (Pauselli et al., 2019; Trumpy & Manzella, 2017). Highest values above 120 mW/m² are observed in the Tyrrhenian Sea and Tuscan domain while the Adriatic Sea and Dinarides record lower values (40–50 mW/m²). In the Pannonian Basin, average heat flow ranges from 80 to 100 mW/m².

cropping out in the northern Tyrrhenian islands and in the Tuscan region (Bianco et al., 2015; Rossetti et al., 1999; Vignaroli et al., 2009). The Northern Tyrrhenian Basin as well as the Ligurian-Tuscan domains are characterized by thin stretched continental crust (e.g., Jolivet et al., 1998; Moeller et al., 2013, 2014; Sartori et al., 2004) modified by extensive volcanism and intruded by large magmatic bodies (e.g., Dini et al., 2005; Rocchi et al., 2010; Serri et al., 1993). This igneous activity features a large range of compositions, from subalkaline to ultra-alkaline and from ultrabasic to acid (Lustrino et al., 2022). The Tyrrhenian Basin began to open during the Tortonian (e.g., Keller & Coward, 1996; Keller et al., 1994; Sartori et al., 2004; Trincardi & Zitellini, 1987), and extension overprinted and partially re-used the compressional structures, as observed also in the axial/eastern sector of the Apennines fold-thrust belt (e.g., Barchi et al., 2021; Bonini & Sani, 2002; Collettini & Barchi, 2002; Curzi et al., 2020; Keller et al., 1994).

The Apennines fold-thrust belt and its undeformed foreland display a complex ENE-directed system of thrust imbricate structures, involving mainly thin-skinned and possibly thick-skinned structural styles (e.g., Bally, 1987; Barchi et al., 1998; Conti et al., 2020; Coward et al., 1999; Massoli et al., 2006; Mazzoli et al., 2005; Molli

ZHANG ET AL. 4 of 24

et al., 2010; Mostardini & Merlini, 1986; Patacca et al., 1990). Compression migrated from the Tyrrhenian area toward the Adriatic foreland from Oligocene to Pliocene-Pleistocene (Doglioni et al., 1996; Keller & Coward, 1996; Noguera & Rea, 2000; Patacca & Scandone, 2001, 2007), whereas coeval extension collapsed the Internal Apennines (Cavinato & DeCelles, 1999; Patacca et al., 1990). The analysis of syn-orogenic and thrust-top deposits allowed the recognition of ~100 and ~200 km progressive eastward migration of the thrust fronts in the last 25 My in the northern and central Apennines, respectively (Boccaletti et al., 1990; Vezzani et al., 2010). The Adriatic Sea, the shared foreland of southern Alps, Apennines, and Dinarides, shows variable tectonic style and age along strike (Cuffaro et al., 2010; Fantoni & Franciosi, 2010; Ghielmi et al., 2010; Scrocca, 2006; Tinterri & Lipparini, 2013; Wrigley et al., 2015) that are controlled by superimposition of pre-shortening (Jurassic rift-related) inherited structures of Adria microplate (Wrigley et al., 2015), and the Apennines and Dinarides orogenic imprint through time (Balling et al., 2021). The well-constrained northern Apennines frontal thrust system displays 45 km of shortening in the last 17 My at shortening rates of 2.9 mm/yr (Basili & Barba, 2007), with slip rates for different thrusts in the 0.26–1.35 mm/yr range (Maesano et al., 2013).

The WSW-directed Dinarides orogenic system is built by multiple orogenic processes related to the progressive closure of the Vardar Ocean since Late Jurassic time (e.g., Channell et al., 1996; Chiari et al., 2011; Gallhofer et al., 2017; Maffione and van Hinsbergen, 2018). The first of these large scale plate tectonic processes was the

The WSW-directed Dinarides orogenic system is built by multiple orogenic processes related to the progressive closure of the Vardar Ocean since Late Jurassic time (e.g., Channell et al., 1996; Chiari et al., 2011; Gallhofer et al., 2017; Maffione and van Hinsbergen, 2018). The first of these large-scale plate tectonic processes was the obduction of the Western Vardar Ophiolite Unit on top of the NE Dinarides with a total displacement of  $\sim$ 180 km. The end of the Vardar oceanic subduction led to the continental collision between Adria (lower plate) and Eurasian (upper plate) along the Sava Suture Zone (Handy et al., 2015; Pamić et al., 1998; Schmid et al., 2008, 2020; Ustaszewski et al., 2010).

The northern and central Dinarides fold-thrust belt is divided into the Internal Dinarides in the east, directly in contact with the Sava Suture Zone, and the External Dinarides in the west (Placer et al., 2010; Schmid et al., 2004; Tari, 2002; Tomljenović et al., 2008). The Internal Dinarides consist of composite thrust sheets (Balling et al., 2021; Schmid et al., 2008, 2020), including obducted Western Vardar Ophiolites (Robertson et al., 2009) and Mesozoic cover rocks (platform carbonates and foredeep deposits) belonging to the NE distal margin of Adria (Tari, 2002; Tomljenović et al., 2008). The External Dinarides are characterized by thrust imbricates of sedimentary cover units, locally involving Paleozoic basement, belonging to the NE margin of the Adria microplate shortened from the Eocene to the Present, although shortening was interrupted by a period of extension in Miocene time (e.g., Schmid et al., 2008; Tari, 2002; Van Unen et al., 2019). Shortening propagated in-sequence from the Sava Suture Zone in the east to the Adriatic foreland in the west (Ustaszewski et al., 2010). Total shortening increases from 50 to 130 km toward the south of Dinarides (Schmid et al., 2020 and references therein; Balling et al., 2021), although these estimates can vary significantly owing to different paleogeographic reconstructions (Korbar, 2009; Pamić et al., 2002). The internal parts of the Dinarides are characterized by abundant Paleogene-middle Miocene calcalkaline to ultrapotassic magmatism, (e.g., Kovács et al., 2007, and references therein).

The Pannonian Basin, to the NE of the Sava Suture Zone, is surrounded by the Alpine, Carpathians and Dinarides orogenic belts and is a Miocene to Present extensional back-arc basin underlain by thinned continental lithosphere (e.g., Horváth, 1995; Horváth et al., 2006; Koroknai et al., 2020). The substratum of the Pannonian Basin is made up by two megatectonic units: the Alpine-Carpathian-Pannonian (AlCaPa) and the Tisza, separated by the WNW-ENE Mid-Hungarian Shear Zone (Csontos & Nagymarosy, 1998; Schmid et al., 2008; Hetényi et al., 2015). The indentation of the Adria microplate during the Pliocene-Quaternary triggered mild compression through the Pannonian Basin (Bada et al., 2007; Horváth et al., 2006; Matenco & Radivojević, 2012). The Pannonian Basin hosts Miocene to recent magmatic rocks with diverse compositions (calc-alkaline, K-alkalic, ultrapotassic and Na-alkalic; Seghedi & Downes, 2011).

### 3. Methods

Modeling of the thermal lithosphere, hereinafter referred to as lithosphere, along the study transect was performed using LitMod2D\_2.0 (Kumar et al., 2020), an updated version of the original 2D software developed by Afonso et al. (2008). Assuming thermal isostasy, thermal steady state and a planar approximation (Cartesian coordinates), the algorithm integrates petrological and geophysical data to study the 2D thermo-chemical structure and the seismic velocity distribution of crust and upper mantle, fitting simultaneously absolute elevation, geoid height, Bouguer gravity anomalies, and SHF (Figure 2).

ZHANG ET AL. 5 of 24

Thorma Physical Pro	parties of the	Crustal Tactonic	Units Along the Profile
Thermo-i mysicai i ro	pernes of me	Crusiui recionic	Omis Along the Fronte

Crustal domains		Density (kg/m <sup>3</sup> )	Thermal conductivity (W/K m)	Radiogenic heat production (μW/m³)
Adria microplate	Sediment	2,450	2.4	1
	Elba granits	2,750	3.1	3.5
	Apennines UC/Tuscany MP	2,750-2,800 (a)	2.7/3.1	1.3/3.8
	Apennines MC/Tuscany MP	2,820	2.7/3.1	0.8/3.0
	Apennines LC/Tuscany MP	2,920	2.1/3.1	0.6/1.0
	Dinarides MC	2,850	2.7	0.8
	Dinarides LC	2,920	2.1	0.6
	Apennines/Dinarides duplicated LC	2,950	2.1	0.6
Tisza microplate	Sava Suture	2,850	2.7	1.3
	Pannonian Basin UC	2,750-2,860 (a)	2.9	2
	Pannonian Basin LC	2,950	2.1	0.6

Note. UC: Upper crust; MP: Magmatic Province; MC: Middle Crust; LC: Lower Crust. (a) Calculated as a function of pressure.

The numerical domain extends from the surface to 400 km depth. It is defined by different crustal and mantle bodies characterized by their individual thermo-physical properties and chemical composition. Crustal bodies are described by the user using thermo-physical properties (e.g., Table 1, thermal conductivity, volumetric heat production rate, density, coefficient of thermal expansion and compressibility), with an option of depth and/or temperature dependence. The composition of upper mantle bodies is defined using the Na<sub>2</sub>O–CaO–FeO–MgO–Al<sub>2</sub>O<sub>3</sub>–SiO<sub>2</sub> (NCFMAS) system (Table 2). The Gibbs free-energy minimization algorithm (Connolly, 2005, 2009) is used to compute stable phases and mineral assemblages within the temperature and pressure ranges of the upper mantle. The density distribution is obtained with an iterative scheme to include the effect of pressure, temperature, and composition. Mantle thermal conductivity is also P-T dependent.

Temperature distribution within the lithosphere is calculated by solving the 2D steady-state heat conduction equation, where boundary conditions are set as two fixed isotherms, that is, 0°C at the surface and 1,320°C at the LAB. Below the LAB, LitMod2D\_2.0 considers a 40-km thick thermal buffer with a temperature of 1,400°C at its base to avoid unrealistic discontinuities between the conductive thermal gradient within the lithosphere and the sublithospheric adiabatic thermal gradient.

 Major Oxides Composition in % of Weight Percent in the NCFMAS System Used for the Lithospheric and Sublithospheric

 Mantle

	Sublithospheric mantle	Mantle wedge	Lithospheric mantle	
Composition	DMM (Workman & Hart, 2005)	DMM—3% (Kumar et al., 2021)	Adriatic mantle (Tc_2) Av. Tecton peridotite (Griffin et al., 2009)	Pannonian mantle (PB_mant) (Alasonati Tašárová et al., 2016; Downes et al., 1992)
SiO <sub>2</sub>	44.7	44.59	45	44.6
$Al_2O_3$	3.98	3.51	3.9	2.9
FeO	8.18	8.21	8.1	8.8
MgO	38.73	39.63	38.7	40.8
CaO	3.17	3.02	3.2	2.6
Na <sub>2</sub> O	0.13	0.082	0.28	0.18
Mg#	89.4	89.58	89.5	90.4
(100 * MgO/[MgO + FeO])				

Note. DMM, Depleted Mid-Oceanic Ridge Mantle; Tc\_2, Average Phanerozoic Mantle; PB\_mant, Pannonian Basin mantle.

ZHANG ET AL. 6 of 24

onlinelibrary.wiley.com/doi/10.1029/2022JB024800 by Csic Organización Central Om (Oficialia Mayor) (Urici), Wiley Online Library on [13/122022]

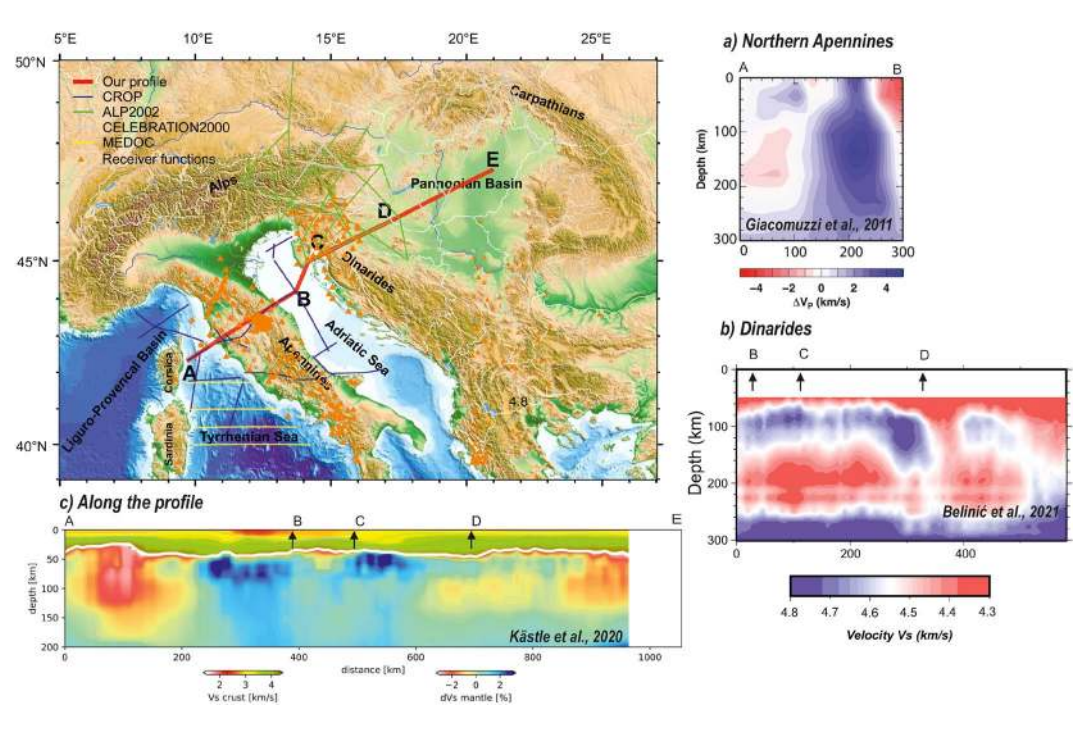


**Figure 3.** Upper mantle characterization from previous studies. (a) P-wave teleseismic tomography from Giacomuzzi et al. (2011). (b) Shear-wave velocity structure beneath the Dinarides from the inversion of Rayleigh-wave dispersion after Belinić et al. (2021) that have been used to constrain the SCLM anomaly below the Dinarides (Figure 5f). (c) Crustal S-wave velocity, Moho depth (white line) and mantle  $V_s$  anomaly from Kästle et al. (2020) model along our profile.

The final density distribution is used to calculate elevation, Bouguer and free air gravity anomalies, and geoid height. Seismic velocities are calculated based on phase and mineral assemblages and on the obtained temperature and pressure conditions and are compared with available velocity and tomography models. LitMod2D approach has been successfully applied in different tectonic settings including continental margins (e.g., Fernàndez et al., 2010; Pedreira et al., 2015) and continental collisional regions (e.g., Carballo et al., 2015; Jiménez-Munt et al., 2019; Kumar et al., 2021; Tunini et al., 2015). For more details about LitMod2D the reader is referred to Afonso et al. (2008) and Kumar et al. (2020).

Moho depth and crustal geometry are mainly constrained by available active and passive seismic experiments (DSS and RFs) and geological cross-sections, as discussed in the following section. The chemical composition of the mantle is obtained from xenoliths data when available, or according to its tectonothermal age as explained in Griffin et al. (2009). The LAB depth and the composition of the mantle (i.e., lateral compositional domains) are subsequently refined based on the fitting of the geophysical observables: elevation, gravity anomaly, geoid high, SHF and mantle seismic velocities (Figure 3; e.g., Belinić et al., 2021; Giacomuzzi et al., 2011; Kästle et al., 2018; Koulakov et al., 2015).

# 4. Lithospheric Structure and Upper Mantle Characterization From Previous Studies

### 4.1. Crustal Structure

During the last three decades, a large amount of geologic and geophysical investigation has been carried out to image the crustal structure of the study region. Along the transect, geophysical data come from deep near-vertical reflection (e.g., Scrocca et al., 2003) and wide-angle reflection/refraction seismic experiments (e.g., Cassinis et al., 2005), RF analyses (e.g., Mele & Sandvol, 2003) and gravity modeling (e.g., Šumanovac, 2010). Additional data come from seismicity distribution at crustal and subcrustal levels (e.g., Chiarabba et al., 2004; De Luca et al., 2009). These studies show that shallow seismicity is mainly concentrated along a narrow band along the backbone of the Apennines while a diffuse activity characterizes the Adriatic region. At crustal levels, focal mechanisms evidence normal faulting below the central part of the Apennines belt and thrust/reverse faulting mechanisms at the outer fronts of the Apennines (e.g., Chiarabba et al., 2014; De Luca et al., 2009). Seismicity

ZHANG ET AL. 7 of 24

21699356, 2022, 12, Downloaded

from https://agupubs.onlinelibrary.wiley.com/doi/10.1029/2022JB024800 by Csic Organización Central Om (Oficialia Mayor) (Urici), Wiley Online Library on [13/12/2022]. See the Term

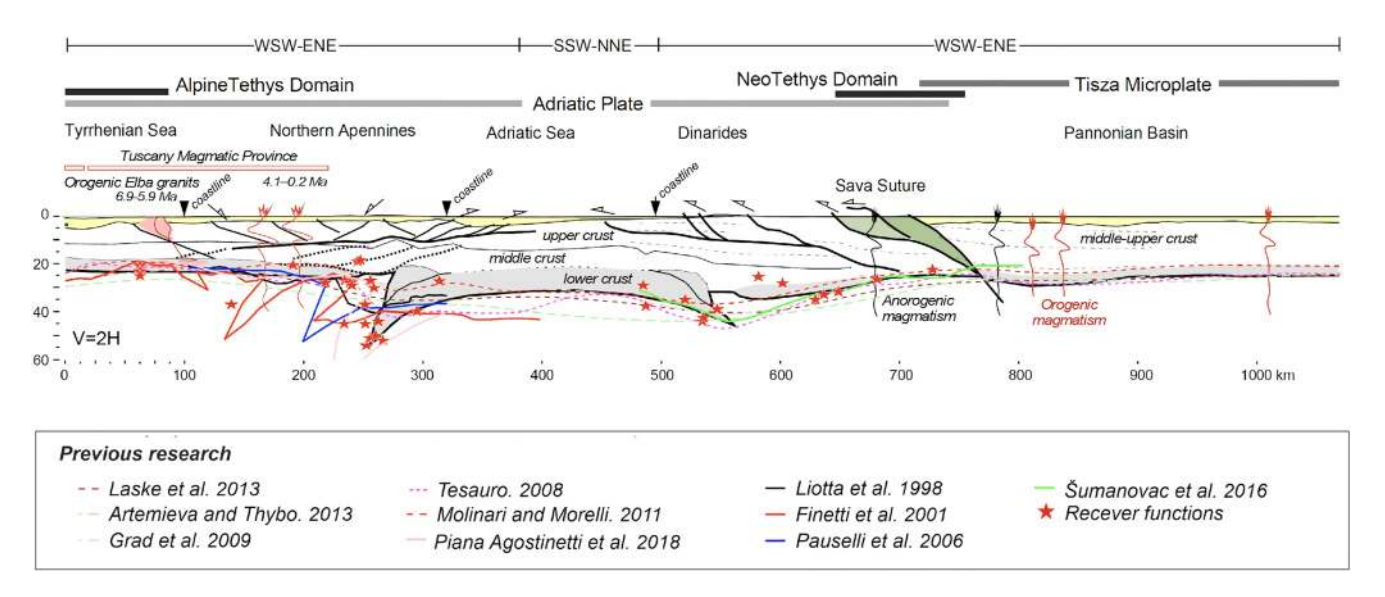


**Figure 4.** Crustal structure from the best fitting model constrained from the available geological and geophysical information listed in the text and in the panel legend. Yellow color is the sediment layer. Moho depths from previous studies and receiver functions (Chiarabba et al., 2014; Diaferia et al., 2019; Mele & Sandvol, 2003; Piana Agostinetti & Amato, 2009; Piana Agostinetti & Faccenna, 2018; Stipčević et al., 2020; Šumanovac et al., 2016) are shown for comparison.

between 25 and 70 km is widespread in the Adriatic region with a tendency to cluster below the Apennines while no deep earthquakes were recorded below the Tyrrhenian Sea (Figures 8 profile E–F of De Luca et al., 2009). The west dipping seismicity, registered down to 70 km depth, is interpreted as the evidence of the subduction of the Adriatic lithosphere beneath the Apennines (De Luca et al., 2009). In the Tyrrhenian basin, the crustal structure is constrained by the CROP line M-12A, while the onshore CROP 03 was used to constrain the crustal geometry of the Apennines and the western region of the Adriatic Sea (Barchi et al., 1998; Finetti et al., 2001; Liotta et al., 1998; Pauselli et al., 2006; Piana Agostinetti & Faccenna, 2018). In the Adriatic Sea we used the CROP M-16 seismic line. For the Dinarides and the western Pannonian Basin, we used the Alp07 profile (Šumanovac et al., 2016) and the earthquake tomography analysis of Kapuralić et al. (2019). In addition to these profiles, we have projected onto the transect the Moho depth data from EUNAseis (Artemieva & Thybo, 2013), CRUST1.0 (Laske et al., 2013) and EPcrust (Molinari & Morelli, 2011) models and the high-resolution Eurasian Moho data set of Tesauro et al. (2008) and Grad et al. (2009). For the Dinarides and Pannonian Basin additional information comes from seismicity distribution (e.g., Kuk et al., 2000 and Bondár et al., 2018, respectively).

There is agreement on the broad features of the crustal structure; however, important discrepancies arise when entering into the details of its internal structure and density distribution. All studies agree that the Moho lies at shallow depths (20-25 km) in the Tyrrhenian Sea and below western Italy, at intermediate depth (30-35 km) along the Adriatic coast, deepening under the Apennines (down to 50 km) and Dinarides (down to 45 km) mountain belts (Figure 3; e.g., Kapuralić et al., 2019; Molinari et al., 2015; Stipčević et al., 2020). In the Apennines, the complex internal crustal structure, the possible presence of a mantle wedge and the top of the subducting slab is reflected in the RFs results where differences in the Moho depth may be as large as 30 km from one study to another (Chiarabba et al., 2014; Mele & Sandvol, 2003; Piana Agostinetti & Faccenna, 2018). Major discrepancies are also observed in the interpretations of multichannel seismic reflection profiles about the internal structure of the crust and the exact location and geometry of the top of the subducting slab (Figure 4). Finetti et al. (2001), based on the interpretation of onshore CROP-03 profile, favor a complex thrust system with thrust faults and shear planes that extend at low angle from the crust to the upper mantle offsetting the Moho. These authors also favor a westward location of the top of the subducting slab, compared to the location proposed by Pauselli et al. (2006) and Piana Agostinetti and Faccenna (2018) who place it right below the External Apennines (Figure 4). This latter interpretation is more in line with RFs and seismicity results of Mele and Sandvol (2003) and Chiarabba et al. (2014, 2020). Receiver functions and seismic tomography indicate that beneath the Internal Apennines the shallowest mantle is characterized by about 5% lower shear wave velocity anomaly and 3% higher  $V_v/V_v$  ratio than the reference values for these depths (Chiarabba et al., 2020). These authors interpreted these anomalies as mantle upwelling with the presence of melts at the base of the crust, extending from the

ZHANG ET AL. 8 of 24



Tyrrhenian to the central Apennines. Below the Dinarides, Kapuralić et al. (2019) using local earthquake tomography inferred Moho depths between 40 and 45 km, similar to those obtained by Šumanovac et al. (2016) using RFs. A quite flat Moho around 25 km depth is observed underneath the back-arc Pannonian Basin (Kapuralić et al., 2019; Šumanovac et al., 2016). From local earthquake tomography, Kapuralić et al. (2019) found high velocities below the northern Dinarides at depths shallower than 10 km, but low velocities in the Pannonian Basin associated with a deep local depression. They also imaged a high-velocity body at 5–15 km depth between the Dinarides and the Pannonian Basin. The Dinaridic crust has been interpreted as two-layered, while the Pannonian crust is interpreted as single-layered (Kapuralić et al., 2019; Šumanovac et al., 2016).

## 4.2. LAB and Upper Mantle Characterization

In the study area a number of RF studies have focused on the LAB (Belinić et al., 2018; Geissler et al., 2010; Miller & Piana Agostinetti, 2012). Tomography, mainly based on teleseismic body-wave (e.g., Koulakov et al., 2009; Lippitsch et al., 2003; Piromallo & Morelli, 2003), P and surface wave tomography (e.g., Belinić et al., 2021; El-Sharkawy et al., 2020; Giacomuzzi et al., 2011; Kästle et al., 2022) and full-wave inversion of body and surface waves (e.g., Beller et al., 2018; Blom et al., 2020; Zhu et al., 2015) have provided images of the upper mantle down to the transition zone. All of them show strong lateral heterogeneities, where the different depths of the discontinuities, and the various shapes and lengths of the imaged slabs highlight the complexity of the region. Although comparison of tomography images is not forthright because mismatch in the location of the anomalies may be partly due to the different methods and sensitivities of the modeled wave types, the 3D structural complexity of the region adds a degree of uncertainty that is reflected in the variety of models proposed so far.

Comparison of available seismic LAB depths shows a high degree of variability between the main tectonic domains. Below the northern Apennines, Miller and Piana Agostinetti (2012), based on S-RFs, highlighted a complex lithospheric structure with two different S-velocity jumps, located at ~90 and 180 km depth. The shallowest one is interpreted as the LAB of the upper plate while the deepest jump is proposed to be associated with the LAB of the subducting lithosphere. This interpretation in terms of subducted/delaminated Adriatic lithosphere below the Apennines agrees with the location and distribution of the west-dipping seismicity down to about 70 km (e.g., Chiarabba et al., 2005; De Luca et al., 2009). Underneath the Dinarides discrepancies of the seismic LAB may reach up to 20 km, from 120 to 100 km depth, shallowing up toward the Adriatic Sea (90 km depth) and Pannonian Basin, where the LAB is placed at a rather constant depth of 70 km (e.g., Belinić, et al., 2018). These studies also highlight the variability of the LAB depth encountered along the Dinarides, with deep LABs in the Northern and Southern regions (100–120 and 90 km depth, respectively) that contrast with the much shallower LAB (~50 km depth) in the central Dinaric region (Belinić et al., 2018; Šumanovac et al., 2017).

As mentioned, tomography images differ substantially depending on the methods used. While global models (e.g., Amaru, 2007 or Zhu et al., 2015) are not conclusive due to their low resolution, regional and local models show a high variability with the presence of subducted slabs, attached slabs of variable lengths and detached slabs (Blom et al., 2020; El-Sharkawy et al., 2020). These studies, based on a high-resolution shear-wave velocity model, find the presence of slab segments in the northern Apennines, beneath the Dinarides and in the central Alps. Below the Apennines, Hua et al. (2017), based on P-wave anisotropic tomography, image a vertically oriented slab extending down to ~300 km, a result that is coincident with that obtained by Benoit et al. (2011), who combined teleseismic P- and S-wave arrival time data. Studies based on P-wave teleseismic tomography find that the slab reaches depths of 400–500 km (Giacomuzzi et al., 2011) and 350–400 km (Hua et al., 2017; Spakman & Wortel, 2004). This result is coincident with that obtained by Koulakov et al. (2015), who, based on body-waves analysis, find a steeply dipping high-velocity anomaly down to 400 km, that they interpret as composed of the continental lithospheric mantle of Adria. Overall, these studies image shallower slab depths than previous models with less resolution (e.g., Lucente et al., 1999; Piromallo & Morelli, 2003), which predicted that the slab penetrates well into the transition zone.

Inversion of Rayleigh-wave dispersion by Belinić et al. (2021) shows a high-velocity anomaly reaching depths of 160 km beneath the northern Dinarides and more than 200 km beneath the southern regions. These results differ slightly from those obtained by Šumanovac and Dudjak (2016) and Šumanovac et al. (2017), who, based on teleseismic tomography, conclude that in the northern Dinarides the pronounced fast anomaly reaches 250 km depth. The observed NE dipping fast anomalies in the northern region extend underneath the entire Dinarides fold-thrust belt, indicating the sinking of cold and rigid material of the Adriatic microplate. Belinić et al. (2021)

ZHANG ET AL. 9 of 24

imaged low velocity zones under the southwestern Pannonian Basin and beneath the central part of Adria, which they interpreted as results of lithospheric thinning and/or upwelling of hot asthenospheric material.

### 5. Results

Here, we summarize the main results of the crustal structure (Figure 4) and the physical properties of the lithospheric and sublithospheric mantle resulting from the best fit model (Figures 5 and 6). The obtained lithospheric model is defined by a series of crustal and mantle bodies, with the crustal physical parameters and the chemical composition of the mantle shown in Tables 1 and 2, respectively. The boundaries of the mantle domains shown in Figure 5f must be understood as transitional (with physical properties changing gradually) and not abrupt, as drawn for simplicity in the figure.

### 5.1. Crustal Structure

Figure 4 shows the modeled crustal structure, which has been constrained by available seismic data and geological-cross sections and slightly modified to match the surface observables, after modifying the geometry and composition of the less constrained mantle bodies. Modifications of the crustal structure are always within the uncertainties of available data. Crustal density values have been taken from previous gravity modeling (Šumanovac, 2010) and calculated by empirical velocity-density relationships (Brocher, 2005), considering the crustal velocity models (e.g., Kapuralić et al., 2019; Molinari et al., 2015). Thermal conductivities and radiogenic heat production come from previous studies (e.g., Norden & Förster, 2006; Trumpy & Manzella, 2017) and from the global compilation by Vilà et al. (2010). Moreover, we consider specific thermal parameters for the Tuscany region and Internal Apennines, where SHF (Figure 2) shows high values probably related to active hydrothermal flow and magmatism, as indicated by the presence of active hydrothermal systems and recent volcanic and magmatic activity (e.g., Pandeli et al., 2013; Sani et al., 2016). We modeled the high SHF within the Tuscany Magmatic Province by high conductivity and radiogenic heat production, which correlates with a crust with magmatic intrusions and the presence of granitoids (Norden & Förster, 2006), cropping out and reached by drill holes in the area (e.g., Dini et al., 2005). In contrast, lower heat flow values (<60 mW/m²) are found in the Internal Apennines and Dinarides, whereas in the Pannonian Basin heat flow values are above 70 mW/m².

According to geological and geophysical information and the best fit of geophysical observables, we distinguish the Adriatic microplate, extending from the Tyrrhenian basin to the Dinarides, and the Tisza microplate, which in the modeled transect encompasses the western half of the Pannonian Basin. These two microplates are separated by the Sava Suture Zone (a remnant of the formerly intervening oceanic domain; Figures 4 and 5) and differ in their internal crustal structure and average densities.

The Moho lies at variable depths, deepening slightly from  $\sim$ 23 km under the Tyrrhenian basin to  $\sim$ 25 km under the Internal Apennines. The Moho depth in the External Apennines increases from ca. 35 km in the east to ca 52 km in the west. Beneath the Adriatic Sea, the Moho remains at a rather constant depth (>30 km) deepening underneath the External Dinarides, where it is locally found at 45 km. East of the Sava Suture Zone, the Tisza microplate shows very little crustal thickness variation, with values decreasing from 30 km in the west to 25 km in the easternmost part of the Pannonian Basin.

In our favored model, three crystalline layers (Figure 4) characterize the crust of the Adriatic microplate. Crustal densities range from 2,750 kg/m³ for the upper crust, 2,820–2,850 kg/m³ for the middle crust and 2,920–2,950 kg/m³ for the lower crust. However, we cannot rule out a two-layered crust, with upper-middle and lower crust with an average density of 2,800 kg/m³ for the upper-middle part. These crystalline layers are covered by a sedimentary layer of variable thickness with an average density of 2,450 kg/m³. In terms of crustal average density, within the Adriatic microplate we can distinguish the Tuscany Magmatic Province with values ~2,780 kg/m³ and the External Apennines, Adriatic Sea and Dinarides ~2,830 kg/m³. The temperature at Moho depth is ~430°C in the Adriatic Sea, gradually increasing with the crustal deepening below the Apennines (~700°C) and the Dinarides (~500°C). The Tuscany Magmatic Province is characterized by high temperatures at shallow levels with values around 100°C at 2 km depth. The Moho temperature increases from 400°C in the western part of the profile in the Tyrrhenian Sea to 530°C in the Internal Apennines. These higher values in an area with thin crust are probably related to upwelling of hot sublithospheric material.

ZHANG ET AL. 10 of 24

21699356, 2022, 12. Downloaded from https://agupubs.onlinelibrary.wiley.com/doi/10.1029/2022JB024800 by Csic Organización Central Om (Oficialia Mayor) (Urici), Wiley Online Library on [13/12022]. See the Terms

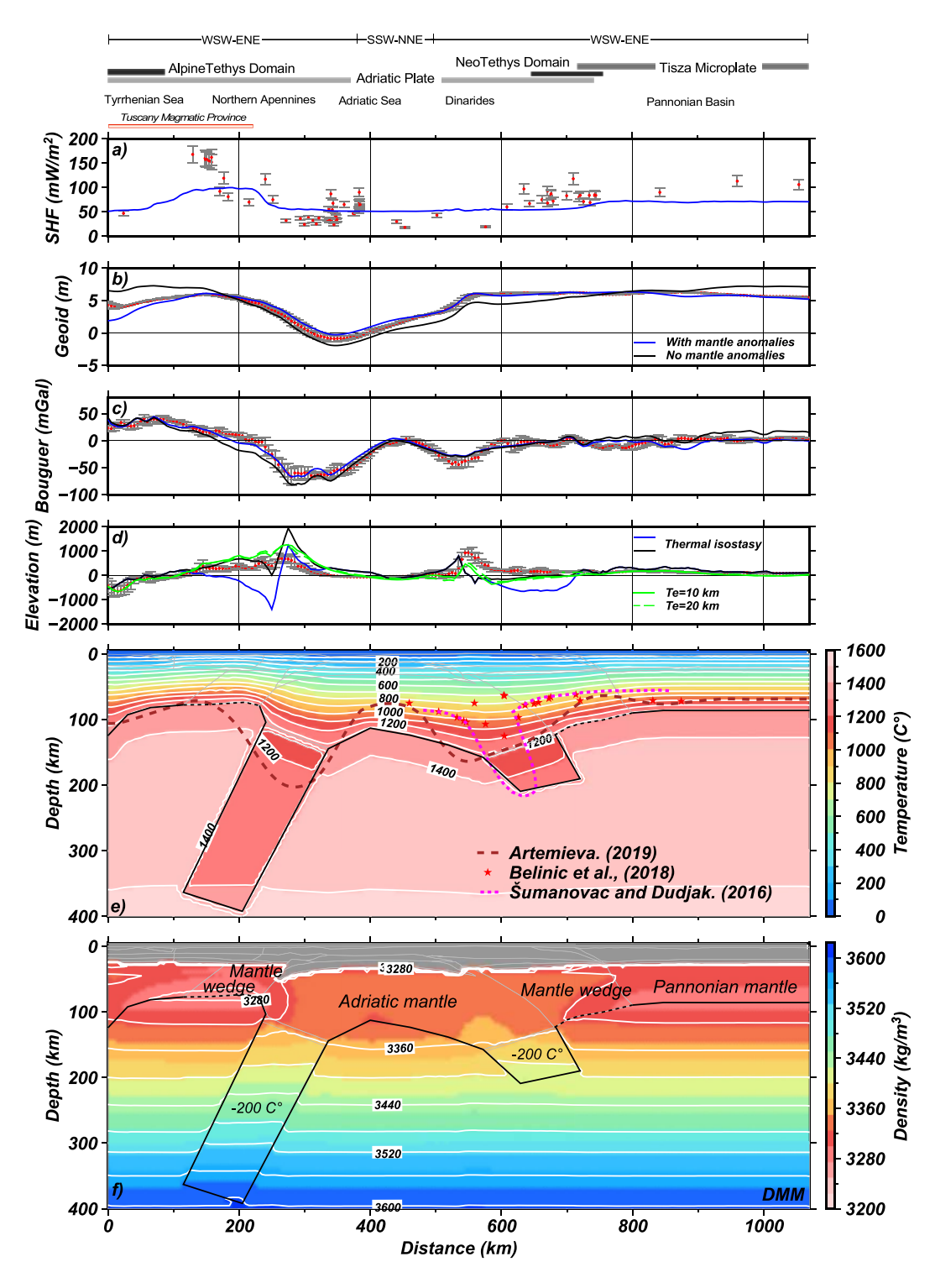


Figure 5. Best fit model. Surface observables (red dots): (a) Surface Heat flow, (b) Geoid height, (c) Bouguer anomaly and (d) absolute elevation, are projected onto the transect at 5 km sampling interval within a strip of 25 km half-width to account for lateral variations perpendicular to the strike. Standard deviations are shown as error bars. Blue and black lines show calculated values with and without sublithosphere anomalies, respectively. In (d) blue and black lines show thermal isostatic elevation (with and without mantle anomalies), and green lines are the calculated flexural elevation with elastic thickness Te = 10 km and dashed line Te = 20 km. Panel (e) shows the temperature distribution for the whole lithosphere. Panel (f) shows the density distribution within the lithospheric mantle along the modeled transect. See Figure 1 for location.

ZHANG ET AL. 11 of 24

21699356, 2022, 12, Downloaded from https://agupubs.onlinelibrary.wiley.com/doi/10.1029/202218/024800 by Csic Organización Central Om (Oficialia Mayor) (Urici), Wiley Online Library on [19/122022]. See the Terms and Conditions (https://onlinelibrary.wiley.

nditions) on Wiley Online Library for rules of use; OA articles are governed by the applicable Creat

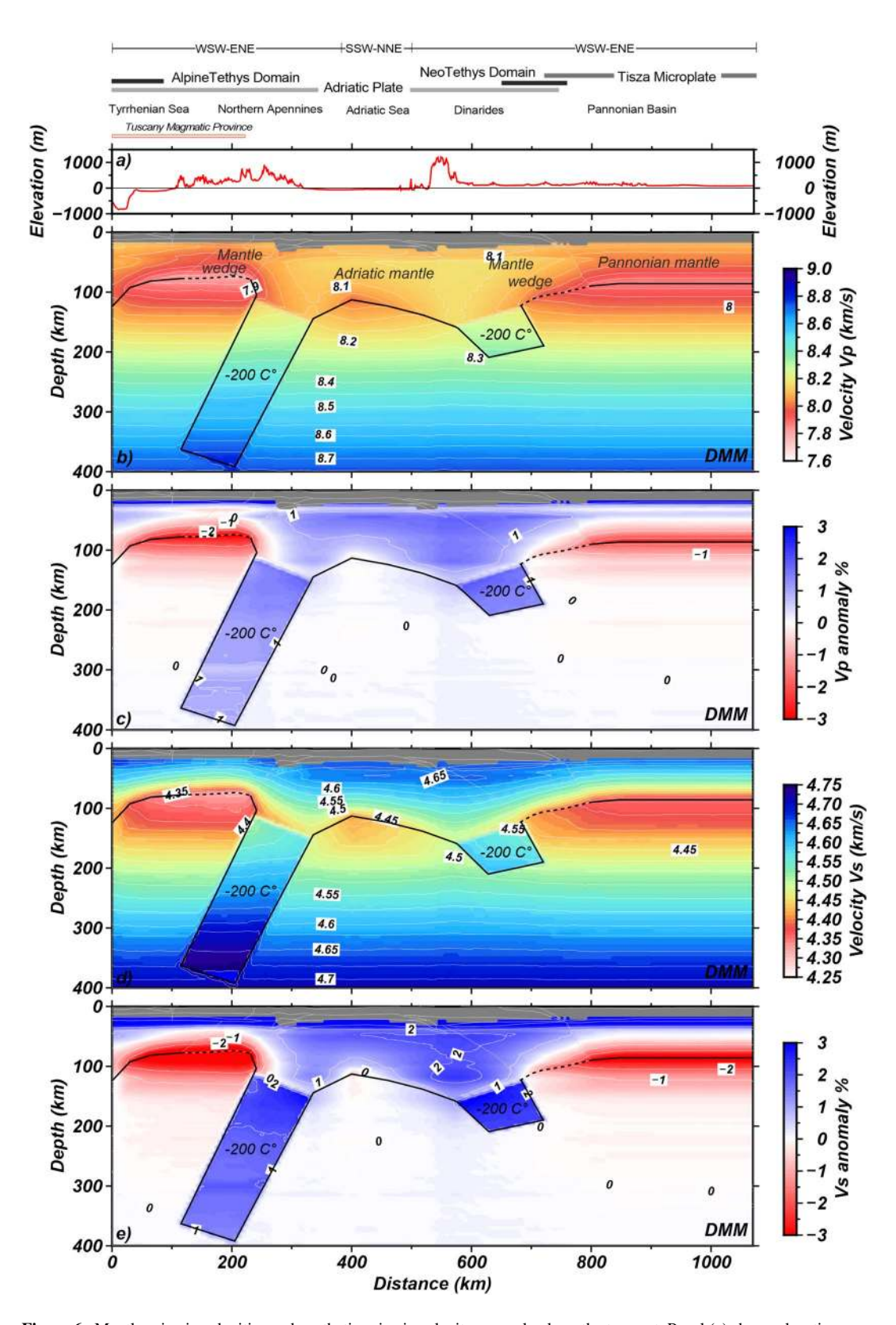


Figure 6. Mantle seismic velocities and synthetic seismic velocity anomaly along the transect. Panel (a) shows elevation profile, (b) and (d) show absolute P- and S-wave velocities and (c) and (d) synthetic P and S-wave anomalies, respectively.

ZHANG ET AL. 12 of 24

The modeled crustal structure of the Pannonian Basin is characterized by a two-layer crystalline crust, covered by a 4–6 km thick sedimentary layer (Figure 4). The upper-middle crust with an average density of 2,750 kg/m<sup>3</sup> extends down to 20 km depth, slightly deepening in its western termination. The lower crust is rather thin all along the basin (5 km) with an average density of 2,950 kg/m<sup>3</sup>. Therefore, the average density of the crust in the Pannonian Basin is between 2,790 and 2,800 kg/m<sup>3</sup>. The model-predicted temperature at Moho levels beneath the Pannonian Basin varies from 500°C in the west to 450°C in the eastern part of the basin.

The Sava Suture Zone was modeled with an average density (2,850 kg/m<sup>3</sup>) higher than in the surrounding crustal rocks (Figures 4 and 5).

### 5.2. LAB and Upper Mantle Characterization

In our best fi model, we distinguish three lithospheric mantle compositions (Figure 5). Beneath the Adriatic microplate (Adriatic mantle, Table 2 and Figure 5f) the lithospheric mantle composition corresponds to a slightly depleted mantle (Tc\_2 of Griffin et al., 2009) with a mean Mg# of 89.5. In the Pannonian Basin (Tisza microplate) the composition of the mantle is the same as obtained by Alasonati Tašárová et al. (2016) and Downes et al. (1992) from the analysis of 20 xenoliths (Pannonian mantle, Table 2 and Figure 5f). Its mean Mg# of 90.4, which indicates the presence of a fertile mantle. The densities and seismic velocities resulting from these two lithospheric mantle compositions are very similar (with maximum differences of ~10 kg/m³ between densities and ~0.01 km/s for  $V_p$  and  $V_s$ ). However, we preferred maintaining the distinction between these different compositions to highlight the different tectonic history between the Adria and Tisza microplates. The third lithospheric mantle composition used is a residual DMM-3% composition (Mantle wedge, Table 2 and Figure 5f) beneath the External Apennines, Dinarides and Sava suture zone. This composition accounts for the presence of a mantle wedge and potential melting of the depleted asthenosphere (DMM) following rollback of the western (hereinafter Apenninic) and the eastern (hereinafter Dinaric) segments of the Adriatic slab. The sublithospheric mantle has been modeled using the DMM composition of Workman and Hart (2005) that is a reference model for an average, non-melted, depleted MORB mantle (more details in Kumar et al., 2020).

The LAB along the Adria microplate domain (Figure 5) is shallow (about 75 km depth) underneath the Tyrrhenian and Tuscany extended terrains and deeper (125–150 km depth) between the External Apennines and the Dinarides. In contrast to the Adriatic domain, the Tisza domain is characterized by a rather flat LAB (~90 km), slightly deeper than the thermal LAB obtained by Artemieva (2019). Figure 5e compares the calculated LAB depth to the thermal LAB of Artemieva (2019) and to the S-RF and P-wave teleseismic LAB of Belinić et al. (2018) and Šumanovac and Dudjak (2016), respectively.

The resulting modeled densities and  $V_{\rm p}$  and  $V_{\rm s}$  seismic velocities for the assumed mantle compositions are shown in Figures 5f and 6. Under the same PT conditions, the density of the Adriatic mantle is slightly higher than that of the Pannonian mantle. Comparing the mantle density profiles of the Adriatic and Pannonian Basin we see that the density of the Adriatic mantle, for example, at 80 km depth, is higher, as much as 50 kg/m³ than that of the Pannonian mantle (Figure 5). The lower values of mantle density are located at the base of the lithosphere in the Tuscany Magmatic Province (<3,280 kg/m³) and in the Pannonian Basin ( $\sim$ 3,300 kg/m³). Similarly, there is also a decrease of  $V_{\rm p}$  and  $V_{\rm s}$  from the Adriatic microplate to the Pannonian Basin (Figure 6c) as observed also by Belinić et al. (2021) at similar depths (Figure 3, panel b). The lowest seismic velocity is obtained in the lithospheric mantle of the Tuscany Magmatic Province with  $V_{\rm p}$  and  $V_{\rm s}$  values from 8.01 to 4.62 km/s below Moho depth to 7.8 and 4.32 km/s at LAB. The highest values of these velocities are found in the lithospheric mantle beneath the Adriatic Sea, with  $V_{\rm p}$  between 8.15 and 8 km/s and  $V_{\rm s}$  from 4.66 to 4.43 km/s. These differences in density and seismic velocity are mainly related to the LAB changes and, then, temperature distribution, more than to compositional changes.

The resulting density of the DMM-3% composition of the mantle wedge is much higher underneath the Dinarides/western Pannonian Basin area than underneath the Tyrrhenian-Tuscany region where the lithospheric thinning results in an increase of the thermal gradient and consequently a decrease in density and seismic velocities.

Furthermore, to better fit the geoid height and Bouguer anomaly (Figures 5b and 5c) and considering seismic tomographic results, we have modeled two sublithospheric thermo-compositional anomalies with an Adriatic mantle composition extending down to 400 km underneath the Apennines and to 250 km below the Dinarides. We keep the same chemical composition (Adriatic mantle) for both slabs considering that geophysical and geological

ZHANG ET AL. 13 of 24

data point to the same Adriatic origin. The positive seismic velocity anomaly (2%-3%) beneath the northern Apennines (Figure 3 profile F-F' of panel A) (Giacomuzzi et al., 2011) and the increase of  $V_{\rm p}$  (8.2–8.4 km/s) and  $V_{\rm s}$  (4.6–4.8 km/s) velocities proposed by Belinić et al. (2021) underneath the Dinarides (Figure 3, panel 2) are both modeled as sublithospheric negative thermal mantle anomalies (-200°C) that extend down to 400 and 250 km, respectively. Our modeling shows that within the sublithospheric anomalies there is a 20 kg/m³ increase in density (Figure 5f) and an increase of ~1.5% for  $V_{\rm p}$  and ~2% for  $V_{\rm s}$ . These thermo-compositional sublithospheric anomalies allow for a better adjustment not just with the seismic tomographic models but also with the geoid height and Bouguer anomaly (Figures 5b and 5c, blue and black lines).

### 6. Discussion

# 6.1. Crustal and Lithospheric Structure

The numerous geophysical surveys carried out in the study region allowed us to have a good constraint on the Moho depth along the northern Apennines and Dinarides (Figure 4 and references therein). Along the transect, we distinguish two main microplates, Adria and Tisza, separated by the Sava Suture to the east of the Dinarides. The geometry of the crustal layers produces the density variations required to fit the observables (Bouguer anomaly, geoid height, and elevation) and it is consistent with the geodynamic context.

The structure of the northern Apennines is complex and the Moho depth differs noticeably in different studies (e.g., Finetti et al., 2001; Liotta et al., 1998; Pauselli et al., 2006). Along the External Apennines, our results agree with those obtained by RFs studies (see references in Figure 4), where the Moho locally reaches maximum depths of ~55 km, in an area where we modeled the top of the Apenninic slab (see next subsection). Beneath the Adriatic Sea, the Moho remains at a rather constant depth, consistent with the results of Molinari and Morelli (2011) and Grad et al. (2009). The Adria crust is deepening underneath the External Dinarides, where it is locally found at 45 km, in agreement with RF data (Stipčević et al., 2020; Šumanovac et al., 2016) and local earthquake tomography (Kapuralić et al., 2019).

According to Pamić et al. (2002) the Sava Suture Zone developed as a back-arc basin during the Cretaceous-Early Paleogene and was subsequently affected by Eocene collisional deformation and metamorphism accompanied by synkinematic granite plutonism, generation of an ophiolite mélange and finally thrusting onto the Dinarides. The high average density that we found for the Sava Suture zone agrees with this geologic history and it also explains the high-velocity body imaged by Kapuralić et al. (2019) at the transition between the Dinarides and the Pannonian Basin.

Figure 5e compares our calculated LAB depths to those reported in other studies. Although there is coincidence with previous models in the regional pattern of lithospheric thickness variations and in the depth of the LAB in the Tyrrhenian and Pannonian basins, there are discrepancies along the External Apennines and Dinarides and in the Adriatic Sea. The predicted LAB is similar to that of Artemieva (2019), except below the Apennines and the Adriatic Sea, likely due to the regional low resolution of Artemieva's model. In addition, our results agree with those of Šumanovac and Dudjak (2016) and Belinić et al. (2018) below the Dinarides, although significant differences are observed below the Pannonian Basin where we find a deeper LAB. The precise determination of the LAB depth depends on the measuring parameters. However, the different definitions should show a similar trend as all of them are imaging the rheologically strong outer layer of the Earth. Jiménez-Munt et al. (2019) found than seismic LAB roughly follows the  $1,000^{\circ}\text{C} \pm 50^{\circ}\text{C}$  isotherm. Along our profile, the trends obtained with different methods are similar, with the thermal LAB deeper than the seismic LAB. The seismic LAB from Šumanovac and Dudjak (2016) roughly follows the isotherm  $1,000^{\circ}\text{C}-900^{\circ}\text{C}$ , whereas below the Dinarides the seimic LAB largely departs from this isotherm, probably related to the presence of the subducted cold slab, which is not in thermal equilibrium (Jiménez-Munt et al., 2019).

# **6.2.** Mantle Composition and Anomalies

It is challenging to identify mantle chemical composition based on density and seismic velocities, because of the non-linear nature of the problem and the lack of uniqueness (Kumar et al., 2020). Hence, the composition of the mantle must be compatible with the geological and geodynamic history of the area. The composition of lithospheric mantle wedges is related to their backarc origin and to the degree of partial melting expected from

ZHANG ET AL. 14 of 24

the nature and volume of magmatic events. The space opened between the trench and the upper plate during slab roll-back processes is replaced by a fertile sublithospheric mantle with DMM composition that will undergo partial melting by adiabatic decompression.

Our best fitting model requires two negative thermal anomalies in the upper mantle below the Apennines and Dinarides in agreement with the interpretation of seismic tomography images (e.g., Belinić et al., 2021; Benoit et al., 2011; El-Sharkawy et al., 2020; Giacomuzzi et al., 2011; Handy et al., 2021; Koulakov et al., 2015; Šumanovac et al., 2017). Beneath the Apennines, the best-fit model indicates the presence of a west-dipping attached cold lithospheric body down to 400 km, in continuation with the west dipping seismicity observed down to 70–80 km below the northern Apennines (De Luca et al., 2009). This deep cold body is characterized by seismic velocities anomalies between 1% and 2%, which coincide with those observed from the seismic tomography (e.g., Figure 3; Giacomuzzi et al., 2011; Kästle et al., 2020). The modeled low mantle velocities around 100 km depth in the Tuscany Magmatic Province (Figure 6) agree with the values (<-2%) predicted by the seismic tomography (e.g., Figure 3a).

Below the Dinarides, a much shorter 125 km-long and east-dipping mantle anomaly is required, resulting in a lithospheric slab down to 250 km. This result is in agreement with Šumanovac and Dudjak (2016), who image a pronounced fast velocity anomaly extending toward the NE direction to at least 250 km depth. Our favored model includes a mantle wedge below the Dinarides and southwest of the Pannonian basin, which is consistent with the S-wave low-velocity zone imaged from the inversion of Rayleigh-wave dispersion by Belinić et al. (2021) (Figure 3b).

### 6.3. Geodynamic Implications

The obtained transect across the northern Tyrrhenian Sea, northern Apennines, northern Dinarides and Pannonian Basin is compatible with previous studies, which indicate an initial configuration based on two main microplates: Adria and Tisza (e.g., Schmid et al., 2020). These microplates were separated by the N-S oriented Vardar Ocean, a Neo-Tethys oceanic branch, and interacted via subduction processes during Mesozoic and Cenozoic time in the framework of the convergence between Africa and Eurasia, which also led to the development of a SE-dipping Alpine-Tethys subduction related to the Alps.

The Adria microplate shows the most complex crustal structure since it encompasses both Apennines and Dinarides fold-thrust belts that show opposing vergence and are separated by the Adriatic Sea foreland. The Apennines orogenic system was built from Oligocene onwards by the deformation of the thinned western continental margin of Adria, after the consumption of the Ligurian-Alpine Tethys in a NW- and W-dipping subduction. This subduction was characterized by roll-back and, likely, later continental delamination, which led to the opening of the Liguro-Provencal and Tyrrhenian backarc basins (Figure 7). We interpret the sublithospheric anomaly observed in our model down to 400 km beneath the Apennines as the remnant slab after these processes. The eastern margin of Adria microplate was deformed over a much longer period spanning the Mesozoic and Cenozoic building of the Dinarides orogenic system (Schmid et al., 2008, 2020; Van Unen et al., 2019).

The Apennines thrust system geometry is still debated, since thin- and thick-skinned models have been proposed (e.g., Butler et al., 2004). Several studies propose that its most recent Neogene evolution is linked to east-directed rollback and subsequent delamination processes (e.g., Benoit et al., 2011; Chiarabba et al., 2014; D'Acquisto et al., 2020). The Internal Dinarides is composed by thrusted tectonic domains, including the Western Vardar Ophiolite Unit (e.g., Schmid et al., 2008), involving Mesozoic cover rocks belonging to the NE distal margin of Adria (Tari, 2002; Tomljenović et al., 2008). Jurassic obduction of Vadar oceanic crust is well preserved and well imaged in our crustal profile by a high-density body about 50 km wide and extending down to the base of the crust.

The northernmost Tyrrhenian Sea and western Tuscany, located onshore and corresponding to the Internal Apennines, are characterized by extensive magmatism (Tuscany Magmatic Province; e.g., Dini et al., 2002; Pandeli et al., 2013; Sani et al., 2016). The Tyrrhenian Sea in this region is characterized by a collection of scattered islands mainly formed by granitic intrusions, in which the largest Elba Island exposes the Monte Capanne and the apophysis of the Porto Azurro granite plutons with ages of 6.9 and 5.9 Ma (Figure 1a) (Pandeli et al., 2013). These granites were mostly derived from melting of the lower crust within an orogenic context (Peccerillo, 2005; Serri et al., 1993). Our crustal model is consistent with the presence of these granitic intrusions and volcanism,

ZHANG ET AL. 15 of 24

21699356, 2022, 12, Downloaded

from https://agupubs.onlinelibrary.wiley.com/doi/10.1029/2022JB024800 by Csic Organización Central Om (Oficialia Mayor) (Urici), Wiley Online Library on [13/12/2022]. See the Terr

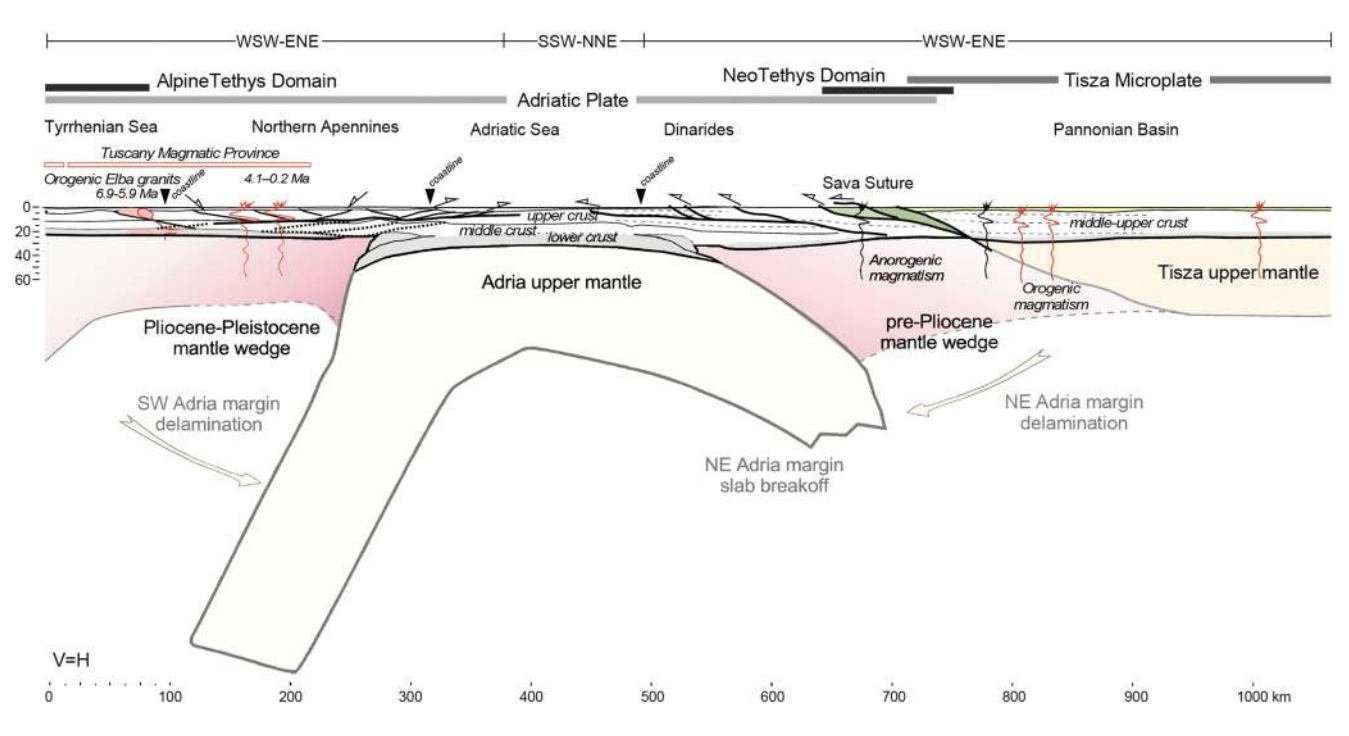


Figure 7. Modeled crust and upper mantle structure along the profile and our geodynamic interpretation.

which are the sources for high thermal conductivity and heat production in the area. The large Tuscany Magmatic Province onshore Italy formed from about 4 to 0.2 Ma extruding along the extensional system of normal faults thinning the Internal Apennines crust (Acocella & Rossetti, 2002). This is compatible with the results from our study, where the Tyrrhenian Sea and the western Apennines are characterized by high thermal gradient and thermal properties (conductivity and heat production) characteristic of magmatic rocks. Provided that continental collision occurred at about 25–30 Ma (e.g., Carminati et al., 2012), these magmatic rocks can be related to either roll-back of a continental slab or to delamination of Adria lithospheric mantle. Some authors proposed that delamination (in the sense of rollback of the lithospheric mantle slab) started at Corsica at about 15 Ma (e.g., Benoit et al., 2011), the resulting slab length should be consistent with the distance from the present-day west coast of Corsica to the crest of the northern Apennines. This distance agrees well with a 400 km deep slab, as modeled in the present study.

The crust is relatively thin below the Northern Tyrrhenian and it thickens toward the Internal-External Apennines boundary where west-dipping thrusts involve basement rocks. This simultaneous crustal thinning in the Tyrrhenian-Tuscan extended terrains and thickening in the External Apennines is consistent with eastward migrating continental subduction and with delamination, as widely acknowledged in the literature. The crust becomes thicker below the Adriatic foreland basin system along the Adriatic Sea, reaching maximum crustal thickness below the Internal Dinarides. This thick crust corresponds to the point of maximum bending of the eastern region of the Adriatic microplate.

The most interesting results, however, are the negative thermal anomalies required at the upper mantle below the Apennines and Dinarides. Beneath the Apennines, we find a west-dipping attached cold lithospheric body down to 400 km. We interpret this anomaly as the Apenninic slab, most likely generated by subduction rollback of oceanic and Adriatic continental lithosphere in a first stage, followed by continental lithospheric mantle delamination, in agreement with previous interpretations (e.g., Benoit et al., 2011; Chiarabba et al., 2014). Assuming only subduction rollback of such a long continental slab is less likely than rollback of the delaminated lithospheric mantle, due to the positive buoyancy of the continental crust.

Below the Dinarides, our model suggests a much shorter east-dipping mantle anomaly, resulting in a lithospheric slab down to 250 km. Šumanovac and Dudjak (2016) interpret this fast velocity anomaly as a downgoing lithosphere slab that has been detached from the crust, sinking steeply beneath the Dinarides. Moreover, our modeled mantle wedge below the Dinarides and southwest of the Pannonian basin is consistent with the low-velocity

ZHANG ET AL. 16 of 24

zone imaged by Belinić et al. (2021). According to Belinić et al. (2021), the high velocity body indicates the possible delaminated lithospheric mantle slab, and the mentioned low-velocity zone the upwelling of hotter asthenospheric material, which agrees with our modeled cold sublithospheric anomaly and the mantle wedge. These two mantle anomalies are located far from the Ligurian Tethys and Vardar (Neo-Tethys) subduction zones. Therefore, these anomalies most likely represent sinking of continental lithosphere. Here we provide a unified view for the origin of these anomalies, as resulting from bidirectional post-collisional delamination of the Adriatic lithospheric mantle below the Apennines and the Dinarides orogens (Figure 7). Delamination related to the Apenninic slab resulted in a near vertical deeper slab and caused crustal and lithospheric thinning and partial melting in the Tyrrhenian-Tuscany region. The shallower anomaly beneath the Dinarides would be consistent with a shorter-lived delamination. On the basis of orogen-wide surface uplift of the Dinarides in Oligo-Miocene times and simultaneous emplacement of igneous rocks (33–22 Ma) in the Internal Dinarides, Balling et al. (2021) proposed post-collisional mantle delamination beginning at 28 Ma and terminated 22 Ma ago.

The thin lower crust below the Tuscany Magmatic Province and Dinarides and the current location of both slabs are compatible with their delamination once the continental collisions of Adria with Corsica Block and Tisza were accomplished with different ages and time lengths. The about 200°C colder bodies with respect to the surrounding rocks, their present size, position and coupling with shallower lithosphere have important consequences for both the evolution of the Apennines and Dinarides orogenic systems and the contribution to their recent dynamic topography.

The calculated isostatic elevation mostly matches the observed elevation except for the External Apennines, Dinarides and the Sava suture zone, where high-amplitude and medium to long-wavelength misfits are observed associated with the subducting slabs (Figure 5d). If we compute the effect of two end-member thermal isostatic models, with and without considering the effect of the sublithospheric anomalies, we observe that in the Apennines and Dinarides the slab deflects the elevation as much as 1,500 m (Figure 5d). This effect is to be expected since as mentioned the sublithospheric velocity anomalies (see Figure 3) are modeled as two thermal anomalies of  $-200^{\circ}$ C (Figures 5 and 6) that result in a colder and higher density zone than the surrounding sublithospheric mantle. Moreover, the thick lithosphere below the Adriatic Sea and the two deepening slabs at both edges pull down the topography of the Adriatic microplate below sea level. For most of the profile, assuming regional isostasy with an elastic thickness (Te) between 10 and 20 km considerably reduces the mismatch between observed and calculated elevation (Figure 5d). The resulting Te agrees with the values obtained by Tesauro et al. (2009), based on thermal and rheological data, which are in the range of 10–20 km along the Tyrrhenian, Apennines and Pannonian Basin, and 20–25 km along the Adriatic Basin and Dinarides (Figure 3 of Tesauro et al., 2009).

# 7. Conclusions

We present a geophysical-petrological model of the crust and upper mantle structure along a transect extending from the northern Tyrrhenian Sea to the Pannonian Basin, crossing the northern Apennines and the northern Dinarides fold-thrust belts. The model offers an integrated view of the complex structure of Adria and Tisza microplates and of the west- and east-dipping slabs occurring along both sides of the Adriatic foreland, building the Apennines and Dinarides orogenic systems. From our results we can draw the following conclusions:

- Adria and Tisza microplates bounded by the Sava Suture Zone have a better fit with the model if they are distinguished by different densities. The best fitting average density for the Adria crust is 2,830 kg/m³ whereas the Tisza crust shows a lower average density between 2,790 and 2,800 kg/m³. This is partly because the lower crust of the Tisza plate is much thinner than that of Adria. The Tyrrhenian Sea and the Internal Apennines are characterized by the presence of elevated temperatures at shallow crustal levels, which is consistent with well-documented magmatic intrusions. We also observe that the crustal structure of the Adria microplate is more complex than that of the Tisza plate, particularly near the collisional zones showing that subduction/ delamination in the area has mainly influenced the Adria domain. This is also observed at Moho levels, where major discrepancies between seismic data are found below the External Apennines and Dinarides. Our modeling permits us to solve these discrepancies and conclude that along the Internal Apennines the Moho lies at depths <25 km while along the External Apennines the Moho is found a depth of 55 km.</p>
- The LAB shows significant lateral variations mainly related to the two crustal domains, recording their different tectonic evolution from the Mesozoic onwards. Beneath the Tyrrhenian Sea the LAB is flat and shallow at ~75 km, slightly deepening toward the westernmost end of the profile. Below the Pannonian Basin the LAB

ZHANG ET AL. 17 of 24

18 of 24

Acknowledgments

We are grateful to Associate Editor

Peter DeCelles and two anonymous

reviewers for their constructive and

detailed comments. We thank Emanuel

David Kästle for making Figure 3c, Tena Belinic and co-authors for sharing their  $V_s$ 

model, and Eugenio Trumpy and Adele

Database obtained within Geothopica

Manzella for providing us the Geothermal

Project. This work is funded by GeoCAM (PGC2018-095154-B-I00) from the Span-

ish Government, the Generalitat de Cata-

lunya Grant (AGAUR 2017 SGR 847)

and ALORBE (PIE-CSIC-202030E10).

WZ is supported by the China Scholar-

ship Council (CSC-201904910470) and

EBG by the Spanish Government Grant

PRE2019-090524. This work has been

done using the facilities of the Labo-

ratory of Geodynamic Modeling from

Geo3BCN-CSIC. Figures were made with

the Generic Mapping Tools (www.soest.

hawaii.edu/gmt; Wessel & Smith, 1998).

ZHANG ET AL.

- remains quite flat although  $\sim$ 20 km deeper than the seismic one. Along the External Apennines and Dinarides we observe that the LAB deepens to 150 km depth but shallowing toward the Adriatic foreland basin reaching 125 km depth.
- Two thermo-compositional sublithospheric anomalies with a *T* anomaly of  $-200^{\circ}$ C relative to the surrounding mantle and with the same composition as the Adria lithospheric mantle are required to fit the geoid height and tomography studies. The presence of these thermal anomalies increases the density by 15–20 kg/m<sup>3</sup> allowing for a better fit of the geoid height and gravity anomaly and it is enough to reproduce the observed  $V_p$  and  $V_s$  anomalies. Below the Apennines, the west-dipping attached cold lithospheric slab reaches 400 km depth, which supports tomography models that favor the presence of a deep and cold anomaly as opposed to models that propose a shallower slab. Below the Dinarides, the east-dipping sublithospheric anomaly is shorter ending at 250 km depth, which agrees with seismic tomographic models.
- The lateral Adria LAB changes and the bidirectional sublithospheric anomalies below the Apennines and Dinarides are responsible for the resulting elevation, with low values in the Adriatic Sea due to its thick lithospheric mantle and the pulling down effect of the sublithospheric anomalies. Most of the elevation along the profile is under thermal isostasy. The observed elevation in the External Apennines, Dinarides and Sava Suture Zone can be explained assuming regional isostasy with an elastic thickness between 10 and 20 km.
- The model is compatible with two different lithospheric mantle compositions, a re-enriched basalt layer beneath the entire Adria microplate and a fertile mantle for the Tisza microplate lithospheric mantle. Moreover, the modeled lithospheric mantle composition below the Apennines and Dinarides is fertile compared to that of the rest of Adria and Tisza microplates. This is consistent with the presence of two sublithospheric mantle wedges, resulting from the bidirectional delamination of the Adria lithospheric mantle.

# **Data Availability Statement**

Software and data used in this work are open access and they can be found in references cited in the main text and figure captions. Data sets for this article are available in Digital CSIC (http://hdl.handle.net/10261/280680, http://dx.doi.org/10.20350/digitalCSIC/14759).

### References

Acocella, V., & Rossetti, F. (2002). The role of extensional tectonics at different crustal levels on granite ascent and emplacement: An example from Tuscany (Italy). *Tectonophysics*, 354(1), 71–83. https://doi.org/10.1016/S0040-1951(02)00290-1

Afonso, J. C., Fernàndez, M., Ranalli, G., Griffin, W. L., & Connolly, J. A. D. (2008). Integrated geophysical-petrological modeling of the lithosphere and sublithospheric upper mantle: Methodology and applications. *Geochemistry, Geophysics, Geosystems*, 9(5), Q05008. https://doi.org/10.1029/2007GC001834

Alasonati Tašárová, Z., Fullea, J., Bielik, M., & Środa, P. (2016). Lithospheric structure of Central Europe: Puzzle pieces from Pannonian Basin to trans-European Suture Zone resolved by geophysical-petrological modeling: Geophysical-petrological modeling. *Tectonics*, 35(3), 722–753. https://doi.org/10.1002/2015TC003935

Amaru, M. L. (2007). Global travel time tomography with 3-D reference models. Utrecht University. Retrieved from http://dspace.library.uu.nl/ handle/1874/19338

Artemieva, I. M. (2019). Lithosphere thermal thickness and geothermal heat flux in Greenland from a new thermal isostasy method. *Earth-Science Reviews*, 188, 469–481. https://doi.org/10.1016/j.earscirev.2018.10.015

Artemieva, I. M., & Thybo, H. (2013). EUNAseis: A seismic model for Moho and crustal structure in Europe, Greenland, and the North Atlantic region. *Tectonophysics*, 609, 97–153. https://doi.org/10.1016/j.tecto.2013.08.004

Bada, G., Horváth, F., Dövényi, P., Szafián, P., Windhoffer, G., & Cloetingh, S. (2007). Present-day stress field and tectonic inversion in the Pannonian basin. *Global and Planetary Change*, 58(1), 165–180. https://doi.org/10.1016/j.gloplacha.2007.01.007

Balling, P., Tomljenović, B., Schmid, S. M., & Ustaszewski, K. (2021). Contrasting along-strike deformation styles in the central external Dinarides assessed by balanced cross-sections: Implications for the tectonic evolution of its Paleogene flexural foreland basin system. *Global and Planetary Change*, 205, 103587. https://doi.org/10.1016/j.gloplacha.2021.103587

Bally, A. W. (1987). Balanced sections and seismic reflection profiles across the Central Apennines, Italy. *Memoirs Geological Society Italy*, 29(8), 11–12.

Barchi, M., Minelli, G., Magnani, B., & Mazzotti, A. (2003). Line CROP 03: Northern Apennines. In *Memorie Descrittive della Carta geologica d'Italia LXII* (Vol. 62, pp. 127–136).

Barchi, M., Minelli, G., & Pialli, G. (1998). The Crop 03 profile: A synthesis of results on deep structures of the Northern Apennines. *Memorie della Societa Geologica Italiana*, 52, 383–400.

Barchi, M., Pauselli, C., Chiarabba, C., Di Stefano, R., Federico, C., & Minelli, G. (2006). Crustal structure, tectonic evolution and seismogenesis in the Northern Apennines (Italy). *Bollettino di Geofisica Teorica ed Applicata*, 47, 249–270.

Barchi, M. R., Carboni, F., Michele, M., Ercoli, M., Giorgetti, C., Porreca, M., et al. (2021). The influence of subsurface geology on the distribution of earthquakes during the 2016–2017 Central Italy seismic sequence. *Tectonophysics*, 807, 228797. https://doi.org/10.1016/j. tecto.2021.228797

Basili, R., & Barba, S. (2007). Migration and shortening rates in the northern Apennines, Italy: Implications for seismic hazard. *Terra Nova*, 19(6), 462–468. https://doi.org/10.1111/j.1365-3121.2007.00772.x

- Belinić, T., Kolínský, P., & Stipčević, J. (2021). Shear-wave velocity structure beneath the Dinarides from the inversion of Rayleigh-wave dispersion. Earth and Planetary Science Letters, 555, 116686. https://doi.org/10.1016/j.epsl.2020.116686
- Belinić, T., Stipčević, J., & Živčić, M. (2018). Lithospheric thickness under the Dinarides. Earth and Planetary Science Letters, 484, 229–240. https://doi.org/10.1016/j.epsl.2017.12.030
- Beller, S., Monteiller, V., Operto, S., Nolet, G., Paul, A., & Zhao, L. (2018). Lithospheric architecture of the South-Western Alps revealed by multiparameter teleseismic full-waveform inversion. *Geophysical Journal International*, 212(2), 1369–1388. https://doi.org/10.1093/gji/ggx216
- Benoit, M. H., Torpey, M., Liszewski, K., Levin, V., & Park, J. (2011). P and S wave upper mantle seismic velocity structure beneath the northern Apennines: New evidence for the end of subduction. *Geochemistry, Geophysics, Geosystems*, 12(6), Q06004. https://doi.org/10.1029/2010GC003428
- Bianco, C., Brogi, A., Caggianelli, A., Giorgetti, G., Liotta, D., & Meccheri, M. (2015). HP-LT metamorphism in Elba island: Implications for the geodynamic evolution of the inner Northern Apennines (Italy). *Journal of Geodynamics*, 91, 13–25. https://doi.org/10.1016/j.jog.2015.08.001
- Blom, N., Gokhberg, A., & Fichtner, A. (2020). Seismic waveform tomography of the central and eastern Mediterranean upper mantle. *Solid Earth*, 11(2), 669–690. https://doi.org/10.5194/se-11-669-2020
- Boccaletti, M., Ciaranfi, N., Cosentino, D., Deiana, G., Gelati, R., Lentini, F., et al. (1990). Palinspastic restoration and paleogeographic reconstruction of the peri-Tyrrhenian area during the Neogene. *Palaeogeography, Palaeoclimatology, Palaeoecology*, 77(1), 41-IN13–IN13. https://doi.org/10.1016/0031-0182(90)90097-O
- Bondár, I., Mónus, P., Czanik, C., Kiszely, M., Gráczer, Z., & Wéber, Z., & the AlpArrayWorking Group. (2018). Relocation of seismicity in the Pannonian basin using a global 3D velocity model. Seismological Research Letters, 89(6), 2284–2293. https://doi.org/10.1785/0220180143
- Bonini, M., & Sani, F. (2002). Extension and compression in the Northern Apennines (Italy) hinterland: Evidence from the late Miocene-Pliocene Siena-Radicofani Basin and relations with basement structures. *Tectonics*, 21(3), 1-1-1-32. https://doi.org/10.1029/2001TC900024
- Brocher, T. M. (2005). Empirical relations between elastic wavespeeds and density in the Earth's crust. *Bulletin of the Seismological Society of America*, 95(6), 2081–2092. https://doi.org/10.1785/0120050077
- Butler, R. W. H., Mazzoli, S., Corrado, S., De Donatis, M., Di Bucci, D., Gambini, R., et al. (2004). Applying thick-skinned tectonic models to
- the Apennine thrust belt of Italy—Limitations and implications.

  Carballo, A., Fernandez, M., Torne, M., Jiménez-Munt, I., & Villaseñor, A. (2015). Thermal and petrophysical characterization of the lithospheric
- mantle along the northeastern Iberia geo-transect. Gondwana Research, 27(4), 1430–1445. https://doi.org/10.1016/j.gr.2013.12.012
- Carminati, E., & Doglioni, C. (2012). Alps vs. Apennines: The paradigm of a tectonically asymmetric Earth. Earth-Science Reviews, 112(1), 67–96. https://doi.org/10.1016/j.earscirev.2012.02.004
- Carminati, E., Lustrino, M., & Doglioni, C. (2012). Geodynamic evolution of the central and western Mediterranean: Tectonics vs. igneous petrology constraints. *Tectonophysics*, 579, 173–192. https://doi.org/10.1016/j.tecto.2012.01.026
- Carminati, E., Petricca, P., & Doglioni, C. (2020). Mediterranean tectonics. In D. Alderton & S. A. Elias (Eds.), Encyclopedia of geology (2nd ed., pp. 408–419). Academic Press. https://doi.org/10.1016/B978-0-08-102908-4.00010-2
- Cassinis, R., Scarascia, S., Lozej, A., & Finetti, I. R. (2005). Review of seismic wide-angle reflection—refraction (WARR) results in the Italian region (1956–1987). In CROP project: Deep seismic exploration of the central Mediterranean and Italy (pp. 31–55). Elsevier Amsterdam.
- Cavinato, G. P., & DeCelles, P. (1999). Extensional basins in the tectonically bimodal central Apennines fold-thrust belt, Italy: Response to corner flow above a subducting slab in retrograde motion. *Geology*, 27(10), 955–958. https://doi.org/10.1130/0091-7613(1999)027<0955:ebittb>2 3 co<sup>2</sup>2
- Channell, J. E. T., Tüysüz, O., Bektas, O., & Sengör, A. M. C. (1996). Jurassic-Cretaceous paleomagnetism and paleogeography of the Pontides (Turkey). *Tectonics*, 15(1), 201–212. https://doi.org/10.1029/95TC02290
- Chiarabba, C., Bianchi, I., De Gori, P., & Agostinetti, N. P. (2020). Mantle upwelling beneath the Apennines identified by receiver function imaging. Scientific Reports, 10(1), 19760. https://doi.org/10.1038/s41598-020-76515-2
- Chiarabba, C., Giacomuzzi, G., Bianchi, I., Agostinetti, N. P., & Park, J. (2014). From underplating to delamination-retreat in the northern Apennines. Earth and Planetary Science Letters, 403, 108–116. https://doi.org/10.1016/j.epsl.2014.06.041
- Chiarabba, C., Jovane, L., & DiStefano, R. (2005). A new view of Italian seismicity using 20 years of instrumental recordings. *Tectonophysics*, 395(3), 251–268. https://doi.org/10.1016/j.tecto.2004.09.013
- 6/10/2014-206. https://doi.org/10.1100/j.etoi.2004.05.013 Chiarabba, C., Pino, N. A., Ventura, G., & Vilardo, G. (2004). Structural features of the shallow plumbing system of Vulcano Island Italy. Bulletin of Volcanology, 66(6), 477-484. https://doi.org/10.1007/s00445-003-0331-9
- Chiari, M., Djerić, N., Garfagnoli, F., Hrvatović, H., Krstić, M., Levi, N., et al. (2011). The geology of the Zlatibor-Maljen area (western Serbia): A geotraverse across the ophiolites of the Dinaric-Hellenic collisional belt. *Ofioliti*, 36(2), 139–166. https://doi.org/10.4454/OFIOLITI.V36.12.3
- Collettini, C., & Barchi, M. R. (2002). A low-angle normal fault in the Umbria region (Central Italy): A mechanical model for the related microseismicity. *Tectonophysics*, 359(1–2), 97–115. https://doi.org/10.1016/s0040-1951(02)00441-9
- Connolly, J. A. D. (2005). Computation of phase equilibria by linear programming: A tool for geodynamic modeling and its application to subduction zone decarbonation. Earth and Planetary Science Letters, 236(1), 524–541. https://doi.org/10.1016/j.epsl.2005.04.033
- Connolly, J. A. D. (2009). The geodynamic equation of state: What and how. Geochemistry, Geophysics, Geosystems, 10(10), Q10014. https://doi.org/10.1029/2009GC002540
- Conti, P., Cornamusini, G., & Carmignani, L. (2020). An outline of the geology of the northern Apennines (Italy), with geological map at 1: 250,000 scale. *Italian Journal of Geosciences*, 139(2), 149–194. https://doi.org/10.3301/ijg.2019.25
- Cosentino, D., Cipollari, P., Marsili, P., & Scrocca, D. (2010). Geology of the central Apennines: A regional review. *Journal of the Virtual Explorer*, 36, 1–37. https://doi.org/10.3809/ivirtex.2010.00223
- Coward, M. P., De Donatis, M., Mazzoli, S., Paltrinieri, W., & Wezel, F. C. (1999). Frontal part of the northern Apennines fold and thrust belt in the Romagna-Marche area (Italy): Shallow and deep structural styles. *Tectonics*, 18(3), 559–574. https://doi.org/10.1029/1999TC900003
- Csontos, L., & Nagymarosy, A. (1998). The Mid-Hungarian line: A zone of repeated tectonic inversions. *Tectonophysics*, 297(1), 51–71. https://doi.org/10.1016/S0040-1951(98)00163-2
- Cuffaro, M., Riguzzi, F., Scrocca, D., Antonioli, F., Carminati, E., Livani, M., & Doglioni, C. (2010). On the geodynamics of the northern Adriatic plate. *Rendiconti Lincei*, 21(1), 253–279. https://doi.org/10.1007/s12210-010-0098-9
- Curzi, M., Aldega, L., Bernasconi, S. M., Berra, F., Billi, A., Boschi, C., et al. (2020). Architecture and evolution of an extensionally-inverted thrust (Mt. Tancia Thrust, Central Apennines): Geological, structural, geochemical, and K–Ar geochronological constraints. *Journal of Structural Geology*, 136, 104059. https://doi.org/10.1016/j.jsg.2020.104059
- D'Acquisto, M., Dal Zilio, L., Molinari, I., Kissling, E., Gerya, T., & van Dinther, Y. (2020). Tectonics and seismicity in the northern Apennines driven by slab retreat and lithospheric delamination. *Tectonophysics*, 789, 228481. https://doi.org/10.1016/j.tecto.2020.228481

ZHANG ET AL. 19 of 24

21699356, 2022, 12, Dov

- De Luca, G., Cattaneo, M., Monachesi, G., & Amato, A. (2009). Seismicity in central and northern Apennines integrating the Italian national and regional networks. *Tectonophysics*, 476(1), 121–135. https://doi.org/10.1016/j.tecto.2008.11.032
- Dewey, J. F., Helman, M. L., Knott, S. D., Turco, E., & Hutton, D. H. W. (1989). Kinematics of the western Mediterranean. *Geological Society, London, Special Publications*, 45(1), 265–283. https://doi.org/10.1144/GSL.SP.1989.045.01.15
- Diaferia, G., Cammarano, F., Piana Agostinetti, N., Gao, C., Lekic, V., Molinari, I., & Boschi, L. (2019). Inferring Crustal temperatures beneath Italy from joint inversion of receiver functions and surface waves. *Journal of Geophysical Research: Solid Earth*, 124(8), 8771–8785. https://doi.org/10.1029/2019JB018340
- Dini, A., Gianelli, G., Puxeddu, M., & Ruggieri, G. (2005). Origin and evolution of Pliocene–Pleistocene granites from the Larderello geothermal field (Tuscan Magmatic Province, Italy). Lithos, 81(1), 1–31. https://doi.org/10.1016/j.lithos.2004.09.002
- Dini, A., Innocenti, F., Rocchi, S., Tonarini, S., & Westerman, D. S. (2002). The magmatic evolution of the late Miocene laccolith–pluton–dyke granitic complex of Elba Island, Italy. *Geological Magazine*, 139(3), 257–279. https://doi.org/10.1017/S0016756802006556
- Doglioni, C. (1991). A proposal for the kinematic modelling of W-dipping subductions—Possible applications to the Tyrrhenian-Apennines system. *Terra Nova*, 3(4), 423–434. https://doi.org/10.1111/j.1365-3121.1991.tb00172.x
- Doglioni, C., Gueguen, E., Sàbat, F., & Fernandez, M. (1997). The western Mediterranean extensional basins and the Alpine orogen. *Terra Nova*, 9(3), 109–112. https://doi.org/10.1046/j.1365-3121.1997.d01-18.x
- Doglioni, C., Harabaglia, P., Martinelli, G., Mongelli, F., & Zito, G. (1996). A geodynamic model of the Southern Apennines accretionary prism. Terra Nova, 8(6), 540–547. https://doi.org/10.1111/j.1365-3121.1996.tb00783.x
- Downes, H., Embey-Isztin, A., & Thirlwall, M. F. (1992). Petrology and geochemistry of spinel peridotite xenoliths from the western Pannonian Basin (Hungary): Evidence for an association between enrichment and texture in the upper mantle. *Contributions to Mineralogy and Petrology*, 109(3), 340–354. https://doi.org/10.1007/BF00283323
- El-Sharkawy, A., Meier, T., Lebedev, S., Behrmann, J. H., Hamada, M., Cristiano, L., et al. (2020). The slab puzzle of the Alpine-Mediterranean region: Insights from a new, high-resolution, shear wave velocity model of the upper mantle. *Geochemistry, Geophysics, Geosystems*, 21(8), e2020GC008993. https://doi.org/10.1029/2020GC008993
- Faccenna, C., Becker, T. W., Auer, L., Billi, A., Boschi, L., Brun, J. P., et al. (2014). Mantle dynamics in the Mediterranean. Reviews of Geophysics, 52(3), 283–332. https://doi.org/10.1002/2013RG000444
- Faccenna, C., Becker, T. W., Lucente, F. P., Jolivet, L., & Rossetti, F. (2001). History of subduction and back are extension in the Central Mediterranean. *Geophysical Journal International*, 145(3), 809–820. https://doi.org/10.1046/j.0956-540x.2001.01435.x
- Fantoni, R., & Franciosi, R. (2010). Tectono-sedimentary setting of the Po plain and Adriatic foreland. Rendiconti Lincei, 21(1), 197–209. https://doi.org/10.1007/s12210-010-0102-4
- Fernàndez, M., Afonso, J. C., & Ranalli, G. (2010). The deep lithospheric structure of the Namibian volcanic margin. *Tectonophysics*, 481(1–4), 68–81. https://doi.org/10.1016/j.tecto.2009.02.036
- Finetti, I. R., Boccaletti, M., Bonini, M., Del Ben, A., Geletti, R., Pipan, M., & Sani, F. (2001). Crustal section based on CROP seismic data across the North Tyrrhenian–Northern Apennines–Adriatic Sea. *Tectonophysics*, 343(3), 135–163. https://doi.org/10.1016/S0040-1951(01)00141-X Fuchs, S., & Norden, B. (2021). The global heat flow database: Release 2021. https://doi.org/10.5880/fidgeo.2021.014
- Fullea, J., Fernàndez, M., & Zeyen, H. (2008). FA2BOUG—A FORTRAN 90 code to compute Bouguer gravity anomalies from gridded free-air anomalies: Application to the Atlantic-Mediterranean transition zone. *Computers & Geosciences*, 34(12), 1665–1681. https://doi.org/10.1016/j.cageo.2008.02.018
- Gallhofer, D., von Quadt, A., Schmid, S. M., Guillong, M., Peytcheva, I., & Seghedi, I. (2017). Magmatic and tectonic history of Jurassic ophiolites and associated granitoids from the South Apuseni Mountains (Romania). Swiss Journal of Geosciences, 110(2), 699–719. https://doi.org/10.1007/s00015-016-0231-6
- Geissler, W. H., Sodoudi, F., & Kind, R. (2010). Thickness of the central and eastern European lithosphere as seen by S receiver functions. *Geophysical Journal International*, 181(2), 604–634. https://doi.org/10.1111/j.1365-246X.2010.04548.x
- Ghielmi, M., Minervini, M., Nini, C., Rogledi, S., Rossi, M., & Vignolo, A. (2010). Sedimentary and tectonic evolution in the eastern Po-plain and northern Adriatic Sea area from Messinian to Middle Pleistocene (Italy). *Rendiconti Lincei*, 21(1), 131–166. https://doi.org/10.1007/s12210-010-0101-5
- Giacomuzzi, G., Chiarabba, C., & De Gori, P. (2011). Linking the Alps and Apennines subduction systems: New constraints revealed by high-resolution teleseismic tomography. Earth and Planetary Science Letters, 301(3), 531–543. https://doi.org/10.1016/j.epsl.2010.11.033
- Gilardoni, M., Reguzzoni, M., & Sampietro, D. (2016). GECO: A global gravity model by locally combining GOCE data and EGM2008. Studia Geophysica et Geodaetica, 60(2), 228–247. https://doi.org/10.1007/s11200-015-1114-4
- Grad, M., & Tiira, T., & ESC Working Group. (2009). The Moho depth map of the European Plate. *Geophysical Journal International*, 176(1), 279–292. https://doi.org/10.1111/j.1365-246X.2008.03919.x
- Griffin, W. L., O'Reilly, S. Y., Afonso, J. C., & Begg, G. C. (2009). The composition and evolution of lithospheric mantle: A re-evaluation and its tectonic implications. *Journal of Petrology*, 50(7), 1185–1204. https://doi.org/10.1093/petrology/egn033
- Handy, M. R., Schmid, S. M., Bousquet, R., Kissling, E., & Bernoulli, D. (2010). Reconciling plate-tectonic reconstructions of Alpine Tethys with the geological–geophysical record of spreading and subduction in the Alps. Earth-Science Reviews, 102(3), 121–158. https://doi.org/10.1016/j. earscirev.2010.06.002
- Handy, M. R., Schmid, S. M., Paffrath, M., & Friederich, W., & the AlpArray Working Group. (2021). Orogenic lithosphere and slabs in the greater Alpine area—Interpretations based on teleseismic P-wave tomography. *Solid Earth*, 12(11), 2633–2669. https://doi.org/10.5194/se\_12\_2633\_2021
- Handy, M. R., Ustaszewski, K., & Kissling, E. (2015). Reconstructing the Alps-Carpathians-Dinarides as a key to understanding switches in subduction polarity, slab gaps and surface motion. *International Journal of Earth Sciences*, 104(1), 1–26. https://doi.org/10.1007/ s00531-014-1060-3
- Hetényi, G., Ren, Y., Dando, B., Stuart, G. W., Hegedűs, E., Kovács, A. C., & Houseman, G. A. (2015). Crustal structure of the Pannonian Basin: The AlCaPa and Tisza terrains and the Mid-Hungarian zone. *Tectonophysics*, 646, 106–116. https://doi.org/10.1016/j.tecto.2015.02.004
- Horváth, F. (1995). Phases of compression during the evolution of the Pannonian Basin and its bearing on hydrocarbon exploration. *Marine and Petroleum Geology*, 12(8), 837–844. https://doi.org/10.1016/0264-8172(95)98851-U
- Horváth, F., Bada, G., Szafián, P., Tari, G., Ádám, A., & Cloetingh, S. (2006). Formation and deformation of the Pannonian Basin: Constraints from observational data. *Geological Society, London, Memoirs*, 32(1), 191–206. https://doi.org/10.1144/GSL.MEM.2006.032.01.11
- Hua, Y., Zhao, D., & Xu, Y. (2017). P wave anisotropic tomography of the Alps. Journal of Geophysical Research: Solid Earth, 122(6), 4509–4528. https://doi.org/10.1002/2016JB013831

ZHANG ET AL. 20 of 24

- Jiménez-Munt, I., Torne, M., Fernàndez, M., Vergés, J., Kumar, A., Carballo, A., & García-Castellanos, D. (2019). Deep seated density anomalies across the Iberia-Africa plate boundary and its topographic response. *Journal of Geophysical Research: Solid Earth*, 124(12), 13310–13332. https://doi.org/10.1029/2019JB018445
- Jolivet, L., Faccenna, C., Goffé, B., Mattei, M., Rossetti, F., Brunet, C., et al. (1998). Midcrustal shear zones in postorogenic extension: Example from the northern Tyrrhenian Sea. *Journal of Geophysical Research*, 103(B6), 12123–12160. https://doi.org/10.1029/97JB03616
- Kapuralić, J., Šumanovac, F., & Markušić, S. (2019). Crustal structure of the northern Dinarides and southwestern part of the Pannonian basin inferred from local earthquake tomography. Swiss Journal of Geosciences, 112(1), 181–198. https://doi.org/10.1007/s00015-018-0335-2
- Kästle, E. D., El-Sharkawy, A., Boschi, L., Meier, T., Rosenberg, C., Bellahsen, N., et al. (2018). Surface wave tomography of the Alps using ambient-noise and earthquake phase velocity measurements. *Journal of Geophysical Research: Solid Earth*, 123(2), 1770–1792. https://doi.org/10.1002/2017JB014698
- Kästle, E. D., Molinari, I., Boschi, L., & Kissling, E., & the AlpArray Working Group. (2022). Azimuthal anisotropy from eikonal tomography: Example from ambient-noise measurements in the AlpArray network. Geophysical Journal International, 229(1), 151–170. https://doi.org/10.1093/gji/ggab453
- Kästle, E. D., Rosenberg, C., Boschi, L., Bellahsen, N., Meier, T., & El-Sharkawy, A. (2020). Slab break-offs in the Alpine subduction zone. International Journal of Earth Sciences, 109(2), 587–603. https://doi.org/10.1007/s00531-020-01821-z
- Keller, J. V. A., & Coward, M. P. (1996). The structure and evolution of the northern Tyrrhenian Sea. Geological Magazine, 133(1), 1–16. https://doi.org/10.1017/S0016756800007214
- Keller, J. V. A., Minelli, G., & Pialli, G. (1994). Anatomy of late orogenic extension: The Northern Apennines case. *Tectonophysics*, 238(1), 275–294. https://doi.org/10.1016/0040-1951(94)90060-4
- Korbar, T. (2009). Orogenic evolution of the External Dinarides in the NE Adriatic region: A model constrained by tectonostratigraphy of Upper Cretaceous to Paleogene carbonates. *Earth-Science Reviews*, 96(4), 296–312. https://doi.org/10.1016/j.earscirev.2009.07.004
- Koroknai, B., Wórum, G., Tóth, T., Koroknai, Z., Fekete-Németh, V., & Kovács, G. (2020). Geological deformations in the Pannonian basin during the neotectonic phase: New insights from the latest regional mapping in Hungary. *Earth-Science Reviews*, 211, 103411. https://doi. org/10.1016/j.earscirev.2020.103411
- Koulakov, I., Jakovlev, A., Zabelina, I., Roure, F., Cloetingh, S., El Khrepy, S., & Al-Arifi, N. (2015). Subduction or delamination beneath the Apennines? Evidence from regional tomography. Solid Earth, 6(2), 669–679. https://doi.org/10.5194/se-6-669-2015
- Koulakov, I., Kaban, M. K., Tesauro, M., & Cloetingh, S. (2009). P- and S-velocity anomalies in the upper mantle beneath Europe from tomographic inversion of ISC data. Geophysical Journal International, 179(1), 345–366. https://doi.org/10.1111/j.1365-246X.2009.04279.x
- Kovács, I., Csontos, L., Szabó, C. S., Bali, E., Falus, G., Benedek, K., & Zajacz, Z. (2007). Paleogene–early Miocene igneous rocks and geodynamics of the Alpine-Carpathian-Pannonian-Dinaric region: An integrated approach. In L. Beccaluva, G. Bianchini, & M. Wilson (Eds.), Cenozoic volcanism in the Mediterranean area. Geological Society of America. https://doi.org/10.1130/2007.2418(05)
- Kuk, V., Prelogović, E., & Dragičević, I. (2000). Seismotectonically active zones in the Dinarides. Geologia Croatica, 53(2), 295–303,
- Kumar, A., Fernàndez, M., Jiménez-Munt, I., Torne, M., Vergés, J., & Afonso, J. C. (2020). LitMod2D\_2.0: An improved integrated geophysical-petrological modeling tool for the physical interpretation of upper mantle anomalies. *Geochemistry, Geophysics, Geosystems*, 21(3), e2019GC008777. https://doi.org/10.1029/2019GC008777
- Kumar, A., Fernàndez, M., Vergés, J., Torne, M., & Jiménez-Munt, I. (2021). Opposite symmetry in the lithospheric structure of the Alboran and Algerian basins and their margins (Western Mediterranean): Geodynamic implications. *Journal of Geophysical Research: Solid Earth*, 126(7), e2020JB021388. https://doi.org/10.1029/2020JB021388
- Lacombe, O., & Jolivet, L. (2005). Structural and kinematic relationships between Corsica and the Pyrenees-Provence domain at the time of the Pyrenean orogeny. *Tectonics*, 24(1). https://doi.org/10.1029/2004TC001673
- Laske, G., Masters, G., Ma, Z., & Pasyanos, M. (2013). Update on CRUST1.0—A 1-degree global model of Earth's Crust. In Geophysical research abstracts EGU2013-2658 (Vol. 15).
- Le Breton, E., Handy, M. R., Molli, G., & Ustaszewski, K. (2017). Post-20 Ma motion of the Adriatic Plate: New Constraints from surrounding orogens and implications for crust-mantle Decoupling. *Tectonics*, 36(12), 3135–3154. https://doi.org/10.1002/2016TC004443
- Liotta, D., Cernobori, L., & Nicolich, R. (1998). Restricted rifting and its consistence with compressional structures: Results from CROP 3 traverse (Northern Apenninies, Italy). Terra Nova, 10(1), 16–20. https://doi.org/10.1046/j.1365-3121.1998.00157.x
- Lippitsch, R., Kissling, E., & Ansorge, J. (2003). Upper mantle structure beneath the Alpine orogen from high-resolution teleseismic tomography. Journal of Geophysical Research, 108(B8), 2376. https://doi.org/10.1029/2002JB002016
- Lucente, F. P., Chiarabba, C., Cimini, G. B., & Giardini, D. (1999). Tomographic constraints on the geodynamic evolution of the Italian region. Journal of Geophysical Research, 104(B9), 20307–20327. https://doi.org/10.1029/1999JB900147
- Lustrino, M., Chiarabba, C., & Carminati, E. (2022). Igneous activity in central-southern Italy: Is the subduction paradigm still valid? In the footsteps of Warren B. Hamilton: New ideas in earth science. Geological Society of America. https://doi.org/10.1130/2021.2553(28)
- Maesano, F. E., Toscani, G., Burrato, P., Mirabella, F., D'Ambrogi, C., & Basili, R. (2013). Deriving thrust fault slip rates from geological modeling: Examples from the Marche coastal and offshore contraction belt, northern Apennines, Italy. *Marine and Petroleum Geology*, 42, 122–134. https://doi.org/10.1016/j.marpetgeo.2012.10.008
- Maffione, M., & van Hinsbergen, D. J. J. (2018). Reconstructing plate boundaries in the Jurassic neo-Tethys from the east and west Vardar ophiolites (Greece and Serbia). *Tectonics*, 37(3), 858–887. https://doi.org/10.1002/2017TC004790
- Malinverno, A., & Ryan, W. B. F. (1986). Extension in the Tyrrhenian Sea and shortening in the Apennines as result of arc migration driven by sinking of the lithosphere. *Tectonics*, 5(2), 227–245. https://doi.org/10.1029/TC005i002p00227
- Massoli, D., Koyi, H. A., & Barchi, M. R. (2006). Structural evolution of a fold and thrust belt generated by multiple décollements: Analogue models and natural examples from the Northern Apennines (Italy). *Journal of Structural Geology*, 28(2), 185–199. https://doi.org/10.1016/j.isg.2005.11.002
- Matenco, L., & Radivojević, D. (2012). On the formation and evolution of the Pannonian Basin: Constraints derived from the structure of the junction area between the Carpathians and Dinarides. *Tectonics*, 31(6), 6007. https://doi.org/10.1029/2012TC003206
- Mazzoli, S., Pierantoni, P. P., Borraccini, F., Paltrinieri, W., & Deiana, G. (2005). Geometry, segmentation pattern and displacement variations along a major Apennine thrust zone, central Italy. *Journal of Structural Geology*, 27(11), 1940–1953. https://doi.org/10.1016/j.jsg.2005.06.002
- Mele, G., & Sandvol, E. (2003). Deep crustal roots beneath the northern Apennines inferred from teleseismic receiver functions. *Earth and Planetary Science Letters*, 211(1), 69–78. https://doi.org/10.1016/S0012-821X(03)00185-7
- Miller, M. S., & Piana Agostinetti, N. (2012). Insights into the evolution of the Italian lithospheric structure from S receiver function analysis. Earth and Planetary Science Letters, 345(348), 49–59. https://doi.org/10.1016/j.epsl.2012.06.028

ZHANG ET AL. 21 of 24

21699356, 2022, 12, Dow

- Moeller, S., Grevemeyer, I., Ranero, C. R., Berndt, C., Klaeschen, D., Sallares, V., et al. (2013). Early-stage rifting of the northern Tyrrhenian Sea Basin: Results from a combined wide-angle and multichannel seismic study. *Geochemistry, Geophysics, Geosystems*, 14(8), 3032–3052. https://doi.org/10.1002/ggge.20180
- Moeller, S., Grevemeyer, I., Ranero, C. R., Berndt, C., Klaeschen, D., Sallares, V., et al. (2014). Crustal thinning in the northern Tyrrhenian Rift: Insights from multichannel and wide-angle seismic data across the basin. *Journal of Geophysical Research: Solid Earth*, 119(3), 1655–1677. https://doi.org/10.1002/2013JB010431
- Molinari, I., & Morelli, A. (2011). EPcrust: A reference crustal model for the European plate. *Geophysical Journal International*, 185(1), 352–364. https://doi.org/10.1111/j.1365-246X.2011.04940.x
- Molinari, I., Verbeke, J., Boschi, L., Kissling, E., & Morelli, A. (2015). Italian and Alpine three-dimensional crustal structure imaged by ambient-noise surface-wave dispersion. Geochemistry, Geophysics, Geosystems, 16(12), 4405–4421. https://doi.org/10.1002/2015GC006176
  Malli, G. (2008). Northern Appraisa. Considerations of the control o
- Molli, G. (2008). Northern Apennine-Corsica orogenic system: An updated overview. Geological Society, London, Special Publications, 298(1), 413-442. https://doi.org/10.1144/SP298.19
- Molli, G., Crispini, L., Malusà, M. G., Mosca, P., Piana, F., & Federico, L. (2010). Geology of the Western Alps-Northern Apennine junction area: A regional review. *Journal of the Virtual Explorer*, 36, 1–49. https://doi.org/10.3809/jvirtex.2010.00215
- Mostardini, F., & Merlini, S. (1986). Appennino centro-meridionale: Sesioni geologiche e proposta di modello strutturale. *Memorie della Societa Geologica Italiana*, 35, 177–202.
- Noguera, A. M., & Rea, G. (2000). Deep structure of the Campanian–Lucanian arc (southern Apennine, Italy). *Tectonophysics*, 324(4), 239–265. https://doi.org/10.1016/S0040-1951(00)00137-2
- Norden, B., & Förster, A. (2006). Thermal conductivity and radiogenic heat production of sedimentary and magmatic rocks in the Northeast German Basin. AAPG Bulletin, 90(6), 939–962. https://doi.org/10.1306/01250605100
- Pamić, J., Balen, D., & Herak, M. (2002). Origin and geodynamic evolution of Late Paleogene magmatic associations along the Periadriatic-Sava-Vardar magmatic belt. Geodinamica Acta, 15(4), 209–231. https://doi.org/10.1080/09853111.2002.10510755
- Pamić, J., Gušić, I., & Jelaska, V. (1998). Geodynamic evolution of the Central Dinarides. Tectonophysics, 297(1), 251–268. https://doi.org/10.1016/S0040-1951(98)00171-1
- Pandeli, E., Principi, G., Bortolotti, V., Benvenuti, M., Fazzuoli, M., Dini, A., et al. (2013). The Elba island: An intriguing geological puzzle in the northern Tyrrhenian Sea. In ISPRA and Soc. Geol. It., Geol. Field Trips, 5(2.1).
- Patacca, E., Sartori, R., & Scandone, P. (1990). Tyrrhenian Basin and Apenninic arcs: Kinematic relations since late Tortonian times. Memorie della Societa Geologica Italiana, 45, 425–451.
- Patacca, E., & Scandone, P. (2001). Late thrust propagation and sedimentary response in the thrust-belt—Foredeep system of the southern Apennines (Pliocene-Pleistocene). In G. B. Vai & I. P. Martini (Eds.), Anatomy of an orogen: The Apennines and adjacent Mediterranean basins (pp. 401–440). Springer Netherlands. https://doi.org/10.1007/978-94-015-9829-3 23
- Patacca, E., & Scandone, P. (2007). Geological interpretation of the CROP-04 seismic line (Southern Apennines, Italy). Bollettino-Societa Geologica Italiana, 7, 297–315.
- Pauselli, C., Barchi, M. R., Federico, C., Magnani, M. B., & Minelli, G. (2006). The crustal structure of the Northern Apennines (Central Italy): An insight by the CROP03 seismic line. *American Journal of Science*, 306(6), 428–450. https://doi.org/10.2475/06.2006.02
- Pauselli, C., Gola, G., Mancinelli, P., Trumpy, E., Saccone, M., Manzella, A., & Ranalli, G. (2019). A new surface heat flow map of the Northern Apennines between latitudes 42.5 and 44.5 N. Geothermics, 81, 39–52. https://doi.org/10.1016/j.geothermics.2019.04.002
- Peccerillo, A. (2005). Plio-quaternary volcanism in Italy: Petrology, geochemistry, geodynamics. Springer.
- Pedreira, D., Afonso, J. C., Pulgar, J. A., Gallastegui, J., Carballo, A., Fernàndez, M., et al. (2015). Geophysical-petrological modeling of the lithosphere beneath the Cantabrian Mountains and the North-Iberian margin: Geodynamic implications. *Lithos*, 230, 46–68. https://doi. org/10.1016/j.lithos.2015.04.018
- Piana Agostinetti, N., & Amato, A. (2009). Moho depth and Vp/Vs ratio in peninsular Italy from teleseismic receiver functions. *Journal of Geophysical Research*, 114(B6), B06303. https://doi.org/10.1029/2008JB005899
- Piana Agostinetti, N., & Faccenna, C. (2018). Deep structure of Northern Apennines subduction orogen (Italy) as revealed by a joint interpretation of passive and active seismic data. *Geophysical Research Letters*, 45(9), 4017–4024. https://doi.org/10.1029/2018GL077640
- Piromallo, C., & Morelli, A. (2003). P wave tomography of the mantle under the Alpine-Mediterranean area. *Journal of Geophysical Research*, 108(B2), 2065. https://doi.org/10.1029/2002JB001757
- Placer, L., Vrabec, M., & Celarc, B. (2010). The bases for understanding of the NW Dinarides and Istria Peninsula tectonics. *Geologija*, 53(1), 55–86. https://doi.org/10.5474/geologija.2010.005
- Plomerová, J., & Babuška, V. (2010). Long memory of mantle lithosphere fabric—European LAB constrained from seismic anisotropy. *Lithos*, 120(1), 131–143. https://doi.org/10.1016/j.lithos.2010.01.008
- Robertson, A., Karamata, S., & Šarić, K. (2009). Overview of ophiolites and related units in the Late Palaeozoic–Early Cenozoic magmatic and tectonic development of Tethys in the northern part of the Balkan region. *Lithos*, 108(1), 1–36. https://doi.org/10.1016/j.lithos.2008.09.007
- Rocchi, S., Westerman, D. S., Dini, A., & Farina, F. (2010). Intrusive sheets and sheeted intrusions at Elba Island, Italy. *Geosphere*, 6(3), 225–236. https://doi.org/10.1130/GES00551.1
- Romagny, A., Jolivet, L., Menant, A., Bessière, E., Maillard, A., Canva, A., et al. (2020). Detailed tectonic reconstructions of the Western Mediterranean region for the last 35 Ma, insights on driving mechanisms. *Bulletin de la Societe Geologique de France*, 191(1), 37. https://doi.org/10.1051/bsef/2020040
- Rosenbaum, G., Gasparon, M., Lucente, F. P., Peccerillo, A., & Miller, M. S. (2008). Kinematics of slab tear faults during subduction segmentation and implications for Italian magmatism: Kinematics of slab tear faults. *Tectonics*, 27(2), TC2008. https://doi.org/10.1029/2007TC002143
- Rossetti, F., Faccenna, C., Jolivet, L., Funiciello, R., Tecce, F., & Brunet, C. (1999). Syn-versus post-orogenic extension: The case study of Giglio island (northern Tyrrhenian Sea, Italy). *Tectonophysics*, 304(1), 71–93. https://doi.org/10.1016/S0040-1951(98)00304-7
- Royden, L. H. (1993). The tectonic expression slab pull at continental convergent boundaries. *Tectonics*, 12(2), 303–325. https://doi.org/10.1029/92TC02248
- Sandwell, D. T., Müller, R. D., Smith, W. H. F., Garcia, E., & Francis, R. (2014). New global marine gravity model from CryoSat-2 and Jason-1 reveals buried tectonic structure. Science, 346(6205), 65–67. https://doi.org/10.1126/science.1258213
- Sani, F., Bonini, M., Montanari, D., Moratti, G., Corti, G., & Ventisette, C. D. (2016). The structural evolution of the Radicondoli–Volterra Basin (southern Tuscany, Italy): Relationships with magmatism and geothermal implications. *Geothermics*, 59, 38–55. https://doi.org/10.1016/j.geothermics.2015.10.008
- Sartori, R., Torelli, L., Zitellini, N., Carrara, G., Magaldi, M., & Mussoni, P. (2004). Crustal features along a W–E Tyrrhenian transect from Sardinia to Campania margins (Central Mediterranean). Tectonophysics, 383(3), 171–192. https://doi.org/10.1016/j.tecto.2004.02.008

ZHANG ET AL. 22 of 24

21699356, 2022, 12, Down

- Schmid, S. M., Bernoulli, D., Fügenschuh, B., Matenco, L., Schefer, S., Schuster, R., et al. (2008). The Alpine-Carpathian-Dinaridic orogenic system: Correlation and evolution of tectonic units. Swiss Journal of Geosciences, 101(1), 139–183. https://doi.org/10.1007/s00015-008-1247-3
   Schmid, S. M., Fügenschuh, B., Kissling, E., & Schuster, R. (2004). Tectonic map and overall architecture of the Alpine orogen. Eclogae Geolog-
- icae Helvetiae, 97(1), 93–117. https://doi.org/10.1007/s00015-004-1113-x
- Schmid, S. M., Fügenschuh, B., Kounov, A., Maţenco, L., Nievergelt, P., Oberhänsli, R., et al. (2020). Tectonic units of the Alpine collision zone between eastern Alps and western Turkey. *Gondwana Research*, 78, 308–374. https://doi.org/10.1016/j.gr.2019.07.005
- Scrocca, D. (2006). Thrust front segmentation induced by differential slab retreat in the Apennines (Italy). Terra Nova, 18(2), 154–161. https://doi.org/10.1111/j.1365-3121.2006.00675.x
- Scrocca, D., Doglioni, C., Innocenti, F., Manetti, P., MAZZOTTI, A., Bertelli, L., et al. (2003). CROP Atlas—seismic reflection profiles of the Italian crust. Ist. Poligrafico e Zecca dello Stato.
- Seghedi, I., & Downes, H. (2011). Geochemistry and tectonic development of Cenozoic magmatism in the Carpathian–Pannonian region. Gondwana Research, 20(4), 655–672. https://doi.org/10.1016/j.gr.2011.06.009
- Serri, G., Innocenti, F., & Manetti, P. (1993). Geochemical and petrological evidence of the subduction of delaminated Adriatic continental lithosphere in the genesis of the Neogene-Quaternary magmatism of central Italy. *Tectonophysics*, 223(1), 117–147. https://doi.org/10.1016/0040-1951(93)90161-C
- Smith, W. H. F., & Sandwell, D. T. (1997). Global Sea floor topography from satellite altimetry and ship depth soundings. *Science*, 277(5334), 1956–1962. https://doi.org/10.1126/science.277.5334.1956
- Spakman, W., & Wortel, R. (2004). A tomographic view on western Mediterranean geodynamics. In W. Cavazza, F. Roure, W. Spakman, G. M. Stampfli, & P. A. Ziegler (Eds.), The TRANSMED Atlas. The Mediterranean region from crust to mantle: Geological and geophysical framework of the Mediterranean and the surrounding areas (pp. 31–52). Springer, https://doi.org/10.1007/978-3-642-18919-7
- Stampfli, G. M., & Borel, G. D. (2002). A plate tectonic model for the Paleozoic and Mesozoic constrained by dynamic plate boundaries and restored synthetic oceanic isochrons. Earth and Planetary Science Letters, 196(1), 17–33. https://doi.org/10.1016/S0012-821X(01)00588-X
- Stipčević, J., Herak, M., Molinari, I., Dasović, I., Tkalčić, H., & Gosar, A. (2020). Crustal thickness beneath the Dinarides and surrounding areas from receiver functions. *Tectonics*, 39(3), e2019TC005872. https://doi.org/10.1029/2019TC005872
- Šumanovac, F. (2010). Lithosphere structure at the contact of the Adriatic microplate and the Pannonian segment based on the gravity modelling. *Tectonophysics*, 485(1), 94–106. https://doi.org/10.1016/j.tecto.2009.12.005
- Tectonophysics, 485(1), 94–106. https://doi.org/10.1016/j.tecto.2009.12.005

  Šumanovac, F., & Dudjak, D. (2016). Descending lithosphere slab beneath the Northwest Dinarides from teleseismic tomography. *Journal of*
- Geodynamics, 102, 171–184. https://doi.org/10.1016/j.jog.2016.09.007

  Šumanovac, F., Hegedűs, E., Orešković, J., Kolar, S., Kovács, A. C., Dudjak, D., & Kovács, I. J. (2016). Passive seismic experiment and receiver functions analysis to determine crustal structure at the contact of the northern Dinarides and southwestern Pannonian Basin. Geophysical Journal International, 205(3), 1420–1436. https://doi.org/10.1093/gji/ggw101
- Šumanovac, F., Markušić, S., Engelsfeld, T., Jurković, K., & Orešković, J. (2017). Shallow and deep lithosphere slabs beneath the Dinarides from teleseismic tomography as the result of the Adriatic lithosphere downwelling. *Tectonophysics*, 712–713, 523–541. https://doi.org/10.1016/j.tecto.2017.06.018
- Tari, V. (2002). Evolution of the northern and western Dinarides: A tectonostratigraphic approach (Vol. 1, pp. 223–236). Stephan Mueller Special Publication Series. https://doi.org/10.5194/smsps-1-223-2002
- Tesauro, M., Kaban, M. K., & Cloetingh, S. A. P. L. (2008). EuCRUST-07: A new reference model for the European crust. *Geophysical Research Letters*, 35(5), L05313. https://doi.org/10.1029/2007GL032244
- Tesauro, M., Kaban, M. K., & Cloetingh, S. A. P. L. (2009). A new thermal and rheological model of the European lithosphere. *Tectonophysics*, 476(3), 478–495. https://doi.org/10.1016/j.tecto.2009.07.022
- Tinterri, R., & Lipparini, L. (2013). Seismo-stratigraphic study of the Plio-Pleistocene foredeep deposits of the Central Adriatic Sea (Italy): Geometry and characteristics of deep-water channels and sediment waves. *Marine and Petroleum Geology*, 42, 30–49. https://doi.org/10.1016/j.marpetgeo.2012.11.004
- Tomljenović, B., Csontos, L., Márton, E., & Márton, P. (2008). Tectonic evolution of the northwestern Internal Dinarides as constrained by structures and rotation of Medvednica Mountains, North Croatia. Geological Society, London, Special Publications, 298(1), 145–167. https://doi.org/10.1144/SP298.8
- Trincardi, F., & Zitellini, N. (1987). The rifting of the Tyrrhenian basin. Geo-Marine Letters, 7, 1-6. https://doi.org/10.1007/BF02310459
- Trumpy, E., & Manzella, A. (2017). Geothopica and the interactive analysis and visualization of the updated Italian National Geothermal Database. *International Journal of Applied Earth Observation and Geoinformation*, 54, 28–37. https://doi.org/10.1016/j.jag.2016.09.004
- Tunini, L., Jiménez-Munt, I., Fernandez, M., Vergés, J., & Villaseñor, A. (2015). Lithospheric mantle heterogeneities beneath the Zagros mountains and the Iranian plateau: A petrological-geophysical study. *Geophysical Journal International*, 200(1), 596–614. https://doi.org/10.1093/gii/ggu418
- Ustaszewski, K., Kounov, A., Schmid, S. M., Schaltegger, U., Krenn, E., Frank, W., & Fügenschuh, B. (2010). Evolution of the Adria-Europe plate boundary in the northern Dinarides: From continent-continent collision to back-arc extension. *Tectonics*, 29(6), TC6017. https://doi.org/10.1029/2010TC002668
- van Hinsbergen, D. J. J., Maffione, M., Koornneef, L. M. T., & Guilmette, C. (2019). Kinematic and paleomagnetic restoration of the Semail ophiolite (Oman) reveals subduction initiation along an ancient Neotethyan fracture zone. *Earth and Planetary Science Letters*, 518, 183–196. https://doi.org/10.1016/j.epsl.2019.04.038
- van Hinsbergen, D. J. J., Torsvik, T. H., Schmid, S. M., Maţenco, L. C., Maffione, M., Vissers, R. L. M., et al. (2020). Orogenic architecture of the Mediterranean region and kinematic reconstruction of its tectonic evolution since the Triassic. *Gondwana Research*, 81, 79–229. https://doi.org/10.1016/j.gr.2019.07.009
- van Unen, M., Matenco, L., Nader, F. H., Darnault, R., Mandic, O., & Demir, V. (2019). Kinematics of foreland-vergent crustal accretion: Inferences from the Dinarides evolution. *Tectonics*, 38(1), 49–76. https://doi.org/10.1029/2018TC005066
- Vezzani, L., Festa, A., & Ghisetti, F. C. (2010). Geology and tectonic evolution of the central-southern Apennines, Italy. Geological Society of America. https://doi.org/10.1130/SPE469
- Vignaroli, G., Faccenna, C., Jolivet, L., Piromallo, C., & Rossetti, F. (2008). Subduction polarity reversal at the junction between the Western Alps and the northern Apennines, Italy. *Tectonophysics*, 450(1), 34–50. https://doi.org/10.1016/j.tecto.2007.12.012
- Vignaroli, G., Faccenna, C., Rossetti, F., & Jolivet, L. (2009). Insights from the Apennines metamorphic complexes and their bearing on the kinematics evolution of the orogen. Geological Society, London, Special Publications, 311(1), 235–256. https://doi.org/10.1144/SP311.9
- Vilà, M., Fernández, M., & Jiménez-Munt, I. (2010). Radiogenic heat production variability of some common lithological groups and its significance to lithospheric thermal modeling. *Tectonophysics*, 490(3), 152–164. https://doi.org/10.1016/j.tecto.2010.05.003

ZHANG ET AL. 23 of 24

- Wessel, P., & Smith, W. H. F. (1998). New, improved version of generic mapping tools released. *Eos, Transactions American Geophysical Union*, 79(47), 579. https://doi.org/10.1029/98E000426
- Workman, R. K., & Hart, S. R. (2005). Major and trace element composition of the depleted MORB mantle (DMM). Earth and Planetary Science Letters, 231(1), 53–72. https://doi.org/10.1016/j.epsl.2004.12.005
- Wrigley, R., Hodgson, N., & Esestime, P. (2015). Petroleum geology and hydrocarbon potential of the Adriatic Basin, offshore Croatia. *Journal of Petroleum Geology*, 38(3), 301–316. https://doi.org/10.1111/jpg.12612
- Zhao, L., Paul, A., Malusà, M. G., Xu, X., Zheng, T., Solarino, S., et al. (2016). Continuity of the Alpine slab unraveled by high-resolution P wave tomography. *Journal of Geophysical Research: Solid Earth*, 121(12), 8720–8737. https://doi.org/10.1002/2016JB013310
- Zhu, H., Bozdağ, E., & Tromp, J. (2015). Seismic structure of the European upper mantle based on adjoint tomography. *Geophysical Journal International*, 201(1), 18–52. https://doi.org/10.1093/gji/ggu492

ZHANG ET AL. 24 of 24



# **JGR** Solid Earth

### RESEARCH ARTICLE

10.1029/2023JB028435

### **Key Points:**

- We unveil the thermochemical structure of the lithosphere and uppermost mantle of the Adria Microplate and its margins
- Results reveal mantle wedges aligning with Apenninic and Dinaric slabs, and cold sublithospheric anomalies beneath NE and SW Adria margins
- In N Apennines the slab is attached while a gap is observed in S Apennines. At Adria's NE margin, the slab penetrates deeper southward

### **Supporting Information:**

Supporting Information may be found in the online version of this article.

### Correspondence to:

M. Torne, mtorne@geo3bcn.csic.es

### Citation:

Zhang, W., Jiménez-Munt, I., Torne, M., Vergés, J., Bravo-Gutiérrez, E., Negredo, A. M., & García-Castellanos, D. (2024). The lithosphere and upper mantle of the Western-Central Mediterranean region from integrated geophysical-geochemical modeling. *Journal of Geophysical Research: Solid Earth, 129*, e2023JB028435. https://doi.org/10.1029/2023JB028435

Received 1 DEC 2023 Accepted 19 MAR 2024

# **Author Contributions:**

Montserrat Torne, Jaume Vergés, Ana M. Negredo Data curation: Wentao Zhang Formal analysis: Wentao Zhang, Estefanía Bravo-Gutiérrez Funding acquisition: Ivone Jiménez-Munt, Daniel García-Castellanos Investigation: Ivone Jiménez-Munt, Montserrat Torne, Jaume Vergés, Estefanía Bravo-Gutiérrez, Ana M. Negredo

Conceptualization: Ivone Jiménez-Munt.

# © 2024. The Authors.

This is an open access article under the terms of the Creative Commons
Attribution-NonCommercial-NoDerivs
License, which permits use and distribution in any medium, provided the original work is properly cited, the use is non-commercial and no modifications or adaptations are made.

# The Lithosphere and Upper Mantle of the Western-Central Mediterranean Region From Integrated Geophysical-Geochemical Modeling

Wentao Zhang<sup>1,2</sup>, Ivone Jiménez-Munt<sup>1</sup>, Montserrat Torne<sup>1</sup>, Jaume Vergés<sup>1</sup>, Estefanía Bravo-Gutiérrez<sup>1</sup>, Ana M. Negredo<sup>3,4</sup>, and Daniel García-Castellanos<sup>1</sup>

<sup>1</sup>Geosciences Barcelona, Geo3BCN-CSIC, Barcelona, Spain, <sup>2</sup>Department of Earth and Ocean Dynamics, University of Barcelona, Barcelona, Spain, <sup>3</sup>Departamento de Física de la Tierra y Astrofísica, Universidad Complutense de Madrid, Madrid, Spain, <sup>4</sup>Instituto de Geociencias, IGEO (CSIC-UCM), Madrid, Spain

**Abstract** This study integrates geophysical-geochemical data to investigate the thermochemical structure of the lithosphere and sublithospheric mantle, along the Southern Tyrrhenian Basin, Apennines, Adriatic Sea, Dinarides, and Carpathians-Balkanides. We present the lithospheric structure of the Adria microplate and the two opposing mantle slabs along its NE and SW margins. The modeling shows the presence of two asthenospheric mantle wedges aligning with the Apenninic and Dinaric continental mantle slab rollback, along with cold (-200°C) sublithospheric anomalies beneath Adria's NE and SW margins. In the northern Adria region, the lithosphere undergoes synchronous thinning in the Tyrrhenian domain and thickening toward the forefront of the northern Apennines. This is associated with the northeastward rollback of the SW Adriatic slab, leading to subsequent delamination of the continental mantle. In the southern Adria region, the complex deep structure results from the variably oriented lithospheric slabs, and nearly 90-degree shift of the tectonic grain between the southern Apennines and the Calabrian Arc. At the SW Adria margin, beneath the northern Apennines, the thermal sublithospheric anomaly is attached to the shallower lithosphere, while a slab gap is modeled in the southern Apennines. One possibility is that the gap is due to a recent horizontal slab tear. Along the NE margin of Adria, the thermal anomaly penetrates to depths of about 200 km in the northern Dinarides and 280 km in the southern Dinarides, shallower than the SW Adria anomaly, which extends to at least 400 km depth.

Plain Language Summary We integrate geological and geophysical data (e.g., elevation, gravity, geoid, seismic tomography) to investigate the density and temperature distribution of the crust and lithospheric mantle down to 400 km, along a profile that extends from the Southern Tyrrhenian Basin and Apennines in Italy to the Southern Dinarides and Carpathians-Balkanides in southern Europe. Taking advantage of our previous research in this region, we provide an integrated view of the lithospheric structure and the uppermost mantle of the Tyrrhenian Basin, Apennines, Adriatic Sea and Dinarides. Our results show notable variations in both the crust and the base of the lithosphere. These variations are observed to be shallower beneath the basins and deeper beneath the mountain belts, particularly in areas with elevated topography. Additionally, our observations highlight the presence of two cold and dense zones situated in the distal margins of the Adria microplate, specifically beneath the Apennines and Dinarides. The thermal anomalies indicate the presence of two oppositely subducting slabs with different geometries and depth of penetration. Their current location, depth and shape have largely controlled the geodynamic evolution of the study region in the last 30 My.

# 1. Introduction

The Western-Central Mediterranean region is a highly active seismic zone, known for its unique tectonic characteristics. It forms part of the Alpine-Mediterranean belt that extends from southern Iberia to the western Aegean Sea. The belt originated from the convergence of the African and Eurasian plates since the Late Cretaceous. It encompasses pre-orogenic rifting and oceanization, activation of several subduction zones and the complete consumption of the Alpine-Ligurian Tethys and Neotethyan oceanic lithospheres, within the continental collision between the Corsica-Sardinia block and Adria microplate during the Late Oligocene–Early Miocene times. Post-collision counterclockwise rotation of the Adria Microplate triggered the opening of the asymmetric Tyrrhenian Basin and the synchronous tectonic tightening along all its margins: the Apennines, the Calabria belt, the

ZHANG ET AL. 1 of 21



# Journal of Geophysical Research: Solid Earth

10.1029/2023JB028435

Montserrat Torne
Project administration: Ivone JiménezMunt, Daniel García-Castellanos
Software: Ivone Jiménez-Munt
Supervision: Ivone Jiménez-Munt,
Montserrat Torne
Validation: Jaume Vergés
Writing – original draft: Wentao Zhang,
Montserrat Torne
Writing – review & editing:
Wentao Zhang, Ivone Jiménez-Munt,
Montserrat Torne, Jaume Vergés,
Estefanía Bravo-Gutiérrez, Ana

M. Negredo, Daniel García-Castellanos

Methodology: Ivone Jiménez-Munt,

Dinarides-Hellenic belt, the Alps and the Carpathian belt (e.g., Carminati et al., 2012, 2020; Handy et al., 2015; Jolivet & Faccenna, 2000; Schmid et al., 2020; van Hinsbergen et al., 2019, 2020; Wortel & Spakman, 2000).

During the opening and subsequent closure of the Alpine-Ligurian Tethys and Vardar oceans, small continental blocks, such as the Alcapa, Tisza, and Dacia microplates (see Figure 1), broke away from the Eurasian Plate. These microplates subsequently collided with Adria with the extrusion of blocks and slab-retreat processes resulting in the formation of the present-day belts and foredeep basins. The Adria microplate is believed to have separated from the African Plate during the early Mesozoic, having drifted toward the NNE with a slight counter clockwise rotation (e.g., Handy et al., 2021; Jolivet, 2023; Le Breton et al., 2017). Consequently, Adria is surrounded by extensively deformed convergent margins, characterized by three plate subductions with different plate polarities. An interesting aspect of these subducted and delaminated slabs is their segmentation and variable lengths at depth, as evidenced by the tomography studies listed below.

It is relatively well accepted (e.g., Carminati et al., 2012) that the current lithospheric structure in the studied region is largely shaped by the subduction of two oceanic domains on either side of the Adria microplate that ended in the retreat of the slabs through rollback processes. The consumption and closure of these oceanic domains triggered the onset of continental subduction followed by delamination beneath the NE and SW margins of the Adria microplate (e.g., Zhang et al., 2022). In this context, we refer to delamination as the Subducting Plate Delamination type as defined by Magni and Király (2020), where the lithospheric mantle and possibly denser continental crust of the subducting plate peels away from the rest of the lithosphere and continues to subduct, leaving only the light continental crust at the surface. Consequently, the Adria microplate plays a significant role in the geodynamics of the Western-Central Mediterranean region. For a comprehensive review of the current geology and geodynamics of the area the reader is referred to the works of Balling et al. (2021), Carminati et al. (2012), Carminati and Chiarabba (2023), Chiarabba et al., 2014, Faccenna et al. (2001), Handy et al. (2015), Jolivet (2023), Schmid et al. (2020), van Hinsbergen et al. (2019, 2020).

Understanding the geodynamic processes within this complex tectonic region requires reliable knowledge of the present-day lithospheric and sublithospheric mantle structure, particularly the evolution of the subducting lithosphere (Giacomuzzi et al., 2022; Magrini et al., 2022). Despite extensive research efforts, ongoing debate persists regarding the structure of the lithospheric and sublithospheric mantle in this region. In particular, there is significant uncertainty about the shapes and sizes of the subducting slabs, and whether they are attached or detached from their shallow counterparts. Global or regional tomography studies, for example, Lucente et al. (1999); Piromallo and Morelli (2003); Spakman and Wortel (2004); Blom et al. (2020); Belinić et al. (2021); El-Sharkawy et al. (2020), Giacomuzzi et al. (2011, 2022) and Rappisi et al. (2022), have not provided conclusive evidence on the details of the mantle structure in the study area. Piromallo and Morelli (2003) show a pronounced, wide and well-resolved fast velocity anomaly below the Southern Apennines while Spakman and Wortel (2004) propose that a short (300–400 km) slab is hanging below them. In the Central Apennines, a slab window is imaged ranging from 140 km (Giacomuzzi et al., 2011) to 250 km (Spakman & Wortel, 2004) depth. In the Southern Apennines, the deep fast Vp velocity anomalies appear continuously connected to the Calabrian slab (e.g., Rappisi et al., 2022).

Three-dimensional anisotropic teleseismic P-wave tomography and S-wave models suggest a positive velocity anomaly under the whole Dinarides (Belinić et al., 2021; Koulakov et al., 2015; Šumanovac & Dudjak, 2016). Positive Vp and Vs regional anomalies beneath the Apennines and Dinarides, located at different depths, are interpreted to be the westward and eastward descending margins of the Adria microplate. Király et al. (2018) describe the two dipping regional anomalies as the bi-directional subduction of Adria. The large amount of deep geophysical data supports the interpretation that the sub-crustal structure beneath Adria is shaped by an intricate array of segmented slabs (e.g., 3-D mapping by Rappisi et al., 2022). These slabs are remnants of the thinned continental margins of Adria that formed during the Pangea break-up, and were subsequently subducted by both the eastwards drift of Adria during the Triassic–Early Cretaceous and by the convergence between Africa and Eurasia since the Late Cretaceous (e.g., Pierantoni et al., 2020).

Zhang et al. (2022) recently modeled a  $\sim$ 1,000 km profile crossing the Northern Apennines and Dinarides, which will be referred to as the Northern Transect (Figure 1, blue dashed line). These authors have demonstrated that bidirectional subducting continental mantle delamination of the Adria microplate can explain the main lithospheric and sublithospheric mantle features within the study region.

ZHANG ET AL. 2 of 21

21699356, 2024, 4, Downloaded from https://agupubs.onlinelibrary.wiley.com/doi/10.1029/2023JB028435 by Readcube (Labtiva Inc.), Wiley Online Library on [30/03/2024]. See the Terms

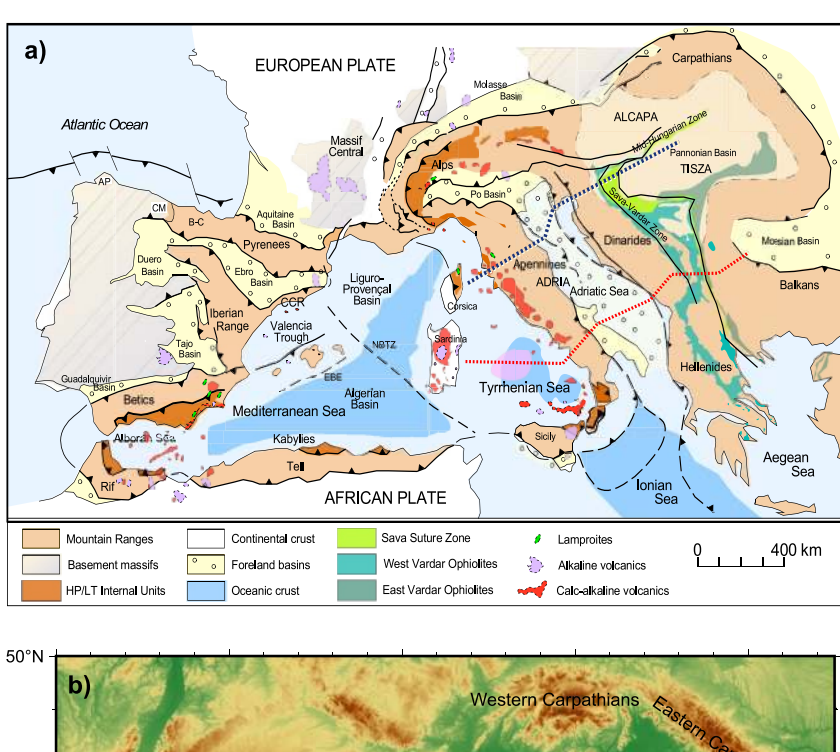




**Figure 1.** (a) Tectonic map of the Western-Central Mediterranean region with the main orogenic belts and foreland basins (based on Melchiorre et al., 2017; Schmid et al., 2020; Vergés & Sàbat, 1999). The blue dashed line shows the location of the northern transect from Zhang et al. (2022). The solid red dashed line shows the location of the southern transect presented in this study. (b) Elevation map. Red triangles show the main volcanoes (Melchiorre et al., 2017).

Considering the longitudinal variations in plate-scale geometries that have been previously identified in various studies of the Apennines and Dinarides slabs, our primary goal is to investigate the lateral continuity between the opposing Apennines and Dinarides slabs. The continuity of these slabs in the Northern Transect has been discussed before (Zhang et al., 2022), and we are now expanding our analysis to encompass the Southern Apennines and Dinarides regions, along the Southern Transect. To accomplish this, we have used the same modeling approach, the LitMod2D\_2.0 software (Kumar et al., 2020), an updated version of the original 2D software developed by Afonso et al. (2008).

ZHANG ET AL. 3 of 21

LitMod2D\_2.0 allows for obtaining the present-day crust and upper mantle structure, down to 400 km depth by integrating available geophysical and petrological data within a self-consistent thermodynamic framework. The Southern Transect spans approximately 1,250 km, crossing the Southern Tyrrhenian Basin, the Southern Apennines, the Adriatic Sea, the Southern Dinarides, and the Carpathians-Balkanides in a roughly SW-NE direction (Figure 1). Its western part corresponds to TRANSMED Project transect III (Carminati et al., 2004). The results along the Southern Transect are the 2D temperature, bulk density, seismic velocity (Vp and Vs), and compositional structure for the entire lithosphere, along with the distribution of temperature anomalies for the sublithospheric mantle. Hence, the geophysical-geochemical integrated model presented here, in conjunction with findings from the Northern Transect, offers valuable insights into the lithospheric and thermochemical structure of the upper mantle beneath the Apennines and Dinarides fold-thrust belts. In this study we integrate the results from the Northern and Southern Adria transects with independent geological and geophysical data (including from earthquakes) to investigate the role of the Adria microplate in the geodynamic evolution of the Western-Central Mediterranean region.

# 2. Lithospheric and Upper Mantle Structure of the Western-Central Mediterranean

### 2.1. Model Parameters and Constraints

The method used combines petrological and geophysical data to determine the 2D thermo-chemical structure and seismic velocity distribution of the crust and upper mantle (down to 400 km), fitting elevation, geoid height, Bouguer gravity, surface heat flow data (Figure S1 in Supporting Information S1) and mantle seismic velocities. Further information regarding the methodology can be found in Afonso et al. (2008); Kumar et al. (2020) and Zhang et al. (2022).

The crustal structure in the central part of the southern Tyrrhenian Basin is mainly based on the MEDOC seismic profile from Prada et al. (2014, 2016). In the southern Apennines data come from the deep crustal seismic reflection (CROP-04) profile (e.g., Akimbekova et al., 2021; Finetti, 2005; Scrocca, 2010). In the eastern section of the profile, the Dinarides and Carpathian-Balkanides crustal structure is mainly constrained by geological data (available crustal cross-sections) (Matenco & Radivojević, 2012; Schmid et al., 2008, 2020). The Moho depth comes from seismic receiver functions (RF) analysis of Piana Agostinetti and Amato (2009); Stipčević et al. (2020) and Kalmár et al. (2021) and the regional crustal models of Mazzoli et al. (2013); Savastano and Piana Agostinetti (2019) and Akimbekova et al. (2021).

The physical parameters for each crustal body are summarized in Table 1. Crustal density values are based on previous studies (e.g., Akimbekova et al., 2021; Prada et al., 2014; Savastano & Piana Agostinetti, 2019; Zhang et al., 2022), that use the velocity-density relationship of Brocher (2005). The density of the sedimentary cover was deduced from the empirical relationships of Nafe and Drake (1963). Thermal conductivities are taken from Norden and Förster (2006) and Trumpy and Manzella (2017), and the radiogenic heat production data come from direct measurements in the Apennines (Verdoya et al., 2019) and from a global compilation of relevant crustal rocks (Hasterok & Webb, 2017; Vilà et al., 2010). Furthermore, the density and thermal conductivity of the exhumed mantle in the central Tyrrhenian Basin were estimated using a thermodynamic approach (see Supporting Information S1 and Figure S2 in Supporting Information S1), while its heat production was assumed to be  $0.02 \,\mu\text{W/m}^3$  (Turcotte & Schubert, 2002).

For characterizing the lithospheric and sublithospheric mantle, we have considered the seismic velocities (Vp and Vs) from the tomography studies of Amaru (2007a, 2007b), Benoit et al. (2011), Giacomuzzi et al. (2011), Koulakov et al. (2015), Šumanovac et al. (2017), El-Sharkawy et al. (2020), Belinić et al. (2021), Handy et al. (2021), and Rappisi et al. (2022).

Considering the previously mentioned geological cross-sections and seismic experiments, Figures 2 and 3 show the crustal and upper-mantle structure that best fit all observables (elevation, geoid height, Bouguer gravity anomaly, surface heat flow and mantle seismic velocities).

# 2.2. Crustal Structure

Along the Southern Transect (Figure 1) we distinguish four main configurations of the crystalline crust that significantly differ in their internal structure and average densities. The westernmost domain consists of the Tyrrhenian Basin, composed in its central region of sediments and a basement that is fundamentally made of

ZHANG ET AL. 4 of 21

21699356, 2024. 4. Downloaded from https://agupubs.onlinelibrary.wiley.com/doi/10.1029/2023JB028435 by Readcube (Labtiva Inc.), Wiley Online Library on [30/03/2024]. See the Terms and Conditions (https://onlinelibrary.wiley.com/rems-and-conditions) on Wiley Online Library for rules of use; OA articles are governed by the applicable Creativa Inc.).

 Table 1

 Thermo-Physical Properties of the Crustal Tectonic Units and Mantle Domains Along the Profile

Tectonic units		Density (kg/m <sup>3</sup> )	Thermal conductivity (W/K m)	Radiogenic heat production (μW/m³)
	Sediment	2,450	2.4	1
Adria Microplate	Tyrrhenian Basin Magmatic UC	2,800	2.7	2
	Tyrrhenian Basin Magmatic LC	2,900	2.1	0.8
	Tyrrhenian Basin EM75	2,870a	1.6	0.02
	Tyrrhenian Basin EM25	2,980a	2.4	0.02
	Apennines UC	2,780	2.7	2
	Apennines LC	2,850	2.1	0.6
	Adriatic Sea UC	2,780-2,840b	2.7	2
	Adriatic Sea MC	2,880	2.1	0.6
	Adriatic Sea LC	3,080	2.1	0.6
	Dinarides UC	2,750-2,820b	2.7	2
	Dinarides LC	2,880	2.1	0.6
Dacia Microplate	Sava Suture	2,850	2.7	1.3
	Balkanides UC	2,750	2.9	2
	Balkanides LC	2,880	2.1	0.6
Mantle	Tyrrhenian LM	DMM-6% (Kumar et al., 2021)		
	Adriatic and Dacia LM	Tc_2 (Griffin et al., 2009)		
	Mantle wedge	DMM-3% (Kumar et al., 2021)		
	Sublithospheric mantle	DMM (Workman & Hart, 2005)		

Note. UC: Upper Crust; MC: Middle Crust; LC: Lower Crust; EM75: Exhumed Mantle 75% serpentinized; EM25: Exhumed Mantle 25% serpentinized; LM: Lithospheric Mantle. (a) The density and thermal conductivity of the exhumed mantle of the central Tyrrhenian Basin is estimated using the thermodynamic approach presented in Supporting Information S1. (b) Calculated as a function of pressure using isothermal compressibility.

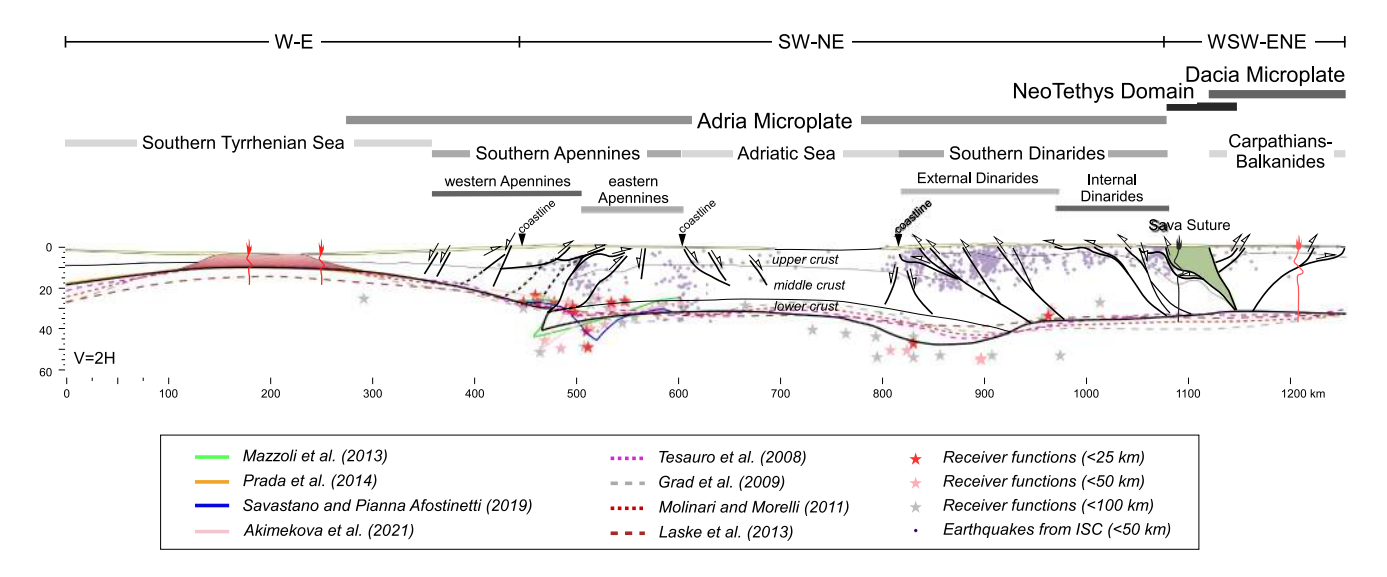


Figure 2. Crustal structure from the best fitting model, which was constrained using available geological and geophysical information as listed in the panel legend and in the main text. Yellow color represents the sediment layer. Degraded red in the central Tyrrhenian Basin shows the serpentinized mantle (75% top, 25% bottom). Moho depths from previous studies are shown with different colors, see bottom legend for color table and references. Stars show Moho locations from receiver function studies of Stipčević et al. (2020) and Piana Agostinetti and Amato (2009). Earthquakes with a magnitude of  $Mb \ge 3.0$  between 2008 and 2021, as recorded in the ISC catalog, are plotted as gray circles projected at 50 km across the transect. Red arrows show the location of main volcanic edifices.

ZHANG ET AL. 5 of 21

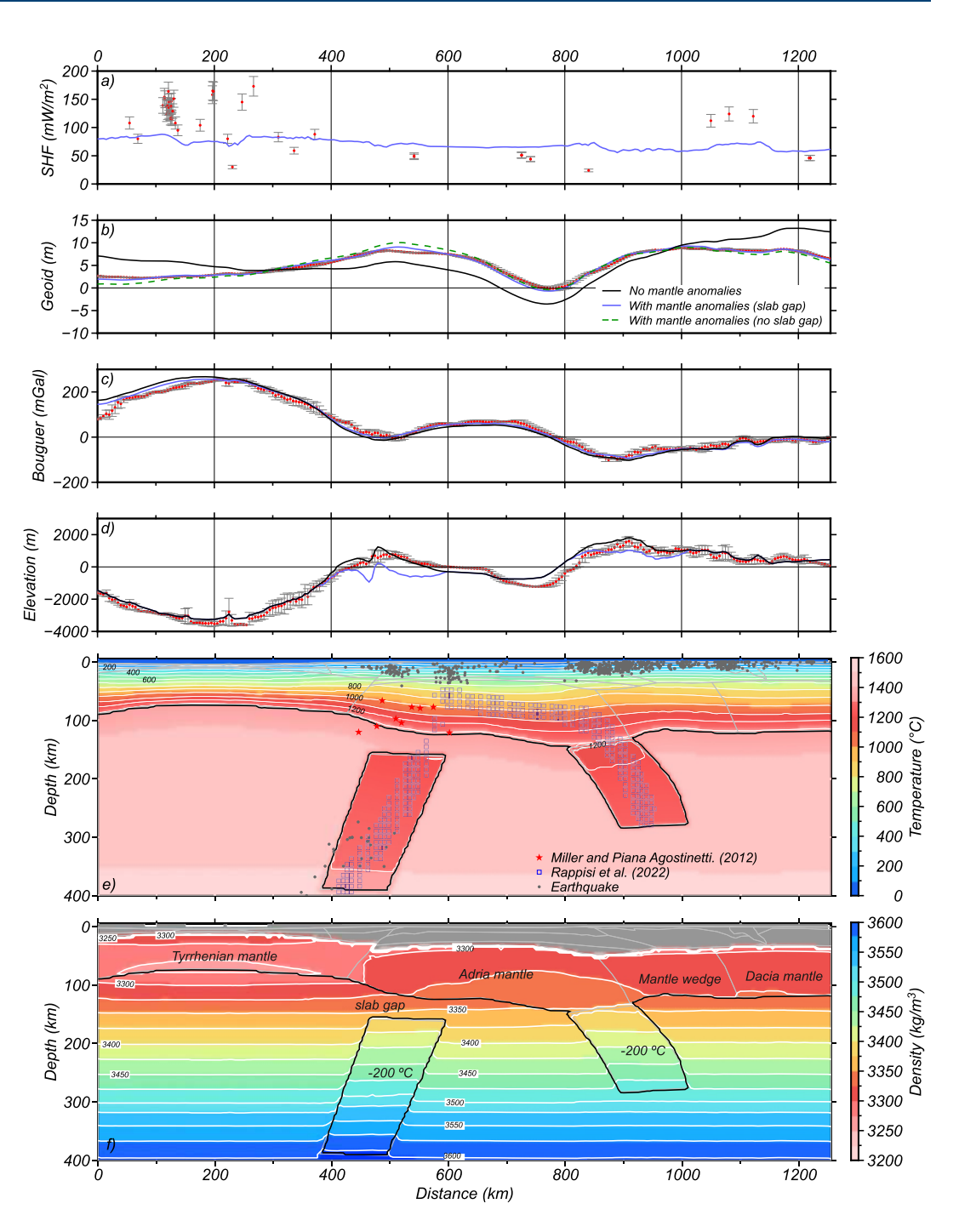


Figure 3. Best fit model, see Figure 1 for location. (a) Surface heat flow. (b) Geoid height. (c) Bouguer gravity anomaly. (d) Elevation. Blue and black lines show modeled results, with and without sublithospheric anomalies, respectively. Red dots show measured data, and vertical bars show the standard deviation calculated across a swath of 25 km half width. (e) Temperature distribution for the entire lithosphere. Continuous black lines highlight the obtained (Lithosphere-Asthenosphere (LAB) depth and location of sublithospheric mantle anomalies. LAB depth from previous studies (red stars) are shown for comparison. Earthquake locations (International Seismological Centre, ISC) with a magnitude of mb ≥ 3.0 between 2008 and 2021, projected 50 km across the transect are shown as solid gray circles. (f) Mantle density distribution. The different compositional domains in the lithospheric mantle are separated by thin gray lines, and major oxide compositions are listed in Table S1. Data from Rappisi et al. (2022) have been taken from https://figshare.com/articles/dataset/iso-\_and\_ani-NEWTON21\_tomographic\_models/19188950 and projected onto the profile.

ZHANG ET AL. 6 of 21

mantle rocks and subordinate oceanic crustal rocks. Moving to the east, in the Adria plain domain, from west to east, we find two more domains: the double-layered crust of the continental slope and the onshore western Apennines and the three-layered crust of the eastern Apennines and Adriatic Sea. To differentiate the Apennines, we define the Southern western Apennines, adjacent to the Tyrrhenian Sea, and the Southern eastern Apennines, bordering the Adriatic Sea. The first region encompasses both offshore and onshore domains in which the crust is thinned and under extension, while the second region is located above a thicker crust under a compressional regime. Our best fitting model shows that the easternmost domain of the profile, including the internal Dinarides (Adria microplate) and the Carpathian-Balkanides (Dacia microplate) is characterized by a two-layered crust of variable thickness, covered by a thick sedimentary cover showing lateral thickness variations. The Adria and Dacia domains are separated by the Sava Suture Zone, exposing remnants of the former Vardar Ocean, which closed at the end of the Cretaceous (e.g., Schmid et al., 2020; Spahić & Gaudenyi, 2022) (Figure 2).

As depicted in Figure 2, significant variations in crustal structure and thickness are observed along the transect. Toward the west, seismic data and drilling results (e.g., Loreto et al., 2021; Prada et al., 2014, 2016) show that the southern Tyrrhenian Basin is characterized by a sedimentary cover with variable thickness and two exhumed mantle layers with different degrees of serpentinization. Our results indicate that serpentinization reaches up to 75% in the upper layer and 25% in the lower layer (Table 1). Their densities have been calculated for different degrees of serpentinization using the thermodynamic approach, plotted in Supporting Information S1 (Figure S2), and ranging from 2,870 to 2,980 km/m³, respectively (Table 1 and Figure 2). Thus, our results are compatible with the central region of the Tyrrhenian Basin characterized by serpentinized mantle and subordinate oceanic rocks, surrounded by a magmatic crust at the western and eastern margins of the basin, where the crust thickens up to 20 km. The magmatic crust consists of two layers, an upper layer that is about 4 km thick, with a density of 2,800 kg/m³, and a lower layer of variable thickness with a density of 2,900 kg/m³ (Table 1 and Figure 2).

The magmatic crust of the eastern Tyrrhenian Basin passes laterally into a two-layered crust that extends from the continental slope to the onshore (Figures 2 and 3). The Moho depth varies from 20 km to almost 30 km with densities of 2,780 kg/m³ for the upper crust and 2,850 kg/m³, for the lower crust. Across the Southern Apennines, Adriatic Sea and external Dinarides, the upper crust has a constant thickness of about 10 km, except in the western and eastern collisional fronts where a thickening of about 5 km is observed. A similar trend is observed in the middle crust, although on average, it is approximately 10 km thicker than the upper crust. Upper and middle crustal densities range from 2,750 to 2,820 kg/m³ for the upper crust and 2,880 kg/m³ for the middle crust (Figure 2). It is worth noting that beneath the Apennines and external Dinarides, the Moho locally reaches depths of 40 and 55 km, respectively. The thickening of the Dinarides crust primarily occurs in the lower crust, which nearly doubles in thickness. A slight thickening is also observed in the upper and middle crust (Figure 2).

Crustal thickening underneath the central and southern external Dinarides is supported by seismic receiver functions (RF) data, which locate the Moho at a depth of 50–55 km (e.g., Stipčević et al., 2020; Sumanovac et al., 2017). Uncertainties found in RF's in this region could be an indication of a double or overlapping Moho (Stipčević et al., 2020). The presence of a high-density lower crust (3,080 kg/m³) is mainly determined by the fitting of the geophysical observables (Figure 3), while also being consistent with the expected densities at those depths.

To the east, the crust exhibits a relatively constant thickness, with the Moho located at 30–35 km depth, slightly deepening toward the internal Dinarides (35 km). The crust is composed of two distinct layers, namely the upper and the middle-lower crust, which have relatively lighter average densities than those observed in the western and central regions of Adria (Table 1). The upper crust, except in the areas surrounding the Sava Suture Zone, is relatively thin ( $\sim$ 5 km) and has an average density of 2,750 kg/m³. The middle-lower crust is significantly thicker and denser, with an average thickness of 25 km and a mean density of 2,880 kg/m³ (Figure 2).

The Adria and Dacia domains are separated by the Sava Suture zone, which stretches from the eastern Alps in the northwest to the Dinarides in the southeast, encompassing a significant portion of the western Balkanides. The suture is mainly composed of a mélange of flysch, ophiolites and metamorphic rocks with densities ranging between 2,200 and 2,800 kg/m³ for the flysch sedimentary rocks and 2,900–3,500 kg/m³ for the metamorphic and ophiolitic rocks (Spahić & Gaudenyi, 2022; Ustaszewski et al., 2010). Our best fitting model shows an average density of 2,850 kg/m³ for the entire Sava Suture Zone complex (Table 1).

ZHANG ET AL. 7 of 21

Our thermal model results also indicate that the temperature at the Moho depth ranges from 300 to 420°C in the western part of the Tyrrhenian Basin to 600–650°C in the Southern western Apennines. In the Adriatic Sea, temperatures are between 600 and 680°C, and they increase rapidly as the base of the crust becomes deeper beneath the external Dinarides, reaching temperatures over 700°C and 800°C, respectively (Figure 3e).

Shallow seismic activity is mainly concentrated along a narrow and nested band along the Southern Apennines and Dinarides (Figure 2). More diffuse activity, mainly located at upper/middle crustal levels (<20 km) is observed in the Sava Suture Zone and Carpathian-Balkanides region. In the inner Southern Apennines normal faulting and thrust/reverse faulting mechanisms occur at the outer fronts of the chain (Chiarabba et al., 2014; De Luca et al., 2009). For most of the region, hypocenters are confined to the upper 20–25 km of the crust with the exception of onshore and offshore areas in the western Adriatic coast where earthquake depths reach the lower crust and uppermost mantle as deep as 40 km depth (Figure 2 and Figure S3 in Supporting Information S1).

Recent seismic activity on the central Apennines and Adriatic Sea has a generally lower magnitude compared to the Southern Apennines (Figure S3 in Supporting Information S1), and it is typically associated with strike-slip and normal faults. In the southern Apennines, major destructive, high-magnitude earthquakes are due to extensional faults. In the Dinarides earthquakes are observed at shallow-intermediate crustal depths and predominantly contractional. Notably, no recent shallow earthquakes have been recorded in the Tyrrhenian Basin where earthquakes primarily occur at depths exceeding 300 km and are related to the Calabrian Wadati-Benioff zone (Figure S3 in Supporting Information S1).

# 2.3. Lithosphere-Asthenosphere Boundary (LAB) and Upper Mantle Structure

In our best-fit model, we have identified three distinct lithospheric mantle compositions: the Tyrrhenian mantle, the Adria and Dacia mantle, and the Dinarides mantle wedge (Table 1 and Table S1 and Figure 3). For the sublithospheric mantle, we used a depleted mid-ocean-ridge (DMM, or Depleted MORB Mantle) composition, as defined by Workman and Hart (2005), which is a reference model for an average, non-melted, depleted MORB mantle. For more details, refer to Kumar et al. (2020) and Zhang et al. (2022).

The lithospheric mantle composition beneath the Southern Tyrrhenian Basin is characterized as DMM-6%, indicating approximately 6% melting of the sublithospheric mantle with a Mg# of 89.72. For the Adria and Dacia mantle, our results reveal a TC\_2 composition (an average Tecton, defined in Griffin et al., 2009), which is a slightly depleted mantle with an average Mg# of 89.5. Below the Dinarides, our best-fit model indicates a DMM-3% composition, which is interpreted as due to the presence of a mantle wedge. This DMM composition with a variable degree of melting accounts for potential melting of both the lithospheric and sublithospheric mantle, likely attributed to the rollback of the Apennines and Dinarides slabs (see Discussion).

The thermal LAB is defined by the depth of the 1,320°C isotherm, a criterion in agreement with the findings of numerical simulations employing realistic viscosities (e.g., Gerya, 2019). The LAB beneath the Southern Tyrrhenian Basin reaches a minimum depth of ~70 km (Figure 3). Toward the Southern Apennines and the external Dinarides, it gradually deepens, and in the Dinarides the lithospheric plate sinks about 280 km below Dacia. From the internal Dinarides to the Carpathian-Balkanides, the LAB is relatively flat at a depth of about 120 km.

These variations in lithosphere thickness along the profile also imply different temperatures between the domains at the same depth. The Tyrrhenian Basin exhibits the highest temperatures, reaching  $\sim 970^{\circ}$ C at a depth of 50 km (Figure 3c and Figure S4 in Supporting Information S1), decreasing toward the margin, where the temperature below the Apennines becomes  $\sim 900^{\circ}$ C. Meanwhile, in the Adriatic Sea and the Dinarides, the temperatures at 50 km depth are  $\sim 780^{\circ}$ C and  $\sim 870^{\circ}$ C, respectively. These lateral temperature variations are reflected in the calculated densities and seismic velocities.

The density distribution of the upper mantle is shown in Figure 3f and Figure S4 in Supporting Information S1. In the 50–120 km depth range Adria's mantle has a slightly higher density (30 kg/m3) than farther to the east. Although the chemical composition of the mantle wedge and the Dacian mantle domain are different, the density differences between the two domains are very small, since they have a similar temperature distribution.

In the Tyrrhenian Basin, the presence of serpentinized mantle at shallow levels (<12 km) results in low densities of 2,870 and 2,980 kg/m<sup>3</sup>. Below that depth, the mantle is devoid of serpentinization and because of the elevated temperatures at shallower depths, the density distribution decreases from 3,320 kg/m<sup>3</sup> at 13 km to 3,270 kg/m<sup>3</sup> at

ZHANG ET AL. 8 of 21

the LAB (Figure S4 in Supporting Information S1). Akimbekova et al. (2021), using a compilation of available active and passive seismic data and gravity modeling, also distinguished between the older, colder and denser Adriatic lithospheric mantle, and the warmer and lighter Tyrrhenian mantle (Figure S4 in Supporting Information S1).

Seismic velocities below the Tyrrhenian Basin are higher at 15–30 km (Vs > 4.6 km/s and Vp  $\sim 8.1$  km/s) decreasing in depth to 4.3 km/s and 7.8 km/s at the LAB. At 50 km depth there is an increase in seismic velocities from the center of the Tyrrhenian Basin to the Adria microplate (Figures S4 and S5 in Supporting Information S1). The highest velocities are observed in the Adria block with Vp values of  $\sim 8.1$  km/s and Vs values between 4.42 and 4.57 km/s (Figures S4 and S5 in Supporting Information S1) while lower values are obtained in the Dacia mantle, although the differences are relatively minor ( $\sim 0.5$  km/s).

Tomography studies show that the sublithospheric mantle at depth between 100 and 160–200 km below the Southern Apennines is characterized by negative Vp anomalies (e.g., Amaru, 2007a, 2007b; Rappisi et al., 2022) and, negative Vs anomalies (e.g., Belinić et al., 2021; El-Sharkawy et al., 2020) whereas positive Vp and Vs anomalies are observed at greater depths (Figure S6 in Supporting Information S1). In contrast, beneath the Southern Dinarides, positive Vp and Vs anomalies extend continuously from the LAB to 280–300 km depth (e.g., Belinić et al., 2021; El-Sharkawy et al., 2020; Rappisi et al., 2022) (Figure S6 in Supporting Information S1).

Based on the 3D anisotropic teleseismic P-wave tomographic model of Rappisi et al. (2022) and the high-resolution shear-wave velocity model of El-Sharkawy et al. (2020) and in order to fit the observed geoid height and elevation data (Figure 3), we have modeled two sublithospheric thermo-compositional anomalies beneath the Southern Apennines and Dinarides. Both anomalies are set to 200°C lower than the surrounding mantle, but with different geometries and extensions. The southwestern anomaly is detached from the overlying plate and extends from 160 to 400 km below the Southern Apennines, whereas the northeastern one is attached and extends to 280 km below the Southern Dinarides. Since both anomalies are related to the sinking of Adria continental lithosphere, we have used the same chemical composition as for the Adria mantle. Our results show that the two sublithospheric anomalies have an increase in density of 20 kg/m3, as well as an increase in Vp and Vs of 1.5% and 2%, respectively (Figure 3 and Figure S5 in Supporting Information S1) with respect to the surrounding lithosphere.

Along the profile seismic activity in the sublithospheric mantle occurs primarily within the Apennine slab and its immediate surroundings at depths  $\geq$ 250 km.

### 3. Discussion

# 3.1. Crustal and Lithospheric Structure

Based on the numerous geological studies and seismic surveys carried out in the study region, we have been able to obtain a well-constrained estimate of the main crustal tectonic units and of the Moho depth for most of the study profile (Figure 2). However, in regions with limited availability of deep seismic data such as the Carpathians and Balkanides, and in regions where there is some uncertainty in the Moho depth estimates, we have refined the depth estimate based on fitting the geophysical observables (Figure S1 in Supporting Information S1). This uncertainty is evident along the Southern Apennines and Dinarides, where the 3D complexity of the crustal structure results in notable differences between the seismic Moho depth and that obtained by regional crustal models (Figure 2).

Although there is coincidence for most of the profile between our results and those obtained from the regional models and seismic data (Figure 2), there are certain discrepancies. In the Tyrrhenian Basin, the main discrepancy is observed with the models proposed by Laske et al. (2013), as these authors suggest a crust that is 5–10 km thicker. The way the Tyrrhenian crust thickens to the west varies among different regional models and our results. Prada et al. (2014, 2016) interpreted anomalously high P-wave velocities as exhumed mantle with variable degrees of serpentinization from 100% below the sedimentary layer to 0% at about 10 km depth. This is compatible with our model results, where we infer a 4 km thick upper layer with 75% serpentinization, and a 2 km thick lower layer with a 25% serpentinized mantle.

To the east, the crustal structure below the Southern Apennines and Dinarides is complex and published estimates of the Moho depth differs noticeably. Below the Apennines, teleseismic RF data from Steckler

ZHANG ET AL. 9 of 21

et al. (2008), Piana Agostinetti et al. (2008), and Piana Agostinetti and Amato (2009) as well as from ambientnoise surface wave dispersion (Molinari et al., 2015) show local differences in Moho depth in the order of
10 km and the presence of a double Moho beneath the western Apennines (Piana Agostinetti & Amato, 2009).
From the compilation of active and passive seismic data along the CROP-04 crustal reflection seismic profile,
Savastano and Piana Agostinetti (2019) concluded that the local crustal thickening is slightly displaced to the
east (~50 km) and deeper than that obtained from our results. However, our results are consistent with those
of Akimbekova et al. (2021), both in terms of the western location and depth of the crustal thickening
(Figure 2). These authors, after a compelling review of the published Moho geometries from both active and
passive seismic methods, performed gravity modeling along CROP-04 (onshore) and M-6B (offshore)
multichannel deep seismic profiles. Our results also agree with the geological crustal model of Mazzoli
et al. (2013) based on the integration of surface geological data and the CROP-04 deep seismic reflection
profile.

Available crustal models agree on a generic crustal thickening below the Southern Dinarides but, there is no consensus on its absolute values. Our findings align closely with the Moho map presented by Zailac et al. (2023) and the RF results of Stipčević et al. (2020). These authors conclude that in the southern external Dinarides, the Moho is located at  $\sim 50$  km, whereas in the Northern Dinarides it is at  $\sim 40$  km (e.g., Stipčević et al., 2020; Zhang et al., 2022). They also report that the uncertainty of the RF data could be indicating the presence of a double or overlapping Moho likely related to the collisional front.

In good agreement with the available regional models our results show a relatively constant Moho depth of 35–40 km depth throughout the Dacia crustal domain, the only difference being a slight crustal thinning in the Sava Suture Zone region (Figure 2). The high average density (2,850 kg/m³) obtained in the suture zone agrees with the high-velocity body imaged by Kapuralićet al. (2019). Subduction and gradual closure of the Vardar Ocean from the Late Cretaceous to the Paleogene resulted in the emplacement of the high density ophiolitic rocks imaged in our modeling results. Zhang et al. (2022), using geophysical-petrological modeling along a northern transect, also found the same average density at the suture zone between the Adria and Tisza microplates. RF results from Miller and Piana Agostinetti (2012) show some local coincidence with our predicted LAB, which is located at about 120 km depth, in the Apennines. However, the majority of seismic studies predict a shallower seismic LAB than our thermal LAB (Figure 3e). The uncertainties in the RF data, which predict the seismic LAB depth ranging from 60 to 120 km, may be associated with the complexity and 3D crustal structure in the subduction front.

In the Southern Tyrrhenian Basin, surface waves dispersion curves constrain the seismic LAB at about 50 km depth (Pontevivo & Panza, 2002; Pontevivo (2003); Panza et al., 2007), much shallower than our thermal LAB, at 70 km depth. This is a widely recognized yet unresolved issue, with the seismic LAB -particularly that obtained from surface waves-usually shallower than the thermal LAB. Jiménez-Munt et al. (2019) found that the seismic LAB roughly follows the  $1,000^{\circ}\text{C} \pm 50^{\circ}\text{C}$  isotherm. As observed in Figure 3e, the seismic LAB obtained by surface wave dispersion roughly follows the 950°C isotherm, which would explain the differences obtained from our study.

# 3.2. Mantle Composition and Sublithospheric Anomalies

Although the relationships between mantle chemical composition, density, and elastic properties is not straightforward due to their non-linear nature and the lack of uniqueness (Kumar et al., 2021), we can still relate the composition of the lithospheric mantle to the primary geodynamic processes. Geoid height and elevation, and to a lesser extent, gravity anomalies should reflect the density anomalies resulting from these processes.

In the Western-Central Mediterranean, the predominant geodynamic processes are extension in the back-arc basins and compression along the front of the subduction-related orogenic system on the SW margins of Adria. Both processes determine by far the type of magmatism and changes in composition of the lithospheric mantle (Lustrino et al., 2011; Peccerillo, 2005).

In the study profile, significant magmatism beneath the Tyrrhenian Basin and Southern Apennines and Dinarides, coupled with geophysical observations, suggest variations in the lithospheric mantle composition and degrees of mantle melting. Subduction processes can chemically enrich the mantle through metasomatism. Subduction accompanied by slab retreat and/or continental delamination, may induce partial melting via adiabatic

ZHANG ET AL. 10 of 21

decompression, leading to mantle depletion. Additionally, regional extensional stresses in the back-arc region can thin the lithosphere, allowing the mantle to rise. Adiabatic decompression and the presence of fluids released by the descending slab may facilitate melting of a partially depleted mantle from the back-arc to the mantle wedge (Peccerillo, 2005; Peccerillo, 2017).

The composition of the Tyrrhenian lithospheric mantle is closely linked to its back-arc origin and degree of partial melting, which can be inferred from the nature and volume of the magmatic events in the area. Based on seismic (surface waves) and petrological modeling, Panza et al. (2007) concluded that the thin crust of Southern Tyrrhenian Basin is underlain by a soft mantle with partial melting reaching 10%, as shown by low velocities (3.0–3.15 km/s) in the uppermost mantle and the presence of mafic tholeitic-to-transitional volcanic rocks with low-to-moderate abundance of incompatible elements.

In the central region of the Southern Tyrrhenian Basin, our best fit model shows exhumed mantle with a degree of serpentinization that decreases with depth, surrounded by a thin magmatic crust toward its margin, which is underlain by a DMM with 6% of partial melting (DMM-6%) (Table S1), in agreement with the results of Panza et al. (2007). From our best fit model, the depleted and partially melted mantle extends laterally to the onshore carbonate platform, where abundant vulcanism is recorded a little farther to the north, for example, Ischia, Vesuvio, Roccamonfina Peccerillo (2005). Additionally, surface wave studies indicate a low velocity zone at the base of the crust ranging from 3.00 to 3.15 km/s below the central Southern Tyrrhenian Basin to 3.85–4.15 km/s below the onshore carbonate platform (Panza et al., 2007).

Beneath the southern external Dinarides, our modeling suggests a mantle wedge with a DMM composition having 3% of melting, based on the fitting of the geophysical observables and considering that the area has undergone continental delamination. The low mantle wedge velocity predicted by our model is also consistent with the low seismic velocity zone proposed by Amaru (2007a, 2007b), Blom et al. (2020) and Belinić et al. (2021). The lithospheric mantle below the remaining Adria and Dacia plates corresponds to a slightly depleted mantle of TC\_2 composition (Griffin et al., 2009; Zhang et al., 2022) (Table S1).

To enhance the fit with geoid height and elevation data, and considering seismic tomography results (e.g., Blom et al., 2020; Amaru, 2007a, 2007b; Benoit et al., 2011; Giacomuzzi et al., 2011; Koulakov et al., 2015; Šumanovac et al., 2017; Blom et al. (2020); Belinić et al., 2021; Belinić et al., 2021; Handy et al., 2021; El-Sharkawy et al., 2020; Rappisi et al., 2022), we have modeled two sublithospheric thermo-compositional anomalies with an Adriatic mantle composition. Our best fitting model shows that the western anomaly, situated below the Southern Apennines, is a west-dipping detached cold (-200°C) anomaly, extending from 160 km down to 400 km. In Figure 4, we compare the observed and calculated elevations under different scenarios, focusing on whether the Apennine slab is detached (Figure 4b) or attached (Figure 4c) to the continental lithosphere. We conclude that the Apennine elevation fits well without considering the slab weight (black line), suggesting detachment. Conversely, the elevation of the Dinarides is consistent with a fully attached slab. Similar observations are seen for the geoid height in Figure 3b, with a mismatch of about 1 m when we consider that the slab is attached to the continental lithosphere. Combining these findings with seismic tomography results (Figure S6 in Supporting Information S1) supports the hypothesis of a slab gap beneath the Southern Apennines. This deep cold body is characterized by seismic anomalies between +1% and +1.5%, which agree with tomography results (e.g., Amaru, 2007a, 2007b; El-Sharkawy et al., 2020; Rapissi et al., 2022) as shown in Figures S5 and S6 in Supporting Information S1.

Below the Southern Dinarides, a much shorter attached east-dipping anomaly is observed, resulting in a lithospheric slab down to 280 km. Our results agree with Rappisi et al. (2022), who observed a pronounced fast velocity anomaly extending along the Northern and Southern Dinarides in a NW-SE direction down to 280 km depth. By contrast, along the Apennines the fast velocity anomaly is mapped down to 400 km.

Deep seismicity, occurring at depths greater than 100 km within the study region, is concentrated in the southern half of the Southern Apennines, Southern Tyrrhenian and Calabrian Arc basins (at depths exceeding 300 km). In contrast, no deep earthquakes have been recorded along the Northern-Central Apennines and Dinarides (Figure S3 in Supporting Information S1). The deep earthquakes observed along the study profile are plausibly linked to the interaction between the deepest segment of the Southern Apennines slab and the Calabria slab (Figure S3 in Supporting Information S1).

ZHANG ET AL. 11 of 21

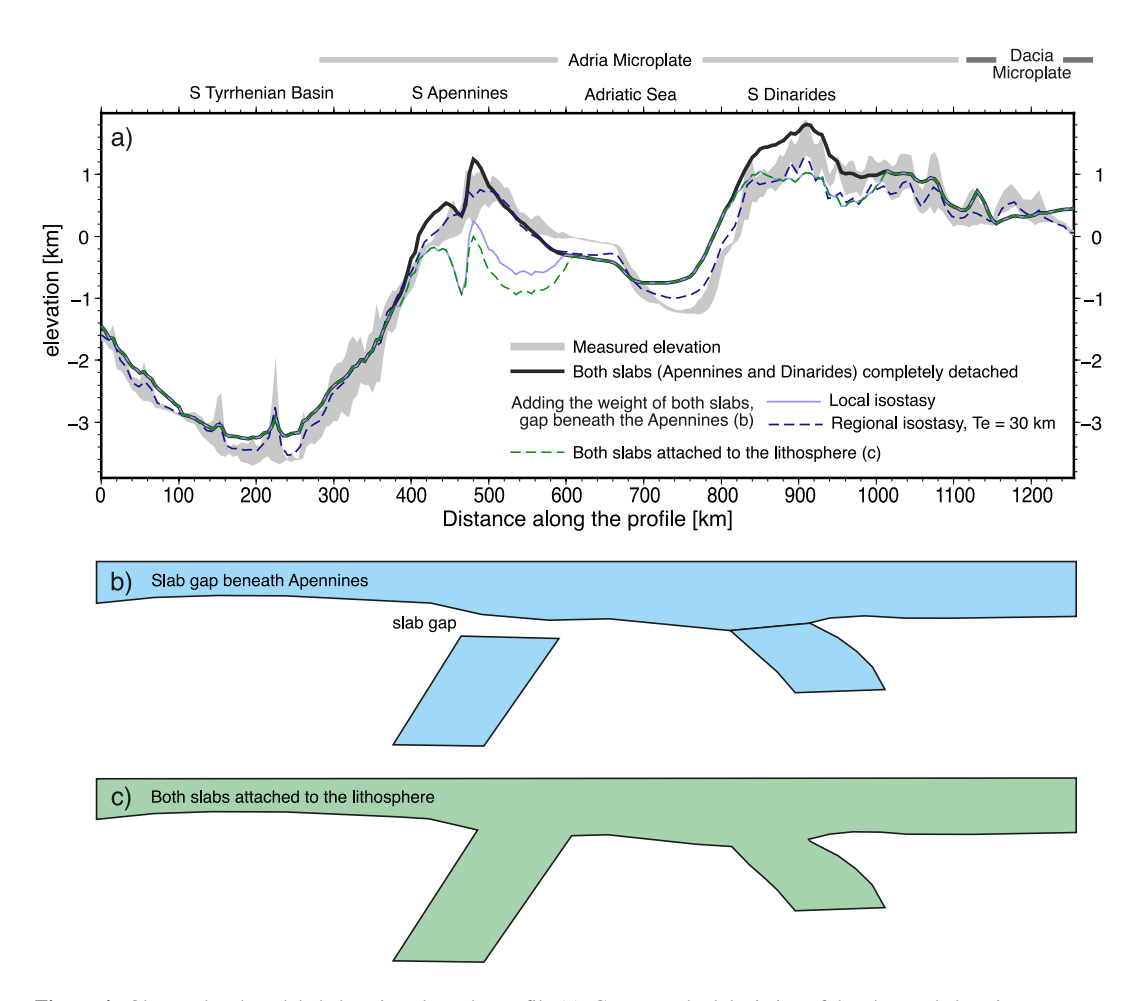


**Figure 4.** Observed and modeled elevation along the profile (a). Gray: standard deviation of the observed elevation across a 50-km-wide swath. Black: local isostasy ignoring the sublithospheric denser anomalies (Apenninic and Dinaric slabs completely detached). Blue: local isostasy considering the weight of the two sublithospheric anomalies, with a slab gap beneath Apennines (b). Dark blue dashed: regional isostasy with an elastic thickness of 30 km, resulting from model (b). Green dashed: local isostasy considering the weight of the two sublithospheric anomalies, with no slab gap beneath Apennines, both slabs attached (c).

# 3.3. N-S Lithospheric Evolution of the Western Alpine-Mediterranean Region: Geodynamic Implications

When comparing the crustal structure of the Northern (Zhang et al., 2022) and Southern profiles (Figure 5), the most significant differences are observed in the Tyrrhenian Basin. The Adria crust, between the Apennines and the Dinarides, has been modeled as a three-layer structure, comprising the upper, middle, and lower crust with relatively similar densities, while beneath the internal Dinarides our results show a two-layer crust (upper-middle and lower crust). Although the best fitting model and geological data indicate a two-layer crust below the internal Dinarides, we cannot rule out the presence of a three-layer crust. The resolution of the geophysical data used is not accurate enough to distinguish between two or three layers, as the response will be the same if the distribution of average density in depth is similar.

Slightly higher densities for the upper-middle crust are obtained along the Southern profile, although they are not large enough to be considered significant. Regarding the base of the crust, the comparison between the Northern and Southern profiles shows a crustal thickening along the eastern Adriatic Sea and southern external Dinarides (Figure 5). The southern external Dinarides have a crust that is about 10 km thicker than in the Northern profile, which agrees with the teleseismic data results of Stipčević et al. (2020). Furthermore, the density of the lower crust is slightly higher, which is coherent with its increasing depth, thus allowing a good fit with geophysical observables.

ZHANG ET AL. 12 of 21

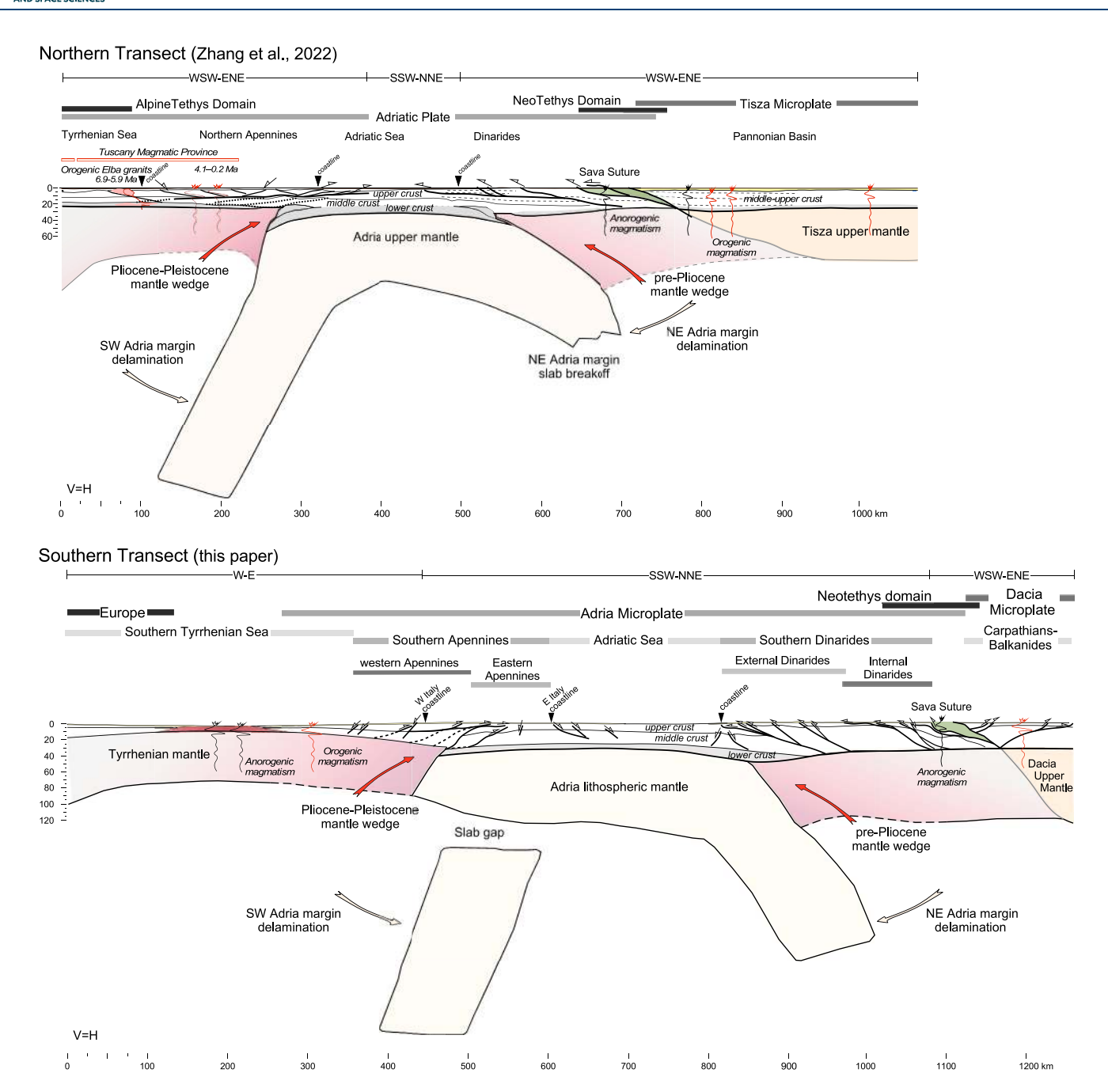


**Figure 5.** Geodynamic interpretation of the lithospheric structure along the Northern (Zhang et al., 2022) and Southern profile (presented in this study). To facilitate comparison of both profiles, we have aligned their origins, which correspond to the coastline of Corsica and Sardinia, respectively. See Figure 1 for their respective locations.

To the west, the Tyrrhenian Basin shows a very distinct organization north and south of 41°N latitude (Figure 5). In the Northern Tyrrhenian Basin, the obtained density depth distribution and crustal structure corresponds to that of a thin continental crust with widespread volcanism, extending to the Tuscany Magmatic Province (e.g., Dini et al., 2002; Pandeli et al., 2013; Sani et al., 2016).

Zhang et al. (2022) show that the western Apennines and Northern Tyrrhenian Basin are characterized by high thermal gradient and thermal properties (conductivity and heat production, 3.1 W/m·K and 3.8–1.0 μW/m³, respectively) characteristic of magmatic rocks. Assuming that the continental collision between the Corsica-Sardinia Block and the Adria microplate took place at 30-25 Ma (Carminati et al., 2012; Molli &

ZHANG ET AL. 13 of 21

Malavieille, 2011; Romagny et al., 2020; Turco et al., 2012), these magmatic rocks could be associated with either the retreat of a continental slab or the continental delamination of the Adria lithospheric mantle, possibly initiated ca 15 Ma, as proposed by Benoit et al. (2011).

For the southern profile, we have modeled a thin sedimentary cover and two exhumed mantle layers that display varying degrees of serpentinization, in agreement with the results of Prada et al. (2014). As in the northern region, volcanism is widespread extending to the onshore Campanian Plain. Magmatism in the central Tyrrhenian Basin is triggered by both extension-induced melting (back-arc basin magmatism) and continental delamination-related processes (Zhang et al., 2022). Moreover, the offshore and onshore continental platform is characterized by volcanic arc-type magmatism. Peccerillo (2017) concludes that magmatism from the Tuscany Province of the Northern Apennines to the Aeolian Arc northwest of Calabria exhibits geochemical markers of source regions that have undergone metasomatism related to subduction processes (involving fluids and subducted sediments). These processes are superimposed upon original mantle components ranging from compositions akin to MORBs to Ocean Island Basalts (OIBs).

In the Northern Adria region, coexisting crustal thinning in the Tyrrhenian domain and thickening toward the forefront of the Northern Apennines fold belt may be explained by NE-ward rollback of the SW Adria slab and its subsequent continental mantle delamination (Zhang et al., 2022). In the Southern Adria region, the deep structure is more complex, primarily due to the nearly 90-degree change in tectonic directions between the Southern Apennines and the Calabrian Arc and their respective slabs (Edwards & Grasemann, 2009; Faccenna et al., 2014). Wadati-Benioff zone earthquakes and local earthquake tomography studies have unveiled the geometry and position of the Calabrian slab, along with its role in the tectonic evolution of the region (e.g., Neri et al., 2020; Presti et al., 2019; Scarfi et al., 2018), showing that the slab might extend to depths of 300–450 km with an approximate northern dip ranging from 60 to 70°, thus reaching the central region of the Southern Tyrrhenian Basin (e.g., Giardini and Velonà (1991); Chiarabba et al., 2005, 2008; Neri et al., 2020).

Regarding the lithospheric mantle composition, in the Northern profile Zhang et al. (2022) propose the existence of two mantle wedges with a DMM-3% composition resulting from the rollback of the Ligurian-Tethys oceanic slab in the SW margin of Adria as well as of the Vardar-Neo-Tethys oceanic slabs in its NE margin. The two opposite and asynchronous subduction rollback processes were followed by the continental mantle delamination of the southwestern and northeastern distal margins of the Adria Microplate.

In the Southern profile and along the Tyrrhenian Basin, considering the age and type of the magmatism and our best-fitting model, we determine that the mantle has a DMM composition with 6% of melting. This anomalous mantle encompasses the Tyrrhenian Basin, the thinned onshore continental margin and the western Apennines. In the Dinarides region, along both profiles, modeling results show a DMM mantle wedge with 3% of melting. The main difference lies in its length, which has been determined based on maintaining the distance from the Sava suture zone to the subduction hinge, while also fitting the geophysical observables.

Along both profiles, the density of the lithospheric mantle underneath the Dinarides is significantly greater than beneath the Tyrrhenian region. This difference arises due to lithospheric thinning in the Tyrrhenian region, leading to an increase of the thermal gradient and, consequently, a decrease in density and seismic velocities.

Underneath the Apennines, our integrated modeling points to a significant cold thermal anomaly  $(-200^{\circ}\text{C})$  that extends to depths of at least to 400 km, reaching the lower boundary of our model. The main difference is that in the Northern profile, the slab is attached to the continental lithosphere. Conversely, in the Southern profile, most seismic tomography studies and the results of our best-fit model show a discontinuity or rupture at depths 120 and 160 km (Figure 3 and Figure S6 in Supporting Information S1).

One possible hypothesis is that the Southern profile intersects a slab gap likely linked to a vertical tear fault that would have favored the initiation of a slab tear, as depicted by the modeled profile (Figure 3). This gap has been commonly interpreted as the detachment of the Southern Apennines slab. It has been explained by different models (Neri et al., 2009; Rosenbaum et al., 2008; Spakman & Wortel, 2004), all of them involving a subhorizontal or vertical lateral tear detachment, with the broken slab dipping like the Northern and Central Apennines slab segments (Figure 6). The slab tear direction would therefore be sub-parallel to the direction of the Apennines rather than sub-perpendicular if it is related to a transform fault defining the segments of the SW Adria margin. From this viewpoint, the modeled slab gap could be the result of incipient slab break-off at the corner of this collision zone (bordered by the transform fault), similar to the 3D numerical model by Boonma et al. (2023)

ZHANG ET AL. 14 of 21

21699356, 2024, 4, Downloaded from https://agupubs.onlinelibrary.wiley.com/doi/10.1029/2023JB028435 by Readcube (Labtiva Inc.), Wiley Online Library on [30/03/2024]. See

Figure 6. Diagram illustrating a simplified view of the slab geometry underneath the western Adriatic margin. Slab geometry is based on the results of integrated lithospheric modeling (Zhang et al., 2022 blue line and this study, red line) and geological and geophysical interpretations, for example, Spakman and Wortel (2004); Rosenbaum et al. (2008); Carminati et al. (2012); Faccenna et al. (2014); Sun et al. (2019); Pierantoni et al. (2020); Rappisi et al. (2022).

and Li et al. (2013). In an alternative view, Carminati and Chiarabba (2023) compare two cross-sections across the southern Apennines and Calabrian arc and identifies similar slab necking structures that they interpreted as slab damage zones. This process of slab weakening would be caused by brittle-ductile damage in the outer rise (Gerya et al., 2021). According to this interpretation, slab weakening would be characterized by low viscosity zones leading slab break-off processes. While we agree with the interpretation of slab damage for deep necking features in both cross sections, our best fitting model, particularly geoid and elevation, suggests that the shallower low seismic velocity anomaly in the Southern Apennines is a small slab gap that could be related to the initiation of a slab break-off process.

Vertical tears due to differential retreat have already been proposed by several authors to explain characteristic features observed in the Tyrrhenian-Apennines system (Doglioni, 1991; Doglioni et al., 1994, 2001; Scrocca, 2006; D'Orazio et al., 2007; Rosenbaum et al., 2008; Petricca et al., 2013; Chiarabba et al., 2016; De Gori et al., 2022; Pierantoni et al., 2020). Pierantoni et al. (2020) following other authors (e.g., Doglioni et al., 1994; Rosenbaum et al., 2008) and based on kinematic reconstructions, postulate that the subduction of the continental part of the slab initiated in the North and progressed toward the South. This could lead to different sinking velocities and, as a result, in the segmentation of the slab along slab tear faults. These tear faults might propagate along the trend of fracture zones and transform faults inherited from the break-up of

Segmented margins have been proposed for other areas within the Western Mediterranean where slab asymmetry and geometric variations were inferred from seismic tomography and lithospheric modeling. For example, the existence of segments of the Jurassic Ligurian-Tethyan lithosphere along the Gulf of Cádiz-Gibraltar Arc region and in the Algerian basin is suggested to explain the observed lithospheric and upper mantle structure, and the double polarity of the subducting slabs (Fernández et al., 2019; Kumar et al., 2021).

A different slab configuration is modeled in the eastern margin of Adria. In the Dinarides the cold thermal anomaly reaches depths of about 200 km in the northern profile and 280 in the southern profile, shallower than those observed at the western margin of Adria (Figure 5). The variations currently observed in the geometry and depth of the western and eastern Adria slabs may potentially stem from differences in subduction and continental delamination histories. The initiation of oceanic subduction along the eastern Adria margin dates back to the Jurassic period, whereas subduction along the western Adria margin commenced during the Oligocene (e.g., Carminati et al., 2012; Gawlick & Missoni, 2019; Schmid et al., 2008; van Hinsbergen et al., 2020). Consequently, the eastern margin seems more evolved as the slab is either largely detached or is partially, if not

ZHANG ET AL. 15 of 21 completely, thermally re-equilibrated with the underlying sub-lithospheric mantle. Based on fission-track ages and isotope geochemistry, Schefer et al. (2010) concluded that (a) following the closure of the Neotethys in the Eocene, the north-eastward Adriatic slab had initiated continental delamination and retreat, and (b) slab break-off may have taken place shortly after the onset of continental delamination. This could explain the depth of the eastern slab, as determined through tomography and our thermal approach.

Adria is encompassed by significantly deformed convergent margins entailing three plate subductions with distinct polarities. One remarkable characteristic of these subducted and delaminated slabs is their diverse geometry and segmentation, as observed in tomographic studies and being compatible with the thermal modeling results presented herein. These segments are divided by lithospheric gaps, which have often been interpreted as having formed during subduction (Faccenna et al., 2014). On the other hand, most of the paleogeographic maps depict a segmentation of the Adria margins, featuring segments separated by transform faults. These segments could indeed be remnants of the Mesozoic Adria plate margins, emphasizing the necessity for a more thorough and comprehensive investigation.

### 4. Conclusions

We present the findings of a geophysical-geochemical model of the lithosphere and uppermost sublithospheric mantle, spanning from the Southern Tyrrhenian Basin to the Carpathians-Balkanides in a roughly SW-NE direction. In conjunction with the earlier investigation of Zhang et al. (2022), our study provides an integrated view of the deep structure of the Adria and Dacia microplates, as well as of the slabs located along the western and eastern Adria margins. Based on our results we can draw the following conclusions:

- In the Southern Tyrrhenian Basin our results fit well with an upper layer of sediments above serpentinized
  mantle rocks. The level of serpentinization decreases from 75% to 25% with depth, laterally transitioning to a
  two-layered magmatic crust.
- In the Southern Adria domain, from west to east, our modeling results reveal two distinct crustal domains: a double-layered crust, which extends along the western Apennines, and the three-layered crust along the eastern Apennines, Adriatic Sea and Southern Dinarides. The maximum Moho depth varies from 40 km beneath the Apennines to 50 km beneath the Dinarides. Crustal thickening primarily occurs at the expense of the lower crust, which nearly doubles its thickness. In the internal Dinarides (Adria microplate) and the Carpathian-Balkanides (Dacia microplate), the crust has a relatively constant thickness of 30–35 km.
- The thermal LAB beneath the Southern Tyrrhenian Basin is shallow, reaching a depth of ~70 km. Toward the
  Southern Apennines and Dinarides, the lithosphere gradually thickens, reaching ~280 km in the Dinarides
  below the Dacia microplate. From the internal Dinarides to the Carpathians-Balkanides, the LAB is relatively
  flat at a depth of about 120 km.
- Our thermo-geochemical model shows two different mantle compositions: a slightly depleted mantle with an average Mg# of 89.5 for the Adria and Dacia microplates, and a more fertile mantle below the Southern Tyrrhenian and Apennines (DMM-6%) and Dinarides (DMM-3%). This is consistent with the presence of two sublithospheric mantle wedges, attributed to the rollback of the Apennines and Dinaric slabs.
- The density distribution and crustal structure of the Northern Tyrrhenian Basin, corresponds to a thin continental crust with widespread volcanism, which extends to the Tuscany Magmatic Province. In contrast, in the Southern Tyrrhenian Basin, the crust is oceanic, with the presence of serpentinized mantle at crustal depths.
- In the Northern Adria region, thinning of the lithosphere in the Tyrrhenian domain and thickening toward the forefront of the Northern Apennines fold belt can be attributed to the northeastward rollback of the SW Adria slab and the resulting continental delamination. In the Southern Adria region, variably oriented lithospheric slabs determine a more complex deep structure, primarily due to the nearly 90-degree shift in tectonic directions between the Southern Apennines, the Calabrian Arc, and their respective slabs.
- The sublithospheric anomaly modeled beneath the Northern Apennines is attached to the shallower lithosphere, while a small slab gap is observed in the Southern Apennines. A possible hypothesis is that this slab gap is the result of a slab horizontal tearing.
- Along the eastern margin of Adria, the cold thermal anomaly penetrates to depths of about 200 km below the Northern Dinarides and 280 km beneath the Southern Dinarides, and thus shallower than those obtained for the western margin of Adria.

ZHANG ET AL. 16 of 21

# **Data Availability Statement**

Tomography data shown in Figure S6 in Supporting Information S1 and used in this study have been downloaded from the Atlas of the Underworld: UU-P07 model (Amaru, 2007a, 2007b), from Appendix C. Supporting Information of Belinić et al. (2021), from IRIS DMC Data Products: EMC-MeRE2020 (El-Sharkawy et al., 2020) and from (Rappisi, 2022, and Rappisi et al., 2022). Elevation and gravity data shown in Figure S1 in Supporting Information S1 and used in the 2D modeling have been taken from Sandwell et al. (2014). Geoid have been downloaded from ICGEM International Center for Global Gravity Field Models (Gilardoni et al., 2016, and Ince et al., 2019) while heat flow data comes from the Global Heat Flow Database Assessment Group (2023). Some of the data visualizations were generated with Generic Mapping Tools (Wessel et al., 2019). Data sets for 2D modeling are available in Digital CSIC (Zhang et al., 2022, and Jiménez-Munt et al., 2024).

### Acknowledgments

We are grateful to Editor Isabelle Manighetti, Associate Editor Peter DeCelles and to W. Cavazza and L. Jolivet for their constructive and detailed comments, which have significantly enhanced the quality of our manuscript. We express our sincere gratitude for the highly constructive discussions and comments provided by Eugenio Carminati. We thank Eugenio Trumpy and Adele Manzella for providing us the Geothermal Database obtained within Geothopica Project and Ajay Kumar for the fruitful discussions on the software code and interpretation. This work is funded by GeoCAM (PGC2018-095154-B-I00) and GEOADRIA (PID2022-139943NB-I00) from the Spanish Government and the Generalitat de Catalunya Grant (AGAUR, 2021 SGR 00410). Wentao Zhang is funded by the China Scholarship Council (CSC-201904910470). This work has been done using the facilities of the Laboratory of Geodynamic Modeling from Geo3BCN-CSIC.

### References

- Afonso, J. C., Fernàndez, M., Ranalli, G., Griffin, W. L., & Connolly, J. A. D. (2008). Integrated geophysical-petrological modeling of the lithosphere and sublithospheric upper mantle: Methodology and applications. *Geochemistry, Geophysics, Geosystems*, 9(5), Q05008. https://doi.org/10.1029/2007GC001834
- Akimbekova, A., Mancinelli, P., Pauselli, C., Minelli, G., & Barchi, M. R. (2021). Forward modelling of Bouguer anomalies along a transect of the Southern Apennines and the Southern Tyrrhenian Sea (Italy). *Italian Journal of Geosciences*, 140(3), 411–421. https://doi.org/10.3301/IJG.
- Amaru, M. L. (2007a). Global travel time tomography with 3-D reference models [Dataset]. ATLAS. https://www.atlas-of-the-underworld.org/uu-p07-model/
- Amaru, M. L. (2007b). Global travel time tomography with 3-D reference models: Geologica Ultraiectina, 274, 174.
- Balling, P., Grützner, C., Tomljenović, B., Spakman, W., & Ustaszewski, K. (2021). Post-collisional mantle delamination in the Dinarides implied from staircases of Oligo-Miocene uplifted marine terraces. Scientific Reports, 11(1), 1. https://doi.org/10.1038/s41598-021-81561-5
- Belinić, T., Kolínský, P., & Stipčević, J. (2021). Shear-wave velocity structure beneath the Dinarides from the inversion of Rayleigh-wave dispersion [Dataset]. Earth and Planetary Science Letters, 555, 116686. https://doi.org/10.1016/j.epsl.2020.116686
- Benoit, M. H., Torpey, M., Liszewski, K., Levin, V., & Park, J. (2011). P and S wave upper mantle seismic velocity structure beneath the northern Apennines: New evidence for the end of subduction. *Geochemistry, Geophysics, Geosystems*, 12(6), Q06004. https://doi.org/10.1029/2010GC003428
- Blom, N., Gokhberg, A., & Fichtner, A. (2020). Seismic waveform tomography of the central and eastern Mediterranean upper mantle. *Solid Earth*, 11(2), 669–690. https://doi.org/10.5194/se-11-669-2020
- Boonma, K., García-Castellanos, D., Jiménez-Munt, I., & Gerya, T. (2023). Thermomechanical modelling of lithospheric slab tearing and its topographic response. Frontiers of Earth Science, 11, 1095229. https://doi.org/10.3389/feart.2023.1095229
- Brocher, T. M. (2005). Empirical relations between elastic wavespeeds and density in the Earth's Crust. *Bulletin of the Seismological Society of America*, 95(6), 2081–2092. https://doi.org/10.1785/0120050077
- Carminati, E., & Chiarabba, C. (2023). Slab damage and the pulsating retreat of the Ionian-Apennines subduction. *Geology*, 51(3), 227–232. https://doi.org/10.1130/G50676.1
- Carminati, E., Doglioni, C., Argnani, A., Carrara, G., Dabovski, C., Dumurdzhanov, N., et al. (2004). TRANSMED transect III. In W. Cavazza, F. Roure, W. Spakman, G. Stampfli, & P. Ziegler (Eds.), *The TRANSMED atlas: The Mediterranean region form crust to mantle*. Springer Verlag. Carminati, E., Lustrino, M., & Doglioni, C. (2012). Geodynamic evolution of the central and western Mediterranean: Tectonics vs. Igneous petrology constraints. *Tectonophysics*, *579*, 173–192. https://doi.org/10.1016/j.tecto.2012.01.026
- Carminati, E., Petricca, P., & Doglioni, C. (2020). Mediterranean Tectonics. In D. Alderton & S. A. Elias (Eds.), Encyclopedia of geology (2nd ed., pp. 408–419). Academic Press. https://doi.org/10.1016/B978-0-08-102908-4.00010-2
- Chiarabba, C., Agostinetti, N. P., & Bianchi, I. (2016). Lithospheric fault and kinematic decoupling of the Apennines system across the Pollino range. *Geophysical Research Letters*, 43(7), 3201–3207. https://doi.org/10.1002/2015GL067610
- Chiarabba, C., De Gori, P., & Speranza, F. (2008). The southern Tyrrhenian subduction zone: Deep geometry, magmatism and Plio-Pleistocene evolution. Earth and Planetary Science Letters, 268(3), 408–423. https://doi.org/10.1016/j.epsl.2008.01.036
- Chiarabba, C., Giacomuzzi, G., Bianchi, I., Agostinetti, N. P., & Park, J. (2014). From underplating to delamination-retreat in the northern Apennines. Earth and Planetary Science Letters, 403, 108–116. https://doi.org/10.1016/j.epsl.2014.06.041
- Chiarabba, C., Jovane, L., & DiStefano, R. (2005). A new view of Italian seismicity using 20 years of instrumental recordings. *Tectonophysics*, 395(3), 251–268. https://doi.org/10.1016/j.tecto.2004.09.013
- De Gori, P., Lucente, F. P., Govoni, A., Margheriti, L., & Chiarabba, C. (2022). Seismic swarms in the Pollino seismic gap: Positive fault inversion within a popup structure. Frontiers in Earth Science, 10, 968187. https://doi.org/10.3389/feart.2022.968187
- De Luca, G., Cattaneo, M., Monachesi, G., & Amato, A. (2009). Seismicity in Central and Northern Apennines integrating the Italian national and regional networks. *Tectonophysics*, 476(1), 121–135. https://doi.org/10.1016/j.tecto.2008.11.032
- Dini, A., Innocenti, F., Rocchi, S., Tonarini, S., & Westerman, D. S. (2002). The magmatic evolution of the late Miocene laccolith–pluton–dyke granitic complex of Elba Island, Italy. *Geological Magazine*, 139(3), 257–279. https://doi.org/10.1017/S0016756802006556
- Doglioni, C. (1991). A proposal for the kinematic modelling of W-dipping subductions Possible applications to the Tyrrhenian-Apennines system. *Terra Nova*, 3(4), 423–434. https://doi.org/10.1111/j.1365-3121.1991.tb00172.x
- Doglioni, C., Innocenti, F., & Mariotti, G. (2001). Why Mt Etna? *Terra Nova*, 13(1), 25–31. https://doi.org/10.1046/j.1365-3121.2001.00301.x Doglioni, C., Mongelli, F., & Pieri, P. (1994). The Puglia uplift (SE Italy): An anomaly in the foreland of the Apenninic subduction due to buckling of a thick continental lithosphere. *Tectonics*, 13(5), 1309–1321. https://doi.org/10.1029/94TC01501
- D'Orazio, M., Innocenti, F., Tonarini, S., & Doglioni, C. (2007). Carbonatites in a subduction system: The Pleistocene alvikites from Mt. Vulture (southern Italy). Lithos, 98(1), 313–334. https://doi.org/10.1016/j.lithos.2007.05.004
- Edwards, M. A., & Grasemann, B. (2009). Mediterranean snapshots of accelerated slab retreat: Subduction instability in stalled continental collision. *Geological Society, London, Special Publications*, 311(1), 155–192. https://doi.org/10.1144/SP311.6

ZHANG ET AL. 17 of 21

18 of 21



ZHANG ET AL.

# Journal of Geophysical Research: Solid Earth

- 10.1029/2023JB028435
- El-Sharkawy, A., Meier, T., Lebedev, S., Behrmann, J. H., Hamada, M., Cristiano, L., et al. (2020). The slab puzzle of the Alpine-Mediterranean region: Insights from a new, high-resolution, shear wave velocity model of the upper mantle [Dataset]. SAGE. https://doi.org/10.17611/dp/emc. 2020 meresvelsh 1
- El-Sharkawy, A., Meier, T., Lebedev, S., Behrmann, J. H., Hamada, M., Cristiano, L., et al. (2020). The slab puzzle of the Alpine-Mediterranean Region: Insights from a new, high-resolution, shear wave velocity model of the upper mantle [Dataset]. *Geochemistry, Geophysics, Geosystems*, 21(8), e2020GC008993. https://doi.org/10.1029/2020GC008993
- Faccenna, C., Becker, T. W., Auer, L., Billi, A., Boschi, L., Brun, J. P., et al. (2014). Mantle dynamics in the Mediterranean. Reviews of Geophysics, 52(3), 283–332. https://doi.org/10.1002/2013RG000444
- Faccenna, C., Becker, T. W., Lucente, F. P., Jolivet, L., & Rossetti, F. (2001). History of subduction and back are extension in the Central Mediterranean. *Geophysical Journal International*, 145(3), 809–820. https://doi.org/10.1046/j.0956-540x.2001.01435.x
- Fernàndez, M., Torne, M., Vergés, J., Casciello, E., & Macchiavelli, C. (2019). Evidence of segmentation in the Iberia–Africa plate boundary: A Jurassic heritage? *Geosciences*, 9(8), 8. https://doi.org/10.3390/geosciences9080343
- Finetti, I. R. (2005). CROP project: Deep seismic exploration of the central Mediterranean and Italy. Elsevier.
- Gawlick, H.-J., & Missoni, S. (2019). Middle-Late Jurassic sedimentary mélange formation related to ophiolite obduction in the Alpine-Carpathian-Dinaridic Mountain Range. Gondwana Research, 74, 144–172. https://doi.org/10.1016/j.gr.2019.03.003
- Gerya, T. (2019). Introduction to numerical geodynamic modelling (2nd ed.). Cambridge University Press. https://doi.org/10.1017/9781316534243
- Gerya, T. V., Bercovici, D., & Becker, T. W. (2021). Dynamic slab segmentation due to brittle-ductile damage in the outer rise. *Nature*, 599(7884), 7884–8250, https://doi.org/10.1038/s41586-021-03937-x
- Giacomuzzi, G., Chiarabba, C., & De Gori, P. (2011). Linking the Alps and Apennines subduction systems: New constraints revealed by high-resolution teleseismic tomography. Earth and Planetary Science Letters, 301(3), 531–543. https://doi.org/10.1016/j.epsl.2010.11.033
- Giacomuzzi, G., De Gori, P., & Chiarabba, C. (2022). How mantle heterogeneities drive continental subduction and magmatism in the Apennines. Scientific Reports, 12(1), 13631. https://doi.org/10.1038/s41598-022-17715-w
- Giardini, D., & Velonà, M. (1991). The deep seismicity of the Tyrrhenian sea. *Terra Nova*, 3(1), 57–64. https://doi.org/10.1111/j.1365-3121.1991. tb00844.x
- Gilardoni, M., Reguzzoni, M., & Sampietro, D. (2016). GECO: A global gravity model by locally combining GOCE data and EGM2008
- [Dataset]. Studia Geophysica et Geodaetica, 60(2), 228–247. https://doi.org/10.1007/s11200-015-1114-4 Global Heat Flow Data Assessment Group, Fuchs, S., Neumann, F., Norden, B., Beardsmore, G., et al. (2023). The global heat flow database:
- Update 2023. V. 1 [Dataset]. GFZ Data Services. https://doi.org/10.5880/fidgeo.2023.008 Griffin, W. L., O'Reilly, S. Y., Afonso, J. C., & Begg, G. C. (2009). The composition and evolution of lithospheric mantle: A re-evaluation and its
- tectonic implications. *Journal of Petrology*, 50(7), 1185–1204. https://doi.org/10.1093/petrology/egn033

  Handy M. R. Schmid, S. M. Paffrath, M. & Friederich, W. & the AlpArray Working Group. (2021). Orogenic lithosphere and slabs in the
- Handy, M. R., Schmid, S. M., Paffrath, M., & Friederich, W., & the AlpArray Working Group. (2021). Orogenic lithosphere and slabs in the greater Alpine area – Interpretations based on teleseismic P-wave tomography. Solid Earth, 12(11), 2633–2669. https://doi.org/10.5194/se-12-2633-2021
- Handy, M. R., Ustaszewski, K., & Kissling, E. (2015). Reconstructing the Alps–Carpathians–Dinarides as a key to understanding switches in subduction polarity, slab gaps and surface motion. *International Journal of Earth Sciences*, 104(1), 1–26. https://doi.org/10.1007/s00531-014-1060-3
- Hasterok, D., & Webb, J. (2017). On the radiogenic heat production of igneous rocks. Geoscience Frontiers, 8(5), 919–940. https://doi.org/10.1016/j.gsf.2017.03.006
- Ince, E. S., Barthelmes, F., Reißland, S., Elger, K., Förste, C., Flechtner, F., & Schuh, H. (2019). ICGEM 15 years of successful collection and distribution of global gravitational models, associated services and future plaw [Dataset]. Earth System Science Data, 11, (2), 647–674. https://doi.org/10.5194/essd-11-647-2019
- Jiménez-Munt, I., Torne, M., Fernàndez, M., Vergés, J., Kumar, A., Carballo, A., & García-Castellanos, D. (2019). Deep seated density anomalies across the Iberia-Africa plate boundary and its topographic response. *Journal of Geophysical Research: Solid Earth*, 124(12), 13310–13332. https://doi.org/10.1029/2019JB018445
- Jiménez-Munt, I., Zhang, W., Torne, M., Vergés, J., Bravo-Gutiérrez, E., Negredo, A. M., et al. (2024). The Lithosphere and Upper Mantle of the Western Mediterranean region from integrated geophysical-geochemical modelling [Dataset]. DIGITAL.CSIC. https://doi.org/10.20350/ digitalCSIC/16154
- Jolivet, L. (2023). Tethys and Apulia (Adria), 100 years of reconstructions. Comptes Rendus Geoscience, 355(S2), 1–20. https://doi.org/10.5802/crgeos.198
- Jolivet, L., & Faccenna, C. (2000). Mediterranean extension and the Africa –Eurasia collision. Tectonics, 19(6), 1095–1106. https://doi.org/10.1029/2000TC900018
- Kalmár, D., Hetényi, G., Balázs, A., Bondár, I., & Group, A. W. (2021). Crustal thinning from orogen to back-arc basin: The structure of the Pannonian basin region revealed by P-to-S converted seismic waves. *Journal of Geophysical Research: Solid Earth*, 126(7), e2020JB021309. https://doi.org/10.1029/2020JB021309
- Kapuralić, J., Šumanovac, F., & Markušić, S. (2019). Crustal structure of the northern Dinarides and southwestern part of the Pannonian basin inferred from local earthquake tomography. Swiss Journal of Geosciences, 112(1), 181–198. https://doi.org/10.1007/s00015-018-0335-2
- Király, Á., Holt, A. F., Funiciello, F., Faccenna, C., & Capitanio, F. A. (2018). Modeling slab-slab interactions: Dynamics of outward dipping double-sided subduction systems. Geochemistry, Geophysics, Geosystems, 19(3), 693–714. https://doi.org/10.1002/2017GC007199
- Koulakov, I., Jakovlev, A., Zabelina, I., Roure, F., Cloetingh, S., El Khrepy, S., & Al-Arifi, N. (2015). Subduction or delamination beneath the Apennines? Evidence from regional tomography. Solid Earth, 6(2), 669–679. https://doi.org/10.5194/se-6-669-2015
- Kumar, A., Fernàndez, M., Jiménez-Munt, I., Torne, M., Vergés, J., & Afonso, J. C. (2020). LitMod2D\_2.0: An improved integrated geophysical-petrological modeling tool for the physical interpretation of upper mantle anomalies. *Geochemistry, Geophysics, Geosystems*, 21(3), e2019GC008777. https://doi.org/10.1029/2019GC008777
- Kumar, A., Fernàndez, M., Vergés, J., Torne, M., & Jiménez-Munt, I. (2021). Opposite symmetry in the lithospheric structure of the Alboran and Algerian basins and their margins (Western Mediterranean): Geodynamic implications. *Journal of Geophysical Research: Solid Earth*, 126(7), e2020JB021388. https://doi.org/10.1029/2020JB021388
- Laske, G., Masters, G., Ma, Z., & Pasyanos, M. (2013). Update on CRUST1.0—A 1-degree global model of Earth's crust (Vol. 15, p. 2658). Le Breton, E., Handy, M. R., Molli, G., & Ustaszewski, K. (2017). Post-20 Ma motion of the Adriatic Plate: New constraints from surrounding
- orogens and implications for crust-mantle decoupling. *Tectonics*, 36(12), 3135–3154. https://doi.org/10.1002/2016TC004443

  Li, Z.-H., Xu, Z., Gerya, T., & Burg, J.-P. (2013). Collision of continental corner from 3-D numerical modeling. *Earth and Planetary Science Letters*, 380, 98–111. https://doi.org/10.1016/j.epsl.2013.08.034

- Loreto, M. F., Zitellini, N., Ranero, C. R., Palmiotto, C., & Prada, M. (2021). Extensional tectonics during the Tyrrhenian back-arc basin formation and a new morpho-tectonic map. *Basin Research*, 33(1), 138–158. https://doi.org/10.1111/bre.12458
- Lucente, F. P., Chiarabba, C., Cimini, G. B., & Giardini, D. (1999). Tomographic constraints on the geodynamic evolution of the Italian region. Journal of Geophysical Research, 104(B9), 20307–20327. https://doi.org/10.1029/1999JB900147
- Lustrino, M., Duggen, S., & Rosenberg, C. L. (2011). The Central-Western Mediterranean: Anomalous igneous activity in an anomalous collisional tectonic setting. Earth-Science Reviews, 104(1), 1–40. https://doi.org/10.1016/j.earscirev.2010.08.002
- Magni, V., & Király, Á. (2020). Delamination. In Reference module in Earth systems and environmental sciences. Elsevier. https://doi.org/10.1016/B978-0-12-409548-9.09515-4
- Magrini, F., Diaferia, G., El-Sharkawy, A., Cammarano, F., van der Meijde, M., Meier, T., & Boschi, L. (2022). Surface-wave tomography of the central-western Mediterranean: New insights into the Liguro-Provençal and Tyrrhenian Basins. *Journal of Geophysical Research: Solid Earth*, 127(3), e2021JB023267. https://doi.org/10.1029/2021JB023267
- Matenco, L., & Radivojević, D. (2012). On the formation and evolution of the Pannonian Basin: Constraints derived from the structure of the junction area between the Carpathians and Dinarides. *Tectonics*, 31(6), TC6007. https://doi.org/10.1029/2012TC003206
- Mazzoli, S., Ascione, A. S. C., Iannace, A., Megna, A., Santini, S., & Vitale, S. (2013). Subduction and continental collision events in the southern Apennines: Constraints from two crustal cross-sections. RENDICONTI ONLINE DELLA SOCIETÀ GEOLOGICA ITALIANA, 25, 78–84. https://doi.org/10.3301/ROL.2013.07
- Melchiorre, M., Vergés, J., Fernàndez, M., Coltorti, M., Torne, M., & Casciello, E. (2017). Evidence for mantle heterogeneities in the westernmost Mediterranean from a statistical approach to volcanic petrology. Lithos, 276, 62–74. https://doi.org/10.1016/j.lithos.2016.11.018
- Miller, M. S., & Piana Agostinetti, N. (2012). Insights into the evolution of the Italian lithospheric structure from S receiver function analysis. Earth and Planetary Science Letters, 345–348, 49–59. https://doi.org/10.1016/j.epsl.2012.06.028
- Molinari, I., Verbeke, J., Boschi, L., Kissling, E., & Morelli, A. (2015). Italian and Alpine three-dimensional crustal structure imaged by ambient-noise surface-wave dispersion. *Geochemistry, Geophysics, Geosystems*, 16(12), 4405–4421. https://doi.org/10.1002/2015GC006176
- Molli, G., & Malavieille, J. (2011). Orogenic processes and the Corsica/Apennines geodynamic evolution: Insights from Taiwan. *International Journal of Earth Sciences*, 100(5), 1207–1224. https://doi.org/10.1007/s00531-010-0598-y
- Nafe, J. E., & Drake, C. L. (1963). Physical properties of marine sediments. In The sea (Vol. 3, pp. 794-815). John Wiley & Sons.
- Neri, G., Orecchio, B., Scolaro, S., & Totaro, C. (2020). Major earthquakes of southern Calabria, Italy, into the regional geodynamic context. Frontiers in Earth Science, 8, 579846. https://doi.org/10.3389/feart.2020.579846
- Neri, G., Orecchio, B., Totaro, C., Falcone, G., & Presti, D. (2009). Subduction beneath southern Italy close the ending: Results from seismic tomography. Seismological Research Letters, 80(1), 63–70. https://doi.org/10.1785/gssrl.80.1.63
- Norden, B., & Förster, A. (2006). Thermal conductivity and radiogenic heat production of sedimentary and magmatic rocks in the Northeast German Basin. *AAPG Bulletin*. 90(6), 939–962. https://doi.org/10.1306/01250605100
- Pandeli, E., Principi, G., Bortolotti, V., Benvenuti, M., Fazzuoli, M., Dini, A., et al. (2013). The Elba Island: An intriguing geological puzzle in the Northern Tyrrhenian Sea. ISPRA and Soc. Geol. It., Geol. Field Trips, 5(2.1), 1–114. https://doi.org/10.3301/gft.2013.03
- Panza, G., Peccerillo, A., Aoudia, A., & Farina, B. (2007). Geophysical and petrological modelling of the structure and composition of the crust and upper mantle in complex geodynamic settings: The Tyrrhenian Sea and surroundings. *Earth-Science Reviews*, 80(1–2), 1–46. https://doi.org/10.1016/j.earscirev.2006.08.004
- Peccerillo, A. (2005). Plio-quaternary volcanism in Italy: Petrology, geochemistry, geodynamics. Springer.
- Peccerillo, A. (2017). Cenozoic volcanism in the Tyrrhenian Sea region. Springer International Publishing. https://doi.org/10.1007/978-3-319-
- Petricca, P., Carafa, M. M. C., Barba, S., & Carminati, E. (2013). Local, regional, and plate scale sources for the stress field in the Adriatic and Periadriatic region. *Marine and Petroleum Geology*, 42, 160–181. https://doi.org/10.1016/j.marpetgeo.2012.08.005
- Piana Agostinetti, N., & Amato, A. (2009). Moho depth and Vp/Vs ratio in peninsular Italy from teleseismic receiver functions. *Journal of Geophysical Research*, 114(B6), B06303. https://doi.org/10.1029/2008JB005899
- Piana Agostinetti, N., Park, J., & Lucente, F. P. (2008). Mantle wedge anisotropy in Southern Tyrrhenian Subduction Zone (Italy), from receiver function analysis. *Tectonophysics*, 462(1–4), 35–48. https://doi.org/10.1016/j.tecto.2008.03.020
- Pierantoni, P. P., Penza, G., Macchiavelli, C., Schettino, A., & Turco, E. (2020). Kinematics of the Tyrrhenian-Apennine system and implications for the origin of the Campanian magmatism. In *Vesuvius, Campi Flegrei, and Campanian volcanism* (pp. 33–56). Elsevier. https://doi.org/10.1016/B978-0-12-816454-9.00003-1
- Piromallo, C., & Morelli, A. (2003). P wave tomography of the mantle under the Alpine-Mediterranean area. *Journal of Geophysical Research*, 108(B2), 2065. https://doi.org/10.1029/2002JB001757
- Pontevivo, A. (2003). Surface-wave tomography and non-linear inversion in Italy and surrounding areas. Ph.D. thesis. University of Trieste. Pontevivo, A., & Panza, G. F. (2002). Group velocity tomography and regionalization in Italy and bordering areas. Physics of the Earth and Planetary Interiors, 134(1), 1–15. https://doi.org/10.1016/S0031-9201(02)00079-1
- Prada, M., Ranero, C. R., Sallarès, V., Zitellini, N., & Grevemeyer, I. (2016). Mantle exhumation and sequence of magmatic events in the Magnaghi–Vavilov Basin (Central Tyrrhenian, Italy): New constraints from geological and geophysical observations. *Tectonophysics*, 689, 133–142. https://doi.org/10.1016/j.tecto.2016.01.041
- Prada, M., Sallares, V., Ranero, C. R., Vendrell, M. G., Grevemeyer, I., Zitellini, N., & de Franco, R. (2014). Seismic structure of the Central Tyrrhenian basin: Geophysical constraints on the nature of the main crustal domains. *Journal of Geophysical Research: Solid Earth*, 119(1), 52–70. https://doi.org/10.1002/2013JB010527
- Presti, D., Totaro, C., Neri, G., & Orecchio, B. (2019). New earthquake data in the Calabrian subduction zone, Italy, suggest revision of the presumed dynamics in the upper part of the subducting slab. Seismological Research Letters, 90(5), 1994–2004. https://doi.org/10.1785/0220190024
- Rappisi, F. (2022). iso- and ani-NEWTON21 tomographic models [Dataset]. figshare. https://doi.org/10.6084/m9.figshare.19188950.v1
- Rappisi, F., VanderBeek, B. P., Faccenda, M., Morelli, A., & Molinari, I. (2022). Slab geometry and upper mantle flow patterns in the central Mediterranean from 3D anisotropic P-wave tomography [Dataset]. *Journal of Geophysical Research: Solid Earth*, 127(5), e2021JB023488. https://doi.org/10.1029/2021JB023488
- Romagny, A., Jolivet, L., Menant, A., Bessière, E., Maillard, A., Canva, A., et al. (2020). Detailed tectonic reconstructions of the Western Mediterranean region for the last 35 Ma, insights on driving mechanisms. *Bulletin de la Societe Geologique de France*, 191(1), 37. https://doi.org/10.1051/bsgf/2020040
- Rosenbaum, G., Gasparon, M., Lucente, F. P., Peccerillo, A., & Miller, M. S. (2008). Kinematics of slab tear faults during subduction segmentation and implications for Italian magmatism: Kinematics of slab tear faults. *Tectonics*, 27(2), TC2008. https://doi.org/10.1029/2007TC002143

ZHANG ET AL. 19 of 21

- Sandwell, D. T., Müller, R. D., Smith, W. H. F., Garcia, E., & Francis, R. (2014). New global marine gravity model from CryoSat-2 and Jason-1 reveals buried tectonic structure. [Dataset]. TOPEX, 346(6205), 65–67. https://doi.org/10.1126/science.1258213
- Sani, F., Bonini, M., Montanari, D., Moratti, G., Corti, G., & Ventisette, C. D. (2016). The structural evolution of the Radicondoli–Volterra Basin (southern Tuscany, Italy): Relationships with magmatism and geothermal implications. *Geothermics*, 59, 38–55. https://doi.org/10.1016/j.geothermics.2015.10.008
- Savastano, L., & Piana Agostinetti, N. (2019). Deep structure of the Southern Apennines as imaged by active and passive seismic data along the CROP-04 (crustal) reflection seismic profile. *Journal of the Geological Society, 176*(6), 1284–1290. https://doi.org/10.1144/jgs2018-201
- Scarfi, L., Barberi, G., Barreca, G., Cannavò, F., Koulakov, I., & Patanè, D. (2018). Slab narrowing in the Central Mediterranean: The Calabro-Ionian subduction zone as imaged by high resolution seismic tomography. Scientific Reports, 8(1), 1. https://doi.org/10.1038/s41598-018-23543-8
- Schefer, S., Egli, D., Missoni, S., Bernoulli, D., Fügenschuh, B., Gawlick, H.-J., et al. (2010). Triassic metasediments in the internal Dinarides (Kopaonik area, southern Serbia): Stratigraphy, paleogeographic and tectonic significance. *Geologica Carpathica*, 61(2), 89–109. https://doi.org/10.2478/v10096-010-0003-6
- Schmid, S. M., Bernoulli, D., Fügenschuh, B., Matenco, L., Schefer, S., Schuster, R., et al. (2008). The Alpine-Carpathian-Dinaridic orogenic system: Correlation and evolution of tectonic units. Swiss Journal of Geosciences, 101(1), 1–183. https://doi.org/10.1007/s00015-008-1247-3
- Schmid, S. M., Fügenschuh, B., Kounov, A., Matenco, L., Nievergelt, P., Oberhänstli, R., et al. (2020). Tectonic units of the Alpine collision zone between Eastern Alps and western Turkey. *Gondwana Research*, 78, 308–374. https://doi.org/10.1016/j.gr.2019.07.005
- Scrocca, D. (2006). Thrust front segmentation induced by differential slab retreat in the Apennines (Italy). Terra Nova, 18(2), 154–161. https://doi.org/10.1111/j.1365-3121.2006.00675.x
- Scrocca, D. (2010). Southern Apennines: Structural setting and tectonic evolution. Journal of the Virtual Explorer, 36. https://doi.org/10.3809/ivirtex.2010.00225
- Spahić, D., & Gaudenyi, T. (2022). On the Sava suture zone: Post-Neotethyan oblique subduction and the origin of the Late Cretaceous minimagma pools. Cretaceous Research, 131, 105062. https://doi.org/10.1016/j.cretres.2021.105062
- Spakman, W., & Wortel, R. (2004). A tomographic view on western Mediterranean geodynamics. In W. Cavazza, F. Roure, W. Spakman, G. M. Stampfli, & P. A. Ziegler (Eds.), *The TRANSMED atlas. The Mediterranean region from crust to mantle: Geological and geophysical framework of the mediterranean and the surrounding areas* (pp. 31–52). Springer. https://doi.org/10.1007/978-3-642-18919-7\_2
- Steckler, M. S., Agostinetti, N. P., Wilson, C. K., Roselli, P., Seeber, L., Amato, A., & Lerner-Lam, A. (2008). Crustal structure in the Southern Apennines from teleseismic receiver functions. Geology, 36(2), 155–158. https://doi.org/10.1130/G24065A.1
- Stipčević, J., Herak, M., Molinari, I., Dasović, I., Tkalčić, H., & Gosar, A. (2020). Crustal thickness beneath the Dinarides and surrounding areas from receiver functions. Tectonics, 39(3), e2019TC005872. https://doi.org/10.1029/2019TC005872
- Šumanovac, F., & Dudjak, D. (2016). Descending lithosphere slab beneath the Northwest Dinarides from teleseismic tomography. *Journal of Geodynamics*, 102, 171–184. https://doi.org/10.1016/j.jog.2016.09.007
- Šumanovac, F., Markušić, S., Engelsfeld, T., Jurković, K., & Orešković, J. (2017). Shallow and deep lithosphere slabs beneath the Dinarides from teleseismic tomography as the result of the Adriatic lithosphere downwelling. *Tectonophysics*, 712–713, 523–541. https://doi.org/10.1016/j.
- Sun, W., Zhao, L., Malusà, M. G., Guillot, S., & Fu, L.-Y. (2019). 3-D Pn tomography reveals continental subduction at the boundaries of the Adriatic microplate in the absence of a precursor oceanic slab. *Earth and Planetary Science Letters*, 510, 131–141. https://doi.org/10.1016/j.epsl.2019.01.012
- Trumpy, E., & Manzella, A. (2017). Geothopica and the interactive analysis and visualization of the updated Italian National Geothermal Database. *International Journal of Applied Earth Observation and Geoinformation*, 54, 28–37. https://doi.org/10.1016/j.jag.2016.09.004
- Turco, E., Macchiavelli, C., Mazzoli, S., Schettino, A., & Pierantoni, P. P. (2012). Kinematic evolution of Alpine Corsica in the framework of Mediterranean mountain belts. *Tectonophysics*, 579, 193–206. https://doi.org/10.1016/j.tecto.2012.05.010
- Turcotte, D. L., & Schubert, G. (2002). Geodynamics (2nd ed.). Cambridge University Press. https://doi.org/10.1017/CBO9780511807442
- Ustaszewski, K., Kounov, A., Schmid, S. M., Schaltegger, U., Krenn, E., Frank, W., & Fügenschuh, B. (2010). Evolution of the Adria-Europe plate boundary in the northern Dinarides: From continent-continent collision to back-arc extension. *Tectonics*, 29(6), TC6017. https://doi.org/10.1029/2010TC002668
- Van Hinsbergen, D. J. J., Maffione, M., Koornneef, L. M. T., & Guilmette, C. (2019). Kinematic and paleomagnetic restoration of the Semail ophiolite (Oman) reveals subduction initiation along an ancient Neotethyan fracture zone. *Earth and Planetary Science Letters*, 518, 183–196. https://doi.org/10.1016/j.eps1.2019.04.038
- van Hinsbergen, D. J. J., Torsvik, T. H., Schmid, S. M., Maţenco, L. C., Maffione, M., Vissers, R. L. M., et al. (2020). Orogenic architecture of the Mediterranean region and kinematic reconstruction of its tectonic evolution since the Triassic. *Gondwana Research*, 81, 79–229. https://doi.org/10.1016/j.gr.2019.07.009
- Verdoya, M., Chiozzi, P., Gola, G., & Jbeily, E. E. (2019). Conductive heat flow pattern of the central-northern Apennines, Italy. *International Journal of Terrestrial Heat Flow and Applied Geothermics*, 2(1), 1–45. https://doi.org/10.31214/ijthfa.v2i1.33
- Vergés, J., & Sàbat, F. (1999). In B. Durand, L. Jolivet, F. Horvath, & M. Séranne (Eds.), Constraints on the Neogene Mediterranean kinematic evolution along a 1000 km transect from Iberia to Africa (Vol. 156, pp. 63–80). Geological Society Special Publication.
- Vilà, M., Fernández, M., & Jiménez-Munt, I. (2010). Radiogenic heat production variability of some common lithological groups and its significance to lithospheric thermal modeling. *Tectonophysics*, 490(3), 152–164. https://doi.org/10.1016/j.tecto.2010.05.003
- Wessel, P., Luis, J. F., Uieda, L., Scharroo, R., Wobbe, F., Smith, W. H. F., & Tian, D. (2019). The generic mapping tools version 6 [Software]. Geochemistry, Geophysics, Geosystems, 20(11), 5556–5564. https://doi.org/10.1029/2019GC008515
- Workman, R. K., & Hart, S. R. (2005). Major and trace element composition of the depleted MORB mantle (DMM). Earth and Planetary Science Letters, 231(1), 53–72. https://doi.org/10.1016/j.epsl.2004.12.005
- Wortel, M. J. R., & Spakman, W. (2000). Subduction and slab detachment in the Mediterranean–Carpathian region. *Science*, 290(5498), 1910–1917. https://doi.org/10.1126/science.290.5498.1910
- Zailac, K., Matoš, B., Vlahović, I., & Stipčević, J. (2023). Referent seismic crustal model of the Dinarides [Preprint]. Crustal structure and composition/Seismics, seismology, paleoseismology, geoelectrics, and electromagnetics/Seismology. https://doi.org/10.5194/egusphere-2023-183
- Zhang, W., Jiménez-Munt, I., Torne, M., Vergés, J., Bravo-Gutiérrez, E., Negredo, A. M., et al. (2022a). Geophysical-petrological model for bidirectional mantle delamination of the Adria microplate beneath the northern Apennines and Dinarides orogenic systems [Dataset]. DIGI-TAL.CSIC. https://doi.org/10.20350/digitalCSIC/14759

ZHANG ET AL. 20 of 21

# **References From the Supporting Information**

- Fullea, J., Fernàndez, M., & Zeyen, H. (2008). FA2BOUG—A FORTRAN 90 code to compute Bouguer gravity anomalies from gridded free-air anomalies: Application to the Atlantic-Mediterranean transition zone. Computers & Geosciences, 34(12), 1665–1681. https://doi.org/10.1016/j.cageo.2008.02.018
- Fuchs, S., & Norden, B., & International Heat Flow Commission. (2021). The global heat flow database: Release 202. *GFZ Data Services*, 73. https://doi.org/10.5880/fidgeo.2021.014
- Pauselli, C., Gola, G., Mancinelli, P., Trumpy, E., Saccone, M., Manzella, A., & Ranalli, G. (2019). A new surface heat flow map of the Northern Apennines between latitudes 42.5 and 44.5 N. *Geothermics*, 81, 39–52. https://doi.org/10.1016/j.geothermics.2019.04.002
- Sandwell, D. T., Müller, R. D., Smith, W. H. F., Garcia, E., & Francis, R. (2014). New global marine gravity model from CryoSat-2 and Jason-1 reveals buried tectonic structure. *Science*, 346(6205), 65–67. https://doi.org/10.1126/science.1258213
- Smith, W. H. F., & Sandwell, D. T. (1997). Global Sea floor topography from satellite altimetry and ship depth soundings. *Science*, 277(5334), 1956–1962. https://doi.org/10.1126/science.277.5334.1956

ZHANG ET AL. 21 of 21